GEOCHEMICAL MODELLING OF ENVIRONMENTAL PROCESSES IN RARE EARTH ELEMENT MINING

Alexandra Crawford

Submitted in accordance with the requirements for the degree of
Doctor of Philosophy

The University of Leeds
School of Earth and Environment

March, 2019

The candidate confirms that the work submitted is her own and that appropriate credit has been given where reference has been made to the work of others.

PhD SETTING

This PhD is part of the SoS RARE consortium project funded by NERC and ESPRC as part of the Security of Supply of Mineral Resources (SoS Minerals) science programme, which is running from 2015 to 2019. The project involves six universities and research institutes (Leeds, Sheffield, St Andrews, Exeter (lead partner), Brighton and BGS), ten industry partners and eight core international research collaborators.

SoS RARE is divided into four work packages, each with specific aims and objectives. This PhD is part of work package four which focuses on the processing of ion adsorption deposits. NERC and UIT (Umwelt- und Ingenieurtechnik GmbH), an industrial partner with considerable numerical modelling experience in the mining industry, co-funded the PhD. As a result, 18 months were spent working with UIT in Dresden, Germany.

ACKNOWLEDGMENTS

I would like to thank my supervisors, Prof Steve Banwart and Dr Barbara Palumbo-Roe, for their useful critiques of this research and their continued guidance and support of my ideas.

I am particularly grateful for the assistance given by Dr Jana Nicolai with experimental design and for many helpful discussions. I would like to express my gratitude to Harald Kalka for his help with all aspects of the modelling, and I am grateful to Dr Horst Märten for his support of my research.

Thanks to Dr Vinzenz Brendler for advice given and to Sabrina Gürlitz and Carola Eckardt for analysis of all my data with ICP-MS and IC. Thanks to Michael Watt and BGS laboratory staff for ICP-MS fusion of my sample material. I am grateful to Dr Elena Tamayo Mas for support using the PEST optimiser and to Dr Sumit Sinha for help getting me started with HYDRUS-1D.

I would also like to thank the project partners from Brighton University, particularly Dr Guilluame Estrade and Dr Samantha Bromfield for XRD analysis of the pits and leach pit transect data. Thanks to the fieldwork team, Dr. Kathryn Goodenough, Dr Megan Barnett, Dr Guilluame Estrade and Eva Marquis for collecting sample material from the study area.

Co-funding from UIT (Umwelt- und Ingenieurtechnik GmbH Dresden), and NERC is gratefully acknowledged.

ABSTRACT

Rare earth elements (REE) are considered indispensable and non-replaceable in many optical, electronic, catalytic and magnetic applications. Indeed they are viewed as critical metals due to the monopoly China has over their supply chain and to their ever increasing demand. Ion adsorption-type deposits (IAD) have attracted much attention in recent years as the relative ease of REE recovery makes these deposits economically significant. At present IAD are only mined in China, which has led to considerable environmental damage.

This study considers an IAD in NW Madagascar which is under active exploration. The research aim was to develop a numerical modelling approach to simulate the mobilisation of REE from IAD. To achieve this, REE exchange reactions with Madagascar IAD minerals in batch reactor tests were modelled, and thermodynamic equilibrium constants were estimated for these reactions. Reactive transport modelling of flow-through laboratory column experiments was undertaken to test the estimated REE exchange constants.

A single exchange constant of log K 2.29 ± 0.5 (experimental standard deviation) was able to describe all the REE exchange reactions with the Madagascar IAD in both batch and column datasets. Exchange constants were also estimated for each individual REE to account for any variation in REE behaviour (e.g. due to the lanthanide contraction). The determined constant only varied to 2 decimal places and the difference between the objective functions for individual log K model (5.71×10^{-11}) and for the single log K model (5.72×10^{-11}) was minimal.

Without further application to different IAD and different sample materials from Madagascar, the exchange constants estimated in this study should not be considered as the standard equilibrium constants for all IAD-REE exchange reactions.

TABLE OF CONTENTS

LIST OF FIGURES

LIST OF TABLES

ABBREVIATIONS

BGS	British Geological Survey
CEC	Cation Exchange Capacity
ESPRC	Engineering and Physical Sciences Research Council
HREE	Heavy Rare Earth Elements
IAD	Ion Adsorption Deposits
IC	Ion Chromatography
ICP-MS	Inductively Coupled Plasma Mass Spectrometry
ISR	In Situ Recovery
IX	Ion Exchange
LLNL	Lawrence Livermore National Laboratory
LREE	Light Rare Earth Elements
NERC	Natural Environment Research Council
PHREEQC	pH Redox Equilibrium
REE	Rare Earth Elements
REO	Rare Earth Oxides
SC	Surface Complexation
SLR	Solid-Liquid Ratio
SoS RARE	Security of Supply of Rare Earth Elements
SD	Standard Deviation
TRLFS	Time Resolved Laser Induced Fluorescence Spectroscopy
UIT	Umwelt und Ingenieurtechnik GmbH Dresden
XRD	X-ray Diffraction

CHAPTER 1

INTRODUCTION

1.1 Motivation

The rare earth elements (REE) are a coherent group of trace elements with regard to their physical, chemical and structural properties (i.e. ionic radius, charge, and mineral site coordination). They comprise the fifteen lanthanides, yttrium and scandium. The REE are considered 'critical' metals because of their extensive applications in the technological sector and China's control over all aspects of the supply chain (EC, 2014; Massari & Ruberti, 2013).

Today, at least 80 % of the global supply of REE comes from China (USGS, 2018), where mining and processing has been concentrated since other large players started leaving the market in the late 1990s. Changes to Chinese industrial policies in the early 2010s led to decreases in their export quota (Mancheri, 2015; Wübbeke, 2013), in turn this led to a surge in global REE exploration activities (Paulick, & Machacek, 2017).

A number of recent exploration projects in Madagascar and Brazil focus on ion adsorption type REE deposits (IAD). These lateritic[1] soils are only commercially processed in China, where they represent the world's main source of heavy REE (HREE). IAD are characterised by the relative ease of REE recovery using a salt solution to mobilise the exchangeable REE cations adsorbed onto the surfaces of clay minerals (Chi & Tian, 2008).

The mining practices associated with REE recovery from IAD (e.g. heap leaching) have led to severe environmental consequences in China, for example soil excavation (Yang *et al.,* 2013). Alternative environmentally focused mining approaches should be considered to develop newly discovered IAD (e.g. in Madagascar) but, prior to this, it is important to understand the mechanism of REE mobilisation during mining, and model this.

A relatively good conceptual understanding of the cation exchange mechanism by which the REE are mobilised from IAD when in contact with a concentrated salt solution (during mining), can be found in the literature (e.g. Coppin *et al.,* 2002). However, the absence of thermodynamic equilibrium constants in the literature (for all the REE) which need to be used to model REE exchange reactions with the minerals in the IAD presents a problem.

[1] Laterite soils are highly weathered tropical or subtropical residual soil, when REE in laterites adsorb onto the surfaces of clay minerals they form IAD.

1.2 Aim

The aim of this research was therefore **to develop a numerical modelling approach that will simulate the mobilisation of the REE from ion adsorption deposits during mining.** This will also involve the consideration of a more environmentally focused extraction method than the techniques currently employed.

1.2.1 Objectives

- Measure the cation exchange capacity of the Madagascar lateritic soil.
- Develop a mathematical modelling approach to determine thermodynamic equilibrium constants using batch reactor experimental data for REE exchange reactions with the Madagascar IAD minerals.
- Determine whether the REE exchange constants can represent REE breakthrough curves from soil column experiments.
- Apply reactive transport modelling at site scale to assess the applicability of an environmentally focused mining approach to recover REE from the Madagascar IAD.

1.3 Madagascar Study Area

A laterite deposit under active exploration was chosen as the study area. This deposit was known as the Tantalus rare earths project and was fully owned by Tantalus Rare Earths AG at the start of this research. As of December 2015, Tantalus Rare Earths AG no longer owns the primary share of the deposit, it will henceforth be termed the Madagascar IAD.

The Madagascar IAD is located on the Ampasindava Peninsula, in the Antsiranana Province in north western Madagascar (see Fig. 1.1). The study area encompasses 283 km^2. The geology comprises a sequence of mainly Jurassic mudstones and siltstones, intruded by the Tertiary alkaline igneous rocks named the Ambohimirahavavy igneous complex.

The Ambohimirahavavy igneous complex is associated with a variety of mineralised rocks: alkaline volcanics; syenitic ring-dykes and late peralkaline granitic and pegmatitic dykes. Two types of REE mineralisation occur in the IAD. REE are hosted by peralkaline rocks in the bedrock and ion adsorption-type REE are present in the overlying laterite profile (SRK, 2013).

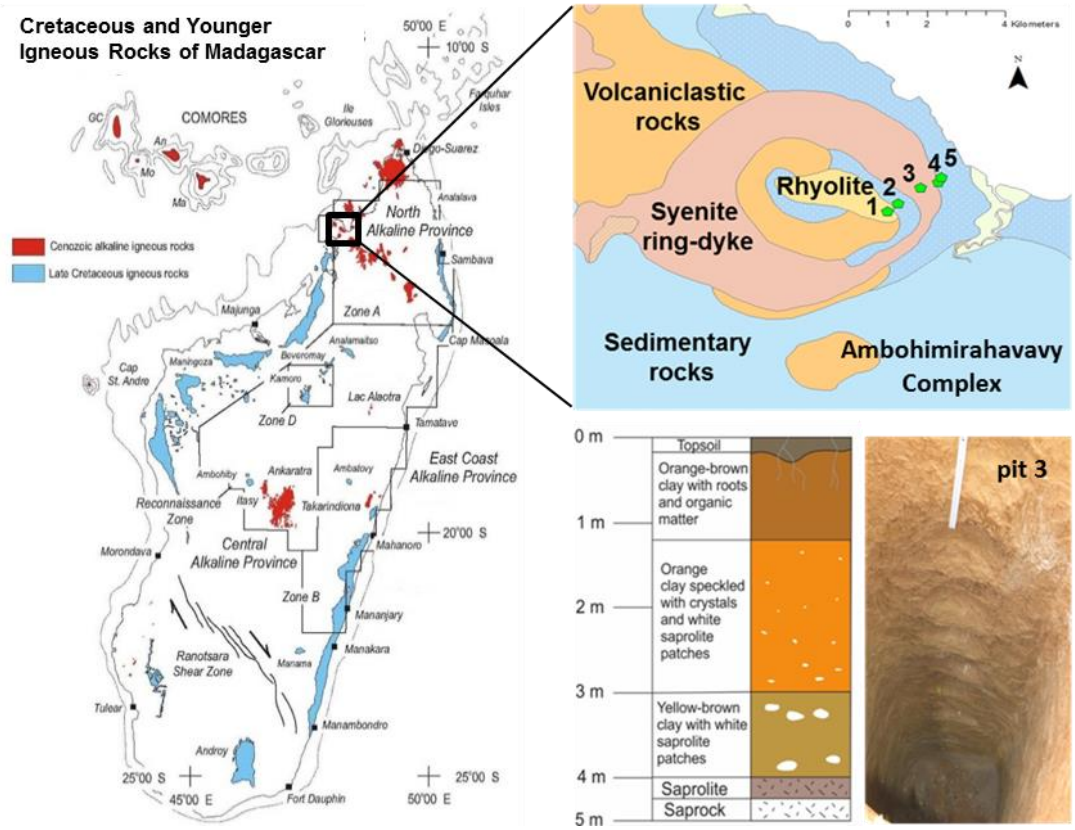

Fig. 1.1 Study area in NW Madagascar (from Kathryn Goodenough).

A typical laterite profile in the Madagascar study area is shown in Fig. 1.2. The minerals present in the profile were identified from a technical report about the Madagascar deposit undertaken by SRK (2013), and from XRD analysis that was performed by SoS Rare project colleagues at Brighton University on samples from a number of localities around the site.

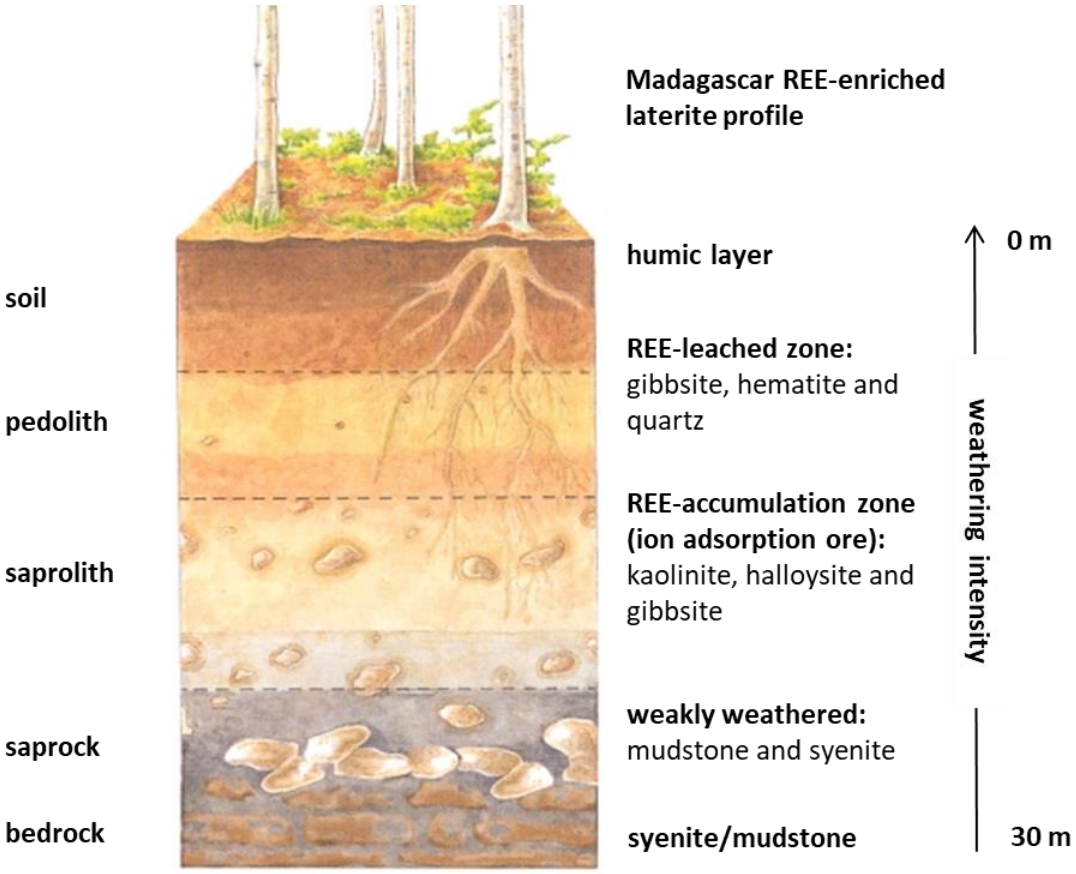

Fig. 1.2 Typical REE-enriched laterite profile in NW Madagascar (adapted from Plummer *et al.,* 1991).

1.3.1 Pit Logging

Fieldwork on the Madagascar study area was carried out in 2016 by SoS RARE project colleagues from BGS and Brighton University. This involved sample collection from five pits at different localities on the Ambohimirahavavy igneous complex. The sampling approach is described in this section.

The five pits sampled on the Ambohimirahavavy complex are shown in the upper right diagram of Fig. 1.1. The pits are located on a microsyenite/rhyolite hill (1), in a river valley (2), on a ridge (3), and on the seaward slope (4, 5). Each pit had a width of 1 m with vertical depths ranging from 1 - 6.5 m.

Bulk samples (2 – 3 kg) from each horizon and smaller 500 g samples at 25 – 30 cm intervals were collected from each pit. Pans were used to scoop the displaced material into bags, during which some mixing would have occurred. Collection began at the lowermost interval to minimise contamination.

All samples were stored in sealed plastic bags and shipped to BGS. The sample material used in this study was collected from pit 3, which was located in a secondary forest (ca. 20

years old) on top of a syenite ring dyke. The pit was excavated manually to a depth of 4.5 m (bottom right diagram in Fig. 1.1).

The bulk sample (593) collected between 3 - 4 m depth in the lower pedolith was chosen for experimental work because it was where the REE were thought to be most concentrated based on the weathering profile development model by Sanematsu & Watanabe (2016). Total REE content in sample 593 is ~ 200 ppm[2].

Within this lateritic section (sample 593), the disturbed material is a fine clayey soil that is brownish-orange in colour and is interspersed with white saprolite patches. There are a few soft chunks present that can be easily broken with a pestle. Some detrital organic materials (i.e. remnants of plants, roots etc.) are also present.

Table 1.1 shows XRD analysis of the pit 3 weathered profile[3]. Kaolinite is observed to be the dominant clay mineral in the IAD. Halloysite is also thought to occur but, because the diffraction signature is very similar to that of kaolinite, it is difficult to differentiate between the two, thus the quantity is unknown.

Table 1.1 XRD analysis of 500 g samples in pit 3 (performed at Brighton University).

500 g Sample	Depth [m]	Kaolinite [%]	Halloysite [%]	Gibbsite [%]	Quartz [%]
578	0.3	78	-	22	-
581	0.9	73	-	27	-
584	1.5	78	-	22	-
589	2.5	62	-	20	18
592	3.2	85	-	-	15
595	3.9	68	-	-	32
597	4.2	26	-	7	67

[2] Determined from Na_2O_2 fusion with an ICP-MS finish by Michael Watt and BGS laboratory staff.
[3] This analysis was performed by SoS RARE project colleagues at Brighton University.

1.4 Thesis Structure

This thesis includes a literature chapter which summarises the prior research underlying this study and a methods chapter where the different analytical techniques are described. Subsequent chapters present data, each being broadly split into the modelling approach and modelling outcomes. The structure of this thesis is as follows:

- CHAPTER 2: Theoretical Background
  - ⇒ Provides a detailed description of the REE and IAD.
  - ⇒ Identifies approaches to mathematically model fluid-rock interactions.
  - ⇒ Introduces REE sorption mechanisms and literature pertaining to this subject.
- CHAPTER 3: Experimental Investigation
  - ⇒ Describes the column and batch experiments undertaken to achieve the research aim and objectives.
- CHAPTER 4: Results and Discussion
  - ⇒ Reports and discusses the outcomes of the experimental investigation described in CHAPTER 3.
- CHAPTER 5: Modelling
  - ⇒ Uses the experimental REE dataset described in CHAPTER 4 to estimate REE exchange constants.
- CHAPTER 6: Alternative Mining Applications
  - ⇒ Reports the results of generic simulations of water flow and solute transport through lateritic soil profiles.
- CHAPTER 7: Conclusion
  - ⇒ Summarises the key outcomes of this research and discusses future work.

CHAPTER 2

THEORETICAL BACKGROUND

This chapter provides the fundamental background knowledge for each of the systems considered in this research:

[1] Rare Earth Elements (REE)

⇒ Introduces the importance of the REE in the technological sector.

[2] Ion Adsorption Deposits (IAD)

⇒ Discusses the importance of IAD as chemically easily leachable deposits.

⇒ Highlights the current challenges associated with mining IAD.

⇒ Discusses the application of environmentally focused mining approaches.

[3] Modelling Fluid-Rock Interactions

⇒ Introduces the thermodynamic equilibrium approach to model ion exchange reactions with the Madagascar IAD.

⇒ Provides an overview of the reactive transport and flow modelling concepts used to simulate the Madagascar IAD system.

[4] REE Sorption Processes

⇒ Introduces the sorption mechanisms occurring during REE mobilisation from IAD.

[5] Sorption Studies

⇒ Summarises literature studies for REE sorption onto common IAD minerals.

2.1 Rare Earth Elements

The REE are a set of seventeen trace metals in the periodic table, including the fifteen lanthanides, yttrium and scandium. Promethium and scandium are excluded from this study because promethium is a radioactive element and scandium behaves considerably differently to the rest of the REE. This leaves a total of fifteen elements.

The term rare earth does not refer to the elements crustal abundances, rather the scarcity of economically concentrated ore deposits. The REE are grouped together because they exhibit similar chemical behaviour. As a result, they tend to occur together in nature and are difficult to separate from one another (Paulick & Machacek, 2017).

The REE are often classified further into light REE (LREE) and heavy REE (HREE):

LREE: La, Ce, Pr, Nd, Pm, Sm, Eu

HREE: Gd, Tb, Dy, Ho, Er, Tm, Yb, Lu and Y

The chemical properties of Sc are not similar enough to classify it as either a LREE or HREE (Gupta & Krishnamurthy, 1992; Jordens *et al.,* 2013).

This division is somewhat arbitrary, but has assisted in the mineral exploitation process (Schoeller & Powell, 1995) as REE-bearing minerals tend to preferentiate towards either the lower or higher atomic numbers (Henderson, 1984). Typically, natural REE ores are dominated by La, Ce and Nd with lower concentrations of the HREE. The HREE are scarcer than LREE because of their low crustal abundances (Table 2.1) and limited reserves (Simandl, 2014).

2.1.1 Chemical and Physical Characteristics

REE are characterised by their chemical similarity. This is related to the occupancy of the 4f electron shell. Electrons are successively added to the 4f sub-shell which lies deep within the 6s sub-shell. La, Gd, Lu and Y are the exceptions which accommodate 1 electron in the 5d shell and 4d shell, respectively. As a result, the 6s shell is filled and the 4f electrons are so well shielded that the REE chemical properties are almost identical (Clark, 1984).

REE chemical similarities allow the trivalent species (REE^{3+}) to occur in an array of minerals (McLennan & Taylor, 2012). The +3 oxidation state is particularly stable. Two of REE can occur in alternate oxidation states in natural systems (Platt, 2012). Ce^{4+} can form under oxidising conditions and Eu^{2+} can form under reducing conditions. Different oxidation states for Sm, Tm and Yb are known, but are rarely seen in nature (Henderson, 1984).

The lanthanide contraction is the main difference between the REE, where the systematic decrease in ionic radii with increasing atomic number is observed. The lanthanide contraction is the result of unit increases in nuclear charge on transition to greater atomic numbers and incomplete shielding by the f orbitals. The importance of this occurrence is reflected in the greater chemical affinity for hydrolysis from La to Lu (Aide & Aide, 2012).

The relative abundance of the REE varies considerably in nature. However, the REE frequently obey the Oddo-Harkins rule. In this regard, elements with an even atomic number will be more abundant than their adjacent odd numbered counterparts (Allaby, 2008). In the Earth's crust, this effect is combined with the general trend of decreasing REE abundance with increasing atomic number. Table 2.1 shows properties of the REE.

Table 2.1 Selected properties of the REE (from Gupta & Krishnamurthy, 2005).

Element	Symbol	Atomic Number	Ground state configuration	Crustal Abundance [ppm]	Radii[1] [nm]	Charge
Scandium	Sc	21	$3d^1 4s^2$	25	0.76	+3
Yttrium	Y	39	$4d^1 5s^2$	24	0.88	+3
Lanthanum	La	57	$5d^1 6s^2$	30	1.06	+3
Cerium	Ce	58	$4f^1 5d^1 6s^2$	60	1.03	+3, +4
Praseodymium	Pr	59	$4f^3 6s^2$	6.7	1.01	+3
Neodymium	Nd	60	$4f^4 6s^2$	27	1.00	+3
Promethium[2]	Pm	61	$4f^5 6s^2$		0.98	+3
Samarium	Sm	62	$4f^6 6s^2$	5.3	0.96	+2, +3
Europium	Eu	63	$4f^7 6s^2$	1.3	0.95	+2, +3
Gadolinium	Gd	64	$4f^7 5d^1 6s^2$	4	0.94	+3
Terbium	Tb	65	$4f^9 6s^2$	0.7	0.92	+3
Dysprosium	Dy	66	$4f^{10} 6s^2$	3.8	0.91	+3
Holmium	Ho	67	$4f^{11} 6s^2$	0.8	0.90	+3
Erbium	Er	68	$4f^{12} 6s^2$	2.1	0.88	+3
Thulium	Tm	69	$4f1^3 6s^2$	0.3	0.87	+2, +3
Ytterbium	Yb	70	$4f^{14} 6s^2$	2.0	0.86	+2, +3
Lutetium	Lu	71	$4f^{14} 5d^1 6s^2$	0.4	0.85	+3

[1]Ionic radii of the M^{3+} ion. [2]Promethium has no natural abundance.

The physical characteristics of the REE are very diverse making them particularly useful in a wide range of applications. The 4f shell determines the optical and electrical properties of the REE. For example, some REE (e.g. La) have sharply defined energy states which can be efficiently used in lighting and laser applications (Ter-Mikirtychev & Ter-Mikirtychev, 2014).

The magnetic properties of the REE originate from the angular momentum of the 4f electrons. REE typically have electrons with magnetic moments[4] occupying the shielded 4f sub-shell (Abaka-Wood *et al.,* 2016). This results in some of the REE (e.g. Nd) having some degree of magnetism and a large magnetic anisotropy[5] (Baczewski *et al.,* 1993).

2.1.2 Mineralogy

The chemical similarities of the REE i.e. the shielding of the 4f electrons, is the reason that the REE are always found as associated groups in minerals and rocks (Clark, 1984). In nature, the REE do not occur in their pure native form as metallic elements, instead they occur either with other REE as accessories in other minerals or as REE minerals.

The REE occur in a range of mineral types including silicates, halides, carbonates, oxides and phosphates. High REE concentrations are required to form their own minerals (e.g.

[4] The magnetic moment of an object is a measure of the object's tendency to align with a magnetic field.
[5] Magnetic anisotropy is the dependence of a materials magnetic properties on direction.

synchysite-(Ce); Möller, 1986). REE-bearing minerals (e.g. carbonates) usually contain most of the REE in varying concentrations, and are often enriched in either the LREE or HREE.

REE mineral deposits occur in an array of metamorphic, sedimentary and igneous rocks. The distribution and concentration of the REE in mineral deposits is primarily influenced by the genetic conditions under which the minerals form such as REE enrichment in magmatic or hydrothermal fluids (Clark, 1984; Murata *et al*., 1959; Neumann *et al*., 1966).

Environments in which REE are enriched are broadly classified into primary deposits formed by hydrothermal and magmatic processes and secondary deposits formed by weathering and sedimentary processes. These two groups are further subdivided on the basis of their occurrence, mineralogy and genetic association (Walters *et al.,* 2011):

- Primary deposits
  - ⇒ carbonatite-associated deposits
  - ⇒ alkaline igneous rocks
  - ⇒ iron-REE deposits
  - ⇒ hydrothermal deposits

- Secondary deposits
  - ⇒ placers
  - ⇒ laterites
  - ⇒ bauxites
  - ⇒ ion adsorption deposits

Despite there being around 200 potential REE ore minerals, there are only a few that are considered economically viable, and even fewer that have been successfully processed and the REE extracted (Jordens *et al.,* 2013). The most commercially significant sources are found in bastnäsite, monazite, xenotime and ion adsorption deposits (Golev *et al.,* 2014).

2.1.3 Importance of the REE

The unique chemical and physical properties of the REE have rendered them indispensable in the hi-tech industry, in low carbon technologies, in electronic devices, and in military and defence applications. As a result of increasing demand in these sectors, the annual global production of rare earth oxides[6] (REO) has grown from c. 72,200 tonnes [t] in 1995 to about 130,000 t in 2017 (USGS, 1996, 2018).

[6] Rare earth oxides are the main way the REE are purchased.

Today, more than 80% of the global REE supply originates from China (USGS, 2018). Mining and processing have been concentrated in China since the late 1990s, where REO production has increased from around 30,000 t in 1995 to a peak of about 130,000 t in 2010 (USGS, 1996, 2011). In the early 2010s, changes were made to Chinese policies limiting REE export quota (Mancheri, 2015; Wübbeke, 2013).

Increasing demand for the REE in modern industrial applications in correlation with China's monopoly over all aspects of the supply chain, the difficulties of substituting the REE for other elements and the low recycling rates, has led to global concerns over the security and supply of these metals. Thus, the REE are considered 'critical' metals (Barteková & Kemp, 2016; Buijs & Sievers, 2011; EC, 2014; Massari, & Ruberti, 2013; Wall, 2014).

Following this designation and the Chinese decreasing their export quota, global exploration activity for REE-bearing mineral deposits surged and by 2012, more than 400 exploration projects were pursuing new prospects with the aim of discovering and developing REE resources (Hatch, 2012). Among the strategies being considered in these projects is the development of processing (i.e. refining, alloying) infrastructure (Humphries, 2013).

2.2 Ion Adsorption Deposits

The term laterite or lateritic soils are used to describe highly weathered tropical or subtropical residual soil, which is rich in clay minerals and usually coated with sesquioxide rich concretions (i.e. Al- and Fe-oxides; Gidigasu, 1972). The colour of these may vary from rusty red to liver brown (Oyelami & Van Rooy, 2016).

The high temperatures and abundant rainfalls found in the tropics and sub-tropics allow laterite weathering profiles to develop in these localities. Laterites are formed when rainwater washes out the bases and the silicic acid, and enriches the soil with aluminium silicates, hydrosilicates and iron (hydr-) oxides (Maji *et al.,* 2007).

When laterites develop on igneous bedrock that includes REE, the REE can be mobilised (and fractionated) into secondary minerals that accumulate within the profile (Berger *et al*., 2014; Goodenough *et al.,* 2018). In a few specific localities, REE in laterites adsorb onto the surfaces of clay minerals to form an IAD.

A deposit that contains ≥ 50% ion-exchangeable REE adsorbed onto clay mineral surfaces is termed an IAD (Chi *et al*., 2005; Wu *et al*., 1990, 1995). An IAD is characterised by

the relative ease of REE extraction (i.e. near the surface and unconsolidated) using a reagent such as ammonium sulphate to mobilise the exchangeable REE into solution.

The stoichiometric ion exchange reaction is shown in Eq. (2.1):

(2.1) $2(Clay)^{3-}REE^{3+} + 3(NH4)_2^{1+}SO_4^{2-} \rightarrow 2(Clay)^{3-}(NH4)_3^{1+} + REE_2^{3+}(SO_4)_3^{2-}$

where the exchange site is $2(Clay)^{3-}$ and the exchangeable ions are REE^{3+} and $(NH4)_3^{1+}$. Because of this relatively simple mechanism of REE recovery, IAD are considered economically significant (Zhang, 1990; Sanematsu *et al*., 2015).

Fig. 2.1 depicts the genesis of an ion adsorption ore. The weathering profile can be broadly divided into the humic layer, the REE leached zone, the REE accumulation zone, the poorly weathered granite and the parent granite. Common IAD minerals include kaolinite, halloysite, gibbsite, goethite, hematite and amorphous iron oxyhydroxides.

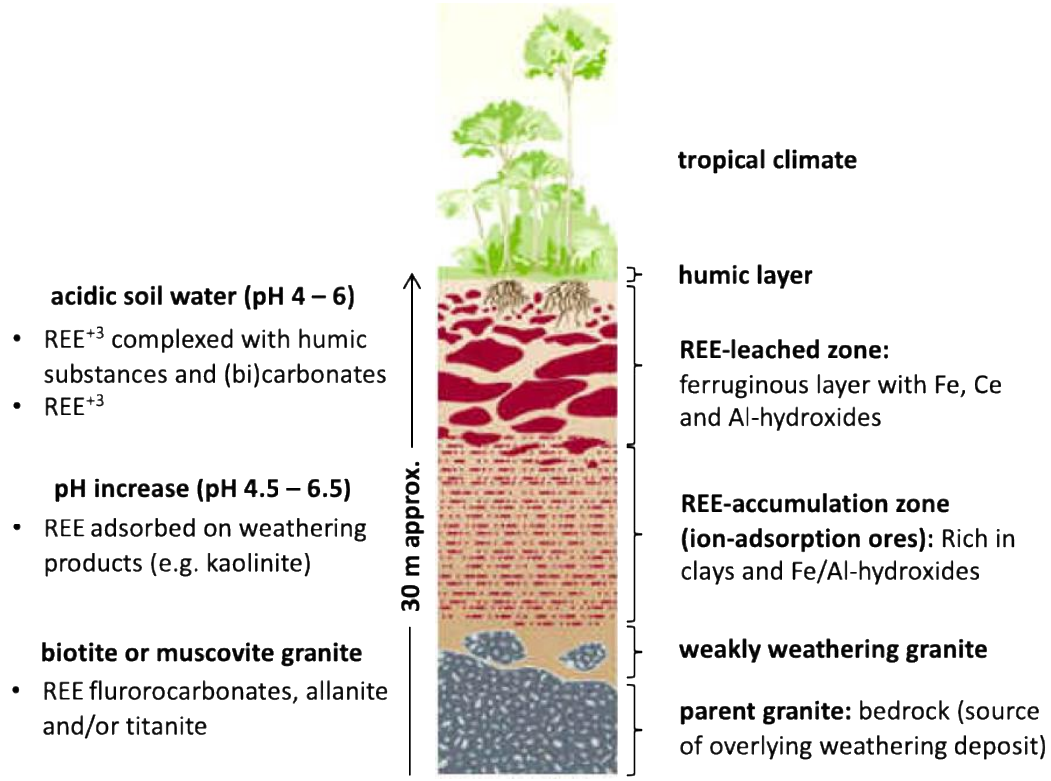

Fig. 2.1 Typical laterite profile depicting the genesis of ion adsorption ore (adapted from Plummer *et al*., 1991).

The majority of IAD occur in areas underlain by granites. Weathering of the granite can release REE-bearing primary magmatic minerals (e.g. allanite) and secondary minerals (e.g. flurorocarbonates) (Aubert *et al.,* 2001). Acidic soil water at shallow levels in the profile can alter and dissolve the REE-bearing minerals released from the weathered granites. Decay of organic material at the surface results in CO_2(g) and its dissolution forms the acidic soil water.

Mobile REE in the soil water are transported down the profile either as trivalent cations or by forming aqueous complexes with humic substances, carbonate and bi-carbonate ions (Tang & Johannesson, 2003). The REE are commonly removed from solution by adsorption onto the surfaces of kaolinite and halloysite, which are abundant, to form an IAD. The amorphous materials present in the IAD are also capable of exchanging REE.

The REE are retained from the aqueous phase due to the adsorption and ion exchange properties of the secondary clay minerals and amorphous materials (§ 2.4.1; Zhao *et al.,* 2001). During weathering, Ce is rarely scavenged from the leached zone, thus fractionation occurs between Ce and the other REE. Fractionation of the LREE and HREE can also occur during weathering and precipitation of secondary minerals (Sanematsu & Watanabe, 2016).

2.2.1 Global Ion Adsorption Deposits

IAD are only commercially processed in China. They account for 35% of world REE production (Yang *et al*., 2013). IAD have been discovered in a few other localities, in Madagascar (this study area, § 1.3), Malawi (Le Couteur, 2011), Brazil (Rocha *et al.,* 2013) and Southeast Asia (Mentani *et al.,* 2010; Sanematsu *et al*., 2013). However, none of these deposits is enriched in HREE to the extent of some of the Chinese deposits.

REE abundances in rocks and sediments are often normalised to another REE pattern to eliminate the complexities of the Oddo-Harkins effect. The most commonly used normalising values are from chondritic meteorites which represent the bulk earth (Wilson, 2007). There is little variation in the relative distributions of REE in estimates of average chondrites (apart from absolute abundances). Therefore, no uniform set of chondrite values is used.

Chondrite normalised REE distribution patterns in the bedrock or weathered profile are often used to describe the fractionation of the LREE and/or the HREE during adsorption. These patterns can be interpreted as being enriched or depleted in the LREE/HREE. Positive or negative anomalies, where one REE is depleted or enriched relative to the other REE, are also prevalent in distribution patterns.

Fig. 2.2 shows chondrite normalised REE patterns of granitic rocks and their weathered profiles from different IAD localities in China (Bao & Zhao, 2008), Laos (Sanematsu *et al*., 2009), and Thailand (Sanematsu *et al*., 2013). For comparison normalised REE leach data from the pit 3 laterite profile in Madagascar is shown (carried out by project colleagues at Brighton University). The data for these plots is provided in Appendix A.

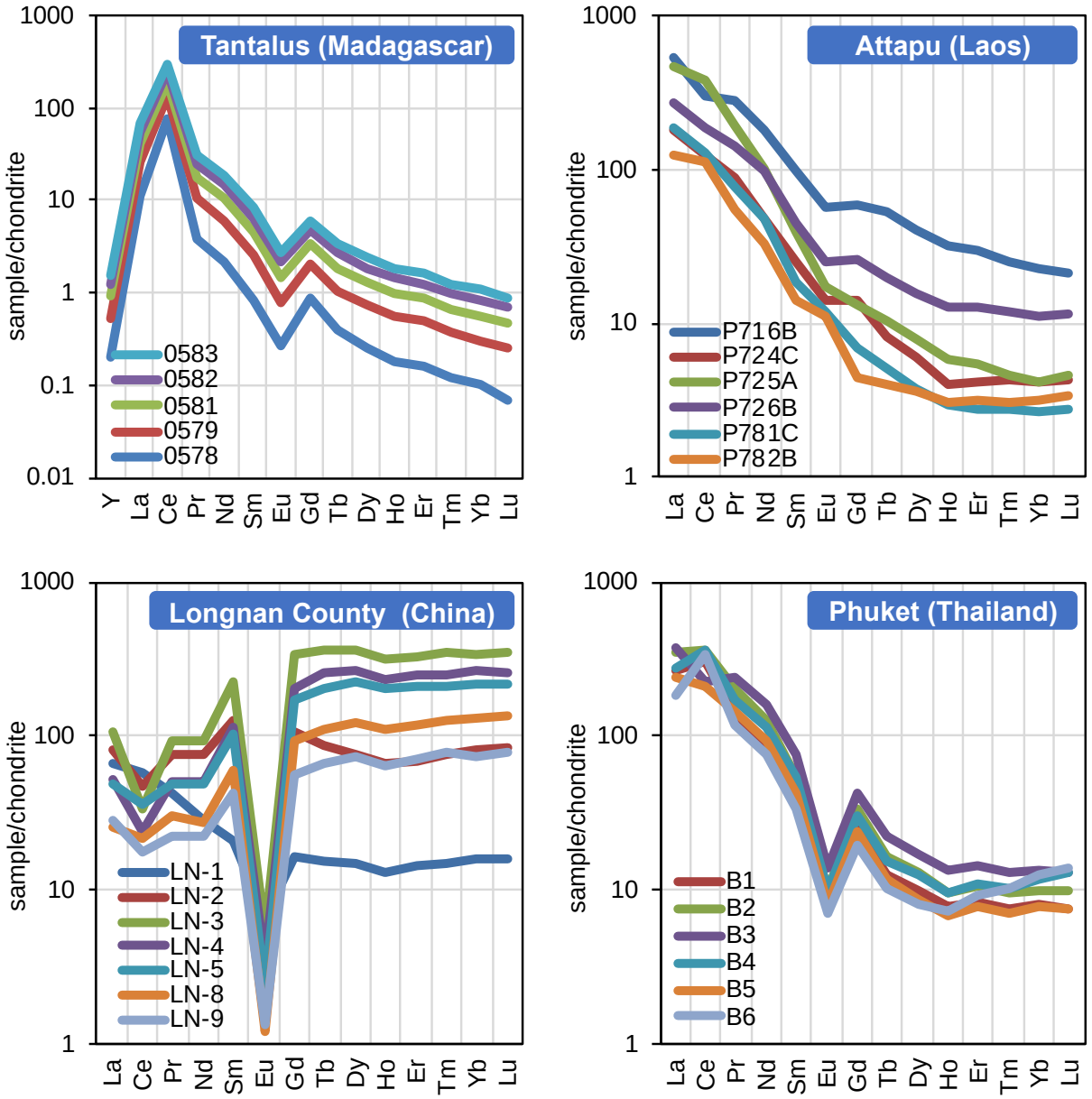

Fig. 2.2 REE distribution patterns from four IAD normalised to chondrite values from Anders & Grevesse (1989) multiplied by a factor of 1.36. Increasing sample numbers correspond to increasing depth.

It is evident from the four distribution patterns that only the Chinese deposit is enriched in the HREE. In addition to their enrichment of the more valuable HREE, Chinese deposits often contain greater REE contents of between 140-6500 ppm (Sanematsu & Wantanabe, 2016) compared to 40-340 ppm (Sanematsu *et al*., 2009), 170-1100 ppm (Sanematsu *et al*., 2013), 130-720 ppm in Laos, Thailand and Madagascar, respectively.

Common anomalies (i.e. positive Ce and negative Eu anomalies) are also observed in the REE patterns. These anomalies are not removed by chondrite normalisation. They are the result of the different oxidation states that Ce and Eu can be found in, under certain redox conditions (§ 2.1.1; Borges *et al*., 2008; Braun *et al*., 1998; Fryer, 1977; Graf, 1978; Tostevin *et al*., 2016; Van Kranendonk *et al*., 2003).

2.2.2 Mining and Processing IAD

There are three important challenges associated with mining and processing of IAD that will be described in this section. These are:

[1] China's monopoly;
[2] Environmental Impacts, and
[3] Economic costs.

The main challenge associated with IAD is that no commercial processing is undertaken outside of China, despite the existence of deposits across the globe (§ 2.2.1). However, the implementation of an export quota by the Chinese government forced other countries to develop their own deposits (e.g. in Madagascar) and invest in new extraction technologies.

Significant environmental consequences are associated with traditional IAD mining and processing technologies (Yang *et al*., 2013). For example, it is estimated that for every t of REO produced from IAD using surface mining and heap leaching (Yang *et al*., 2013):

- 300 m^2 of vegetation and topsoil are removed;
- 1000 t of wastewater containing concentrated $(NH_4)_2SO_4$ and heavy metals are produced, and
- 2000 t tailings are disposed into adjacent valleys and streams.

For two decades (~1990-2010) surface mining of IAD was the dominant driver of land-use change and degradation in southern China (Yang *et al.,* 2013). This has led to permanent ecological, environmental and health problems. An example of these damages is observed in

the Ganzhou region, where REE mining has left 153 km^2 of destroyed forests, 302 abandoned mines and 191 million tonnes of tailings (Guo, 2012; Yang *et al.,* 2013).

Economic issues with developing IAD include a large leach residue (tailings), overexploitation and significant environmental restoration costs (e.g. reclamation of Ganzhou's REE mines cost an estimated $5.8 billion; Ding, 2012; Yang *et al.,* 2013). In addition, grade and tonnages of IAD have been steadily decreasing. This has led to greater extraction costs because more reagent is required to recover the REE (Tian *et al.,* 2013).

2.2.3 REE Extraction

It is widely accepted that commercial production of REO from many conventional REE ore deposits (such as carbonatites) is far from environmentally sustainable. This is because large amounts of material and energy are required along with the generation of significant quantities of solid waste, and air/water emissions (Navarro & Zhao, 2014; Vahidi *et al.,* 2016). IAD are unique in the relative ease of REE extraction.

Surface mining is the primary method of REE extraction for IAD because of their near surface nature. This type of mining is generally considered safer and more economic than operation of underground mines (Palmer *et al*., 2010). In most cases, this method involves removing the overburden (including topsoil and vegetation), digging or blasting the ore and then removing it for further processing (Walters *et al.,* 2011).

REE in IAD mainly occur in the exchangeable phase (60 - 90%) as adsorbed species on clay mineral surfaces, where they can be easily mobilised into solution with a chemical cation exchange reagent (Eq. (2.1)); Chi *et al.,* 2006; Jun *et al.,* 2010). This makes processing of IAD fairly simple. The remaining 10 - 40% are not recovered to date because more aggressive leaching conditions are required (Voβenkaul *et al*., 2015).

The different processing methods that have been implemented in China over the last 50 years include heap and tank/pool leaching and in-situ recovery (Yang *et al.,* 2013). Heap leaching involves heaping the ore into a pile on an impermeable layer. A reagent that is sprayed at the surface seeps downward solubilising the REE. The enriched solution is then collected in a solution sump (Papangelakis & Moldoveanu, 2014).

Tank leaching is quite similar to heap leaching except the material mined from the IAD is placed in a tank and soaked with a reagent (Zhao *et al*., 2001). Formerly, tank and heap leaching were the widely most used methods to process IAD. However, the related environmental impact (ground clearance, tailings discharge, and ground water contamination)

is one of the main reasons cited by the Chinese government for imposing an export quota (Vahidi *et al.,* 2016).

In addition to the export quota, the government enforced a ban on surface mining and tank/heap leaching while implementing in situ recovery (ISR) to develop IAD (Anonymous cited in Yang *et al.,* 2013). ISR is now the dominating technology, because there is minimal surface disturbance associated since surface mining is not required beforehand and the process can be performed on site (Schüler *et al.,* 2011).

The economic and environmental advantages and disadvantages of ISR over traditional heap or tank leaching approaches are outlined in Table 2.2.

Advantages	Disadvantages
• ISR can achieve extraction efficiencies greater than 90%, with final products of purity 90–92% (Roskill, 2007).	• Chemical reagents contaminating groundwater and surface water (Zhu *et al.,* 2011).
• No ore beneficiation (extraction purely through hydrometallurgical processes).	• High power demand for ISR site (in the 100 kW range (Li, 2011).
• One fifth less top soil and vegetation is removed (Yang *et al*., 2013)	• One third of top soil removed (Navarro & Zhao, 2014).

Table 2.2 Advantages and disadvantages of ISR compared to heap/tank leaching.

It is evident that ISR is advantageous over heap/tank leaching from an environmental standpoint. However, current ISR operations are still associated with some environmental and economic issues (see Table 2.2). Therefore the implementation of ISR to tackle environmental problems (i.e. ground clearance and ammonium sulphate contamination of water bodies) associated with REE mining and extraction remains highly contentious (Li *et al.,* 2010).

2.2.4 Standard Application of In situ Recovery

For the reasons stated in § 2.2.3, this study will focus on ISR. Implementation of ISR involves setting up a wellfield of vertical injection and extraction wells that span the breadth of the ore body. A reagent is injected into the ore body under saturated conditions, it flows through the pores of the deposit, mobilising the exchangeable REE into solution. The REE-enriched solution is then pumped to the surface for additional processing via extraction wells (Fig. 2.3).

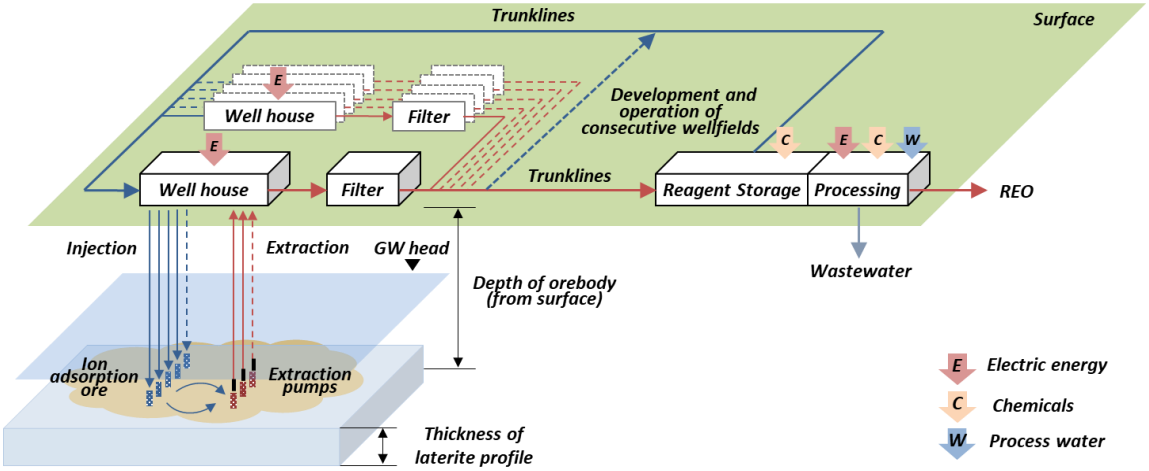

Fig. 2.3 Application of ISR to selectively mobilise REE from ion adsorption ore (from Nicolai *et al.,* 2017).

The main features of ISR are illustrated in Fig. 2.3:

- Injection and extraction wells are distributed throughout the mine site. Spacing between the wells and depth of the wells is primarily dependent on the deposit conditions. A sufficient groundwater head is required to maintain the productivity of the operating pumps.
- Well houses disseminate the injection solution to the injection wells at a specified injection pressure/flow rate.
- The trunk line network consists of two pipe systems: one to transport the reagent (and for fresh water flushing at the end of mining) and the other to transport the enriched solution pumped to the surface for further processing.
- The main operating costs are energy consumption for the pumps (E) and chemical requirements (C).

A number of different salts ($(NH_4)_2SO_4$, Na_2SO_4, NH_4Cl, NaCl) can be used to mobilise the REE (Moldoveanu & Papangelakis, 2012; Navarro & Zhao, 2014). The most commonly used is ammonium sulphate, although NaCl (seawater) is considered the most environmentally viable. Following leaching (after 150 – 400 days), fresh water is injected to flush out the remaining REE-bearing solution and to minimise groundwater contamination.

To recover the REE from solution, precipitation is carried out with oxalic acid ($H_2C_2O_4$) or ammonium bicarbonate (NH_4HCO_3) (Jun *et al.,* 2011; Yu *et al.,* 1990). The precipitate is then pressed to remove water and then calcined at 750–850 °C to produce REO. If required the REO can be separated into individual REE by dissolution in hydrochloric acid (HCl) and fractional solvent extraction (Walters *et al.,* 2011).

2.2.4.1 Feasibility Criteria for ISR application

An IAD must meet certain criteria before ISR can be considered at a mine site (Fig. 2.4). This includes (Mudd, 2001; Nicolai *et al.,* 2017; Sarangi & Beri, 2000):

- Ore body hosted in a porous, permeable rock formation;
- Confinement of ore body, below by continuous impermeable strata;
- Deposit located below the water table and therefore saturated with naturally occurring groundwater (ensures hydraulic head for extraction wells);
- Ore body in a geological formation with little to no irregularities (i.e. tectonic faults), to minimise the potential for migration of the reactive solution;
- Minimal heterogeneities with regard to the hydrological and mineralogical/geochemical conditions;
- Deposit has suitable mineral matrix i.e. sufficient REE content with little to no interfering minerals.

Therefore, as part of the feasibility study, geophysical surveying and drilling/borehole logging should be undertaken to determine the ore morphology and the hydrogeology of the deposit, in addition to core drilling and assay to determine the chemical and mineralogical aspects of the deposit (Vahidi *et al*., 2016).

Wellfield design and the performance concept are the two most important aspects of an efficient ISR operation (see Fig. 2.4; Nicolai *et al*., 2017):

- Part I: Hydrology
  - $\Rightarrow$ Establishing optimum contact (interface) between the reagent and the ore body.
  - $\Rightarrow$ The wellfield design determines the achievable flow rate Q, usually quantified with reference to the effective pore volume V_P.
  - $\Rightarrow$ The pore volume exchange (PVE) rate is defined by $q = Q/V_P$.
  - $\Rightarrow$ Reagent flow includes transport of the solution into the orebody and transport of REE-enriched solution out of the ore body.
- Part II: Desorption Chemistry and Kinetics
  - $\Rightarrow$ Setup of the most effective desorption chemistry relies on definition of the chemical conditions, pH, redox, and reagent composition, particularly to optimise leaching kinetics for maximum productivity.

Both the PVE rate (q) and the kinetic rate of desorption (r) determine the achievable production rate (product of flow rate and REE concentration in the enriched solution) as a function of wellfield operation time (Fig. 2.4).

The determination and optimisation of the wellfield design and desorption chemistry parameters are subject to reactive transport simulations. These simulations should be based on laboratory and field tests at local and regional scale. Advanced feasibility studies can be used to link the assessment of feasibility criteria to economic models (e.g. OPEX and CAPEX).

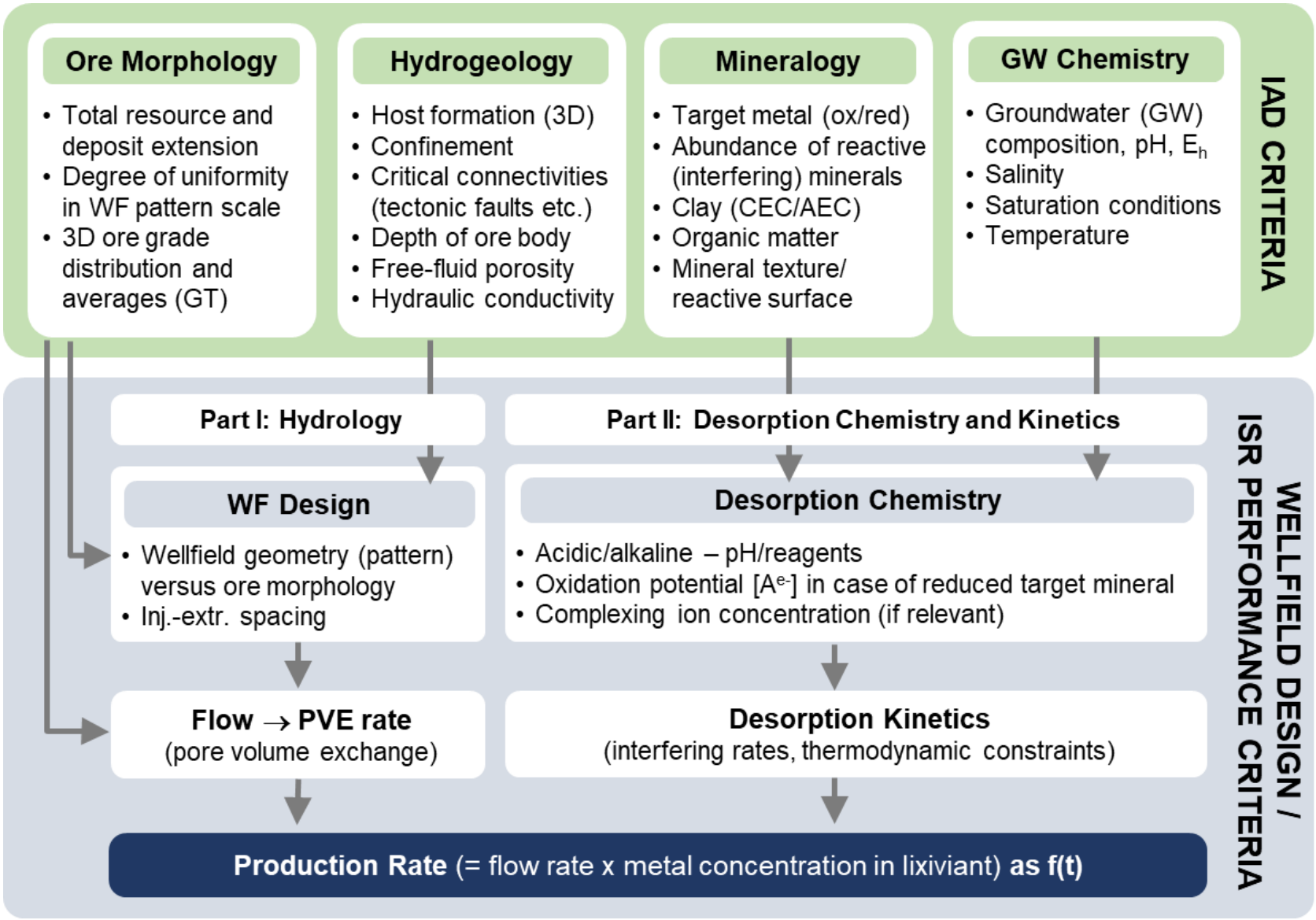

Fig. 2.4 Feasibility criteria for the application of ISR and the corresponding conditions for wellfield design and performance (from Nicolai *et al*., 2017).

2.2.5 Potential for In Situ Recovery in Madagascar

One objective of this study was to apply reactive transport modelling at site scale to assess the applicability of an environmentally focused mining approach (e.g. ISR) to develop the Madagascar IAD. This was related to the commercial driver of this research, to develop a conceptual model of the geochemical reactive transport processes in ISR of IAD and to consider environmental improvements to implement at sites (e.g. Madagascar).

A simplified ISR approach to the standard application (Fig. 2.3) is shown in Fig. 2.5, where the wellfield is installed close to a hillslope. The reagent is injected into the ore body, the REE-enriched solution is then transported along a collection tunnel in the lower levels of the profile. The solubilised REE accumulate in collection pools built close to the hillside and organised in terraces which is then channelled into tanks for further processing.

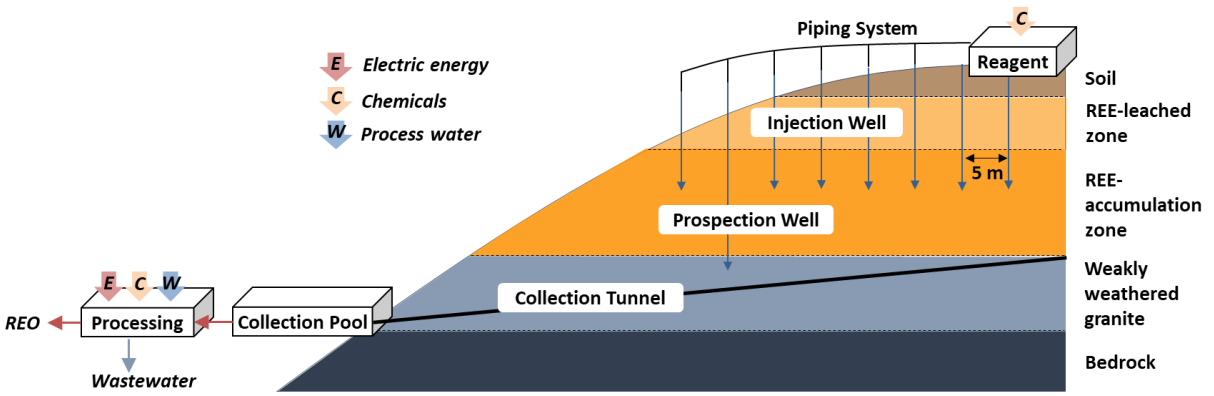

Fig. 2.5 In situ recovery on a hillslope (adapted from Vahidi *et al*., 2016).

Bearing in mind the environmental and economic challenges outlined in § 2.2.2, it is clear that the responsible development of any IAD project would need to meet much stricter environmental regulations for mining and restoration. This should involve comprehensive risk assessments, geophysical surveys and reactive transport modelling being undertaken prior to the mining and processing stage (Goodenough *et al*., 2018).

2.3 Modelling Fluid-Rock Interactions

Simplified and practical models are often implemented to deal with the complexity of fluid-rock systems. Early studies adopted a primarily thermodynamic approach focusing on geochemical reactions without consideration of transport processes (e.g. Thompson, 1959), with the implicit or explicit assumption of equilibrium between the fluid and the rock. As a result, these early models were fundamentally static rather than dynamic in nature.

Helgeson (1968) introduced the concept of an irreversible reaction path which, in addition to treating the reaction network as a dynamically evolving system, allowed for the consideration of a multicomponent geochemical system where multiple minerals and species appear as both reactants and products. A kinetic basis was given to the approach in subsequent studies (including the introduction of real time) (Aagaard & Helgeson, 1982).

Thermodynamic models for fluid-rock interactions have been more extensively developed than kinetic models because they require fewer parameters (Stumm & Morgan, 2012). Nevertheless, thermodynamic models are powerful tools in which Gibbs free energies (chemical potentials) are used to describe the thermodynamically stable state and characterise the direction and extent of processes approaching equilibrium.

In the last three decades, kinetic and empirical equilibrium models have been applied with varying degrees of success to describe REE transport in soil environments. These models include retention and release reactions (i.e. ion exchange, adsorption/desorption) for REE species (Selim, 2012). The next section provides an overview of the modelling concepts used in this research to simulate the flow, transport and reaction processes in the Madagascar IAD.

2.3.1 The Thermodynamic Approach

Ion exchange is thought to be the most important mechanism of REE mobilisation from the Madagascar IAD. In this study, the approach used to model ion exchange is based on equilibrium thermodynamics (Appelo, 1994; Helfferich, 1995).

The law of mass action and electroneutrality allow the calculation of activities of exchangeable cations from a given solution when the equilibrium constant (K) is known (e.g. Fletcher & Sposito, 1989). For a reaction of the generalised type:

(2.2) $$aA + bB \leftrightarrow cC + dD$$

the distribution at equilibrium of the species on the both sides of the reaction is given by:

(2.3) $$K = \frac{[C]^c[D]^d}{[A]^a[B]^b}$$

where the bracketed quantities denote activities (also known as effective concentrations, the units are noted below).

The law of mass action is only valid for the activity of ions, which is the measured total concentration corrected for the effects of electrostatic shielding and for the presence of aqueous complexes (Appelo & Postma, 2005).

The activity in the law of mass action is a measure of the effective concentration of the species, which can indicate how, for example, an Al^{3+} ion would behave when there are no interactions with other ions in solution, i.e. at infinite dilution.

In thermodynamics, the activity of gases, adsorbed ions and solutes are expressed as a fraction relative to a standard state, and as a fraction, the activity is always dimensionless. The standard state for a solid is a pure solid, similarly for gases it is a pure gas phase at 1 atm.

The standard state for an ion exchanger is an exchanger filled by a single ion and for aqueous solutes the standard state is defined as an ideal solution with a solute concentration of 1 mol/kg H_2O = 1 molal, where 'ideal' means a 1 M solute behaving as at infinite dilution.

The activity is related to the molal concentration by an activity coefficient which corrects for non-ideal behaviour. For aqueous solutes, the relation is:

$$[i] = \gamma_i \cdot m_i / m_i^0 \equiv \gamma_i \cdot m_i \tag{2.4}$$

where [i] is the activity of ion i (dimensionless), γ_i is the activity coefficient (dimensionless), m_i is the molality [mol/kg H_2O], m_i^0 is the standard state i.e. 1 mol/kg H_2O.

Activity coefficients may vary, but if ion i is present at trace concentration, and no other ions are present, then $\gamma_i \rightarrow 1$. Activity coefficients for solutes are calculated using the Debye-Hückel theory, which defines the ionic strength[7] I as:

$$I = {}^1/_2 \sum (m_i/m_i^0 \cdot z_i^2) \equiv {}^1/_2 \sum m_i \cdot z_i^2 \tag{2.5}$$

where z_i is the charge number of ion i, and m_i is the molality of i. Similar to the definition of activity, the ionic strength becomes dimensionless by division with the standard state m_i^0.

[7] The ionic strength describes the number of electrical charges in the solution.

For dilute electrolyte solutes, I < 0.1, the Debye-Hückel equation describes the electrostatic interaction as:

$$\log \gamma_i = \frac{Az_i^2 \sqrt{I}}{1 + B\mathring{a}_i \sqrt{I}} \quad (2.6)$$

where A and B are temperature dependent constants: at 25 °C A = 0.5085 and B = 0.3285 x 10^{10}/m and $\mathring{a}_i$ is the empirical ion-size parameter.

Various equations have been proposed to derive activity coefficients at ionic strength values greater than 0.1 (Davies, 1962; Langmuir, 1997; Nordstrom & Munoz, 1994; Parkhurst, 1990; Truesdell & Jones, 1974). The Davies equation can apply up to an ionic strength of 0.5:

$$\gamma_i = Az_i^2 \left(\frac{\sqrt{I}}{1 + \sqrt{I}} - 0.3I \right) \quad (2.7)$$

where A is the same temperature dependent coefficient as in Eq. (2.6).

The Truesdell-Jones equation is a reasonable approximation up to ionic strength values of about 2 in dominantly chloride solutions

$$\log \gamma_i = \frac{Az_i^2 \sqrt{I}}{1 + Ba_i \sqrt{I}} + b_i I \quad (2.8)$$

where A and B are the temperature dependent coefficient from Eq. (2.6) and a_i and b_i are ion-specific fit parameters.

In order to calculate mass action constants for the reaction in Eq. (2.2):

$$\Delta G_r = \Delta G_r^0 + RT \ln \frac{[C]^c[D]^d}{[A]^a[B]^b} \quad (2.9)$$

where ΔG_r is the change in Gibbs free energy [kJ/mol] of the reaction, ΔG_r^0 is the standard Gibbs free energy of the reaction and equal to ΔG_r when each product or reactant is present at unit activity (so that the log term becomes zero) at a specified standard state (25 °C 1 atm), R is the gas constant [8.314 x 10^{-3} kJ/mol/deg] and T is the absolute temperature [Kelvin].

The direction in which the reaction will proceed is indicated by ΔG_r. In the case of equilibrium Eq. (2.9) reduces to:

$$\Delta G_r^0 = -RT \ln \frac{[C]^c[D]^d}{[A]^a[B]^b} \quad (2.10)$$

The activity product in the last term is equal to the mass action constant K (Eq. (2.3):

$$\Delta G_r^0 = -RT \ln K \quad (2.11)$$

Back substitution of Eq. (2.10) in ((2.9) results in

$$\Delta G_r = -RT \ln K + RT \ln \frac{[C]^c[D]^d}{[A]^a[B]^b} \quad (2.12)$$

In Eq. (2.12) the distance from equilibrium is expressed in terms of the mass action constant.

2.3.2 Transport Processes

Later models clarified the application of reaction path models to water-rock interactions involving transport by demonstrating that they could be used to describe pure advective transport through a porous medium (Lichtner, 1988).

Transport is essential in the fluid interaction process because:

- It provides the driving force for many of the reactions that take place by continuously introducing fluid out of equilibrium with respect to the reactive solid phase and,
- It provides a characteristic time scale that can be compared with the rates of reaction.

Advection involves the translation in space of dissolved or suspended material at the rate of movement of the bulk fluid phase. The advective flux, J_{adv}, of a dissolved species in porous media can be described mathematically as:

$$J_{adv} = \emptyset v C_i \quad (2.13)$$

where $\emptyset$ is the porosity, v is the average linear velocity [m/s] in the media and C_i is the concentration of the ith species.

The fluid velocity in porous and fractured media is usually described with Darcy's Law (Darcy, 1856), which states that the volumetric flux of water [$m^3_{fluid}/m^2_{medium}/s$], q, is a vector proportional to the gradient in the hydraulic head:

$$q = \emptyset v = -K\nabla h \tag{2.14}$$

where h is the hydraulic head [L] and K is the hydraulic conductivity [m/s].

The hydraulic conductivity is defined as:

$$K = \frac{k\rho g}{\mu} \tag{2.15}$$

where k is the permeability [m^2], g is the acceleration due to gravity [9.81 m/s^2] and μ is the dynamic viscosity [Pa·s]. Darcy's Law can also be written in terms of the fluid pressure by defining the hydraulic head as:

$$h = z + \frac{P}{\rho g} \tag{2.16}$$

where z is the depth [L] P is the fluid pressure [Pa] and p is the fluid density [kg/m^3]. The gradient in hydraulic head can be defined as:

$$\nabla h = \frac{dh}{dl} = \frac{h_1 - h_2}{length} \tag{2.17}$$

where ∇h is the gradient in hydraulic head [dimensionless], dh is the difference between two hydraulic heads [L] and dl is the flow path between the two piezometers [L].

In addition to flow, molecular diffusion should be taken into account, if transport through low porosity and permeability material is to be considered (Steefel & Maher, 2009). Molecular diffusion is often described in terms of Fick's First Law, which states that the diffusive flux (shown only for a single coordinate direction x) is proportional to the concentration gradient:

$$J_i = -D_i \frac{\delta C_i}{\delta x} \tag{2.18}$$

D_i is referred to as the diffusion coefficient and is specific to the chemical component considered as indicated by the subscript i.

Fluid-rock interactions typically take place in porous media, thus it is important to account for the effect of tortuosity. Tortuosity T_L is defined as:

(2.19) $$T_L = \left(\frac{L}{L_e}\right)^2$$

where L is path length the solute would follow in water alone and L_e is the tortuous path length the solute would follow in porous media.

In this definition of tortuosity, its value is always < 1 (Bear, 1972). The effective diffusion coefficient in porous media is obtained by multiplying the tortuosity by the diffusion coefficient for the solute in pure water. Using this formulation, the diffusion coefficient is given by:

(2.20) $$D_i^* = T_L D_i$$

The diffusive flux is then given by

(2.21) $$J_j^{diff} = -\emptyset D_j T_L \frac{\delta C_j}{\delta x} = -\emptyset D_j^* \frac{\delta C_j}{\delta x}$$

where C_j is the concentration of the jth species.

The spreading of the solute mass as a result of dispersion is a diffusion-like process that has led to the use of Fick's First Law to describe the process in one dimension as:

(2.22) $$J_j^{disp} = -D_h \frac{\delta C_j}{\delta x}$$

where D_h is the hydrodynamic dispersion coefficient. The coefficient of hydrodynamic dispersion is defined as the sum of a molecular diffusion and mechanical dispersion (Eq. (2.23), since these effects are not separable where flow is involved (Bear, 1972).

(2.23) $$D_h = D^* + D$$

2.3.3 Reactive Transport Modelling

This section outlines the basics of reactive transport models, which combine the transport processes (described in § 2.3.2) with the expressions for kinetically controlled geochemical reactions (Mayer *et al.,* 2002; Prommer *et al*., 2003; Walter *et al.,* 1994).

For a system with transport of a non-reactive tracer, an expression for the conservation of solute mass can be derived by accounting for the flux of solute across the faces a volume element. For a 1-D system (fluxes in the Y and Z directions = 0), the net flux is obtained from:

(2.24) $$\frac{\delta J_i}{\delta x} = \lim_{\Delta x \to 0} \frac{J_i\, I_{x+\Delta x} - J_i\, I_x}{\Delta x}$$

In a multidimensional system involving porous media, the accumulation of solute mass is given by the difference of the fluxes summed over all of the faces of the element:

(2.25) $$\frac{\delta(\emptyset C_i)}{\delta t} = -\nabla \cdot J_i = -\left(\frac{\delta J_i}{\delta x} + \frac{\delta J_i}{\delta y} + \frac{\delta J_i}{\delta z} \right)$$

where J_i is the flux vector. Substitution of Eq.(2.13) and (2.18) into Eq. (2.25) yields:

(2.26) $$\frac{\delta(\emptyset C_i)}{\delta t} = -\nabla(\emptyset v C_i) + (\emptyset D_i^* \nabla C_i)$$

To include reactions, the 1-D version of the advection-dispersion equation is shown in Eq. (2.26). For a constant porosity, tortuosity and flow system characterised by first-order precipitation and dissolution reaction that can be described in terms of a single chemical component, the advection-dispersion equation becomes:

(2.27) $$\emptyset \frac{\delta C}{\delta t} = -\emptyset v \frac{\delta C}{\delta x} + D^* \frac{\delta^2 C}{\delta x^2} + Ak\left(1 - \frac{C}{C_{eq}}\right)$$

where k is the rate constant [moles $m^{-2}s^{-1}$], A is the reactive surface area of the mineral [m^2m^{-3}] and C_{eq} is the solubility of the mineral [moles m^{-3}].

Reactive transport models have evolved considerably as diagnostic and prognostic tools, and make a significant contribution to elucidating the inherently complex dynamics of engineered and natural environments (Appelo, 1994; Steefel *et al.,* 2005; Han *et al.,* 2010).

2.3.3.1 Soil-Column Studies

Soil column experiments have been widely used to determine the fate and migration of metals through soils (Camobreco *et al.,* 1996; Dontsova *et al*., 2006; Masipan *et al.,* 2016). Thus, reactive transport models are often based on laboratory or field-site investigations.

Soil columns are also a good way to characterise ion exchange reactions, in which a solution is passed through a fixed bed of ion exchange material, and its composition is changed either by ion exchange or sorption.

The time at which the cations first appear in the effluent is termed the breakthrough point. The breakthrough curve and the breakthrough point depend on the composition of the injected solution, the operating conditions and the ion exchanger properties (Helfferich, 1995).

One factor that has been shown to greatly increase the mobility and velocity of solute movement to the groundwater is preferential flow (Steenhuis *et al.,* 1995). The term preferential flow implies that, infiltrating water does not have sufficient time to equilibrate with slowly moving groundwater in the bulk of the soil matrix (Jarvis, 1998).

Different forms exist. In fine soils, high conductivity paths form the network for preferential flow. In unstructured sandy soils, preferential flow is caused by sloping textural interfaces (Kung, 1990) or by instability at the wetting front (Glass *et al*., 1989). Thus physical nonequilibrium conditions can occur in many soil types (Flurry *et al.,* 1994).

Water added to the soil can rapidly flow through this preferential network, bypassing most of the soil matrix. In soil column experiments, where a homogenous mixture has been ensured by experimental design, preferential flow has still been observed to increase metal movement (Masipan *et al.,* 2016; Seyfried & Rao*,* 1987).

There are a number of simulation models that have been developed to account for preferential water flow and solute transport, such as the dual/single porosity models (Gerke & van Genuchten, 1993; Saxena *et al.,* 1994; Šimůnek *et al.,* 2003). The single porosity model considers one only pore domain, the mobile water region.

The dual porosity approach assumes that the porous medium consists of two regions, one associated with the macropore or fracture network (known as the mobile water region) and the other with a less permeable pore system of soil aggregates or rock matrix blocks (known as the stagnant water region) (Gerke & van Genuchten, 1993).

Each pore domain is characterised by a porosity, a water content and a solute concentration. Vertical water and solute transport are calculated in each domain, with mass exchange between domains treated as source/sink terms in the model. The mass exchange is calculated using approximate first-order equations (Gerke & van Genuchten, 1993).

2.4 REE Sorption Processes

The aim of this research was to model REE mobilisation from the Madagascar IAD during mining processes. Because the mobility of the REE once released from geological deposits is largely controlled by sorption processes, it was important to gain a comprehensive understanding of REE behaviour in the soil matrix.

This section provides an overview of REE sorption processes and the oxide and clay minerals involved in REE sorption in IAD systems. Sorption describes the uptake of an ion or

compound onto a contiguous mineral surface. The term includes any retention mechanism that controls availability and mobility.

Sorption can be divided into adsorption, absorption and ion exchange. Adsorption describes the binding of solutes or ions to solid surfaces to form complexes, absorption describes the incorporation of a solute into the solid and ion exchange describes the stoichiometric replacement of ions on a surface (Fig. 2.6; Postma & Appelo, 2005).

Ion exchange and adsorption reactions are related in that one ionic solute species may replace another ionic solute species already on the surface site and may form a surface complex. In practice, it is difficult to distinguish between these processes as they often occur simultaneously. Thus, the general term sorption is applied when the mechanism is unknown.

Ion exchange at clay mineral surfaces accounts for a part of trace metal sorption in soil systems. However, adsorption of trace metals at the variable charge surfaces of phyllosilicates, metal (hydr)oxides, and humic substances, is thought to account for the majority of sorption in natural environments (Appelo & Postma, 2005).

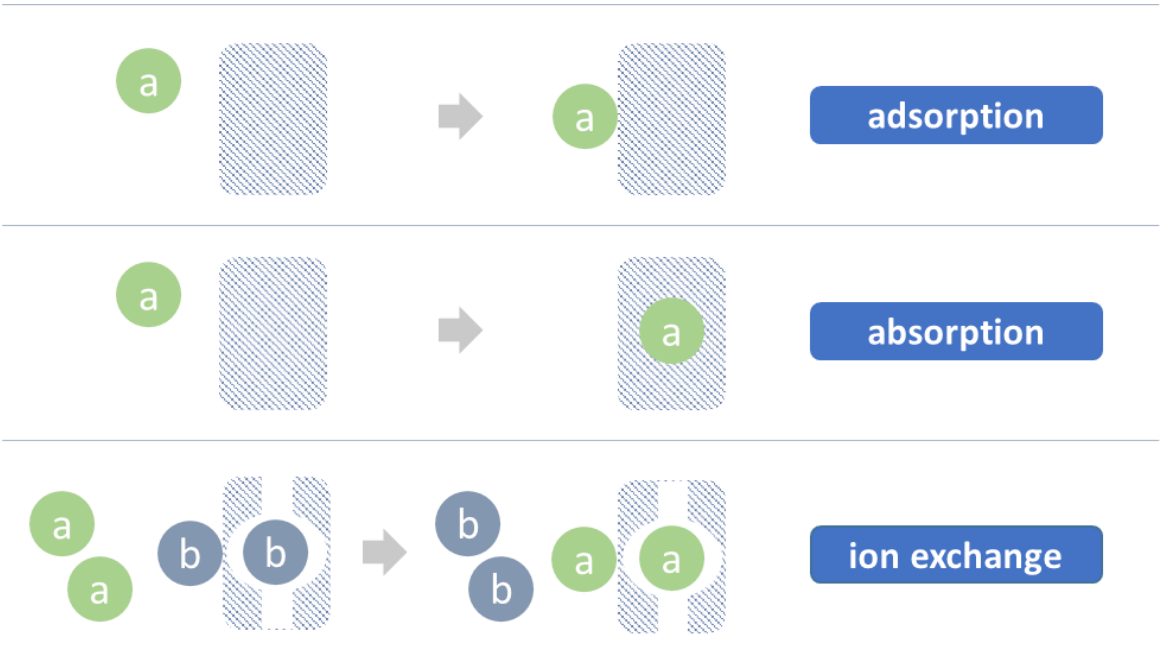

Fig. 2.6 Sorption processes at the mineral-water interface (adapted from Appelo & Postma, 2005).

Mineral surface interactions lead to different adsorptive behaviours involving electrostatic attraction of charged aqueous species or chemical binding. In the presence of water, the surfaces of silicates and oxides are covered by different surface hydroxyl groups, which are coordinated to one or more metal atoms (terminal hydroxyls) in the crystal lattice.

Ions in solution may become attached as aqueous complexes. Inner-sphere complexation involves terminal hydroxyl groups, which behave as Lewis bases[8] and interact with Lewis acids such as metal ions. The direct coordination of the metal ion to the surface hydroxyl groups leads to the release of water molecules from the ion's hydration sphere.

Outer-sphere complex formation occurs when charged aqueous species attach to surface hydroxyl groups of opposite charge (Del Nero *et al*., 2004). The inner-/outer-sphere state is gradual and fluctuates in time (Stumm & Morgan, 2012). Fig. 2.7 shows inner- and outer-sphere complex formation at the mineral surface.

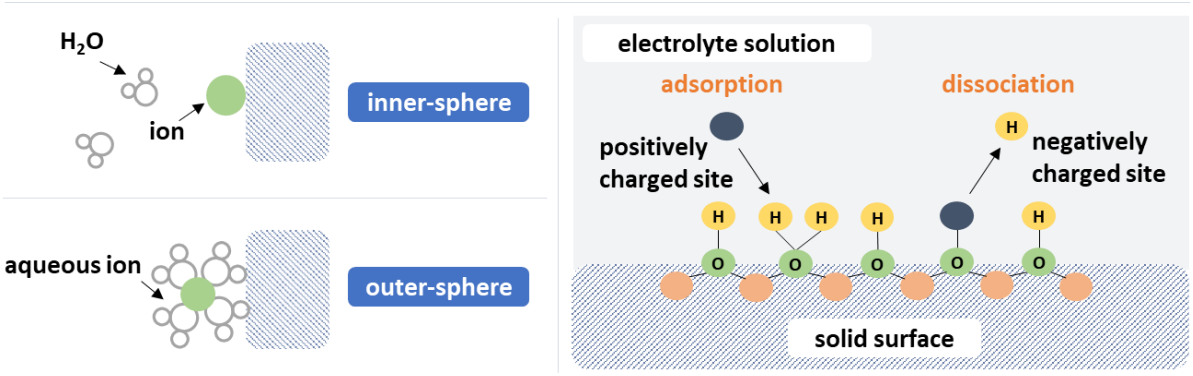

Fig. 2.7 Inner- and outer-sphere complex formation at the solid surface.

2.4.1 Sorption at Mineral Surfaces

2.4.1.1 Clay Minerals

Clay minerals are formed at the earth's surface by diagenetic and hydrothermal alteration of silicate minerals. They are characterised by their ability to absorb certain ions and retain them in an exchangeable state. The most common exchangeable cations in order of relative abundance, are Ca^{2+}, Mg^{2+}, H^{+}, K^{+}, NH_4^{+}, Na^{+} (Grim, 1968).

Structurally, the clay minerals are composed of planes of cations, arranged in sheets, which may be tetrahedrally or octahedrally coordinated with oxygen and hydroxyl. These sheets are in turn arranged into layers (Hillier, 2003). Clays can be classified according to the type of layer structure. These are shown in Fig. 2.8.

[8] In the Lewis theory of acid-base reactions, bases donate pairs of electrons and acids accept pairs of electrons.

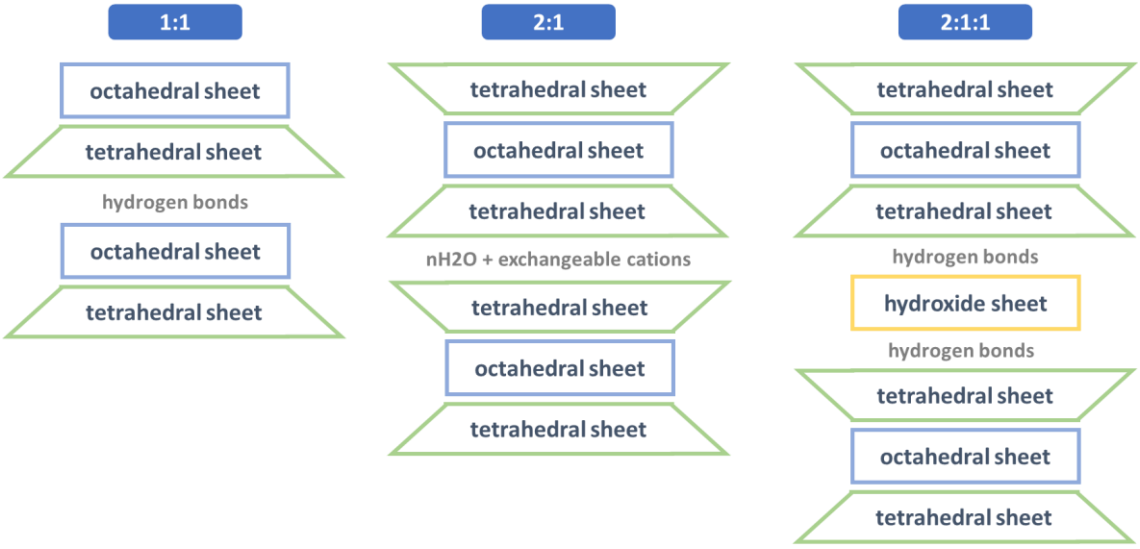

Fig. 2.8 Classification of the 1:1, 2:1 and 2:1:1 clay mineral structure.

Clay minerals can acquire a surface charge when they are in contact with an aqueous phase. This produces an electrical imbalance at the solid-solution interface influencing the distribution of neighbouring ions. Clay minerals can develop a surface charge in two ways:

[1] From chemical reactions at the solid surface, where ionisable functional groups (i.e. –OH) are present and charge depends on solution pH, and

[2] Isomorphic substitution (of Al^{3+} for Mg^{2+} or Si^{4+} for Al^{3+}) within the lattice and lattice imperfections at the solid surface resulting in a permanent negative surface charge.

As a result, clays exhibit two different site types on their surfaces: interlayer sites and edge sites (Stumm & Morgan, 1996). The literature suggests that exchange reactions dominate at interlayer sites while surface complexation (SC) mechanisms dominate at edge sites (e.g. Coppin *et al.,* 2002). This will be discussed further in § 2.4.

Fig. 2.9 shows the development of a surface charge on kaolinite when in contact with the aqueous phase. A permanent negative charge develops on the T faces due to isomorphic substitution of Si^{4+} for Al^{3+} or Al^{3+} for Mg^{2+} and a pH-dependent charge develops on the edges and O face OH groups due to surface protolytic reactions.

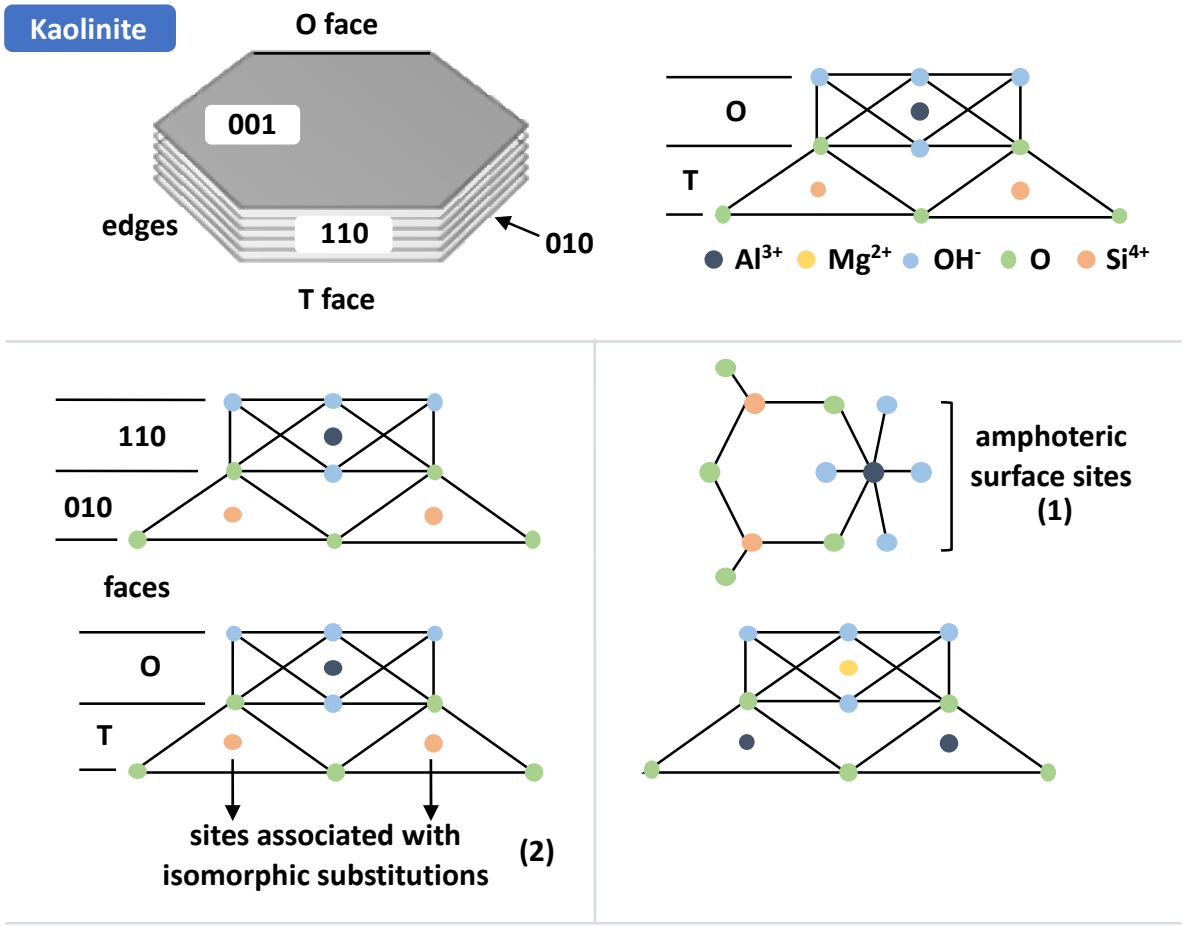

Fig. 2.9 Development of surface charge on kaolinite when in contact with an aqueous phase (atom arrangement in silica tetrahedral (T) and alumina octahedral (O) layers).

The total charge and the sites responsible for charge development depend on the structure of the clay mineral. Table 2.3 shows the charge characteristics of common clay and oxide minerals, including the cation exchange capacity (CEC). The CEC defines the extent to which a mineral can hold exchangeable cations on their negative charge sites.

Cation exchange sites are found primarily on clay minerals and organic matter surfaces. The CEC has two origins described in [1] and [2] at sites where a negative surface charge develops. The interlayer part of the CEC is considered to be constant since it is insensitive to the pH of the system. The CEC at the edge sites is pH dependent because the acidity of the aluminol groups is weak and the edge charges depend on pH (Lagaly, 1981). 2:1 clays have a higher net negative charge than 1:1 clays, as a result they have a greater CEC.

Some clay and oxide minerals can have an anion exchange capacity (AEC) in addition to a CEC (Ma & Eggleton, 1999). The AEC is the degree to which a soil can adsorb and exchange anions. The CEC is relatively low in 1:1 clays, and the influence of the AEC is consequentially more significant (see Fig. 2.10).

Anion exchange arises from the protonation of hydroxyl groups on the edge sites of minerals. The AEC is pH dependent and increases with decreasing pH. This is because at low pH an additional hydrogen ion is associated with the hydroxyl group, leaving a net positive charge (Pansu & Gautheyrou, 2007).

Fig. 2.10 relates the charge characteristics of aluminosilicate soils to weathering intensity. Less weathered soils will have a CEC under acidic, neutral and basic conditions, but no AEC. Whereas highly weathered will develop a CEC under neutral and basic conditions or an AEC under acidic conditions (Brady & Weil, 2002).

Table 2.3 Charge characteristics of colloids (from Brady & Weil, 2002).

Colloid	Charge at pH 7[1] [meq/100g]	Constant[1] [%]	Variable[1] [%]	Variable[2] [meq/100g]	CEC [meq/100g]
Kaolinite	8	65	35	2	3 - 15
Smectite	100	95	5	0	80 - 150
Vermiculite	150	95	5	0	100 - 150
Chlorite	30	80	20	0	10 - 40
Gibbsite	4	0	100	5	4
Goethite	4	0	100	5	up to 100
Quartz	0	0	0	0	0

[1] = negative, [2] = positive

Fig. 2.10 Clay charge characteristics related to their weathering intensity (adapted from Brady & Weil, 2002).

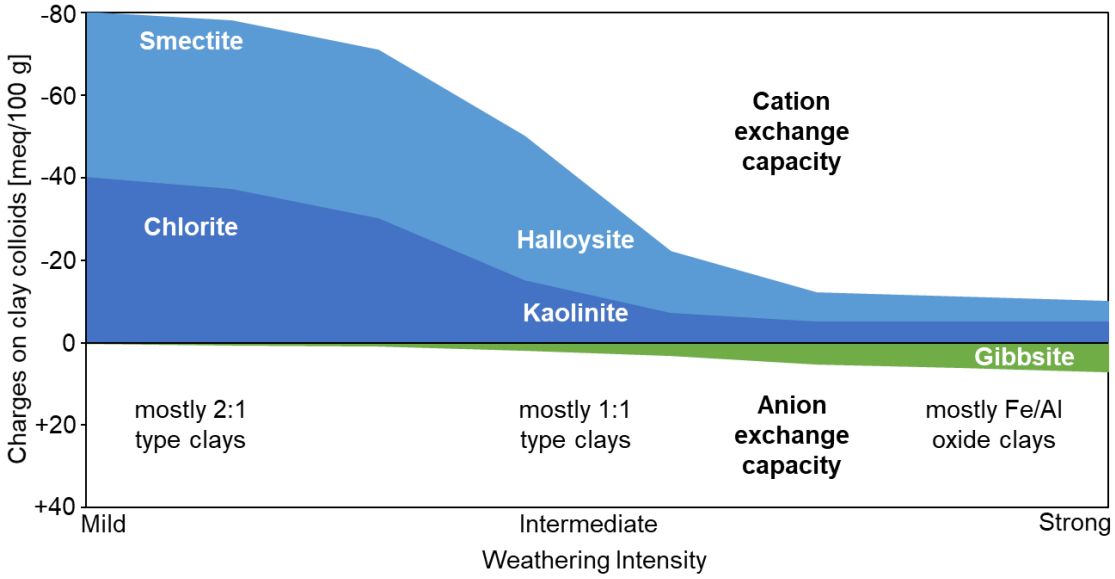

Kaolinite ($Al_2Si_2O_5(OH)_4$) has a 1:1 layered structure (Fig. 2.11). Repeating layers of the mineral are joined together by hydrogen bonds and weak Van der Waals forces[9] (Bear, 1965). The hydrogen bonds are the main source of the cohesive energy between layers. They are also the reason for the absence of layer charge and the low CEC (Ma & Eggleton, 1999; Miranda-Trevino & Coles, 2003; Uddin, 2017).

It is widely accepted that the variable charges on the edges of kaolinite particles is due to protonation or deprotonation of exposed hydroxyl groups and therefore dependent on solution pH. On the other hand the basal siloxane surfaces carry a constant (negative) structural charge due to isomorphic substitution of Si^{4+} for Al^{3+} (McBride, 1976; Rand & Melton, 1977; van Olphen, 1977; Williams & Williams, 1978).

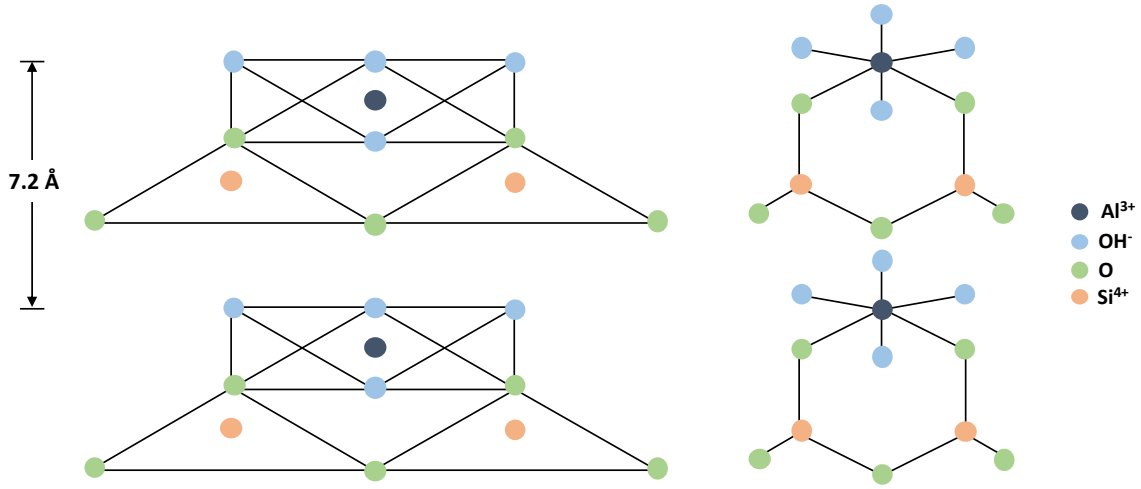

Fig. 2.11 *Left*: structure of kaolinite. *Right*: surface hydroxyl groups covering the octahedral sheet

2.4.1.2 Metal Oxide Minerals

The oxide minerals typically present in soils comprise oxides, hydroxides, oxyhydroxides, and hydrated oxides of Si, Fe, Mn, Al, and Ti. Oxides of Fe, Mn, and Al may exhibit a high surface area, with reactive surface sites which strongly bind oxyanions and metal cations, thereby impacting the mobility of trace metals (Hillel & Hatfield, 2005).

Many hydrous metal oxides contain ionisable functional groups at their surfaces (Smith, 1999). A surface charge can develop as a result of dissociation of these functional groups. Inner- and outer-sphere complexation reactions can occur between ionised functional groups and the ions in solution (see Fig. 2.7).

[9] Van der Waals forces are relatively weak electric forces that attract neutral molecules to one another.

Proton exchange reactions for surface functional groups of oxides are expressed as:

(2.28) $>XOH_2^+ = >XOH + H^+$

(2.29) $>XOH = >XO^- + H^+$

where >XOH is a surface-binding site, and $>XOH_2^+$ and $>XO^-$ are proton-exchange surface complexes.

The charge at the oxide mineral surface depends on the pH of the surrounding solution. In general, neutral or alkaline pH conditions will result in a net negatively charged surface, while under acidic pH conditions an excess of protons are retained at the surface yielding a net positively charged surface:

(2.30) $>XOH_2^+ \leftrightarrow >XOH \leftrightarrow >XO^-$
(low pH) (high pH)

The net surface charge can be zero when the surface oxygens are protonated just enough to compensate broken bonds and a small internal charge (Appelo & Postma, 2005). This point is termed the point of zero charge (PZC):

(2.31) $[>XOH_2^+] = [>XO^-]$

The PZC for several minerals is shown in Table 2.4.

Table 2.4 PZC for a variety of minerals (from Smith, 1999).

Mineral	pH_{PZC}[10]
Hydrous ferric oxide (amorphous)	8.1
Goethite	6-7
Hematite	4.2-6.9
Gibbsite	10
SiO_2 (amorphous)	3.5
Kaolinite	4.6
Montmorillonite	2.5

Surface charge can affect the distribution of neighbouring solutes, since a decrease in the pH of the surrounding water will attract anionic species from solution. Conversely, increasing the pH will attract cationic species from solution (Smith, 1999).

Fig. 2.12 shows oxide surfaces changing their charge with pH due to ionisable water molecules bound on the surface metal sites. The upper diagram highlights dissociation of the

[10] These values were determined by different researchers using different methods and electrolyte solutions (Smith, 1999).

hydroxyl group in an aqueous solution and point of zero charge and the lower diagram shows the formation process of hydroxyl group on a metal oxide.

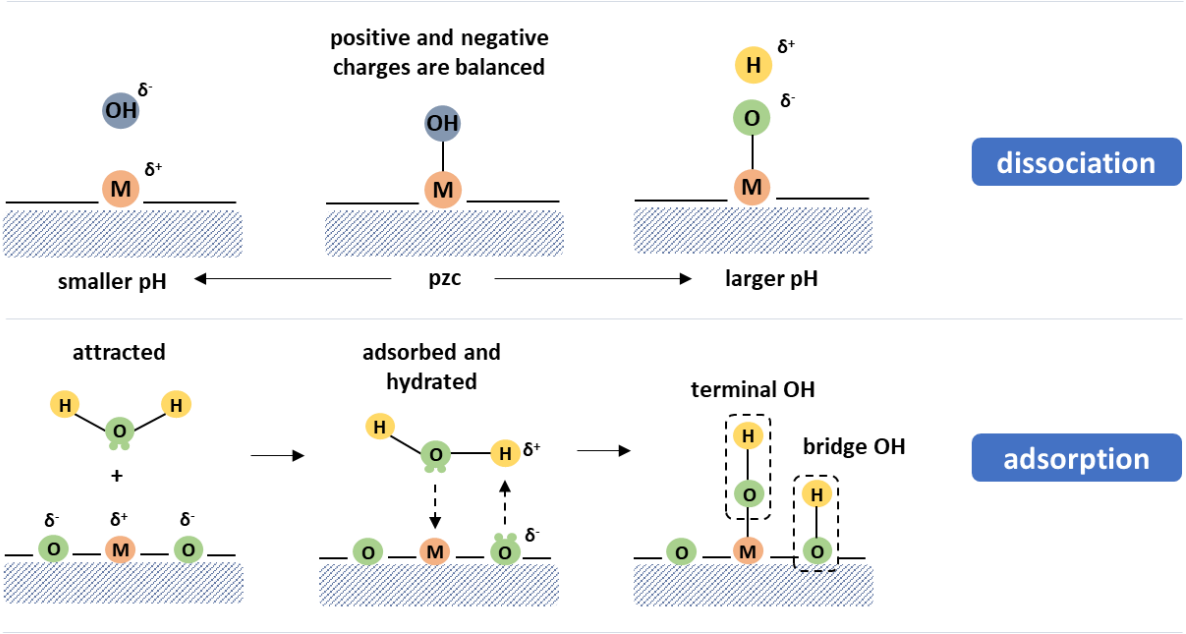

Fig. 2.12 pH-dependent variable charge sites at oxide solid surfaces.

Amorphous iron oxyhydroxide is commonly found in natural aqueous systems as a discrete mineral phase and as a surface coating on particulate matter (Davies *et al.,* 1978). It is thought to play a significant role in sequestering elements because of its large surface area and strong affinity for many elements (Jenne, 1968; Singh *et al.,* 1984).

Amorphous materials are capable of exchanging REE because they have permanent charge and/or pH-dependent surface charge, which can be expressed as the PZC. The surfaces of minerals and amorphous materials are more positively charged below their own PZC, and they are more negatively charged above the PZC (Sanematsu & Watanabe, 2016).

Gibbsite (α-$Al(OH)_3$) is formed by weathering of aluminous minerals, thus it is common in lateritic soils. Gibbsite also forms in low temperature hydrothermal and metamorphic environments, replacing aluminous minerals (Saalfeld & Wedde, 1974). Similar to most hydrous metal oxides, gibbsite can adsorb metal ions, anions and ligands onto its surface.

The basic structure forms stacked sheets of linked octahedrons of aluminium hydroxide held together by weak residual bonds (Fig. 2.13). The octahedrons comprise of aluminium ions bonded to six octahedrally coordinated hydroxides. Each OH^- is bonded to two Al^{3+} atoms leaving a third of the octahedrons vacant a central Al^{3+} atom (Parfitt *et al*., 1977). The result is a neutral sheet (no charge between sheets).

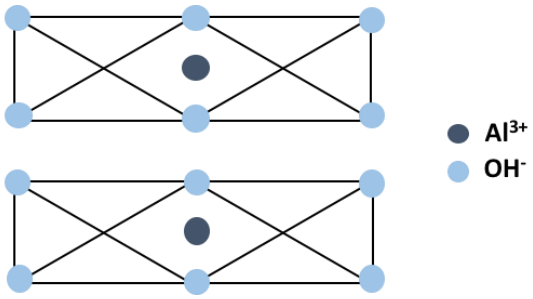

Fig. 2.13 Dioctahedral gibbsite $Al(OH)_3$.

Goethite (α-FeOOH) is one of the most widespread forms of iron oxyhydroxides in terrestrial soils, sediments and ore deposits. Goethite forms from the weathering of other iron-rich minerals, and thus is commonly found in laterite soils. The mineral has a high specific surface area in excess of 200 m^2/g and as a result is able to adsorb large amounts of metal cation and anions onto its surface (Tunega, 2012).

The crystal structure of goethite is orthorhombic and consists of edge sharing $FeO_3(OH)_3$ octahedra (Cornell & Schwertmann, 2003). The octahedral units are arranged in double rows separated by empty sites. Each Fe^{3+} cation is surrounded by three O^{2-} and three OH^- anions in a distorted octahedral configuration. This distortion is enhanced by the formation of intrastructural hydrogen bonds (Tunega, 2012).

2.5 Sorption Studies

Many literature studies have investigated REE sorption interactions. This is due to their importance as chemical analogues for the trivalent actinides within the framework of strategies for radioactive waste disposal and because of their role as geochemical tracers (e.g. the degree of REE fractionation in a mineral can indicate its genesis).

A summary of the REE sorption studies on common IAD minerals such as kaolinite, goethite, hematite and amorphous materials is presented in this section. No REE-gibbsite or REE-halloysite sorption studies were found in the literature.

Numerous mechanistic sorption studies on clay minerals (Aja, 1998; Coppin *et al.,* 2002; Stumpf *et al*., 2002; Tertre *et al.,* 2006a, 2006b, 2008; Xiangke *et al*., 2001) point to the existence of two kinds of fundamental processes taking place:

- Cation exchange with pre-existing cations linked to the surface by electrostatic bonds on interlayer sites, and
- Surface complexation with hydrolysed edge sites such as silanol (>SiOH), ferrinol (>FeOH) and aluminol (>AlOH).

These conclusions are based on macroscopic properties (distribution coefficients) and acidity–basicity, as well as spectroscopic studies. These observations correspond with the permanent and variable surface charges sites attributed to clay surfaces (see § 2.4.1.1).

Given the complexity of sorption processes, it is important to understand the mechanisms which can influence REE patterns. In solution, trace metals such as the REE can be influenced by complexation reactions, by anionic ligands, the dissolution and/or precipitation of minerals containing or incorporating REE into their structure, as well as by redox reactions and adsorption onto mineral or organic solid phases.

The presence of competing metals has been observed to significantly affect REE sorption (Kookana & Naidu, 1998; McBride, 1994). For example, in the presence of Ca^{2+}, Mg^{2+} and Al^{3+} the sorption of Eu^{3+}/Gd^{3+} onto kaolinite decreased significantly, whereas in their absence sorption is almost 100 % (Kautenburger & Beck, 2010). Verma & Mohapatra (2016) also observed this effect for Eu^{3+} sorption on kaolinite in the presence and absence of Na^{+}.

Competitive sorption can lead to fractionation of the REE during particle-solution interactions (Piper, 1974). This is governed by the chemical properties of the REE and the solid surface. A number of studies have observed the selective retention of the HREE to clay surfaces at high ionic strength and neutral pH (Aagard, 1974; Bonnot-Courtois & Jaffrezic-Renault, 1982; Byrne & Kim, 1990; Coppin *et al*., 2002; Tertre *et al*., 2005).

Early studies interpreted this trend as being due to decrease of the ionic radius with increasing atomic number (i.e. the lanthanide contraction) (Aagard, 1974; Bonnot-Courtois & Jaffrezic-Renault, 1982). Coppin *et al.* (2002) suggest that the concentration of cations in solution interferes with this phenomenon (i.e. the salt effect). Two possible explanations are offered that take into account the salt effect:

[1] The presence of concentrated Na^{+} at the particle surface inhibits sorption of competitors with a larger ionic radius, as observed with the LREE when compared to the HREE (lanthanide contraction).

[2] Sorption at the variable charge sites at the edges of the clay is occurring, indicating desolvation of cations to form inner-sphere complexes. Fractionation reflects the variation in desolvation energy with the atomic number of the REE.

The assumption that the REE are sorbed as inner sphere-complexes at the variably charged surfaces of metal oxides (e.g. hematite) is well documented (Bau, 1999; Kawabe *et al.,* 1999; Rabung e*t al.,* 1998). In contrast, the steric effects of Na^{+} was negligible in the experiments conducted at low ionic strength and all the REE were sorbed to the same extent.

A number of REE sorption studies onto metal oxides observed the opposite fractionation, where the LREE are preferentially retained over the HREE (Koeppenkastrop *et al*., 1991; Koeppenkastrop & De Carlo, 1992). This trend could be explained by a stronger complexation of HREE with carbonate ions than the LREE (Cantrell & Byrne, 1987).

2.5.1 Distribution Coefficients

Sorption can be expressed in terms of a distribution coefficient (K_d), which combines the effects of various processes determining the reversible partitioning between the solid surface and the aqueous phases, including surface complexation and ion exchange (Payne *et al*., 2013). The distribution coefficient is defined as:

$$K_d = \frac{\text{amount of adsorbed metal}}{\text{amount of metal in solution}} \tag{2.32}$$

where K_d typically has units such as mL/g or L/kg and the amount of metal in both the numerator and denominator can be expressed in convenient units (such as moles).

K_d values are determined in batch sorption experiments, where a solution containing a known quantity of a REE is in contact with the mineral phase of interest under controlled conditions. The concentration of the REE adsorbed on the mineral surface can be determined by measurement of the REE concentration remaining in the aqueous phase.

The experimental results can be converted to a K_d value:

$$K_d = \frac{C_i - C_{eq}}{C_{eq}} \cdot \frac{V}{m} \tag{2.33}$$

where C_i and C_{eq} denote the initial and equilibrium concentrations of the metal ion and V and m are the volume of the aqueous phase and the mass of the mineral, respectively.

High values of K_d indicate that the metal has been retained by the solid through sorption reactions, while low values of K_d indicate that most of the metal remains in solution where it is available for transport and geochemical reactions (Anderson & Christensen, 1988). Table 2.5 summarises K_d values reported for REE sorption onto common IAD minerals.

Table 2.5 Distribution coefficients reported for REE sorption onto common IAD minerals.

Mineral	REE	Temp [°C]	log K_d [mL/g]	pH	Background electrolyte	Reference
Kaolinite	Nd	25	3.75 - 6.22	1.20 - 2.74	none	Aja (1998)
	Nd	25	4.48 ± 0.03	8.14 ± 0.03	none	Aja (1998)
	Nd	25	3.69 - 6.37	4.02 – 6.02	0.7 M NaCl	Aja (1998)
	Eu	25	2.85 - 5.32	2.65 - 11.32	0.1 M $NaClO_4$	Bradbury & Baeyens (2009)
	Ho	25	1.83 - 4.23	3.03 - 7.12	0.5 M $NaClO_4$	Coppin *et al.* (2002)
	Ho	25	2.65 - 4.71	3.07 - 6.96	0.025 M $NaClO_4$	Coppin *et al.* (2002)
	Sm	25	1.43 - 4.31	4.27 - 6.88	0.5 M $NaClO_4$	Coppin *et al.* (2003)
	Sm	25	3.41 - 4.47	4.22 - 6.50	0.025 M $NaClO_4$	Coppin *et al.* (2003)
	Eu	25	1.60 - 4.91	2.50 - 9.50	0.5 M $NaClO_4$	Tertre *et al.* (2006a)
	Eu	40	1.10 - 8.00	2.50 - 9.50	0.5 M $NaClO_4$	Tertre *et al.* (2006a)
	Eu	80	1.88 - 5.12	2.50 - 9.50	0.5 M $NaClO_4$	Tertre *et al.* (2006a)
	Eu	150	1.62 - 4.97	2.50 - 9.50	0.5 M $NaClO_4$	Tertre *et al.* (2006a)
	Eu	25	1.16 - 6.54	2.77 - 10.41	0.1 M $NaClO_4$	Huittenen *et al*. (2010)
	Eu	25	1.78 - 4.31	5.0 ± 0.02	0.01 M $NaClO_4$	Kautenberger & Beck (2010)
	Gd	25	1.82 - 4.48	5.0 ± 0.02	0.01 M $NaClO_4$	Kautenberger & Beck (2010
	Eu	25	2.52	4.2 ± 0.1	1 M NaCl	Xiangke *et al.* (2001)
Goethite (cr)	REE	25	6.0	7.8	seawater	Koeppenkastrap & De Carlo (1992)
Goethite (am)	REE	25	6.0	7.8	seawater	Koeppenkastrap & De Carlo (1992)
Hematite	Eu	25	-2.45 - 0.65	3.66 - 5.81	0.1 M $NaClO_4$	Rabung *et al.* (1998)

K_d values are only applicable under specific conditions where sorption and desorption are the dominant partitioning mechanism (i.e. dilute solutions), in contrast to the controlling partitioning mechanism being the aqueous saturation of a species with respect to a specific mineral phase or congruent dissolution (Meeussen *et al.,* 2009).

K_d values are linear extrapolations of an empirical value applicable to specific experimental conditions. They are not mechanistic except in the Henry's Law regime[11] (i.e. dilute solutions) (Payne *et al.,* 2013). Thus, their application to aqueous concentrations and conditions beyond their initial definition should be performed with care.

2.5.2 Sorption Isotherms

An isotherm is a curve that describes the retention of a substance onto a solid at various concentrations. The remaining solute concentration of a compound C [mol L^{-1} or kg L^{-1}] can be compared with the concentration of this compound retained on solid particles Q [mol kg^{-1} or kg kg^{-1}]. The relationship Q = f(C) is termed the sorption isotherm.

There are four main types of isotherms (Giles *et al.,* 1974):

[1] The C isotherm
- ⇒ The curve is a line of zero-origin, this means that the ratio between the concentration of the compound remaining in solution and adsorbed on the solid is the same at any concentration.
- ⇒ This ratio is usually termed the distribution coefficient.
- ⇒ The C isotherm is often a simple approximation for a narrow range of concentrations.

[2] The L isotherm
- ⇒ The ratio between the concentration of the compound remaining in solution and adsorbed on the solid decreases when the solution concentration increases, providing a concave curve.
- ⇒ This curve suggests progressive saturation of the solid.

[3] The H isotherm
- ⇒ This is a particular case of the L isotherm, where the initial slope is very high.

[4] The S isotherm
- ⇒ The curve is sigmoidal and thus has got a point of inflection.
- ⇒ This type of isotherm is always the result of at least two opposite mechanisms.

[11] Henry's Law states that the amount of dissolved gas is proportional to its partial pressure in the gas phase.

The concave isotherm (L or H isotherms) is the most widely met isotherm. An example is the Freundlich (1909) model, which is empirical and is based on the following relation:

(2.34) $Q = FC^n$

where F [L kg^{-1}] and n [dimensionless] are two constants (n<1).

Eq. (2.34) Q = FCn is easily linearisable:

(2.35) $\log Q = \log F + n \log C$

In accordance with the Freundlich equation, the isotherm does not reach a plateau as C increases.

Another example is the Langmuir (1918) model, which is based on reaction hypotheses. The solid is assumed to have a limited adsorption capacity Q_{max}. All the adsorption sites (i) are sterically independent of the adsorbed quantity, (ii) each site retains one molecule of the given compounds and (iii) all sites are assumed to be identical (Limousin *et al.,* 2007).

The reaction, free site + solute ↔ surface complex, is then considered. The law of mass action cannot be directly applied to this reaction because the activities of the adsorbed species are not clearly defined (thermodynamically). Nevertheless, the surface activity coefficients are assumed equal to unity and the activities are calculated with conditional stability constants:

(2.36) $$L = \frac{[\text{surface complex}]}{[\text{solute}][\text{free site}]} = \frac{Q_{max}}{C(Q_{max} - Q)}$$

where Q is the solid concentration of the retain compound on the solid and $Q_{max} – Q$ is the solid concentration of the free adsorptive site.

Therefore the Langmuir isotherm is:

(2.37) $$Q = Q_{max} \frac{LC}{1 + LC}$$

Eq. (2.37) can be linearised by Eq. (2.38):

(2.38) $$\frac{Q}{C} = Q_{max} L - LQ$$

where the constant L corresponds to the affinity of the compound for the solid, while Q_{max} corresponds to the adsorption capacity of the solid.

According to the initial assumption, the isotherm reaches a plateau Q_{max}. The constant $Q_{max}L$ is the initial slope of the isotherm and is often used as the K_d when the concentrations are low enough to justify this approximation (Limousin *et al.,* 2007).

In cases where the concentration of the studied compound is higher than a trace concentration, more complicated models than the Freundlich or the Langmuir must be applied (Kinniburgh, 1986). Hinz (2001) proposed an equation to describe any type of isotherm:

$$Q = Q_{max} \sum_{i=1}^{\omega} f_i \prod_{j=1}^{\tau_i} \left(\frac{A_{i,j} C^{pi,j}}{1 + B_{i,j} C^{qi,j}} \right)^{ri,j} \quad (2.39)$$

where f_i is the fraction of sites of type i, ω is the total number of different site types, Q_{max} is the asymptotic amount of adsorption at high concentrations, τ_i gives the number of interaction terms between different site types. $A_{i,j}$ and $B_{i,j}$ are empirical affinity constants and $p_{i,j}$, $q_{i,j}$ and $r_{i,j}$ are dimensionless empirical parameters.

Despite the fact that Eq. (2.39) is fully empirical, and includes many fitting parameters, it has the advantage of reducing any isotherm into different site types. Sorption isotherms do not have an intrinsic thermodynamic definition, their significance depends entirely on the experimental conditions from which they were obtained. This means that the measurement method has a strong influence on the results.

Sorption isotherms are a well-established approach to describe a range of retention/release phenomena. This is very useful in the prediction and comprehension of the mobility of sorbing substances in the environment. However, these isotherms are empirical and macroscopic. Hence, this does not on its own make clear the complex mechanisms involved (Ho, 2004; Limousin *et al.,* 2007).

2.5.3 Surface Complexation Models

Quantitative modelling of sorption by advanced surface complexation models (SCM) has been widely implemented to gain a fundamental understanding of sorption processes at mineral surfaces (Bradbury *et al*., 2005; Bradbury & Baeyens, 2002, 2005 2009, 2011; Kulik *et al*., 2000; Marmier *et al.,* 1994, 1997; Quinn *et al.,* 2006a, 2006b; Rabung *et al*., 2000; Tang & Johannesson, 2005; Tertre *et al.,* 2006a, 2006b, 2008).

SCM are based on thermodynamic principles. They provide a mechanistic interpretation of sorption processes. Because sorption processes are better defined using specific surface

complexes and charge and mass balanced chemical reactions (Sposito, 1983), SCM are considered advantageous over empirical adsorption models (e.g. sorption isotherms).

These models generally consider two sorption mechanisms to be taking place on clay mineral surfaces at:

- permanent sites ⇒ sub model: ion exchange
- variable charge sites ⇒ sub model: surface complexation

where the permanent sites account for the majority of sites for clays (Table 2.3). This study will only implement the ion exchange model, although a literature study with an example of a surface complexation model will be discussed in this section.

Surface complexation models require a significant number of parameters, some need to be fitted (e.g. formation constants), but many must be constrained by physical measurements (e.g. the surface potential of the mineral). In practice, however, surface complexation parameters are rarely derived from experiments due the difficultly in producing reliable and accurate results. Therefore, there are large gaps in the thermodynamic dataset.

Models based on ion exchange are considered much more robust than those based on surface complexation. Parameterisation requires the determination of an exchange constant (log K) from experimental measurement (Eq. (2.3)). A number of exchange constants for species such as AlX_3 are present in standard thermodynamic databases (see § 5.1.1.1). There are however no databases that contain REE exchange constants.

2.5.3.1 Thermodynamics

Sorption involves two effects: a chemical bond between the ion and the surface atoms, and an electrostatic effect that depends on the surface charge. These yield two terms in the equation for the Gibbs free energy of surface complexation:

(2.40) $\Delta G = \Delta G_{intr} + \Delta G_{coul}$

where ΔG_{intr} is the intrinsic energy at zero surface charge and ΔG_{coul} is the coulombic term[12] defined as:

(2.41) $\Delta G_{coul} = F\psi_S$

[12] The Coulombic terms reflects the electrical work required to move ions away from a charged surface

where F is the Faraday constant [96,485 C/mol] and ψ_S is the surface potential [V]. The relationship between the Gibbs free energy and the equilibrium constant (K):

(2.42) $\Delta G = -RT \ln K$

can be used to transform Eq. (2.42) to

(2.43) $$\log K = \log K_{intr} - \frac{F\psi_S}{2.3 \cdot RT}$$

where R is the gas constant [8.31 J/mol/K^0], T is the temperature [K] and K_{intr} is the intrinsic equilibrium constant that enters the thermodynamic database as the log K value.

The diffuse double layer model (Dzombak & Morel, 1990; Stumm *et al.,* 1970) has been implemented in the literature to describe REE sorption on kaolinite (Tertre *et al.,* 2006a). This model considers the charged surface to be balanced by a parallel layer of counter ions.

According to the Gouy Chapman theory (for a symmetrical electrolyte with valence Z), the surface charge density [σ, in C/m^2] is related to the ψ_S by:

(2.44) $$\sigma = (8000\, RT\varepsilon\varepsilon_0 c)^{\frac{1}{2}} \cdot \sinh\left(\frac{Z\psi_S F}{2\,RT}\right)$$

where ε is the dielectric constant of water [dimensionless], ε_0 is the permittivity of free space [8.854×10^{-12} C/V·m] and c is the molar electrolyte concentration [mol/L]. At low potential, Eq (2.44) can be linearised as:

(2.45) $\sigma = \varepsilon\varepsilon_0 \kappa \psi_S$

where the double layer thickness 1/k [metres] is defined by:

(2.46) $$k^2 = \frac{2F^2 I \times 10^3}{\varepsilon\varepsilon_0 RT}$$

The ionic strength I [mol/L] is defined as:

(2.47) $I = 0.5 \sum(Z_i^2 \cdot c_i)$

At 25 °C [T = 298 K], the dielectric constant of water is 78.5 and Eq. (2.44) and (2.45) become:

(2.48) $\sigma = 0.1174 c^{1/2} \sinh(Z\psi_S \cdot 19.46)$

(2.49) $\sigma = 2.5 I^{1/2} \psi_S$

In the case of an asymmetrical electrolyte, a different charge-potential relationship is involved but, except for very low potentials, it is approximately the same as that for a symmetrical electrolyte which has the valence of the counter ion (Hunter, 1981). The double layer model cannot be used for high ionic strength > 0.1 M (Hayes *et al.,* 1991).

2.5.3.2 Diffuse Layer Model

Sorption of Eu^{3+} onto kaolinite from 25 to 150 °C was interpreted by Tertre *et al.* (2006a) using the diffuse layer model (DLM) formalism. The CEC of the pure kaolinite was 3.7 meq/100g[13]. The experimental and spectroscopic analyses indicated that two types of reactive sites should be considered, implying the existence of two distinct mechanisms, an exchange reaction with the compensating Na^+ cations described by:

(2.50) $3{>}XNa + Eu^{3+} = {>}X_3Eu + 3Na^+$ (K_{ex})

and a surface complexation reaction on the amphoteric aluminol sites described by:

(2.51) $>AlOH + Eu^{3+} = >AlOEu^{2+} + H^+$ (K_{edge})

A number of inputs were required to parameterise the DLM for it to be able to describe sorption of Eu^{3+} onto kaolinite. These include: (1) exchange constants over the entire range of ionic strength; (2) values of the site densities (aluminol sites and structural negative sites), and (3) values of the acid/base constants for the aluminol sites and exchange reactions at the studied temperatures (Tertre *et al.,* 2006a).

Time resolved laser induced fluorescence spectroscopy (TRLFS) was used to constrain the number of Eu complexes and the stoichiometry of reactions. The acidity constants of the amphoteric aluminol sites were taken from Tertre *et al*. (2006b). Potentiometric titrations (at 25 and 60 °C in 0.025 – 0.5 M $NaClO_4$ solutions) were used to quantify the influence of the negative structural charge on the acid/base surface chemistry of kaolinite.

The acid/base model considers one negative exchange site and two edges, to take into account the crystalline structure of kaolinite (Tertre *et al.,* 2006b). The negative exchange site, $>X^-$, can react with both H^+ and Na^+ according to the reactions:

(2.52) $>X^- + H^+ = >XH$

(2.53) $>X^- + Na^+ = >XNa$

[13] The method used to calculate the CEC was not included in the paper.

For the edge sites, the assumption was made that kaolinite possesses silanol [>SiOH] and aluminol [>AlOH] sites. In correlation with the literature data, the aluminol sites were considered to be amphoteric (Brady, 1994; Tombacz *et al*., 2004) whereas the silanol sites were considered to be neutral or negative in the studied range of pH (Brady *et al.,* 1996). As a result, three reactions are taken into account:

(2.54) $>AlOH + H^+ = >AlOH_2^+$

(2.55) $>AlOH = >AlO^- + H^+$

(2.56) $>SiOH = >SiO^- + H^+$

The experimental results were then fitted to the model, with the parameters used in the acid/base model (Table 2.6).

Table 2.6 Sorption constants used to model Eu^{3+} sorption onto kaolinite (from Tertre *et al.,* 2006a).

Kaolinite	**log K**				
	25 - 150 ºC	25 ºC	40 ºC	80 ºC	150 ºC
Sorption reactions					
$3>XNa + Eu^{3+} = >X_3Eu + 3Na^+$	11.0 ± 0.4		-		
$>AlOH + Eu^{3+} = >AlOEu^{2+} + H^+$	-	-2.3 ± 0.3	-1.4 ± 0.2	0.2 ± 0.2	2.7 ± 0.4
Reactions of the acid/base model					
$>X^- + H^+ = >XH$	-2.2		-		
$>X^- + H^+ = >XNa$	5.1		-		
$>AlOH + H^+ = >AlOH_2^+$	-	4.8 ± 0.3			
$>AlOH = >AlO^- + H^+$	-	-6.1 ± 0.3			
$>SiOH = >SiO^- + H^+$	-	-7.7 ± 0.3			

Total site densities (in µmol/m^2): AlOH = 0.83; SiOH = 0.83; X^- = 3.7.

The numerical values of intrinsic sorption constants used for modelling Eu^{3+} sorption onto kaolinite are shown in Table 2.6 (Tertre *et al.,* 2006a). The exchange mechanism for Eu^{3+} sorption reactions was assumed to be temperature independent, whereas the complexation constant increases from log K = -2.3 at 25 ºC to 2.7 at 150 ºC. The exchange constant for the Na/Eu reaction on kaolinite was log K = 11.0 ± 0.4.

2.6 Summary

This chapter describes the prior research that motivated this study, and is divided into sections that focus on:

- The significance of the REE in the high-tech industry and their geochemistry;
- The importance of IAD and the application of more environmentally responsible mining technologies to recover the REE;
- The application of thermodynamic equilibrium and reactive transport models to describe solute transport, water flow and geochemical reactions in complex systems;
- The REE sorption mechanisms associated with common IAD minerals, and
- Literature studies that determine REE exchange constants with kaolinite.

The REE are a coherent group of 17 trace metals. Their unique physical and chemical behaviour has made them indispensable in many aspects of the technological industry. However, the growing demand for these elements poses considerable technical and economic challenges to the preservation of a reliable and affordable supply for present and future use.

A laterite deposit containing > 50% ion exchangeable REE adsorbed onto clay mineral surfaces is termed an IAD. The importance of this type of REE-bearing ore stems from the chemical ease of REE extraction. China is the only country to commercially process IAD. Nonetheless, active exploration projects are underway for IAD in Madagascar and Brazil.

Several environmental concerns are associated with mining IAD using surface mining and heap leaching (e.g. groundwater contamination, vegetation clearance and soil excavation). ISR is now implemented in China because it is considered more environmentally acceptable. However, ground clearance and $(NH_4)_2SO_4$ contamination is still linked with ISR.

This highlights the need to consider environmental improvements before ISR should be implemented for potential deposits such as the Madagascar IAD. In addition, the Madagascar IAD must meet certain feasibility criteria (§ 2.2.4.1). Reactive transport modelling in addition to laboratory and field tests should be undertaken to determine deposit suitability.

1-D reactive transport models are capable of simulating solute transport, ion exchange reactions and water flow through dynamic natural environments such as the Madagascar IAD system. Soil column experiments have been widely used to evaluate reactive transport models and determine the fate of trace metals through soils.

REE sorption on the common IAD minerals such as kaolinite and amorphous materials are capable of exchanging and adsorbing REE because they have permanent (negative)

charge sites and/or pH dependent charge sites. Fractionation is commonly observed during REE-mineral sorption, this reflects the variation in desolvation energy with atomic number.

There are a number of empirical and mechanistic approaches that have been used to investigate REE sorption on mineral surfaces. Distribution coefficients and sorption isotherms have been widely used to understand the mobility of sorbing substances. However, their significance depends entirely on the experimental conditions on which they are based.

Surface complexation models provide a more complete, mechanistic understanding of sorption processes. However, many surface complexation parameters are required in these models. Some of these parameters are difficult to constrain by physical measurements, therefore there is limited amount of accurate thermodynamic data.

REE exchange reactions in ion exchange models are described by thermodynamic equilibrium constants (log K). There are no databases which contain REE exchange constants. In the literature, a log K is reported for the Eu exchange reaction with pure kaolinite (Tertre *et al.,* 2006a). No literature studies with exchange constants for all the REE were found.

CHAPTER 3

EXPERIMENTAL INVESTIGATION

This chapter considers the experimental procedures that were carried out in order to model REE mobilisation from the Madagascar IAD.

Three types of experiments were performed:

- CEC determination of the Madagascar IAD ⇒ model input
- Batch tests to determine log K for REE-IAD exchange ⇒ model input
- Column tests ⇒ log K verification

In preparation for the batch and column tests the disturbed subsamples (introduced in § 1.3.1) were weighed and placed onto trays. The material was left to air dry for 14 days (it was not oven-dried at 40 °C, because it was thought that high drying temperatures could alter the material characteristics). Once dry, the samples were weighed again to determine the moisture content. The dried samples were then ground manually with a mortar and pestle.

The reagents used in this research are of analytical grade obtained from VWR™. Solutions were prepared using ultrapure water. The vessels used were rinsed with ultrapure water before use to remove possible contamination sources. The sample preparation, experimental work, and analyses were performed under normal room conditions of pressure (1 atm) and the temperature was kept constant within a measured range of 20 °C to 23 °C.

Each experiment was performed in duplicate or triplicate to provide a measure of the experimental variance. Two blank solutions for each of the reactive solutions used in the experiments were prepared following the relevant experimental procedure. The blank solutions were analysed in addition to the replicates to measure for interference during spectral analysis and to trace sources of artificially introduced contamination.

A digital pH meter (inoLab Multi 9630) calibrated using a 3-point calibration and electrode (SenTix®980) was used to measure pH. A high precision electrical balance (Ohaus SP6000 Scout Pro Portable Balance) was used for weighing. Ion Chromatography (Thermo Scientific ISQ EC Single Quadrupole) and Inductively Coupled Plasma Mass Spectroscopy (Perkin Elmer NexION 350x) were used to measure element concentrations.

3.1 Cation Exchange Capacity

The CEC of the Madagascar soil was derived using the approach of Hendershot & Duquette (1986). This provided a direct measure of the bulk soil CEC. Determination of the CEC was important when modelling REE mobilisation from the Madagascar IAD because the CEC provides the exchange composition[14] of the laterite.

The permeant and variable charge sites on clay surfaces (§ 2.4.1.1) attract exchangeable ions (counterions) to form an exchange complex (Carter, 1993). The CEC method aims to saturate the exchange complex with a cation, forcing the exchangeable cations present on the charged surface into solution (law of mass action).

In the approach of Hendershot & Duquette (1986), a high solid-liquid ratio (SLR) was used with the assumption that all the exchangeable cations on the material would be mobilised into solution. In addition to the barium chloride reagent that Hendershot & Duquette (1986) used, this study performed two further CEC tests with two different reagents.

The three reagents used are:

[1] 0.5 M barium chloride ($BaCl_2$)
[2] 1 M ammonium chloride (NH_4Cl)
[3] 1 M ammonium acetate (NH_4Ac)

The method involved transferring 4.0 g of air dried material to a 50 mL polyethylene tube. Forty mL of a reactive solution (1, 2 or 3) was then added to the tube, giving a 1:10 SLR. The SLR is defined by:

$$\text{SLR} = \frac{m}{V} \tag{3.1}$$

where m is the mass [g] of the Madagascar sample and V is the volume [mL] of the reagent.

The pH of the initial solution was measured. The tube was placed in a rotary shaker and shaken at 11 rpm for 2 hours (the kinetics of exchange was investigated by UIT, where the reaction was found to reach completion within 5 minutes, 2 hours ensured the removal of all exchangeable cations from the material).

The tube was centrifuged at 1,000 rpm for 30 minutes. The final pH of the supernatant

[14] The exchange composition refers to the distribution of exchangeable cations on the deposit.

was recorded. The supernatant was then filtered through a 0.45 µm filter paper. The eluent was separated into two fractions. One fraction was analysed for cation concentrations with ICP-MS. This procedure was repeated twice for each of the three reagents to give duplicates.

The CEC [meq/100g] of the Madagascar IAD was calculated from this fraction as:

$$(3.2) \qquad CEC = \left[\sum_i \frac{C_i}{M_i/z_i}\right] / 1000$$

where C_i is the aqueous concentration [mg/L] of the ion i, M_i is the molar mass of i and z is the charge of i. The measured elements used to calculate the CEC were Na, K, Mg, Ca, Mn, Cu, Ni, Zn, Al, Y, La, Ce, Pr, Nd, Sm, Eu, Gd, Tb, Dy, Ho, Er, Tm, Yb, Lu and Si[15].

The other fraction was tested for colloids. Initially ICP-MS was used to determine the major element concentrations, then light scattering and ultracentrifugation were employed to separate any colloids. ICP-MS was repeated following separation to ascertain whether cation concentration changes indicated the presence of colloids in the non-centrifuged samples[16].

3.2 Batch Reaction Tests

Thermodynamic equilibrium constants to describe REE exchange reactions with the Madagascar IAD were estimated from batch tests. These tests were defined operationally as achieving chemical equilibrium during which pH was observed to become constant with time. The tests were performed at 9 SLR conditions which are shown in Table 3.1.

Table 3.1 SLR conditions for 9 batch tests.

	m [g]	**V [mL]**	**SLR [g/mL]**
1	5	45	0.11
2	7.5	42.5	0.18
3	10	40	0.25
4	12.5	37.5	0.33
5	15	35	0.43
6	17.5	32.5	0.54
7	20	30	0.67
8	22.5	27.5	0.82
9	25	25	1.00

The experimental approach involved transferring the 0.5 M barium chloride solution to a 50 mL polyethylene tube containing the Madagascar material, in one of the predefined SLR shown in Table 3.1. The pH of the initial solution was measured. The tube was shaken in a

[15] All the measured elements above the detection limit where used in the CEC equation.
[16] ICP-MS analysis showed the presence of colloids to be negligible.

rotary shaker for 2 hours at 13 rpm; it was then centrifuged for 30 minutes at 1,000 rpm.

The final pH of the supernatant was recorded before it was filtered through a 0.45 µm filter, and separated into two fractions for analysis of the major element concentrations with ICP-MS and IC. This procedure was repeated three times for each SLR condition to give triplicates. Fig. 3.1 shows some of the batch tests in different SLR conditions.

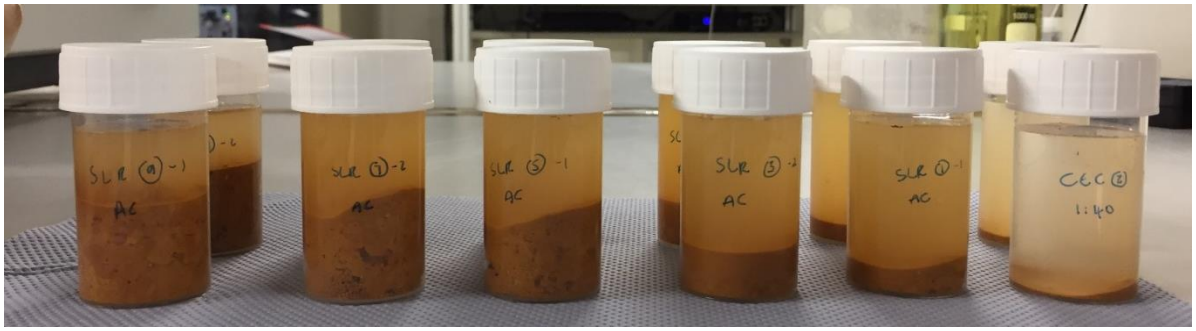

Fig. 3.1 Batch tests in different SLR conditions.

The use of 9 different SLR meant that each test would comprise a different exchangeable REE concentration. Thus, the C_{TOT} [meq/L], which is defined in Eq. (3.3), varied.

$$C_{TOT} = CEC \cdot \frac{m}{V} = CEC \cdot SLR \tag{3.3}$$

Different exchangeable species distributions in each SLR condition were important when extracting REE equilibrium constants from the batch dataset. This is because these different distributions ensured that all the exchange reactions with the Madagascar IAD in a range of experimental conditions were adequately described.

3.3 Soil Columns

Soil column experiments were performed with the Madagascar material to test whether the REE equilibrium constants estimated from the batch tests (described in § 3.2) could describe reactive transport through the REE column breakthrough curves.

A continuous flow column transport system usually provides a better approximation of the field conditions. Thus, reactive transport calculations based on the soil columns were used in this study to model the field site, incorporating flow, transport and ion exchange reactions.

The protocol involved adding the air-dried sample to each column in 10 g portions. The sample was compressed between each addition to obtain a uniform bulk density. A porous plate with 8-12 µm filter was placed at either end of the column, allowing the solution but not the material to flow from the columns. The columns are shown during packing in Fig. 3.2.

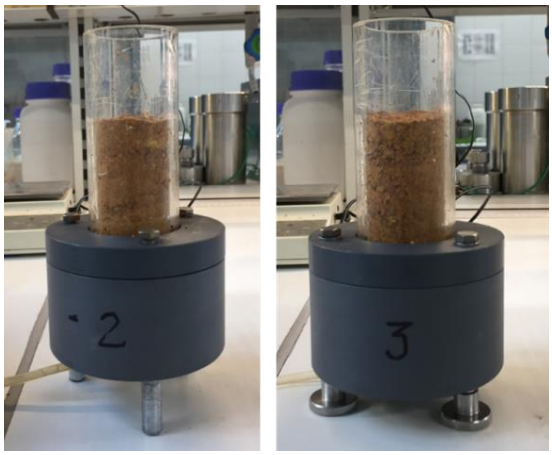

Fig. 3.2 The columns during the packing procedure.

Each column had a length of L = 15 cm, an inside diameter of 4 cm (area A = 12.6 cm^2) and a volume of 188 cm^3. Once packed, the columns were installed in the column test facility (Fig. 3.4). Two column experiments were performed, each using a different reactive solution:

[1] 0.05 M barium chloride ($BaCl_2$)

[2] 0.1 M ammonium chloride (NH_4Cl)

For each solution, two columns in replicate were run in parallel. In the first experiment, de-ionised water was used to saturate the column for 7 days. This period was sufficient to allow equilibrium conditions to be attained (to ensure this, pH was measured frequently).

The material was then flushed with a barium chloride solution for 16 days. Preliminary reactive transport calculations suggest this amount of time was sufficient to elute all elements from the material. The column flow conditions are shown in Fig. 3.3.

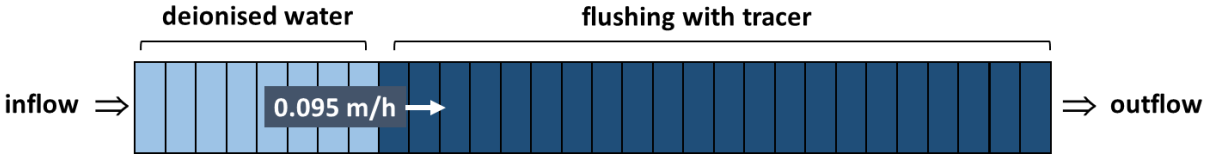

Fig. 3.3 Column flow conditions.

Because the breakthrough curves in the first experiment indicated that not all the elements were completely eluted from the column, the methodology of second experiment was altered. In this de-ionised water was used to saturate the column for 8 days and then the column was flushed for 24 days with ammonium chloride.

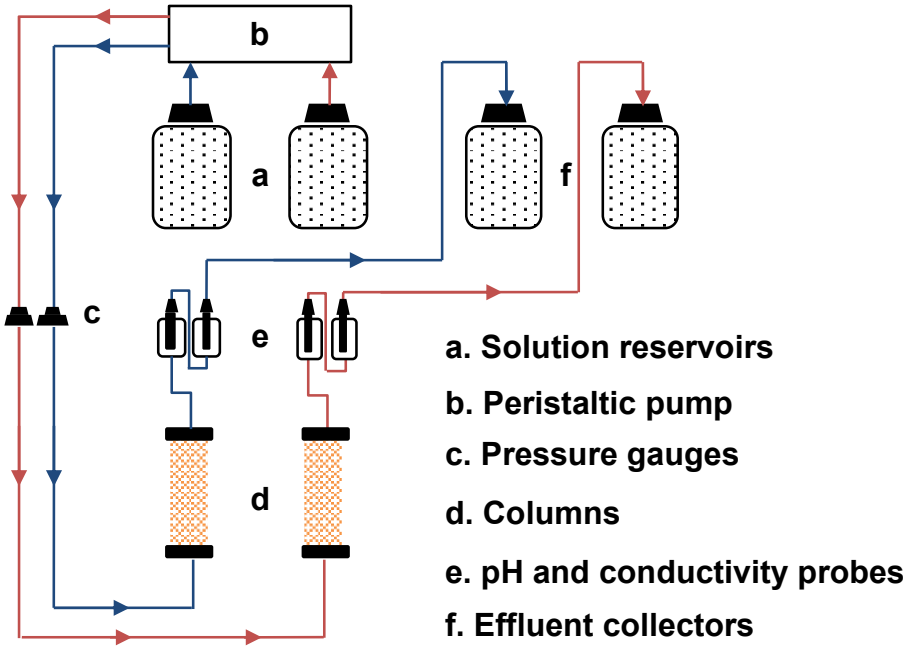

Fig 3.4 Column Test Facility at UIT.

The columns were operated with an upward flow of Q = 0.02 mL/min using a peristaltic pump. The flow rate was checked at least once a day and adjusted accordingly (the flow rate varied marginally in the range of 0.001 mL/min to 0.003 mL/min). Pressure within the test facility was monitored throughout the entire experiment and recorded every 5 hours.

Bulk density and porosity were determined gravimetrically by weighing the column before and after saturation:

(3.4) bulk density: $\rho_b = 1.3\ g/cm^3$

(3.5) porosity: $\varepsilon = 0.19$

The eluates were collected approximately every 12 hours. pH and conductivity were measured immediately following sample collection. This was in addition to online pH and conductivity measurements recorded every five hours. The eluates were filtered through a 0.45 µm filter before analysis of the major and trace element concentrations with ICP-MS and IC.

Numerous column experiments had been performed prior to the two experiments described in this section. This was to determine an optimum set of column pre-conditions (i.e. flow rate, packing procedure, concentration of the salt solution and length of solution injection) since it was not easy to maintain a flow through the clay-rich soil.

3.4 Summary

This chapter describes the experimental investigation undertaken in this research. Three different types of experiments were performed with sample material from Madagascar to determine input parameters to be used to model REE mobilisation from the IAD.

Determination of the CEC using a number of reactive solutions was important for the modelling of REE ion exchange reactions because it provides the exchange composition of the Madagascar IAD (i.e. the concentration of exchangeable species).

Batch reaction tests were undertaken at 9 SLR conditions to provide a REE dataset from which to estimate REE exchange constants with the Madagascar IAD minerals. Cation exchange reactions in the tests were indicated by the fast equilibrium kinetics.

Column experiments with different reagents were carried out to determine whether the estimated exchange constants could also describe REE breakthough curves and to improve current understanding of solute transport and water flow through the Madagascar laterite.

CHAPTER 4

RESULTS AND DISUCSSION

This chapter will present the results of the experimental investigation and provide a descriptive account of the key findings. In addition, the results will be interpreted to provide a basis for CHAPTER 5, which will use these results in reactive transport and equilibrium calculations to model REE mobilisation from the Madagascar IAD.

4.1 CEC

The Madagascar IAD in contact with three solutions leads to the following results:

- 0.5 M **$BaCl_2$** (initial pH 6.4) $\Rightarrow$ CEC = 10.34 ± 0.07 meq/100g (final pH 4.0)
- 1.0 M **NH_4Cl** (initial pH 5.0) $\Rightarrow$ CEC = 10.25 ± 0.05 meq/100g (final pH 4.1)
- 1.0 M **NH_4Ac** (initial pH 7.0) $\Rightarrow$ CEC = ~10.28 ± 0.12[17] meq/100g (final pH 6.5)

The analogous values indicate that the CEC was independent of pH (as expected, § 2.4.1.1). A significant pH decrease was observed between the initial and final chloride solutions ($BaCl_2$ and NH_4Cl) but not in the acetate solution. A CEC of 10.3 meq/100g was used in subsequent model calculations (in CHAPTER 5). The CEC data is given in Appendix B.

Fig. 4.1 shows the exchangeable element solution composition in each CEC test. Most of the element concentrations were similar in each test, except for Al which was strongly influenced by the pH of the different reactive solutions. High exchangeable Al concentrations were present in the chloride solutions (at pH 4), but not in the acetate solution (at pH 6.5).

Equilibrium modelling of all the CEC experiments was undertaken in PHREEQC in the presence and absence of Al to gain a better understanding of the reason for the pH drop in the chloride solutions and for the low exchangeable Al concentration in the acetate solution. This modelling will be discussed in § 5.1.2.

[17] . The NH_4Ac CEC value is estimated. This is based on modelling of the CEC experiment which is discussed in detail in § 5.1.2.

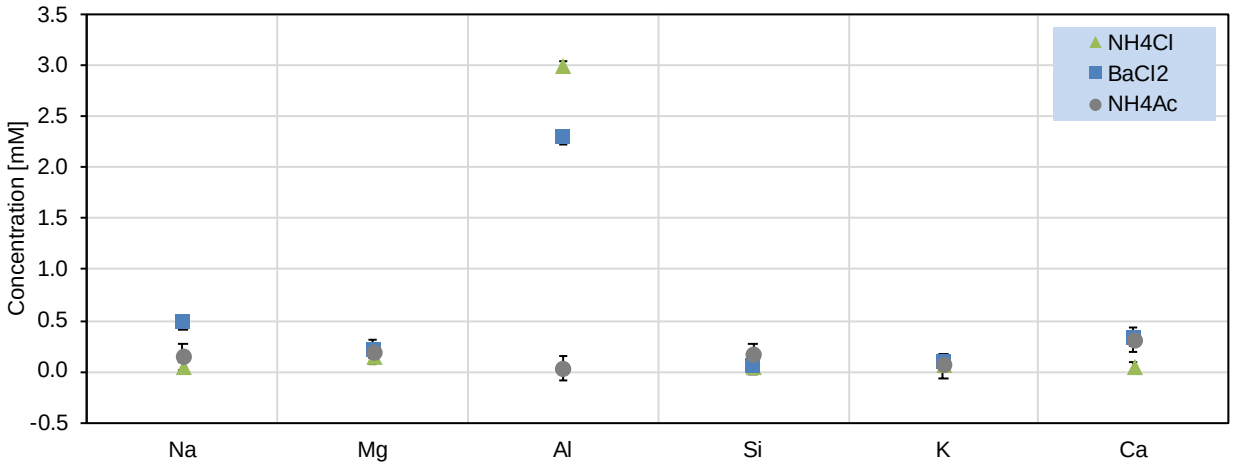

Fig. 4.1 Major aqueous element composition for 3 CEC tests. Error bars signify standard error of replicates.

4.2 Batch Reaction Tests

The C_{TOT} for each of the 9 SLR conditions is shown in Table 4.1 (calculated with Eq. (3.3)). C_{TOT} will enter the equilibrium calculations (described in CHAPTER 5) as an important input parameter. For example, in case of SLR = 0.11 g/mL

$$C_{TOT} \equiv 10.3 \frac{meq}{100g} \cdot 0.11 \frac{g}{mL} \cdot 10 = 11.3 \frac{meq}{L} \tag{4.1}$$

The entire batch dataset is presented in Appendix B.

Table 4.1 The C_{TOT} values for each SLR condition.

	m [g]	V [mL]	SLR [g/mL]	C_{TOT} [meq/L]
1	5	45	0.11	11.3
2	7.5	42.5	0.18	18.5
3	10	40	0.25	25.8
4	12.5	37.5	0.33	33.9
5	15	35	0.43	44.3
6	17.5	32.5	0.54	55.6
7	20	30	0.67	69.0
8	22.5	27.5	0.82	84.5
9	25	25	1.00	103

The exchangeable cation concentrations for Al^{3+}, Ca^{2+}, Mg^{2+} and Na^{+} following the ion exchange reaction are shown in Fig. 4.2 at 9 SLR conditions. The final pH for these tests decreased with increasing SLR, from pH 4.0 to 3.6. Al and Mg illustrate the expected trend, where the exchangeable concentration increased with increasing SLR. This reflected an increasing number of exchange sites.

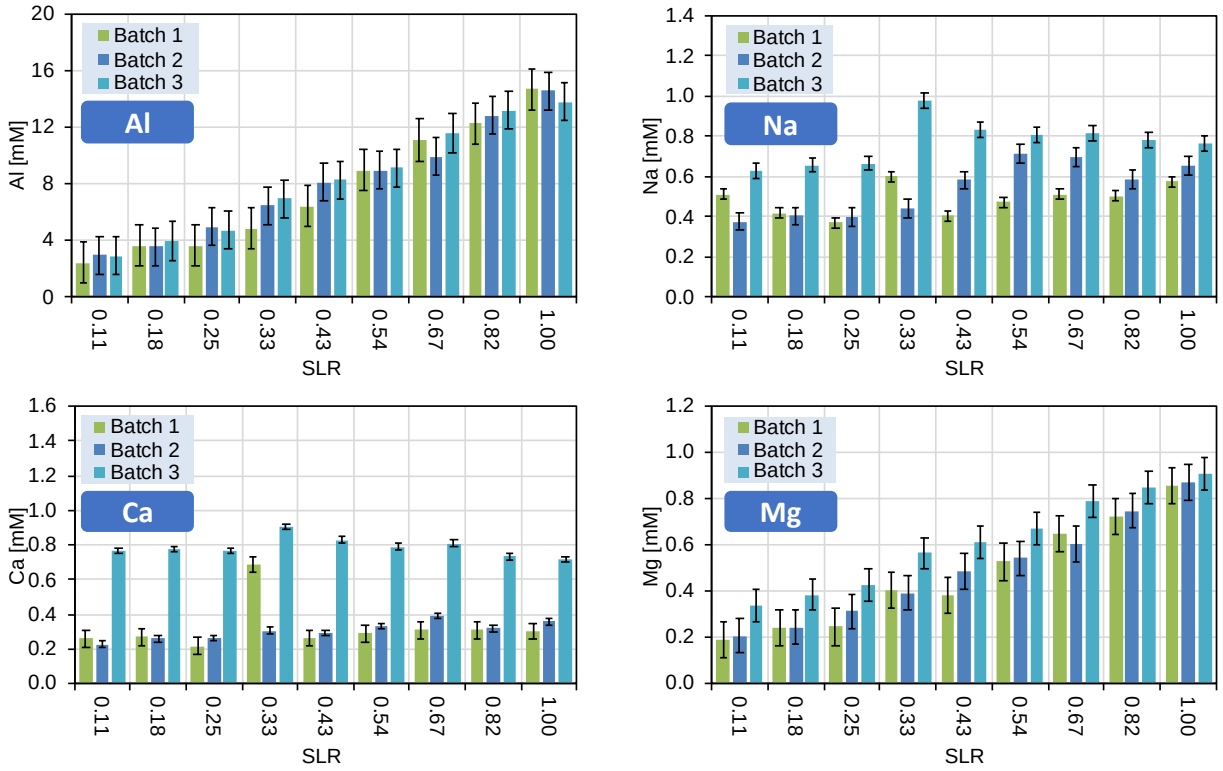

Fig. 4.2 Exchangeable cation concentrations for 9 SLR conditions. Error bars signify standard error of triplicates.

Systematic differences observed between the batches, such as consistently higher Na, Ca, Mg concentrations in solution after the ion exchange reaction in batch 3 could demonstrate the natural variability in exchange surface composition within an IAD. This provides a possible explanation for the varied trend observed in the Ca and Na concentrations in Fig. 4.2.

In correlation with the CEC results, Al^{3+} was observed to be the major exchangeable cation on the Madagascar IAD with concentrations increasing from 2.4 mM to 14.6 mM as a function of SLR. This is in addition to its occurrence in kaolinite's mineral structure (the dominant clay exchanger in the Madagascar sample; Table 1.1).

The exchangeable REE fraction mobilised into solution at 9 SLR conditions are shown in Fig. 4.3. For the most part the REE behaved as anticipated, the concentration of exchangeable REE mobilised into solution increased with increasing SLR. The reproducible nature of the dataset was supported by the similarity of the repeat tests (batch 1, 2 and 3).

The analytical data showed Sm and Eu behaving differently to the rest of the REE, where the exchangeable fraction decreased with increasing SLR (in each repeat test). The literature indicates that spectral interference during analysis could explain this trend (summarised in § 4.2.1). Thus, the geochemical behaviour of the REE does not differ, the measured data does.

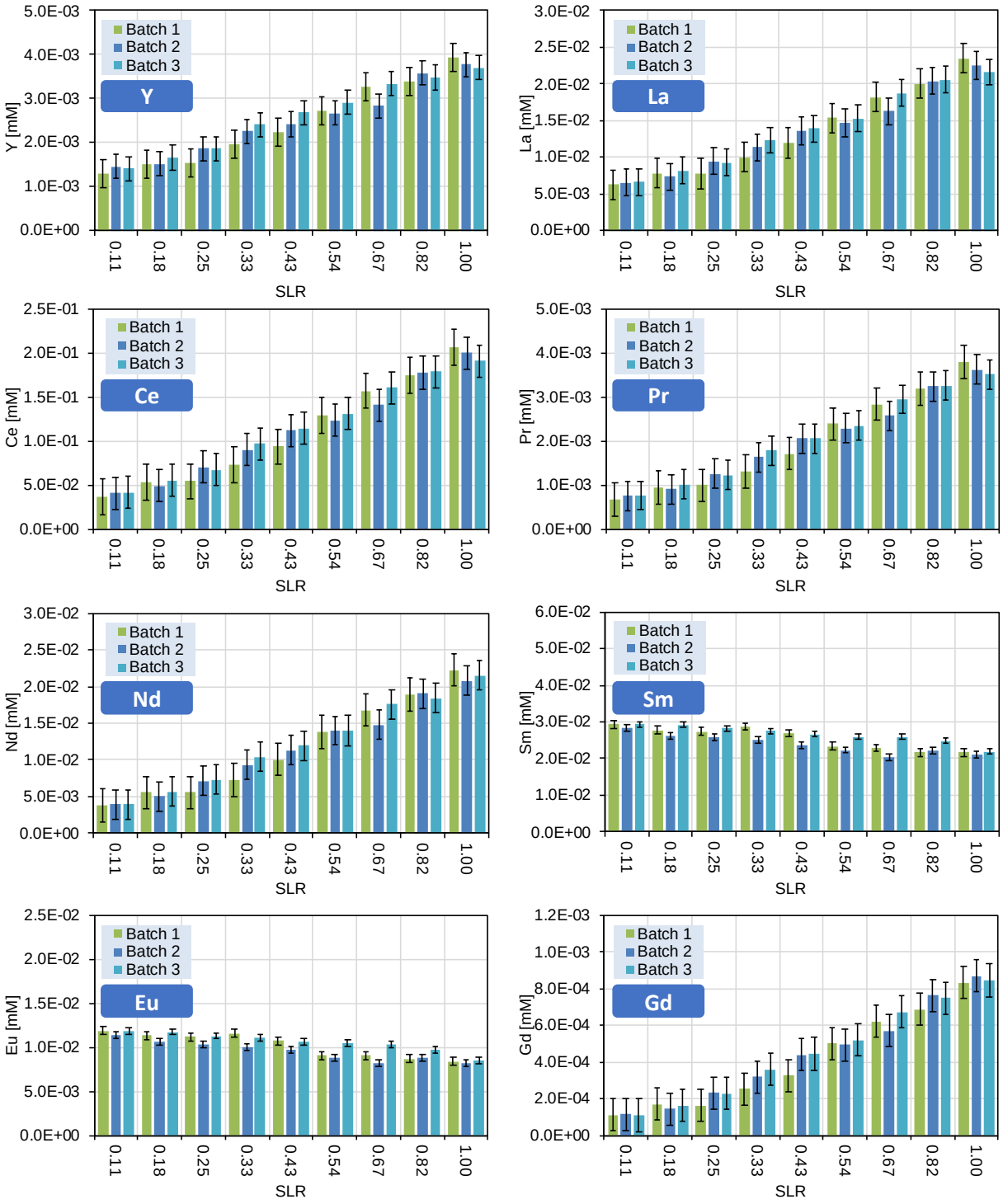
Batch 1
Batch 2
Batch 3
Y
Y [mM]
5.0E-03
4.0E-03
3.0E-03
2.0E-03
1.0E-03
0.0E+00
La
La [mM]
3.0E-02
2.5E-02
2.0E-02
1.5E-02
1.0E-02
5.0E-03
0.0E+00
Ce
Ce [mM]
2.5E-01
2.0E-01
1.5E-01
1.0E-01
5.0E-02
0.0E+00
Pr
Pr [mM]
5.0E-03
4.0E-03
3.0E-03
2.0E-03
1.0E-03
0.0E+00
Nd
Nd [mM]
3.0E-02
2.5E-02
2.0E-02
1.5E-02
1.0E-02
5.0E-03
0.0E+00
Sm
Sm [mM]
6.0E-02
5.0E-02
4.0E-02
3.0E-02
2.0E-02
1.0E-02
0.0E+00
Eu
Eu [mM]
2.5E-02
2.0E-02
1.5E-02
1.0E-02
5.0E-03
0.0E+00
Gd
Gd [mM]
1.2E-03
1.0E-03
8.0E-04
6.0E-04
4.0E-04
2.0E-04
0.0E+00
0.11
0.18
0.25
0.33
0.43
0.54
0.67
0.82
1.00
SLR

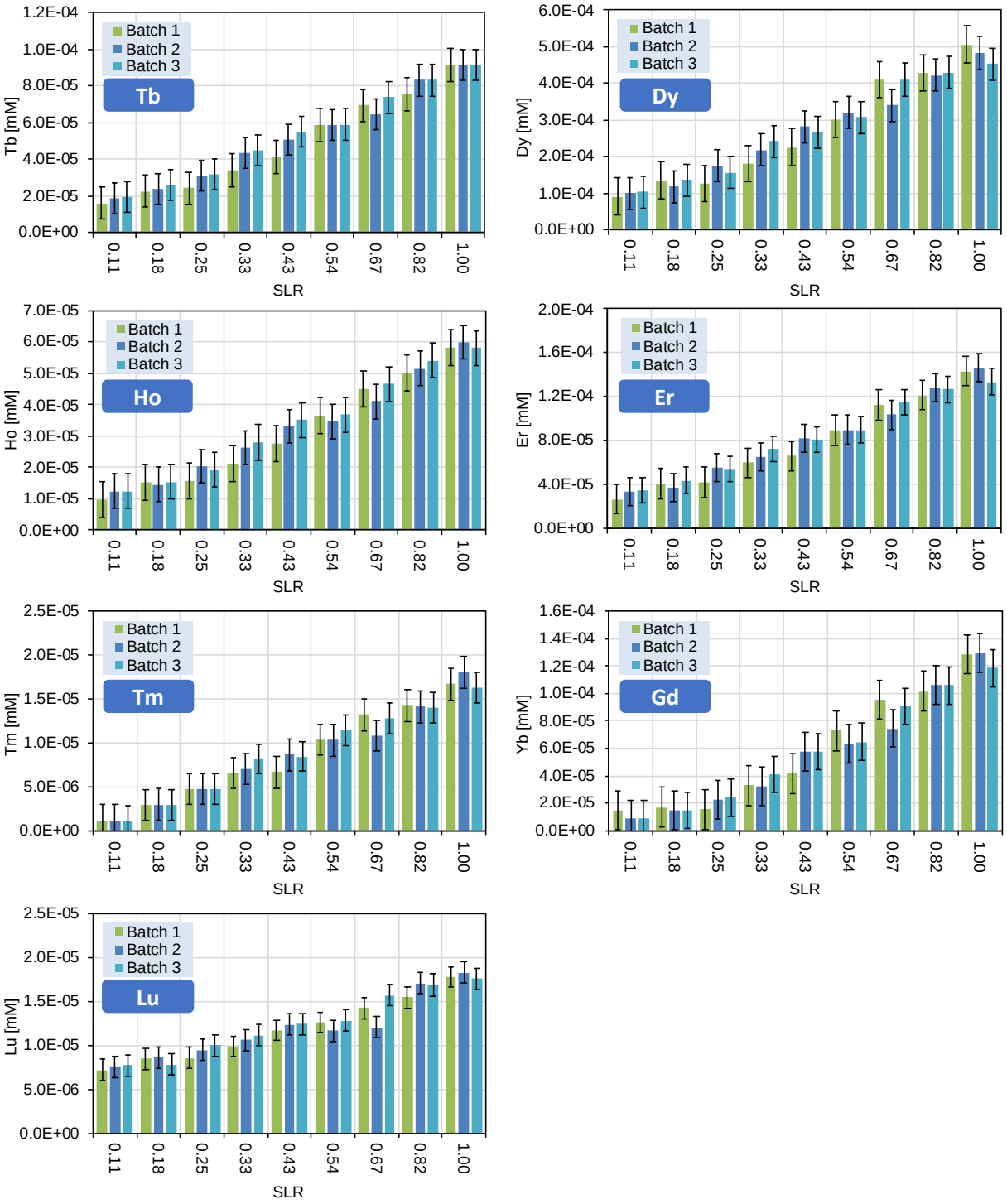

Fig. 4.3 Exchangeable REE concentrations for 9 SLR conditions. Error bars signify standard error of triplicates.

4.2.1 Interferences during Spectral Analysis

Spectral interferences can occur when atomic- or polyatomic ion masses differ by less than 0.5 mass units from the analyte ion (Dams *et al.,* 1995). These isobaric interferences are caused by the overlap of isotopes of different elements. Potential sources of spectral interference that arise in the presence of the REE and high Ba concentrations (during ICP-MS

analysis) will be discussed and used to interpret the Sm and Eu trend (Fig. 4.3).

Spectral overlap of polyatomic ions is caused by the production of ionised molecular species within the plasma (Jarvis *et al*., 1991). The polyatomic ions, BaO^+ and $BaOH^+$, were found to significantly affect the intensity of the middle REE isotopes from ^{146}Nd through to ^{155}Gd (Cao *et al.,* 2001). Particular complexities arises from the formation of BaO^+ which interferes with both ^{151}Eu and ^{153}Eu, leaving no Eu isotope entirely free from interference (Jarvis, 1989).

Both the LREE and Ba can form oxide species (between 0.2–1.2%; Gray & Williams, 1987) during ICP-MS analysis. Under optimum operating conditions, oxide interference is typically low as the magnitude of interference is within accepted analytical precision (Jarvis, 1988). However, samples that contain high levels of Ba and/or strong fractionation of the LREE relative to the HREE, are subject to substantial interference effects (Kent, 2005).

The following results were observed in the batch dataset under discussion:

- The exchangeable REE fraction was determined with a highly concentrated barium chloride solution, and
- The material exhibited a strong fractionation of the LREE relative to the HREE.

These results fulfil both of the criteria outlined above to cause a significant interference effect.

To further confirm the presence of spectral interference, Jarvis *et al*. (1989) recommends measuring the Ba concentration. Measurement of the Ba concentration in the batch tests following the ion exchange reaction were consistently higher than the initial concentration (500 mM) in the 9 SLR conditions. That is values of 730 mM, 995 mM and 1473 mM were reported. The analysis was repeated several times with the same outcome[18].

In addition, Sm and Eu concentrations in blanks of the concentrated $BaCl_2$ solution, were an order of magnitude greater than the rest of the lanthanides (Fig. 4.4). This trend strongly suggests an interfering effect. Solvent extraction was considered to correct for interference by separating Ba from the analyte system prior to analysis. However, this approach was not carried out because it was limited by incomplete REE recovery (Shabani *et al.*, 1990).

[18] Analysis with ICP-MS can lead to overestimated concentrations when highly concentrated solutions are being measured as in the batch tests.

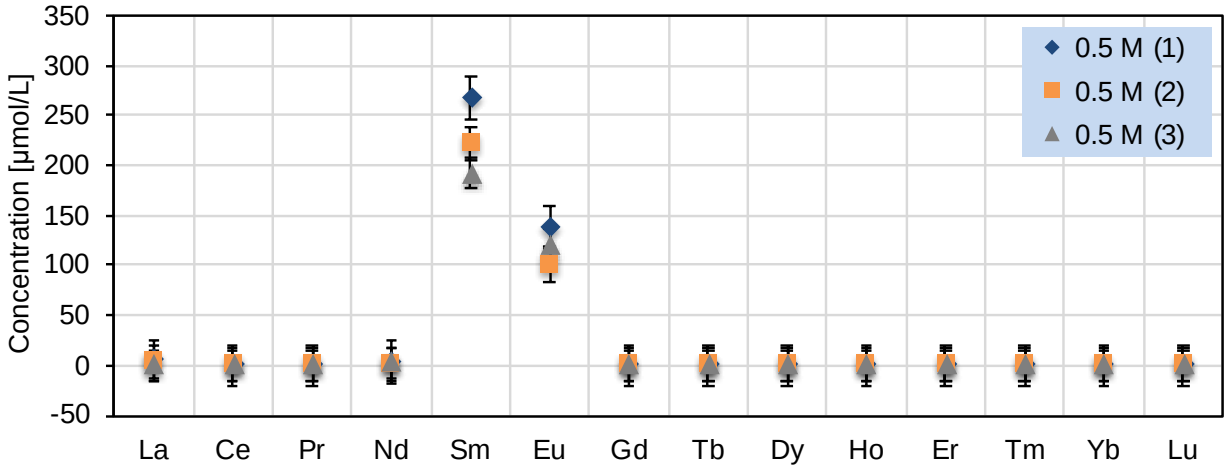

Fig. 4.4 REE concentrations in blank 0.5 M BaCl2 solutions, in triplicate. Error bars = standard error of triplicates.

4.3 Soil Column Experiments

Fig. 4.5 shows the breakthrough curves (effluent concentration vs time) for the major ions and the REE for the column experiments in which a barium chloride solution was used. The curves of the duplicate column were analogous (only one column is shown). The entire column dataset is shown in Appendix B.

The important time points within the columns are:

- start of column test with deionised water: $t_0 = 0$
- 0.05 M $BaCl_2$ is added to solution reservoir: $t_1 = 168$ h (7 days)
- $BaCl_2$ enters column (after flowing through tubes): $t_2 = 168$ h + 100 h = 268 h
- estimated Cl breakthrough (tracer) assuming ε[19] = 0.19: $t_3 = 268$ h + 30 h[20] = 298 h
- Al and REE breakthrough (measured): $t_4 = 350$ h
- retarded Ba breakthrough (measured): $t_5 = 400$ h

Al and the REE breakthrough simultaneously. The breakthrough of Ba^{2+} was retarded because the cation was exchanging for the REE^{3+} and Al^{3+} on the IAD surface prior to breakthrough. The overall trend of the REE breakthrough curves was similar. Sm and Eu were the exceptions as their concentration steadily increased with time (explained in § 4.2.1).

[19] ε was determined at the start of the column experiment: $\varepsilon = V_{column}/W_{content} = 35.7$ g / 188.5 cm^3 = 0.19
[20] Time for 1 pore-volume exchange: PV = $\varepsilon V/Q$ = 0.19·188 mL / (1.2 mL/h) = 30 h.

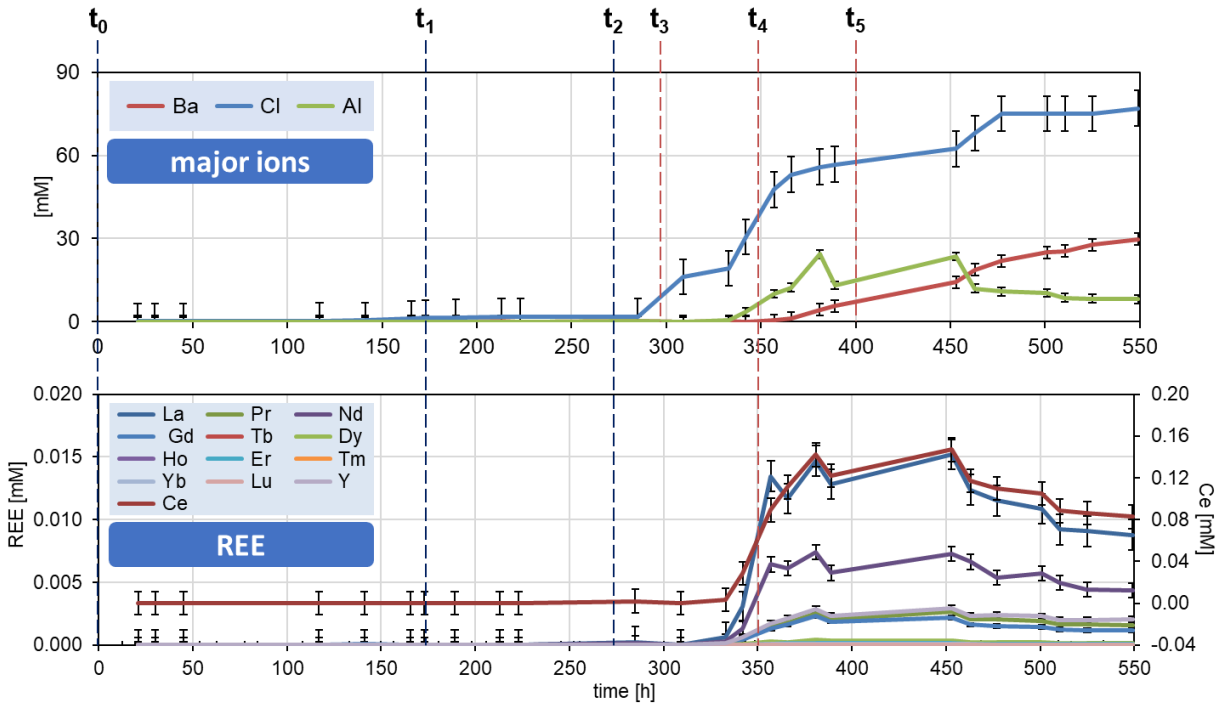

Fig. 4.5 Elution behaviour of Ba, Cl, Al, (upper) and the REE (lower). Error bars signify standard error of replicates.

Breakthrough curves for the column in which an ammonium chloride solution was used to desorb elements are shown for the major ions and the REE in Fig. 4.6. The curves of the replica column were comparable, thus only one column is shown.

Typical time points in the columns are:

- start of column test with deionised water: $t_0 = 0$
- 0.1 M NH_4Cl is injected into solution reservoir: $t_1 = 192$ h (8 days)
- NH_4Cl enters column (after flowing through tubes): $t_2 = 192$ h + 100 h = 292 h
- estimated Cl breakthrough assuming $\varepsilon = 0.19$: $t_3 = 292$ h + 30 h = 322 h
- Al and REE breakthrough (measured): $t_4 = 400$ h

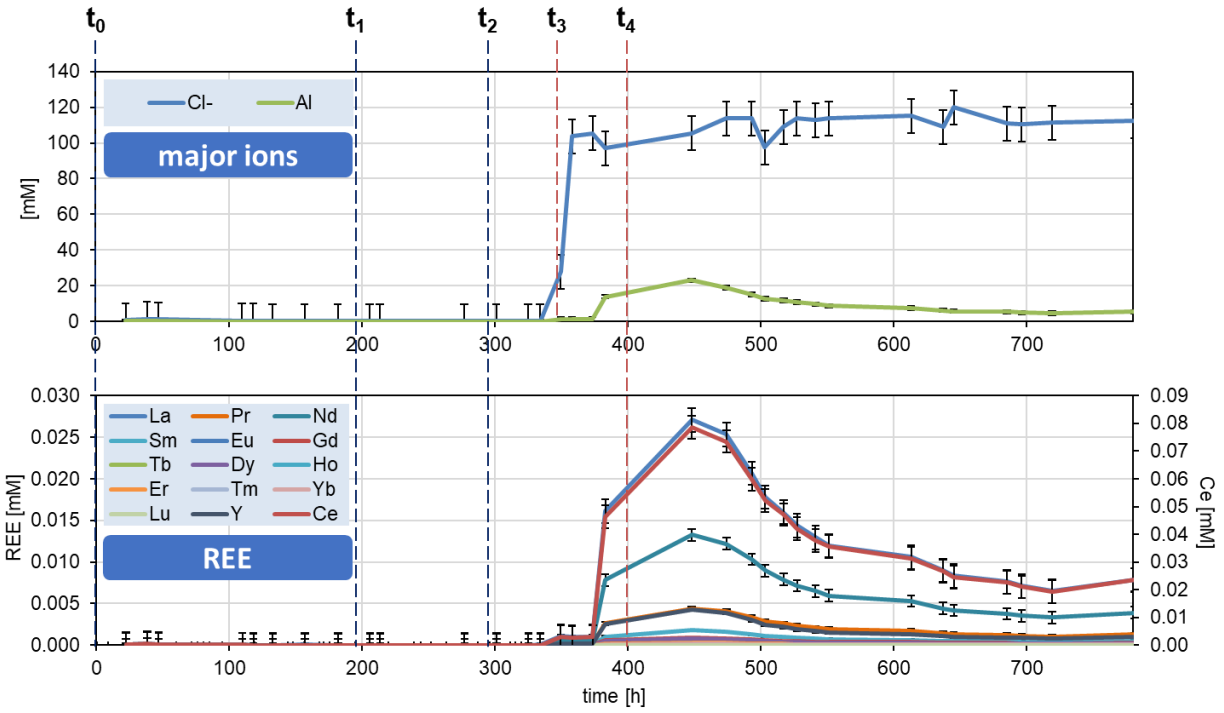

Fig. 4.6 Elution behaviour of Cl, Al, (upper) and the REE (lower). Error bars signify standard error of replicates.

Ammonia concentrations could not be accurately resolved due to the well-known measurement difficulties (Harper, 2005). However, retardation of NH_4^+ was expected as the cation substitutes for Al^{3+} and the REE^{3+} on the IAD. All the REE breakthrough curves behaved similarly. Preferential flow was indicated by the rapid breakthrough of the Cl tracer.

4.4 Madagascar IAD Mineralogy

The minerals identified in the Madagascar sample material (pit 3) with XRD analysis were kaolinite, gibbsite and quartz (shown in Table 1.1). Kaolinite is identified as the dominant mineral and the principal exchanger surface. However, no wet chemistry analysis was performed to determine whether amorphous iron oxyhydroxides were also present.

Amorphous iron oxyhydroxides are commonly found in weathered laterites. They are also important exchangers of cations (§ 2.4.1.2). The extent to which the amorphous materials contribute to the deposit's exchange capacity is unknown. For this reason, it was important to consider the exchange capacity of the laterite profile as a whole.

Hence, the exchange constants estimated in this study will represent REE exchange reactions with all potential exchange surfaces in the Madagascar IAD (§ 5.1.3), rather than just for REE-kaolinite exchange reactions.

4.5 Key Conclusions

There are two main outcomes of the CEC tests:

[1] The CEC of Madagascar IAD is 10.34 ± 0.07 meq per 100g of dry soil.

[2] The major exchangeable cation on the Madagascar IAD is Al^{3+} (in addition to its occurrence in the kaolinite's mineral structure).

The main outcome of the batch equilibrium tests was that all the REE (incl. Sm and Eu) behave coherently when mobilised into solution by a reactive solution. Spectral interference during analysis was the only reason for the different measured behaviour of Sm and Eu.

Cation exchange reactions were observed in the soil column experiments by the retardation of the injected cation (Ba^{2+} or NH_4^+) breakthrough, as the injected cation was exchanging for the REE^{3+}, Al^{3+} and the other trace elements in the column.

Minerals commonly associated with IAD include: kaolinite, halloysite, gibbsite, and amorphous materials. The amorphous mineral content in the Madagascar IAD was not determined. But, in this study all potential REE exchanging minerals will be considered in the estimation of REE exchange constants with the Madagascar IAD.

CHAPTER 5

MODELLING

This chapter outlines the modelling approach used to estimate REE exchange constants from the batch reaction dataset. Reactive transport modelling of the soil columns was also undertaken to test whether the estimated REE exchange constants could also describe the breakthrough curves. The results of these simulations are discussed and evaluated where relevant to the research aims of this study. The model inputs are shown in Appendix C.

5.1 Modelling REE Exchange

Equilibrium calculations were performed in PHREEQC to model REE ion exchange with the Madagascar IAD minerals (§ 4.2) and to estimate exchange constants for these reactions from the experimental data and reaction stoichiometry. Cation exchange reactions in the CEC experiments (§ 4.1) with three reactive solutions were also modelled in PHREEQC to determine the role of aluminium in the Madagascar IAD.

5.1.1 PHREEQC Model Description

PHREEQC version 3 (Parkhurst & Appelo, 2013) is a geochemical modelling code capable of performing a wide variety of aqueous geochemical calculations. The programme is based on the equilibrium chemistry of aqueous solutions interacting with other components such as ion exchange surfaces, sorbing surfaces, minerals, gases and solid solutions.

PHREEQC is written in the C and C++ programming languages and implements several types of aqueous models. These include two ion-association aqueous models (the Lawrence Livermore National Laboratory model and WATEQ4F), the Specific ion Interaction Theory (SIT) aqueous model, and the Pitzer specific-ion-interaction aqueous model.

Using any of these aqueous models, PHREEQC has capabilities for:

[1] speciation and saturation index calculations;
[2] batch-reaction and 1D transport calculations with reversible and irreversible reactions which include ion-exchange equilibria, surface complexation and kinetically controlled reactions, and
[3] inverse modelling.

In batch-reaction calculations, PHREEQC is oriented towards system equilibrium as opposed to just aqueous equilibrium. Thus, for an equilibrium calculation, all of the moles of each element in the system will be distributed among the aqueous, pure and gas phases, solid solutions, surface sites and exchange sites to attain system equilibrium.

Exchange reactions are modelled in PHREEQC as ion association reactions in the form of two half reactions. For example, the exchange of Na for REE is defined with the reaction:

(5.1) $3NaX + REE^{3+} \leftrightarrow REEX_3 + 3Na^+$

which is split into

(5.2) $REE^{3+} + 3X^- = REEX_3$ log K

(5.3) $Na^+ + X^- = NaX$ log K

where X^- represents the exchanger.

Eq. (5.2) and (5.3) can be combined to provide the full exchange equation in Eq. (5.1) and corresponding thermodynamic constant. In the default database file, sodium (NaX) is used as the reference and the reaction $Na^+ + X^- = NaX$ is given a log K of 0.0 (see also Eq.(5.7)).

The default ion exchange formulation assumes that the thermodynamic activity of the exchangeable species is equal to its equivalent fraction. The equivalent fraction E of an ion is the ratio of this ion equivalent concentration and the sum of equivalent concentrations of all present ions (Zagorodni, 2006):

(5.4) $$E_{Ion_i} = \frac{z_i[Ion_i]}{\sum_{j=1}^{n} z_j[Ion_j]} \quad 0 \le E \le 1$$

where z_i and $[Ion_i]$ are charge and molar concentration of the ion number i. Optionally, the equivalent fraction can be multiplied by a Debye-Hückel activity coefficient to define the activity of an exchange species (Appelo, 1994).

Other formulations use other definitions of activity (e.g. mole fraction instead of equivalent fraction) and may be included in the database with appropriate rewriting of species or solid solutions. In most cases, modelling of ion exchange reactions requires experimental data on material from the study site for appropriate model application (e.g. Tertre *et al.,* 2008).

5.1.1.1 Thermodynamic Databases

Reliable and consistent thermodynamic data form the basis for chemical and speciation modelling of equilibrium and reactive transport of constituents within complex systems (Meeussen *et al.,* 2009). These data can consist of equilibrium constants (log K) for stoichiometric reactions that describe the:

[1] Formation of dissolved species in aqueous solution;
[2] Dissolution and precipitation of solid phases between aqueous and solid phases, and
[3] Exchange of cations between aqueous and solid phases.

In practice, however, there are many instances where thermodynamic data are limited, have not been measured, or where it is not possible to provide accurate quantification of the equilibrium chemistry.

Nine thermodynamic databases are provided with PHREEQC, two of which are important in this research: *llnl.dat* and the *wateq4f.dat*. The *llnl.dat* (Johnson *et al.,* 2000) uses thermodynamic data compiled from the Lawrence Livermore National Laboratory (LLNL). The LLNL aqueous model includes reliable data for a number of minerals and aqueous species in a temperature range of 0 to 300 °C.

The *wateq4f.dat* file is derived from WATEQ4F (Ball & Nordstrom, 1991). The database was developed by the U.S. Geological Survey and it contains most of the major and trace species, mineral phases and gas phases in natural water systems. It was developed to be used in a temperature range of 0 to 100 °C. All databases rely on different extensions of the Debye-Hückel expression (e.g. Davis; Eq. (2.6 – (2.8)) for the activity coefficient calculations.

One limitation of PHREEQC is the lack of internal consistency in the databases (Postma & Appelo, 2013). All of the databases are collections of log K and enthalpies of reactions from various literature sources. However, no systematic attempt has been made to determine the aqueous model used to develop the individual log K or the consistency of the aqueous models with the original experimental data. Thus, the databases should be thought of as preliminary.

5.1.1.2 Exchange Constants for the Cation Exchange Model (IX model)

An objective of the thesis was to estimate REE exchange constants. The problems with existing databases that contain exchange constants such as WATEQ4F and LLNL are: there are no log K values for the REE; the log K for exchange species available should be considered

for montmorillonite only (according to Tournassat *et al.,* 2007), and there are few or no references.

The equilibrium calculations based on the batch and CEC experimental datasets were implemented with exchange constants obtained from the WATEQ4F database. These are equivalent to those found in the LLNL database except for the exchange species AlX_3 which has log K = 0.41 and the additional species $AlOHX_2$ (which was added to *wateq4f.dat*).

The exchange reactions for the major and trace cations and the log K for the exchange reactions are:

(5.5) $H^+ + X^- = HX$ log K = 1.0

(5.6) $K^+ + X^- = KX$ log K = 0.7

(5.7) $Na^+ + X^- = NaX$ log K = 0.0

(5.8) $NH_4^+ + X^- = NH_4X$ log K = 0.6

(5.9) $Ca^{2+} + 2X^- = CaX_2$ log K = 0.8

(5.10) $Mg^{2+} + 2X^- = MgX_2$ log K = 0.6

(5.11) $Mn^{2+} + 2X^- = MnX_2$ log K = 0.52

(5.12) $Ba^{2+} + 2X^- = BaX_2$ log K = 0.91

(5.13) $Zn^{2+} + 2X^- = ZnX_2$ log K = 0.8

(5.14) $AlOH^{2+} + 2X^- = AlOHX_2$ log K = 0.89

(5.15) $Al^{3+} + 3X^- = AlX_3$ log K = 0.67

(5.16) $Fe^{3+} + 3X^- = FeX_3$ log K = 0.67

The log K values for the REE were determined using Eq. (5.17):

(5.17) $$K = \frac{[REEX_3]}{\{REE^{3+}\} \cdot [X^{3-}]}$$

where $[REEX_3]$ is the concentration of adsorbed species and $\{REE^{3+}\}$ is the activity of the aqueous REE species.

In the equilibrium calculations, activity corrections for all exchange species were considered using the parameter-free Davies formula in Eq. (2.7). This was due to the high ionic strength of the salt solution used in the experiments.

5.1.2 Verification of the CEC Results

Equilibrium calculations are presented to elucidate the CEC findings (§ 4.1) and to establish an explanation for the varying aluminium concentration in the presence of different

reactive solutions. Two different equilibrium calculations with each reactive solution were considered in PHREEQC (based on the log K values in Eq (5.5) to (5.16)):

- **Case 1:** without Al adsorbed on the clay
- **Case 2:** with Al adsorbed on the clay (as the major species occupying 72 %)

These two scenarios are shown to highlight the importance of Al in the Madagascar IAD.

In each calculation, the exchange composition of the IAD was taken from the CEC results shown in Appendix B. The initial load was put in equilibrium with each of the three solutions (in accordance with the experimental method) where the highly-concentrated cation, Ba^{2+}/NH_4^+, substituted for all other exchangeable cations on the clay.

The equilibrium calculations for both cases are shown in Fig 5.1, Fig 5.2 and Fig 5.3 with the $BaCl_2$, NH_4Cl and NH_4Ac solutions, respectively. In the chloride solution calculations, the aqueous species distribution mirrored the initial exchangeable load on the clay in both cases (Fig 5.1 and Fig 5.2). The main difference was the final pH.

Only case 2, in the presence of exchangeable Al, could reproduce the experimentally recognised drop in pH to pH 4. This suggests that high concentrations of exchangeable Al being mobilised into solution by a highly-concentrated cation was the reason for the pH drop. This result also indicates that it is the major exchangeable species on the Madagascar IAD.

An additional effect was observed in the case 2 theoretical calculations with NH_4Ac (Fig 5.3). NH_4^+ still replaces all the exchangeable cations on the clay (including Al), but, because the NH_4Ac solution acts as a buffer, resisting a pH change, the exchangeable Al was instead precipitated as gibbsite. As a result, no exchangeable Al was mobilised into solution.

When other Al oxide phases such as amorphous $Al(OH)_3$ were assumed to form, the model result did not agree with the measurement. This supported the assumption that the exchangeable Al precipitated in the form of gibbsite. However, this has not been confirmed by additional experimentation or analysis.

The NH_4Ac CEC shown in § 4.1 is an estimated value. It was recalculated to include precipitated Al (the concentration added to the CEC calculation was approximately 2.8 mM in correlation with concentration of Al measured in $BaCl_2$ and NH_4Cl CEC tests). The theoretical findings provide an explanation for the near absence of measured Al in the NH_4Ac CEC test (Fig. 4.1).

Fig 5.1 Chemical equilibrium calculations with a $BaCl_2$ solution.

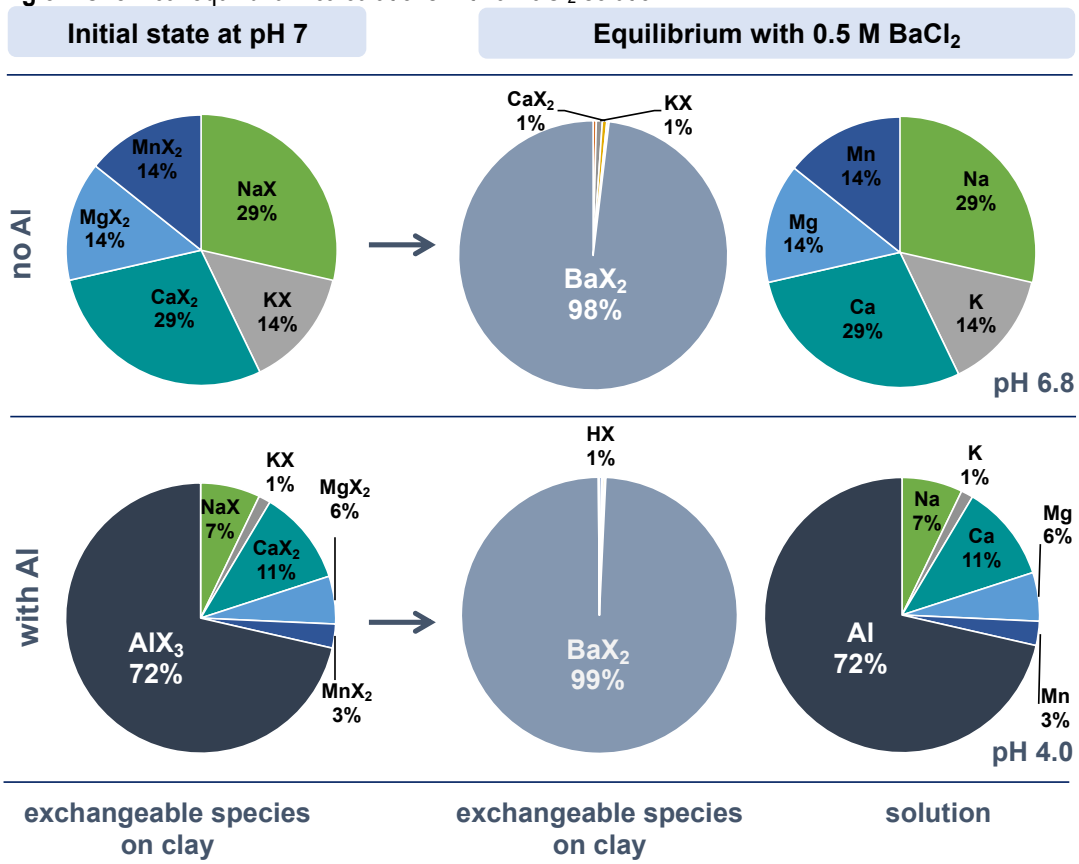

Fig 5.2 Chemical equilibrium calculations with a NH4Cl solution.

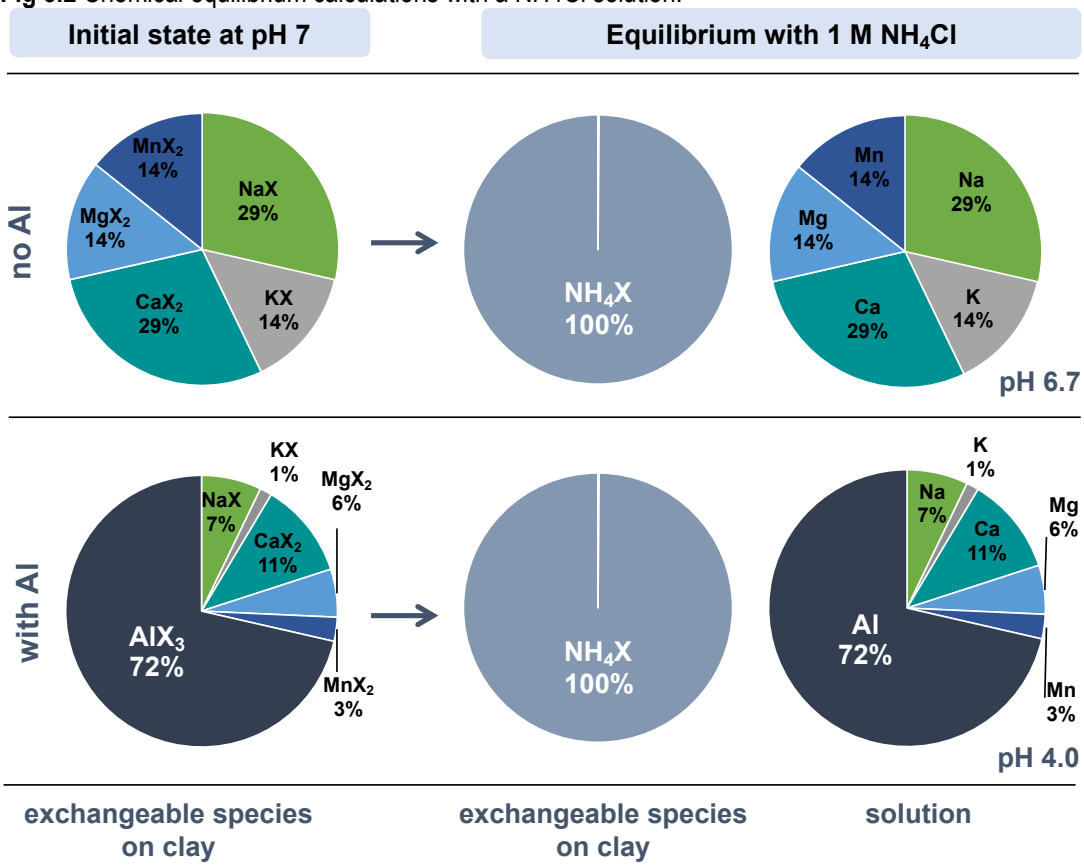

Fig 5.3 Chemical equilibrium calculations with a NH_4Ac solution.

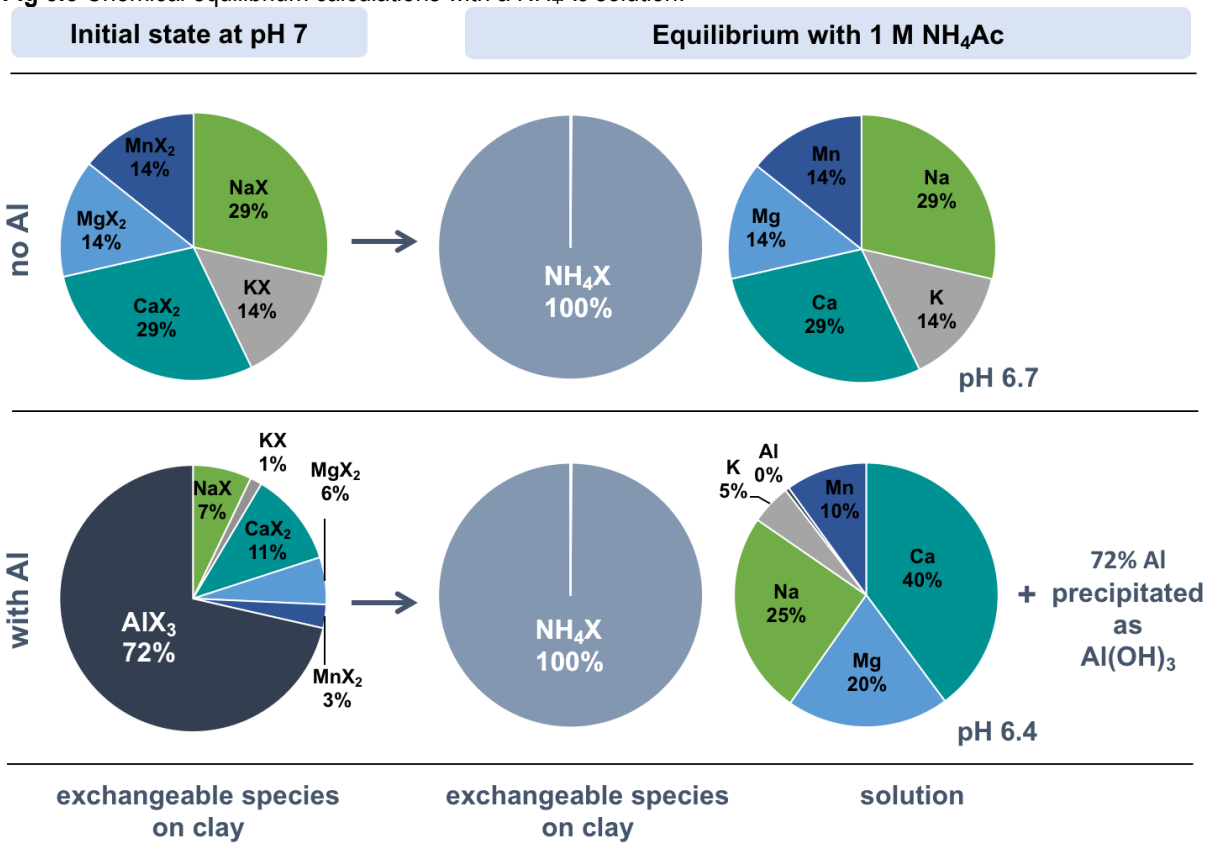

5.1.3 Modelling Approach to Estimate REE Exchange Constants

Equilibrium calculations were performed in PHREEQC to estimate the log K values that best fit the experimental data (in § 4.2) to describe REE exchange reactions with the Madagascar IAD. The modelling approach involved:

- Parameter study
  - ⇒ Test a variety of REE exchange constants (log K) to narrow the range within which to fit the parameter.
- Determination of a single log K for all REE
  - ⇒ The lanthanides have similar physicochemical properties, therefore, the assumption was made that one log K could describe REE-IAD exchange reactions.
- Sensitivity study
  - ⇒ Test the sensitivity of the exchange surface mineralogy by adjusting the exchange constants of the major cations.
- Improve the fit of the log K

⇒ Determine whether the log K fits the dataset better when a log K is estimated for each of the LREE and HREE and the REE.

The approach outlined above was used to estimate exchange constants for 13 of the REE (Y, La, Ce, Pr, Nd, Gd, Tb, Dy, Ho, Er, Tm, Yb and Lu). Exchange constants for Sm and Eu were estimated using a different approach (see § 4.2.1), which will be discussed in the following section (§ 5.1.4).

Equilibrium calculations were performed for each of the 13 REE. Because the modelled REE all showed the same trend, only 4 REE are shown in the figures in this section. La, Ce, Nd and Dy were chosen to represent the lanthanides because they are considered important in terms of their industrial applications and crustal abundance (§ 2.1.3).

Error bars that represent the standard deviation (SD) from triplicate batch tests are shown in all the figures for each of the 4 REE. The SD was included to represent the variance of the experimental dataset and thus the variance in the estimate exchange constants. The confidence intervals for La, Ce, Nd and Dy are ± 0.01, ± 0.1, ± 0.01 and ± 0.0003, respectively.

5.1.3.1 Parameter Study

The experimental dataset comprises exchangeable REE concentrations at 9 SLR that were mobilised into the aqueous phase by a concentrated barium chloride solution. Different SLR conditions were used to ensure that a different exchange composition from the Madagascar IAD would be seen in each of the 9 SLR (Fig. 4.3).

The log K values estimated from this dataset using the modelling approach (outlined in § 5.1.3) should therefore be able to describe REE exchange reactions in various experimental conditions. The dataset showed that the exchangeable REE concentration mobilised into solution increased with increasing SLR (the experimental dataset is shown in Appendix B).

A parameter study was undertaken to narrow the range within which to fit the REE exchange constants. It was assumed that one log K can describe ion exchange of all the REE. The modelling approach in PHREEQC was as follows:

[1] Define the exchange composition of the Madagascar IAD for each SLR condition using the C_{TOT} (Table 4.1; Eq. (5.18));

[2] Choose an initial seed value to use as the REE exchange constant;

[3] Run the PHREEQC simulation using the exchange composition in equilibrium with 0.5 M $BaCl_2$ solution (allowing exchange of REE^{3+} and major cations on clay for Ba^{2+}) and the chosen log K for all the SLR conditions (see Appendix C for model inputs);

[4] Compare the modelled exchangeable REE concentrations to measured concentrations, and

[5] Repeat step (2) with another log K value until the best description of the REE batch reactor dataset was achieved.

For each SLR condition, the exchange composition of the Madagascar IAD is calculated by:

$$C_{TOT} \equiv CEC \frac{meq}{100g} \cdot SLR \frac{g}{mL} \cdot 10 \quad (5.18)$$

The equivalent element fractions used to calculate the CEC with the barium chloride solution are shown in Table 5.1.

Table 5.1 Equivalent element fraction used to calculate the CEC.

	Element	Charge	Equivalent Fraction [meq/100g]
major and trace elements	Na	+1	0.47
	K	+1	0.08
	Ca	+2	0.63
	Mg	+2	0.41
	Mn	+2	0.01
	Zn	+2	1.41
	Ni	+2	0.00
	Cu	+2	0.24
	Al	+3	6.85
	Si	+4	0.02
REE	Y	+3	3.88E-03
	La	+3	1.65E-02
	Ce	+3	9.34E-02
	Pr	+3	1.69E-03
	Nd	+3	9.88E-03
	Sm	+3	6.23E-02
	Eu	+3	3.44E-02
	Gd	+3	1.51E-04
	Tb	+3	4.68E-05
	Dy	+3	2.33E-04
	Ho	+3	2.76E-05
	Er	+3	7.46E-05
	Tm	+3	1.78E-05
	Yb	+3	1.73E-05
	Lu	+3	1.82E-05
CEC [meq/100g]			10.34

The contribution of each exchange species in each SLR condition to the exchange composition of the Madagascar IAD was calculated by:

$$X_e \equiv E_e \frac{meq}{100g} \cdot SLR \frac{g}{mL} \cdot 10 = E_x \frac{meq}{L} \quad (5.19)$$

where X is the exchange species of element e, E is the equivalent fraction of element e in the CEC experiment [meq/100g] and E_x is the equivalent fraction of the exchange species X contribution to the C_{TOT} [meq/L].

For example, the major and trace exchange species in the 0.11 SLR condition are defined as:

$$NaX \equiv 0.47 \frac{meq}{100g} \cdot 0.11 \frac{g}{mL} \cdot 10 = 0.52 \frac{meq}{L} \quad (5.20)$$

$$KX \equiv 0.08 \frac{meq}{100g} \cdot 0.11 \frac{g}{mL} \cdot 10 = 0.09 \frac{meq}{L} \quad (5.21)$$

$$CaX_2 \equiv 0.63 \frac{meq}{100g} \cdot 0.11 \frac{g}{mL} \cdot 10 = 0.70 \frac{meq}{L} \quad (5.22)$$

$$MgX_2 \equiv 0.41 \frac{meq}{100g} \cdot 0.11 \frac{g}{mL} \cdot 10 = 0.45 \frac{meq}{L} \quad (5.23)$$

$$MnX_2 \equiv 0.01 \frac{meq}{100g} \cdot 0.11 \frac{g}{mL} \cdot 10 = 0.01 \frac{meq}{L} \quad (5.24)$$

$$ZnX_2 \equiv 1.41 \frac{meq}{100g} \cdot 0.11 \frac{g}{mL} \cdot 10 = 1.55 \frac{meq}{L} \quad (5.25)$$

$$CuX_2 \equiv 0.24 \frac{meq}{100g} \cdot 0.11 \frac{g}{mL} \cdot 10 = 0.27 \frac{meq}{L} \quad (5.26)$$

$$AlX_3 \equiv 6.85 \frac{meq}{100g} \cdot 0.11 \frac{g}{mL} \cdot 10 = 7.53 \frac{meq}{L} \quad (5.27)$$

Table 5.2 defines the entire exchange composition for SLR condition = 0.11. The cations Si^{4+} and Ni^{2+} are not included in the ion exchange modelling because there are no exchange constants for the species SiX_4 and NiX_2 in any of the PHREEQC databases.

Table 5.2 Input conditions that define the exchange composition for SLR condition = 0.11.

	IX species	Reaction	log K	Equivalent Fraction [meq/L]
major and trace exchange species	NaX	$Na^+ + X^- = NaX$	0.0	0.52
	KX	$K^+ + X^- = KX$	0.7	0.09
	CaX_2	$Ca^{2+} + 2X^- = CaX_2$	0.8	0.70
	MgX_2	$Mg^{2+} + 2X^- = MgX_2$	0.6	0.45
	MnX_2	$Mn^{2+} + 2X^- = MnX_2$	0.52	0.01
	CuX_2	$Cu^{2+} + 2X^- = CuX_2$	0.6	0.27
	ZnX_2	$Zn^{2+} + 2X^- = ZnX_2$	0.8	1.55
	AlX_3	$Al^{3+} + 3X^- = AlX_3$	0.67	7.53
REE	YX_3	$Y^{3+} + 3X^- = YX_3$	2.29	4.27E-03
	LaX_3	$La^{3+} + 3X^- = LaX_3$	2.29	1.81E-02
	CeX_3	$Ce^{3+} + 3X^- = CeX_3$	2.29	1.03E-01
	PrX_3	$Pr^{3+} + 3X^- = PrX_3$	2.29	1.86E-03
	NdX_3	$Nd^{3+} + 3X^- = NdX_3$	2.29	1.09E-02
	GdX_3	$Gd^{3+} + 3X^- = GdX_3$	2.29	1.67E-04
	TbX_3	$Tb^{3+} + 3X^- = TbX_3$	2.29	5.15E-05
	DyX_3	$Dy^{3+} + 3X^- = DyX_3$	2.29	2.56E-04
	HoX_3	$Ho^{3+} + 3X^- = HoX_3$	2.29	3.04E-05
	ErX_3	$Er^{3+} + 3X^- = ErX_3$	2.29	8.21E-05
	TmX_3	$Tm^{3+} + 3X^- = TmX_3$	2.29	1.95E-05
	YbX_3	$Yb^{3+} + 3X^- = YbX_3$	2.29	1.91E-05
	LuX_3	$Lu^{3+}\ 3X^- = LuX_3$	2.29	2.00E-05
			C_{TOT} [meq/L]	11.3

Fig 5.4 illustrates an example from the parameter study, where calculated and measured REE concentrations are compared. For each SLR condition, three equilibrium calculations are shown that are based on three log K values:

- log K = 1.3
- log K = 2.3 ⇐ best visual fit value
- log K = 3.3

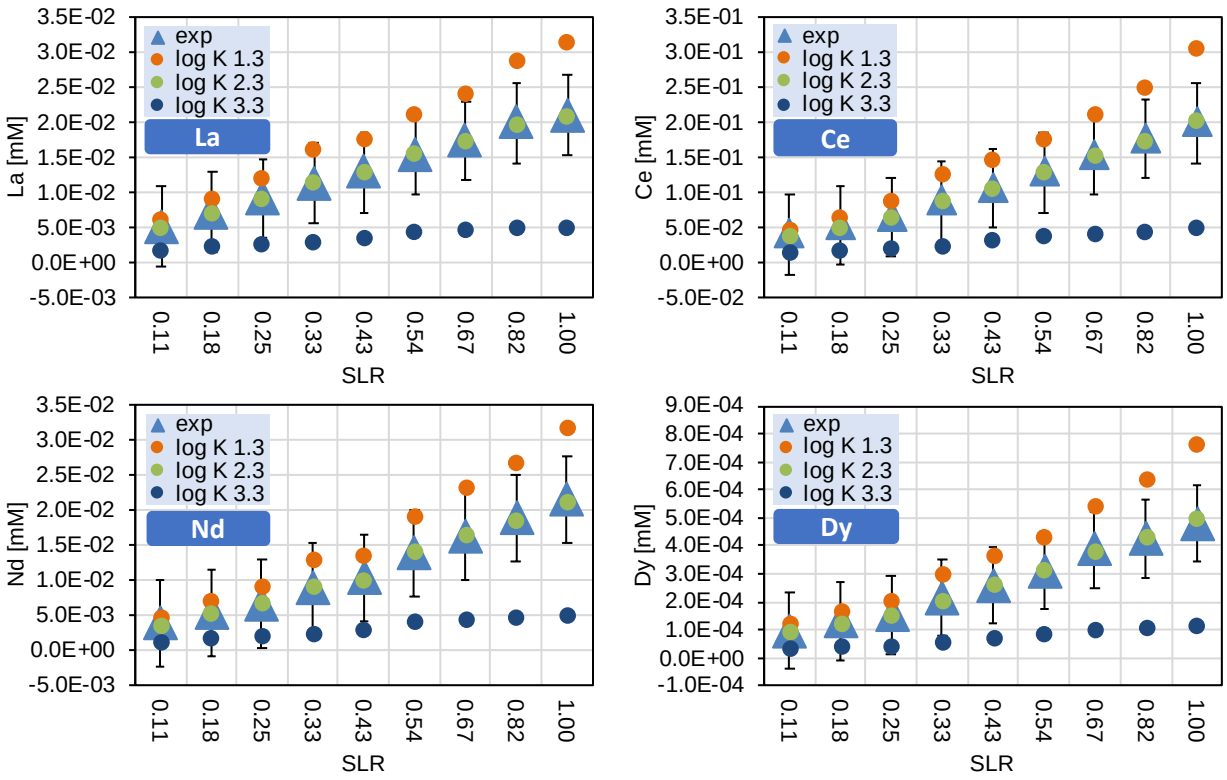

Fig 5.4 Parameter study of different log K for all the REE. The error bars represent the standard deviation.

The model showed that increasing the log K decreased the exchangeable REE concentration mobilised into solution. This was because the REE were more strongly bound to the exchanger surface. Since there is only a literature source that contains an exchange constant describing Eu exchange reactions with kaolinite surfaces (Tertre *et al.,* 2006a), the parameter study narrowed the range to fit the log K.

The results of the parameter study (in Fig 5.4) are also shown in Fig 5.5 for the major exchangeable cation (Al^{3+}) on the Madagascar IAD, where the three equilibrium calculations for the REE are compared to calculated and measured Al concentrations. The equilibrium model in which a log K = 2.3 represents all REE exchange reactions with the Madagascar IAD was observed to best fit the Al dataset.

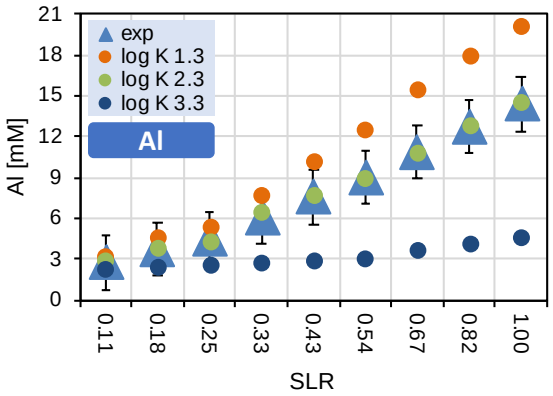

Fig 5.5 Exchangeable Al with different REE log K models.

5.1.3.2 Determination of a Single log K value for all the REE

PEST (Doherty, 1994), a parameter optimisation tool, was used in conjunction with PHREEQC to extract the equilibrium constants from the REE experimental dataset that describe REE exchange reactions with the Madagascar IAD.

PEST was able to take control of the existing PHREEQC model (described in § 5.1.3.1). Parameter optimisation was achieved using the Guass-Marquardt-Levenberg method for which the discrepancies between the model-generated numbers and the corresponding measured data were reduced to a minimum in the weighted least squares sense.

A single equilibrium constant was assumed to describe all REE exchange reactions with the Madagascar IAD. The equilibrium model that best described the REE dataset with PHREEQC (visual fit) and PEST (least squares fit) are shown in Fig 5.6. The best fit log K value for all of the REE was:

(5.28) $REE^{3+} + 3X^{-} = REEX_3$ log K = 2.30 ± standard deviation in PHREEQC

(5.29) $REE^{3+} + 3X^{-} = REEX_3$ log K = 2.29 ± standard deviation in PEST

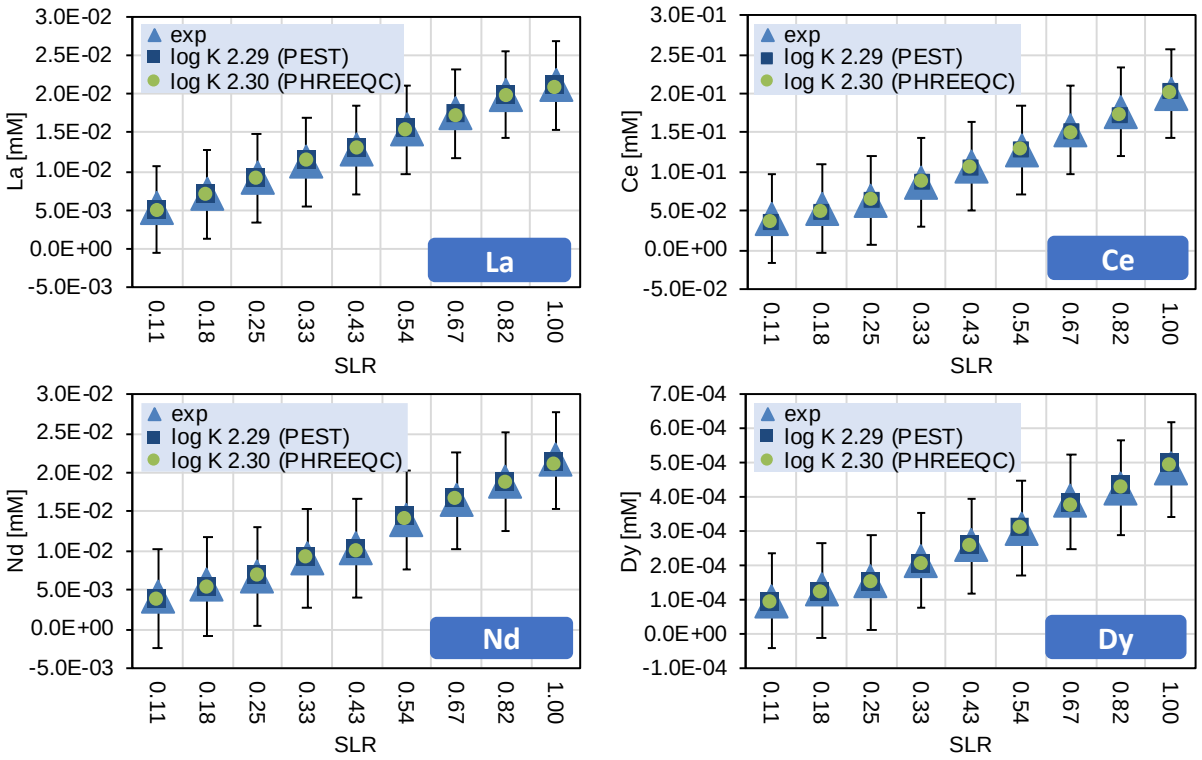

Fig 5.6 PEST and PHREEQC equilibrium calculations compared to the measured REE dataset.

PEST produces an objective function value for each model calculation. The objective function of a linear programming problem is to minimise or to maximise a numerical value. In the case of optimisation in PEST, the objective function to be minimised is the difference between the experimental data and the corresponding model generated numbers.

The objective function takes the following general form:

(5.30) minimise or maximise $Z = \sum_{i=t}^{n} c_i X_i$

where c_i is the objective function coefficient corresponding to the i^{th} variable, and X_i is i^{th} the decision variable.

The objective function was also determined for the PHREEQC calculation using Eq (5.30). The PEST calculation leads to a lower objective function (5.724×10^{-11}) than the PHREEQC calculation (9.281×10^{-11}). Thus the log K in Eq. (5.29) provides a better fit.

PEST produces 95% confidence upper and lower limits, thus the log K value becomes:

(5.31) $REE^{3+} + 3X^{-} = REEX_3$ log K = 2.290 ± 0.005

However this does not take into account the standard deviation of the experimental dataset. Therefore, the standard deviation was shown in Fig. 5.6 to signify the range within which the log K values could vary for each REE.

5.1.3.3 Sensitivity Study

The log K values in Eq. (5.5) to (5.15) were used in all the model calculations shown in § 5.1.3.1 and § 5.1.3.2. However, there are little to no references for these constants and they should be considered for montmorillonite only (Tournassat *et al.,* 2007).

Therefore, it was important to consider whether adjusting the ion exchange constants for the major exchange species would be able to improve the model of the experimental REE dataset and thus be considered for kaolinite (Table 1.1).

The log K values for the ion exchange reactions of the major cations (Ba^{2+} and Al^{3+}) were varied in PHREEQC to test the sensitivity of the estimated REE exchange constants to exchange surface mineralogy by comparing different constants to those used in the database for montmorillonite.

Ba^{2+} was considered a major cation in addition to Al^{3+} because a highly concentrated barium chloride solution was used in the batch reactor tests to saturate the clay, where Ba^{2+} exchanged for all the cations on the clay.

Fig 5.7 compares calculated and measured exchangeable REE[21] concentrations for nine SLR values. For each SLR three equilibrium models, each with different log K values for BaX_2 exchange species, are shown:

(5.32) $Ba^{2+} + 2X^- = BaX_2$ log K = -0.09

(5.33) $Ba^{2+} + 2X^- = BaX_2$ log K = 0.91 $\Leftarrow$ best visual fit value

(5.34) $Ba^{2+} + 2X^- = BaX_2$ log K = 1.91

In each model, LaX_3 was given the standard value of log K = 2.29.

[21] La^{3+} represents the entire lanthanide series

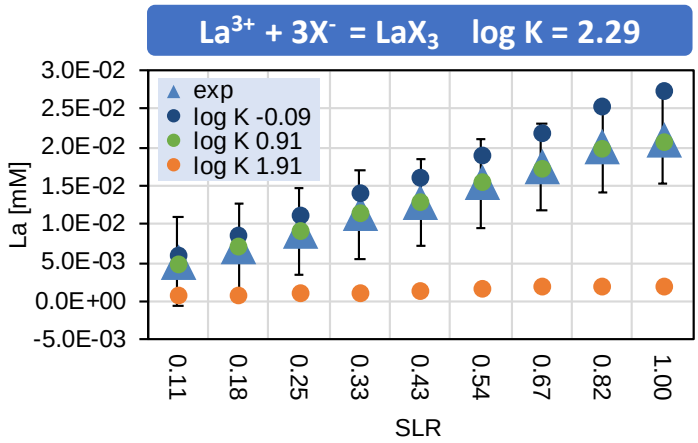

Fig 5.7 Sensitivity study investigating the effect of Ba on the REE.

The log K for the BaX_2 exchange species in Eq. (5.12) from the WATEQ4F thermodynamic database provides the best description of the experimental REE concentrations. The different models also highlight that the REE are very sensitive to changes in the log K value for BaX_2 exchange species.

The log K of the $REEX_3$ and BaX_2 were also adjusted to determine whether further improvements to the parameter values of the estimated REE exchange constants were possible. Fig 5.8 shows a sensitivity study in which the log K values for BaX_2 and the $REEX_3$ were varied. In each diagram, a single log K was assigned to all the $REEX_3$:

(5.35) $La^{3+} + 3X^- = LaX_3$ log K = 0.29

(5.36) $La^{3+} + 3X^- = LaX_3$ log K = 1.29

(5.37) $La^{3+} + 3X^- = LaX_3$ log K = 3.29

Each diagram shows three equilibrium models where the log K of BaX_2 was varied (see Eq. (5.32) to (5.34)).

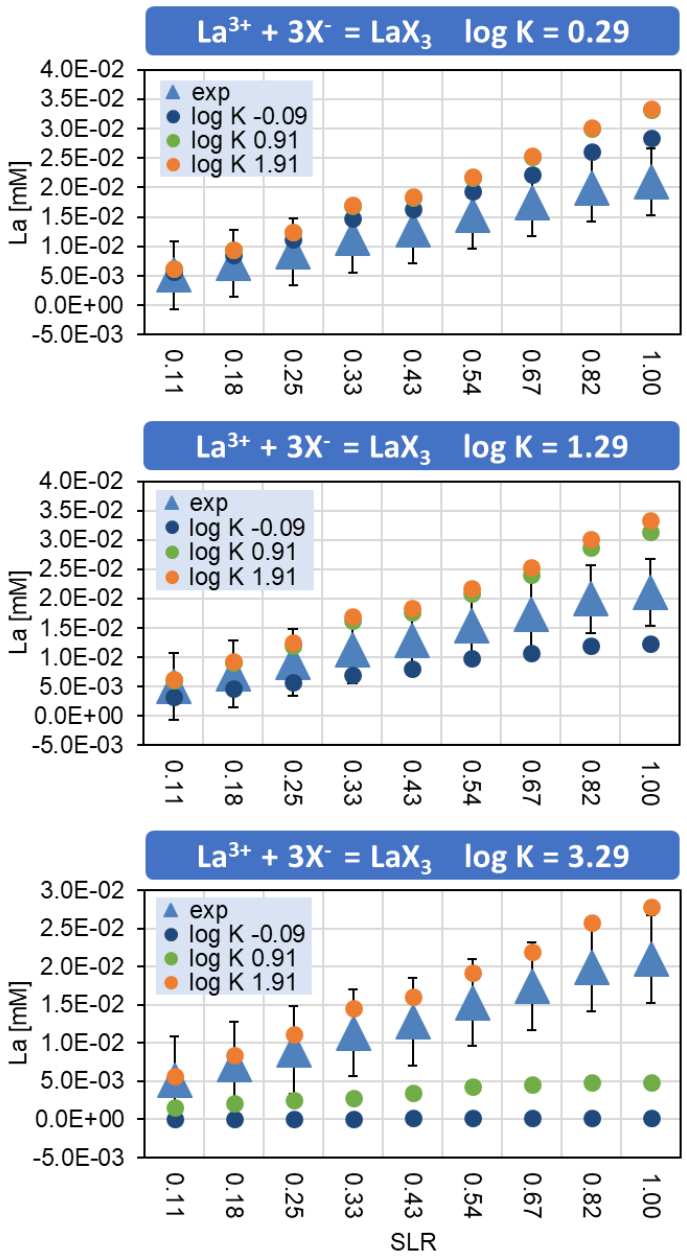

Fig 5.8 Sensitivity study investigating the effect of Ba on the REE.

The model calculations in Fig 5.8 show that the calculated exchangeable REE concentration mobilised into solution was affected by changes to the log K values, especially when the log K for the REE was higher. However, a better description of the experimental dataset with the constants in Eq. (5.35) to (5.37) was not achieved.

The experimental CEC results indicated that Al^{3+} was the major exchangeable cation on the Madagascar IAD (see § 4.1). Thus, changing the log K value for the AlX_3 exchange species was expected to strongly affect the exchangeable REE concentration.

Fig 5.9 compares calculated and measured exchangeable REE concentrations for nine SLR conditions. For each SLR three equilibrium models each with different log K values for AlX_3 exchange species are shown:

(5.38) $Al^{3+} + 3X^- = AlX_3$ log K = -0.06

(5.39) $Al^{3+} + 3X^- = AlX_3$ log K = 0.67 ⇐ best visual fit value

(5.40) $Al^{3+} + 3X^- = AlX_3$ log K = 1.67

In each model, LaX_3 was assigned the standard value of log K = 2.29.

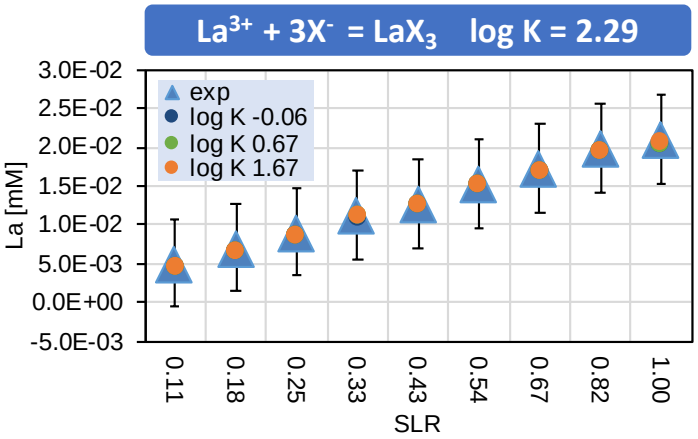

Fig 5.9 Sensitivity study investigating the effect of Al on the REE[22].

It was apparent from the adjustments made to the log K value for AlX_3 (each by an order of magnitude) and the minor variation in the exchangeable REE concentrations that the REE are relatively insensitive to Al. Thus, the log K value in Eq. (5.15) from the WATEQ4F database was found to best describe REE exchange with the Madagascar IAD.

The log K values of the $REEX_3$ and AlX_3 were adjusted. Fig 5.10 shows the results of a sensitivity study where the exchange constants for AlX_3 and the $REEX_3$ were varied. A single log K value was assigned to all the REE (see Eq. (5.35) to (5.37)). Each diagram shows three equilibrium models where the log K of AlX_3 was varied (see Eq. (5.38) to (5.40)).

[22] The data points are not affected by changes to the log K of AlX_3, thus they overlap.

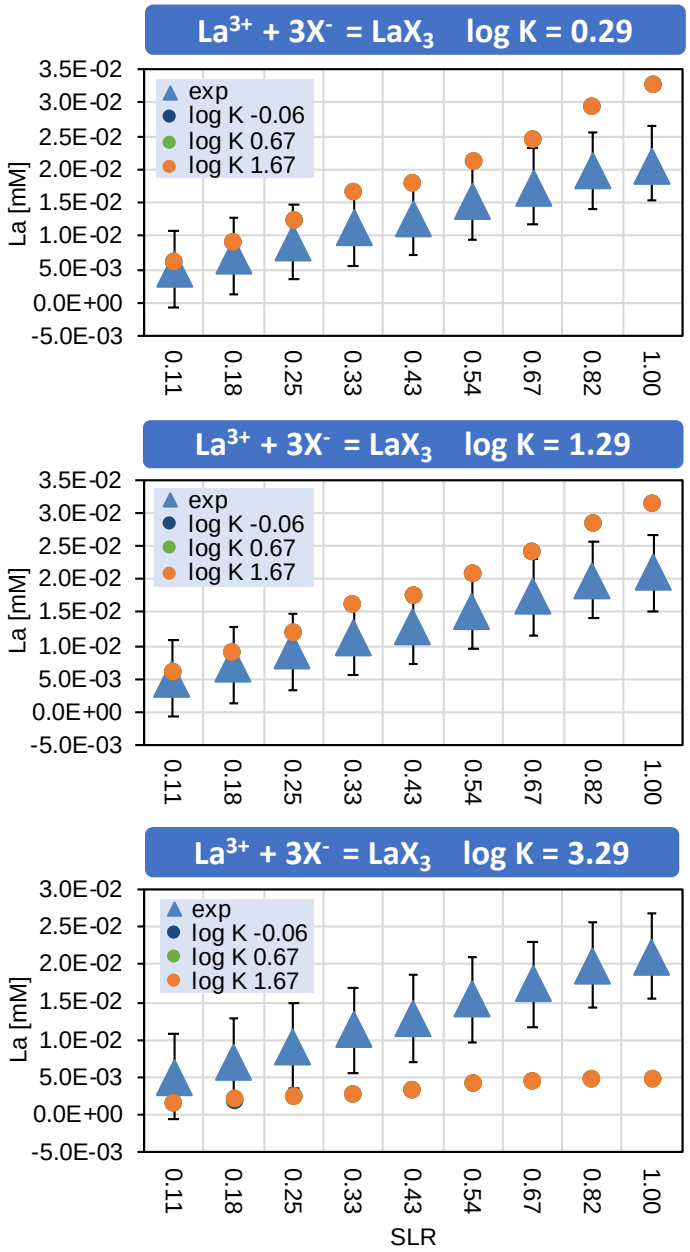

Fig 5.10 Sensitivity study for Al and the REE[23].

The equilibrium calculations indicate that the modelled REE and Al concentrations were unaffected by changes to the log K values. The only observed effect was seen when the log K for the $REEX_3$ exchange species was varied. The different Al models did not influence the modelled REE concentrations.

The outcomes of the sensitivity study with the major exchangeable cations and REE support the model calculations in § 5.1.3.2, where the ion exchange reactions in the experimental REE dataset were best described by log K = 2.29 and log K values from the WATEQ4F database for minor and major cations (in Eq. (5.5) to (5.15)).

[23] The data points are not affected by changes to the log K of AlX_3, thus they overlap.

The study also indicates that the non-REE ions are not sensitive to the mineral exchange surface assuming that the exchange constants in the database are based on montmorillonite (stated in Tournassat *et al.,* 2007). This because the model calculations above demonstrate the database values are consistent with observations on kaolinite.

Another interesting outcome of the log K = 2.29 model for all the $REEX_3$ exchange species implies that the REE are more strongly bound to the IAD exchanger surface than the other trivalent species, AlX_3 and FeX_3, in the WATEQ4F database, which both have a log K = 0.67 (Eq. (5.15) and (5.16)).

5.1.3.4 log K values for the LREE and HREE

Once the single log K for all REE was determined in § 5.1.3.2 and a sensitivity study supported the findings in § 5.1.3.3, improvements to the modelling approach were undertaken using the PEST optimiser.

Fractionation between the LREE and HREE was observed in Madagascar IAD (Fig. 2.2), where the HREE are more strongly bound than the LREE. Therefore, an equilibrium model was implemented, in which one log K value was assigned to the HREE and one to the LREE.

The model calculations for the LREE and HREE are compared to the experimental dataset in Fig 5.11. Optimisation in PEST indicated that:

(5.41) log K = 2.289 for LREE (La, Ce, Pr and Nd)

(5.42) log K = 2.283 for HREE (Gd, Tb, Dy, Ho, Er, Tm, Yb, Lu and Y)

best described the measured REE concentrations. Very small differences between the log K value for the LREE and HREE (to 3 decimal places) were observed.

The least squares objective function for this calculation was 5.723×10^{-11} compared to 5.724×10^{-11} in the single log K model. This indicates that a slightly better fit was observed when one log K was assigned to both the HREE and LREE rather than when a single exchange constant was used to describe all REE exchange reactions with the Madagascar IAD.

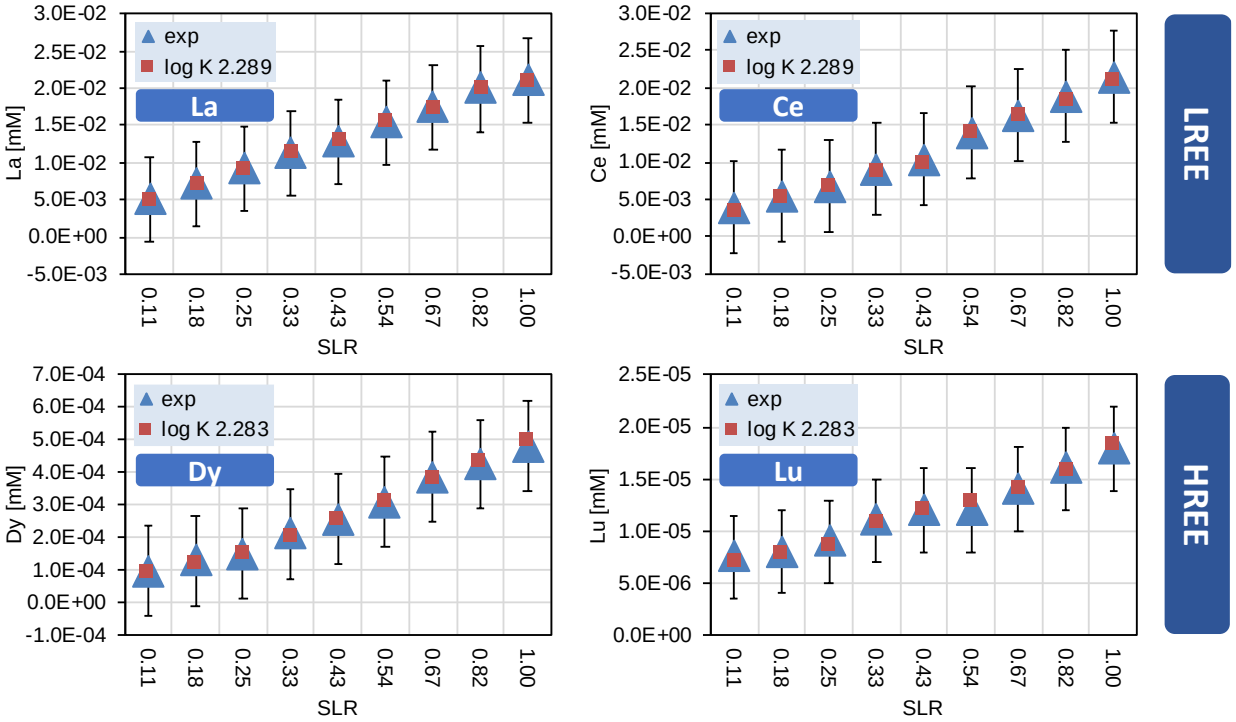

Fig 5.11 LREE and HREE log K parameter set compared to measured REE exchangeable concentrations.

5.1.3.5 Individual log K values for REE

The REE are a chemically similar group of trace elements. However, there are small chemical differences between the REE (i.e. the decrease in ionic radii with increasing atomic number, § 2.1.1). These differences could be observed in their exchange behaviour.

Fine-tuning of the modelling approach showed that an individual log K for each REE (in PEST) would better be able to describe REE exchange reactions. Table 5.3 includes the individual equilibrium constants for REE exchange with the Madagascar IAD.

Table 5.3 Equilibrium constants for REE exchange reactions.

IX Species	Reactions	log K ± SD
YX_3	$Y^{3+} + 3X^- = YX_3$	2.27978 ± 0.00174
LaX_3	$La^{3+} + 3X^- = LaX_3$	2.28539 ± 0.01141
CeX_3	$Ce^{3+} + 3X^- = CeX_3$	2.28987 ± 0.11344
PrX_3	$Pr^{3+} + 3X^- = PrX_3$	2.26463 ± 0.00208
NdX_3	$Nd^{3+} + 3X^- = NdX_3$	2.28198 ± 0.01245
GdX_3	$Gd^{3+} + 3X^- = GdX_3$	2.29588 ± 0.00053
TbX_3	$Tb^{3+} + 3X^- = TbX_3$	2.29588 ± 0.00005
DyX_3	$Dy^{3+} + 3X^- = DyX_3$	2.29793 ± 0.00028
HoX_3	$Ho^{3+} + 3X^- = HoX_3$	2.301131 ± 0.00003
ErX_3	$Er^{3+} + 3X^- = ErX_3$	2.28808 ± 0.00008
TmX_3	$Tm^{3+} + 3X^- = TmX_3$	2.28764 ± 0.00001
YbX_3	$Yb^{3+} + 3X^- = YbX_3$	2.29237 ± 0.00008
LuX_3	$Lu^{3+} + 3X^- = LuX_3$	2.29434 ± 0.00001

Fig 5.12 compares the single and individual log K best fit calculations to the measured REE dataset. The visible differences between the single log K model and the individual log K model were minimal. The objective function value reflects this, decreasing from 5.72 x 10^{-11} for the single log K model compared to 5.71 x 10^{-11} for the different log K model.

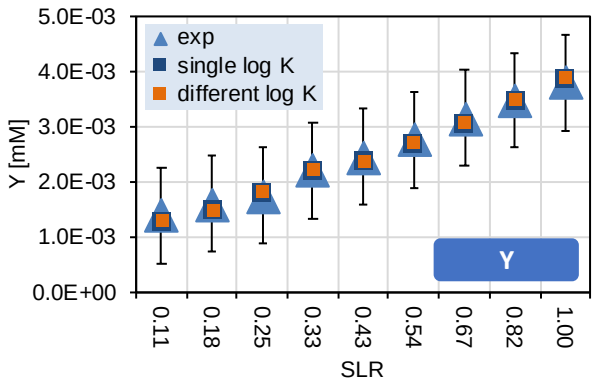

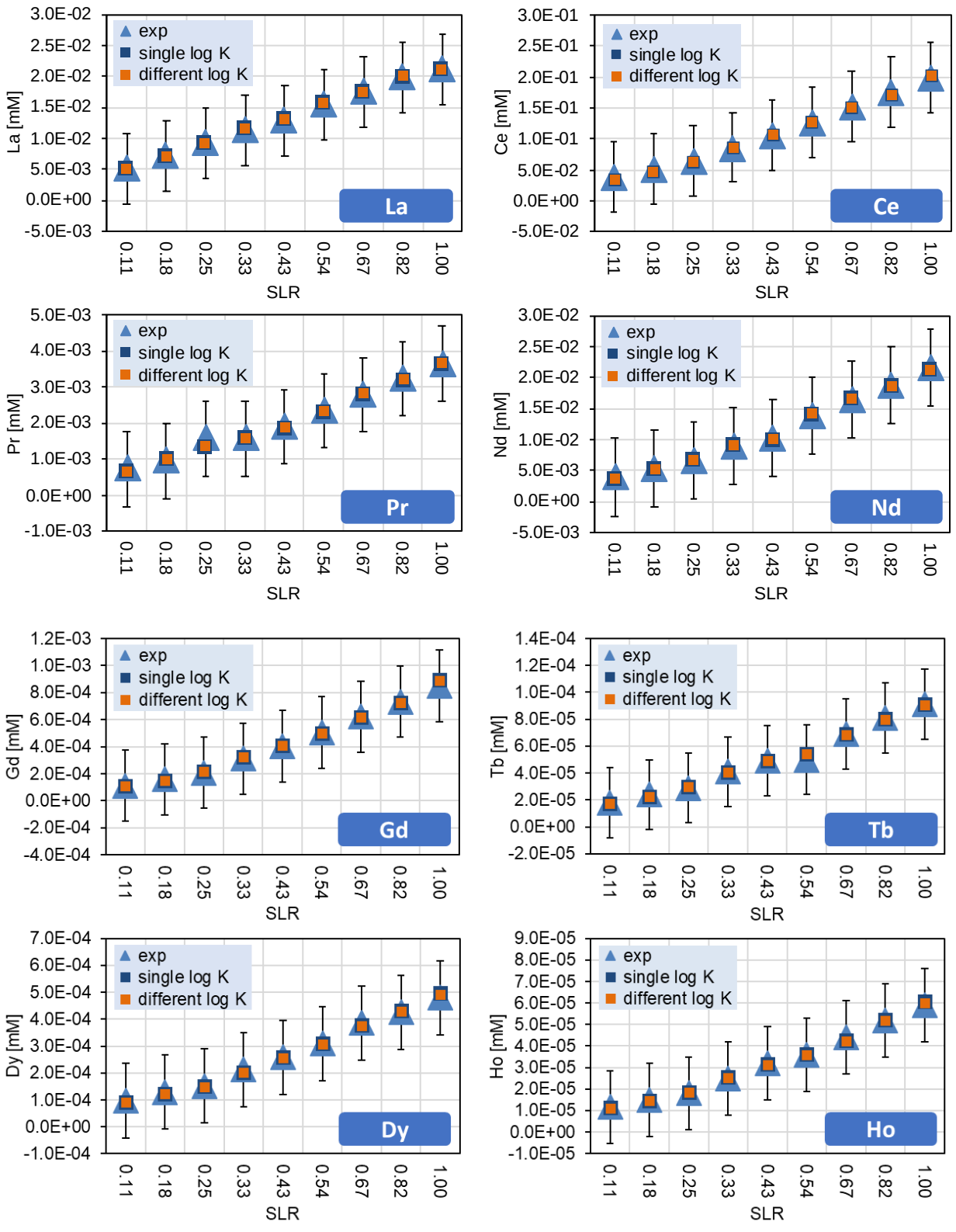
exp
single log K
different log K
La [mM]
3.0E-02
2.5E-02
2.0E-02
1.5E-02
1.0E-02
5.0E-03
0.0E+00
-5.0E-03
La
Ce [mM]
3.0E-01
2.5E-01
2.0E-01
1.5E-01
1.0E-01
5.0E-02
0.0E+00
-5.0E-02
Ce
Pr [mM]
5.0E-03
4.0E-03
3.0E-03
2.0E-03
1.0E-03
0.0E+00
-1.0E-03
Pr
Nd [mM]
3.0E-02
2.5E-02
2.0E-02
1.5E-02
1.0E-02
5.0E-03
0.0E+00
-5.0E-03
Nd
Gd [mM]
1.2E-03
1.0E-03
8.0E-04
6.0E-04
4.0E-04
2.0E-04
0.0E+00
-2.0E-04
-4.0E-04
Gd
Tb [mM]
1.4E-04
1.2E-04
1.0E-04
8.0E-05
6.0E-05
4.0E-05
2.0E-05
0.0E+00
-2.0E-05
Tb
Dy [mM]
7.0E-04
6.0E-04
5.0E-04
4.0E-04
3.0E-04
2.0E-04
1.0E-04
0.0E+00
-1.0E-04
Dy
Ho [mM]
9.0E-05
8.0E-05
7.0E-05
6.0E-05
5.0E-05
4.0E-05
3.0E-05
2.0E-05
1.0E-05
0.0E+00
-1.0E-05
Ho
0.11
0.18
0.25
0.33
0.43
0.54
0.67
0.82
1.00
SLR

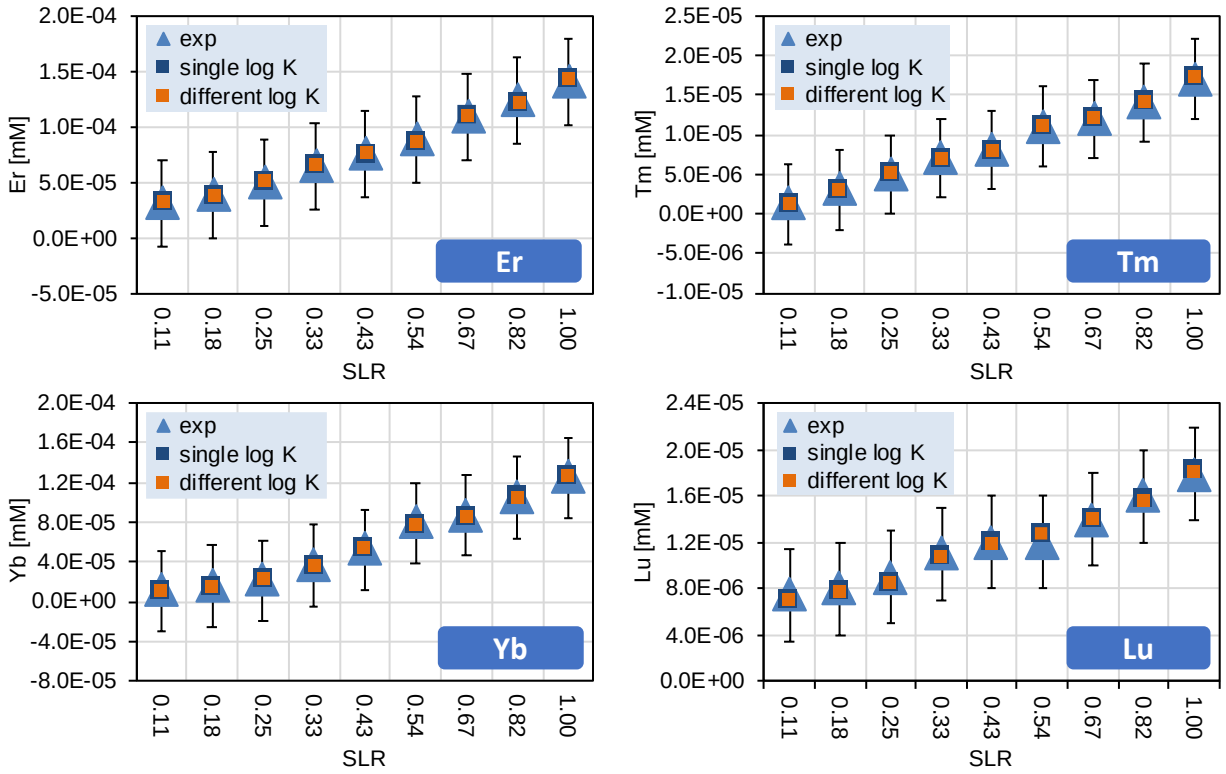

Fig 5.12 The single and individual log K best fit calculations are compared the measured REE dataset.

5.1.4 Extrapolation of Exchange Constants for Sm and Eu

Sm and Eu could not be accurately resolved from the experimental dataset (see § 4.2.1). This meant that their exchange constants could not be determined using the modelling approach described in § 5.1.3. This section describes the modelling approach to estimate the equilibrium constants for Sm and Eu exchange with the Madagascar IAD.

Because the lanthanides are chemically similar in atomic structure, they also behave similarly in terms of chemical reaction properties including the free energy of ion exchange reactions and the corresponding thermodynamic constants (see § 2.1.1). Therefore, Sm and Eu were expected to behave as the rest of the REE did in the batch reactor dataset (§ 4.2).

The majority of the REE in the Madagascar IAD are bound to the clay mineral surface in the exchangeable position (Chi *et al.,* 2006; Jun *et al.,* 2010) and, when in contact with a concentrated salt solution, these exchangeable cations will be mobilised into solution. The batch and CEC experiments and PHREEQC equilibrium calculations support this assertion.

The assumption was therefore made that the solid Sm and Eu concentrations measured for the IAD sample[24] represent the total exchangeable amount of each species and experimental value for the 1:1 (1.00) SLR condition (i.e. where the highest exchangeable concentration was observed). The solid concentrations for the other 13 REE were also compared to the reliable experimental values for the 1:1 SLR condition and found to be similar.

The remaining 8 SLR conditions (0.11 – 0.82) were approximated from the exchangeable REE concentration differences between SLR 1.00 and SLR 0.82 to give a Sm and Eu values for the 0.82 SLR condition, then the exchangeable REE concentration differences between SLR 0.82 and 0.67 to provide values for the 0.67 SLR condition etc. Table 5.4 shows the expected Sm and Eu concentrations for the experimental dataset.

Table 5.4 Estimated Sm and Eu concentrations.

SLR [g/mL]	Sm [mM]	Eu [mM]
0.11	0.00029	0.000037
0.18	0.00042	0.000044
0.25	0.00048	0.000049
0.33	0.00052	0.000059
0.43	0.00069	0.000084
0.54	0.00086	0.000119
0.67	0.00119	0.000145
0.82	0.00173	0.000182
1.00	0.00209	0.000231

Once the experimental dataset was defined, an equilibrium model was developed in PHREEQC and, in conjunction with PEST, a single exchange constant was calculated:

(5.43) $REE^{3+} + 3X^{-} = REEX_3$ $\log K = 2.29$

This value correlates exactly with the previously calculated log K to describe all the REE exchange reactions with the Madagascar IAD with a single constant.

Fine-tuning of the modelling approach considered an individual log K for each REE:

(5.44) $Sm^{3+} + 3X^{-} = SmX_3$ $\log K = 2.28164 \pm 0.00057$[25]

(5.45) $Eu^{3+} + 3X^{-} = EuX_3$ $\log K = 2.28131 \pm 0.00006$

[24] BGS measured total element concentrations in sample 593 by Na_2O_2 fusion with an ICP-MS finish. Total Sm and Eu in the sample 593 was 2.08 mg/kg and 0.35 mg/kg, respectively.

[25] Estimated standard deviation of Sm and Eu.

In this model, the log K values for the 13 other lanthanides were given the estimated individual exchange constants reported in Table 5.3.

Fig 5.13 compares the single and individual log K best fit calculations to the measured Sm and Eu dataset. It is important to note that while the log K for SmX_3 and EuX_3 reflect the behaviour of the rest of REE (as expected) these values should be considered preliminary.

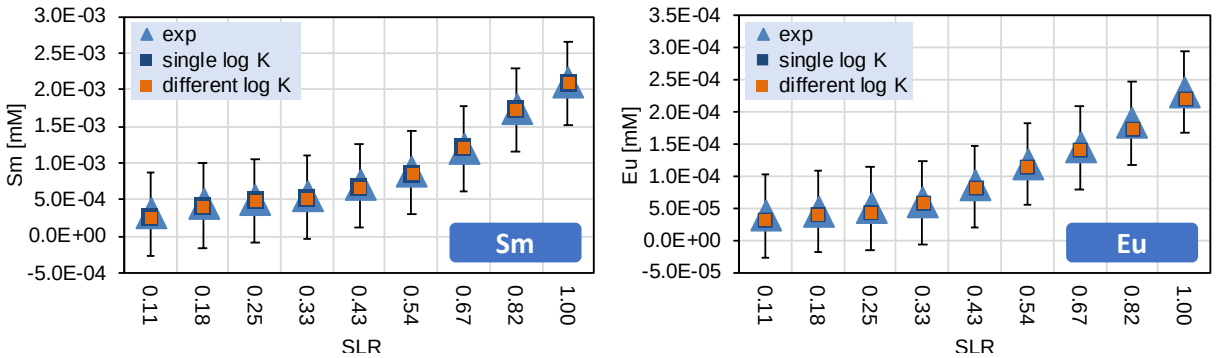

Fig 5.13 The single and individual log K best fit calculations are compared to the extrapolated Sm and Eu dataset

5.2 Reactive Transport Modelling

Reactive transport calculations were performed in TRN (UIT's in-house software) to simulate solute transport in IX columns (sorption/elution) by modelling REE breakthrough curves with the exchange constants that were estimated in § 5.1.3. The input files for the TRN models are shown in Appendix C.

5.2.1 TRN Model Description

The reactive transport model, TRN (Kalka, 2018), combines transport with geochemical reactions (thermodynamics and kinetics) and comprises three main parts (see Fig 5.14). The model has a modular design consisting of groups of independent subroutines that carry out specific simulation tasks with PHREEQC version 3 (Parkhurst & Appelo, 2013).

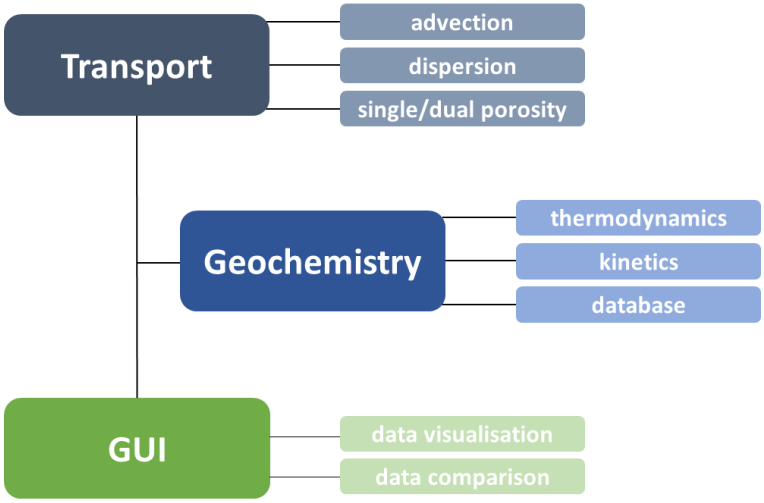

Fig 5.14 Modular structure of TRN (Kalka, 2018).

Reactive transport models that discretise the advection reaction dispersion (ARD) equation (Eq. (2.27)) may incur problems because small concentration variations are not apparent due to numerical dispersion. TRN adopted the ideas of Appelo & Postma (2013) and is free from numerical dispersion.

The time-spatial discretisation (Δx, Δt) for a numerical dispersion free simulation depends on the flow velocity, v (m/h)

$$v = \frac{\Delta x}{\Delta t} \tag{5.46}$$

No numerical dispersion means the calculated concentration fronts are only influenced by calculated effects of hydrodynamic dispersion as represented in the transport equation.

The three components of the ARD equation are calculated sequentially in TRN for a 1D column or flowline. The column is divided into a number, N, of cells. Fig 5.15 illustrates the discretisation of the flowline in a number of cells. One timestep (also known as a shift in PHREEQC) moves the mobile cell contents into the next cell.

Subsequently, the reactions between the immobile entities (exchangers, minerals etc.) and the solution are calculated. Dispersion is then calculated for each timestep by mixing the contents of the adjacent cells. This is followed by calculating reactions between the mobile and immobile entities. During the next timestep, everything is repeated.

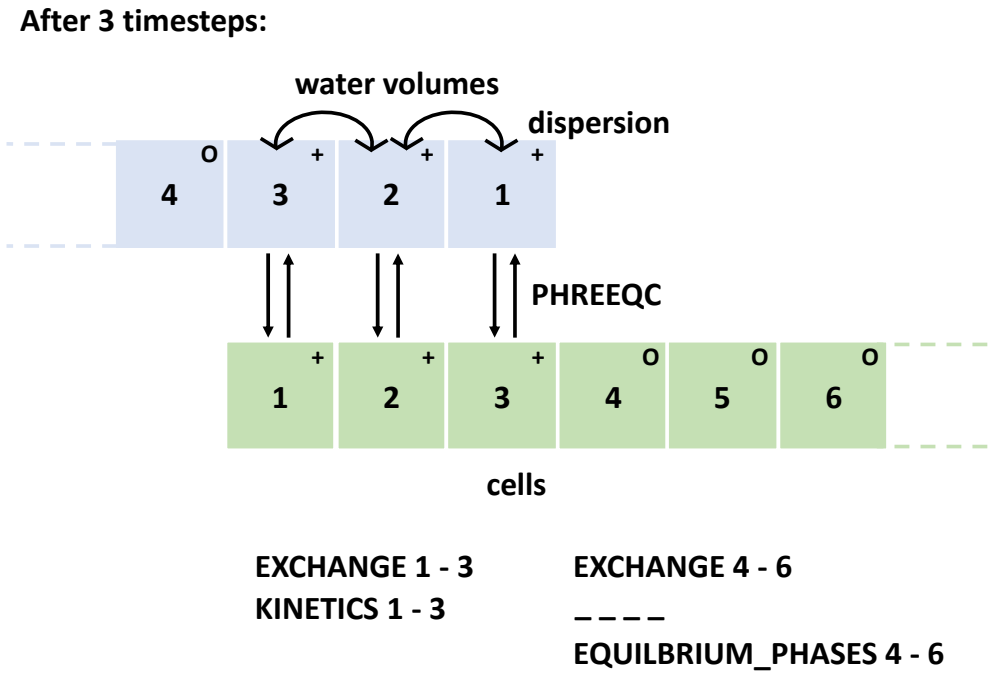

Fig 5.15 Cell structure of a 1D reactive transport column (from Appelo & Postma, 2005).

There are two approaches that are often considered to describe flow and transport through columns: the dual porosity and the single porosity model (Arbogast *et al.,* 1990; Gerke & van Genuchten, 1993; Jarvis, 1998; Larsson & Jarvis, 1999). TRN is able to implement both. Fig 5.16 shows a 1D reactive transport flow path with the dual porosity model.

The dual porosity model requires the porosity of the mobile, ε_F, and the stagnant regions, ε_P, and the mass exchange rate, α, between the two regions to be defined in TRN. It is also to possible in TRN to define where ion exchange takes place, either in the mobile water, in the stagnant water, or in both regions.

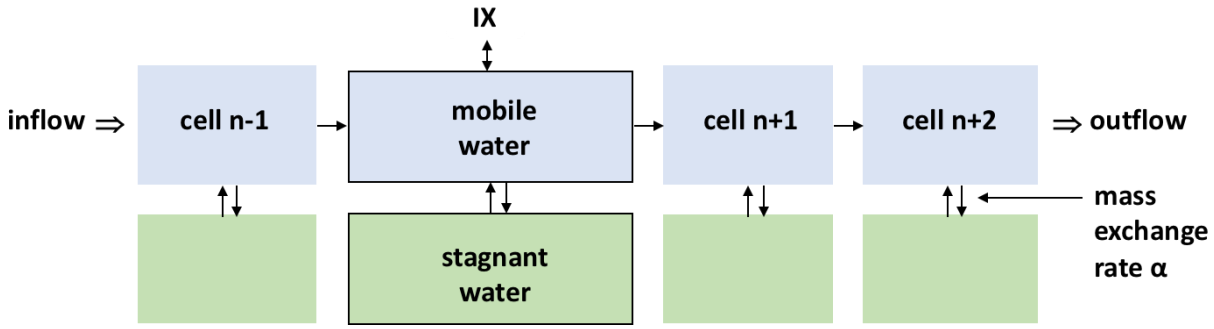

Fig 5.16 1-D reactive transport model using the dual porosity approach in TRN.

5.2.2 Modelling Approach

TRN was used to simulate solute transport, thermodynamic reactions and ion exchange in the Madagascar IAD. The approach used to model reactive transport in the column experiments with both reagents (barium chloride and ammonium chloride) involved:

- Adjustment of Column Hydraulics
  - ⇒ Determine the column hydraulics by fitting the model to the chloride (tracer ion) breakthrough curve.
- Ion Exchange in the Dual Porosity Model
  - ⇒ Establish where ion exchange is taking place (i.e. in the mobile region, stagnant region or both) by comparing each model to the measured major cation breakthrough curves.
- Major Element Breakthrough Curves
  - ⇒ Determine whether the model can adequately describe the major element breakthroughs.
- REE Breakthrough Curves
  - ⇒ Determine whether the extracted log K values can model the measured REE breakthroughs.

Using Microsoft Excel, analysis of variance (ANOVA) and statistical methods were used to determine whether the model simulations differed significantly from measured breakthrough curves. The modelling approach and the results will be described in the following sections.

5.2.1.1 Adjustment of Column Hydraulics

The reactive transport modelling was focused on the chemical processes triggered by the reagent injection. That is, the flushing period with deionised water was not considered. Hence, all models start at t_2, the estimated point of reagent injection (see Fig. 4.5 and Fig. 4.6).

The equilibrium conditions achieved in the column with deionised water were used to simulate the initial column solution in the model.

A tracer (Cl^-) was used to estimate the flow and storage properties of the Madagascar IAD. The chloride ion was assumed to act as a conservative tracer that did not undergo chemical reactions with exchange surfaces or aqueous species in the column.

The hydraulic properties of the columns could therefore be determined by fitting the 1-D reactive transport model to the measured chloride breakthrough curve in the absence of any calculated reactions involving Cl^-.

The fixed geometric and hydraulic parameters of the model setup were:

(5.47)	column length	L = 0.15 m
(5.48)	cross section	A = 12.6 cm^2
(5.49)	volumetric flow	Q = 1.2 mL/h

The other inputs that were required in TRN to set up the reactive transport model to reproduce the column conditions were the fitted parameters. These included:

- mobile porosity ε_F
- immobile porosity ε_P
- mass exchange rate α
- longitudinal dispersivity a_L

Each of these parameters was varied in numerous simulations until the best representation of the Cl breakthrough curve was achieved, using both the single and dual porosity approaches.

Fig 5.17 displays some of the hydraulic parameter variations that were used to model the measured Cl breakthrough curve in both sets of column experiments:

- 1st diagram: single porosity ε = 0.19
- 2nd diagram: dual porosity ε_F = 0.10, α = 0.55, ε_P = 0.10
- 3rd diagram: dual porosity ε_F = 0.10, α = 0.55, ε_P = 0.30
- 4th diagram: dual porosity ε_F = 0.10, α = 0.55, ε_P = 0.50
- 5th diagram: dual porosity ε_F = 0.10, α = 0.55, ε_P = 0.70

Fig 5.18 presents the residual plots for the hydraulic parameter variation models in Fig 5.17. The R^2 value for each of the residuals is shown in Table 5.5.

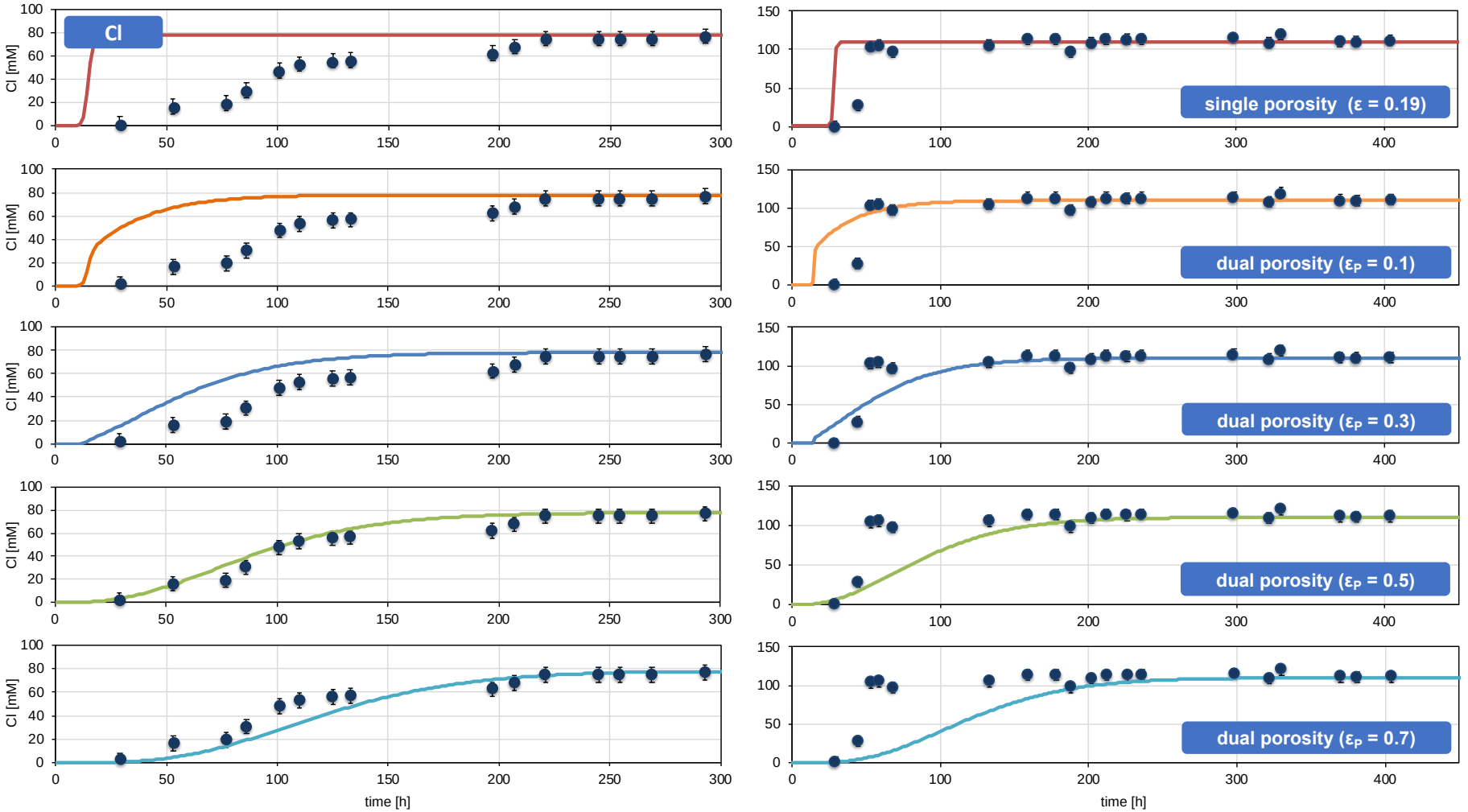

Fig 5.17 Parameter variation for the Cl breakthrough. Left: tracer curves in BaCl2 column. Right: tracer curves in NH4Cl column. Error bars signify standard error of replicates.

Fig 5.18 Residuals for modelling the Cl breakthrough. Left: in the BaCl2 column. Right: in the NH4Cl column.

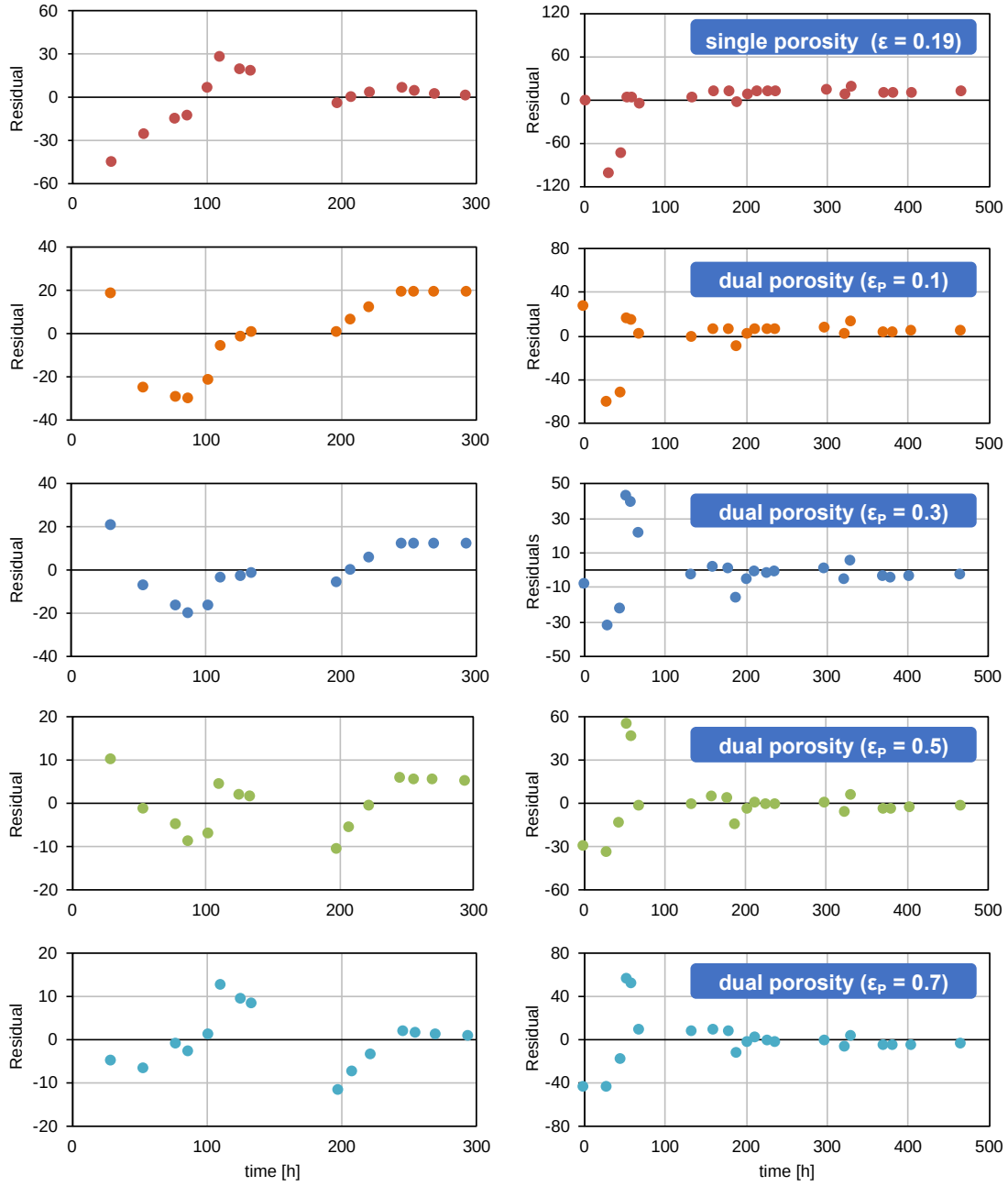

Table 5.5 R^2 value for the corresponding Cl models.

	Cl Model	R^2
Barium chloride column	single porosity (ε = 0:19)	0.540
	dual porosity (ε_P = 0.1)	0.527
	dual porosity (ε_P = 0.3)	0.793
	dual porosity (ε_P = 0.5)	0.947
	dual porosity (ε_P = 0.7)	0.921
Ammonium chloride column	single porosity (ε = 0:19)	0.817
	dual porosity (ε_P = 0.1)	0.694
	dual porosity (ε_P = 0.3)	0.786
	dual porosity (ε_P = 0.5)	0.821
	dual porosity (ε_P = 0.7)	0.611

The uppermost diagrams in Fig 5.17 represent the single porosity approach, where the measured total porosity (ε = 0.19) was used to simulate the chloride breakthrough curve. However, the single porosity models in both columns were not able to accurately represent the tracer[26]. The R^2 values and residuals agree with the visual interpretation.

Numerous simulations to account for the tracer behaviour show that the best description was achieved by the dual porosity approach and the 4th parameter set. The highest R^2 values were observed for this model as were the lowest residual values. Thus, the column hydraulics could be described by:

(5.50) mobile porosity $\varepsilon_F = 0.1$

(5.51) flow velocity $v = 0.095$ m/h (from Eq. (5.46)

Assuming 10 cells in the column, this leads to the following discretisation:

(5.52) number of cells $N = 10$

(5.53) cell length $\Delta x = L/N = 0.015$ m

(5.54) time bin $\Delta t = \Delta x/v = 0.158$ h

In the dual porosity approach, longitudinal dispersivity a_L is of less importance, thus it was given a value of $a_L = 0.001$ m (i.e. 1/15-th of the cell length). The two dual-porosity parameters α and ε_P were adjusted to the Cl breakthrough curve:

(5.55) mass-exchange rate $\alpha = 0.055\ h^{-1}$

(5.56) stagnant porosity $\varepsilon_P = 0.5$

During the different parameter variations, it was apparent that adjusting α has less effect on the shape of the breakthrough curve than adjusting ε_P.

Preferential flow was unavoidable when undertaking the column experiments due to the heterogeneous nature of the sample material and width of the soil columns. Preferential flow was indicated by the fast breakthrough of the tracer in the ammonium column (Fig. 4.6), when compared to the breakthrough in the barium chloride column (Fig. 4.5).

Preferential flow in the columns could not be completely characterised by the parameter set, despite use of the dual porosity model. However, the dual porosity model is considered to

[26] The measured porosity could not represent the tracer behaviour, therefore time was used along the x axis in all figures as opposed to the more commonly used pore volumes (which is calculated from total porosity).

be sufficiently accurate to model the tracer breakthrough. This is confirmed by the lowest residual values for the parameter set (Fig 5.18).

5.2.1.2 Ion Exchange in the Dual Porosity Model

The precise simulation of ion exchange reactions through the soil columns was the main aim of this reactive transport modelling study. In the dual porosity model, the region where ion exchange is taking place can be defined either in the mobile region, the stagnant region or both regions (see Fig 5.16).

Neither stagnant nor mobile porosities for clays are available in the literature for the dual porosity model. As a result these parameters were fitted to the measured breakthrough curves. TRN simulations in which ion exchange occurred in the mobile region, in the stagnant regions, and in both regions of the column are shown in Fig 5.19.

The simulations are compared to the measured breakthroughs for the major cation in each column, and were based on the adjusted hydraulic parameter set in § 5.2.1.1. In the model calculations shown, no changes were made to the database values of the cation equilibrium constants for all the cation-clay exchange reactions (Eq. (5.5) to (5.15)).

The residual plots for the dual porosity models are shown in Fig 5.20. The R^2 value for each of the residual plots is shown in Table 5.6. The model indicates that the best representation of measured breakthrough curves was observed when ion exchange reactions were taking place in both the mobile and stagnant phases.

The highest R^2 values (0.76 for Ba; 0.89 for Al) were observed using the ‘both’ model as were the lowest residual values, this supports the visual representation. Therefore the ‘both’ model that considers ion exchange to be occurring in both the mobile and stagnant regions was used in further simulations to model the major cation and REE breakthrough curves.

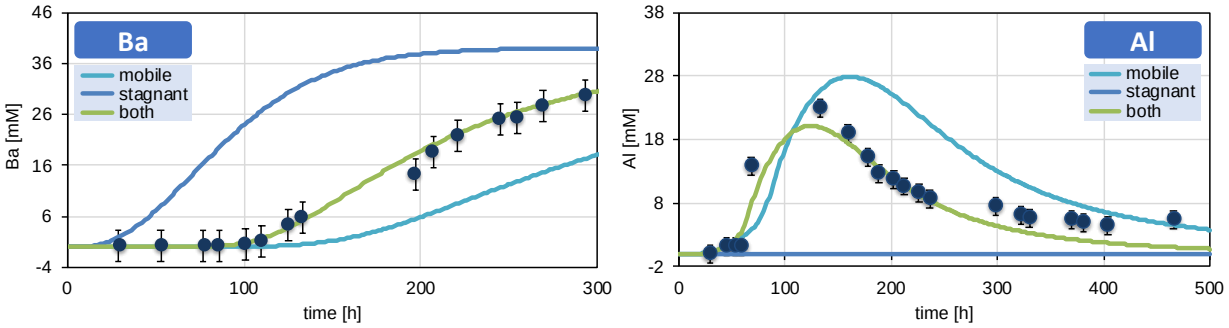

Fig 5.19 Simulations varying IX. *Left*: Ba breakthrough in $BaCl_2$ column. *Right:* Al breakthrough in NH_4Cl column.

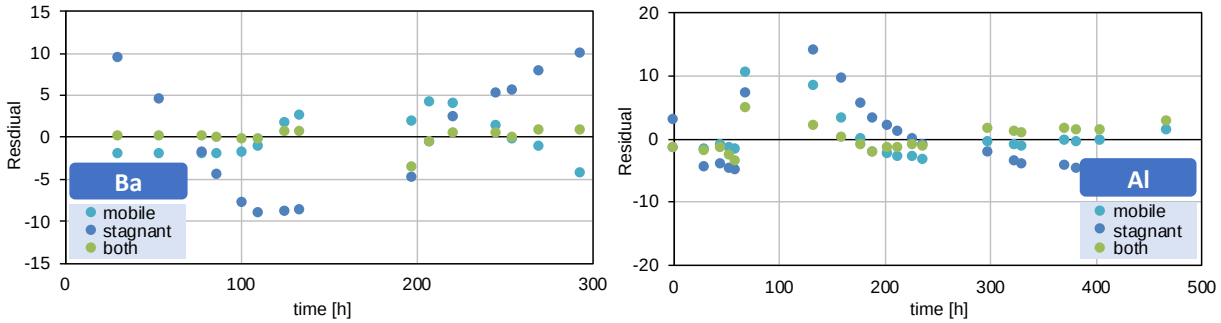

Fig 5.20 Residual plots for ion exchange porosity models of Ba and Al.

Barium chloride column	**Ba Model**	**R^2**
	mobile	0.668
	stagnant	0.501
	both	0.775
Ammonium chloride column	**Al Model**	**R^2**
	mobile	0.690
	stagnant	0.237
	both	0.890

Table 5.6 R^2 value for the corresponding Ba and Al models.

5.2.1.3 Major Element Breakthrough Curves

An important indicator of whether or not the TRN model can accurately represent reactive transport through the columns is how well the model characterises the breakthrough curves of the major elements.

TRN simulations for the major elements (Ba, Al) are compared with the measured outflow concentrations in the barium chloride column (Fig 5.21). The simulations were based on the adjusted hydraulic parameter set in § 5.2.1.1. The cation equilibrium constants for all the cation-clay exchange reactions used in the model calculations are found in Eq. (5.5) to (5.15).

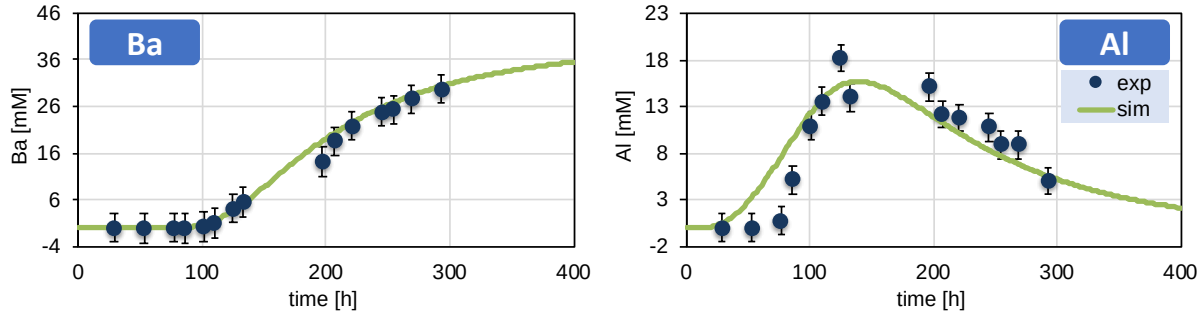

Fig 5.21 Calculated and measured element concentrations in the outflow solution of the barium chloride column

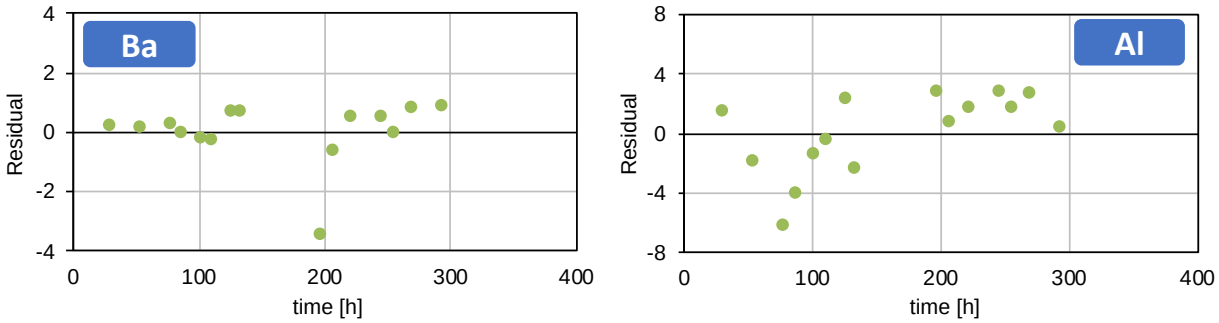

Fig 5.22 Residuals for the calculated and measured element breakthrough curves in the barium chloride column.

The residuals for the modelled and measured breakthrough curves in the barium chloride column are shown in Fig 5.22. The low residual values indicate the model can adequately represent the major elements.

Fig 5.23 shows the TRN model for the major element (Al) in the ammonium chloride column compared to the measured outflow concentrations. The residuals for the model are also displayed in Fig 5.23. Again, the low residuals indicate that a relatively good representation of the column breakthrough curve is given by the model.

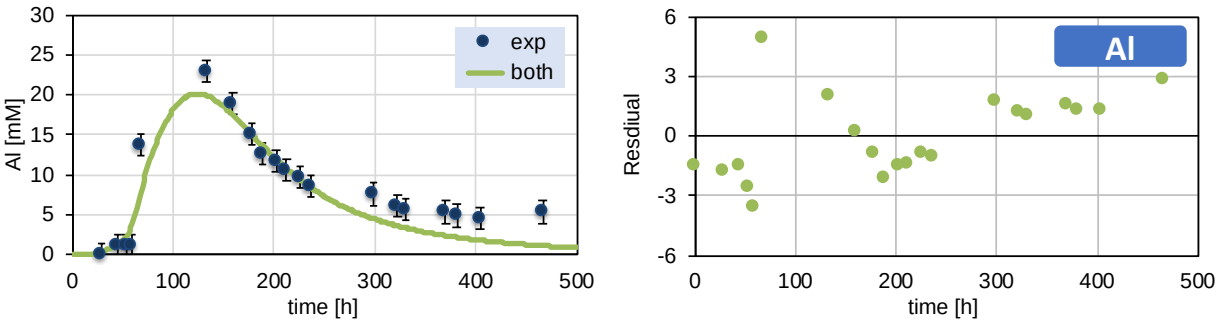

Fig 5.23 Left: calculated and measured Al breakthrough in the NH4Cl column. Right: residual plot of the Al model.

5.2.1.4 REE Breakthrough Curves

The main reason for modelling the column experiments was to determine whether the REE equilibrium constants estimated from the batch tests (described in § 5.1.3) could account for reactive transport through the column breakthrough curves.

TRN calculations for all REE are compared with the measured outflow concentrations in both sets of column tests (based on the hydraulic parameters in § 5.2.1.1). Four simulations are shown in Fig 5.24 and Fig 5.26, each representing a different log K value:

- log K = 2.19
- log K = 2.29 ⇐ best fit value
- log K = 2.39
- log K = 2.49

Different log K values were simulated to highlight the sensitivity of the REE to small changes in the equilibrium constant. The exchange constants for all major and minor cations were taken from the WATEQ4F database (see Eq. (5.5) to (5.15)).

Residual plots for the four models in both columns are displayed in Fig 5.25 and Fig 5.27. The R^2 value for each of the residual plots is shown in Table 5.7.

Table 5.7 R^2 values for the corresponding REE models.

	Model	R^2 in barium chloride column	R^2 in ammonium chloride column
La	log K 2.19	0.659	0.898
	log K 2.29	0.705	0.903
	log K 2.39	0.683	0.902
	log K 2.49	0.652	0.901
Ce	log K 2.19	0.619	0.897
	log K 2.29	0.685	0.904
	log K 2.39	0.669	0.903
	log K 2.49	0.648	0.901
Nd	log K 2.19	0.630	0.889
	log K 2.29	0.690	0.908
	log K 2.39	0.676	0.906
	log K 2.49	0.625	0.904
Dy	log K 2.19	0.718	0.890
	log K 2.29	0.749	0.896
	log K 2.39	0.743	0.893
	log K 2.49	0.733	0.894

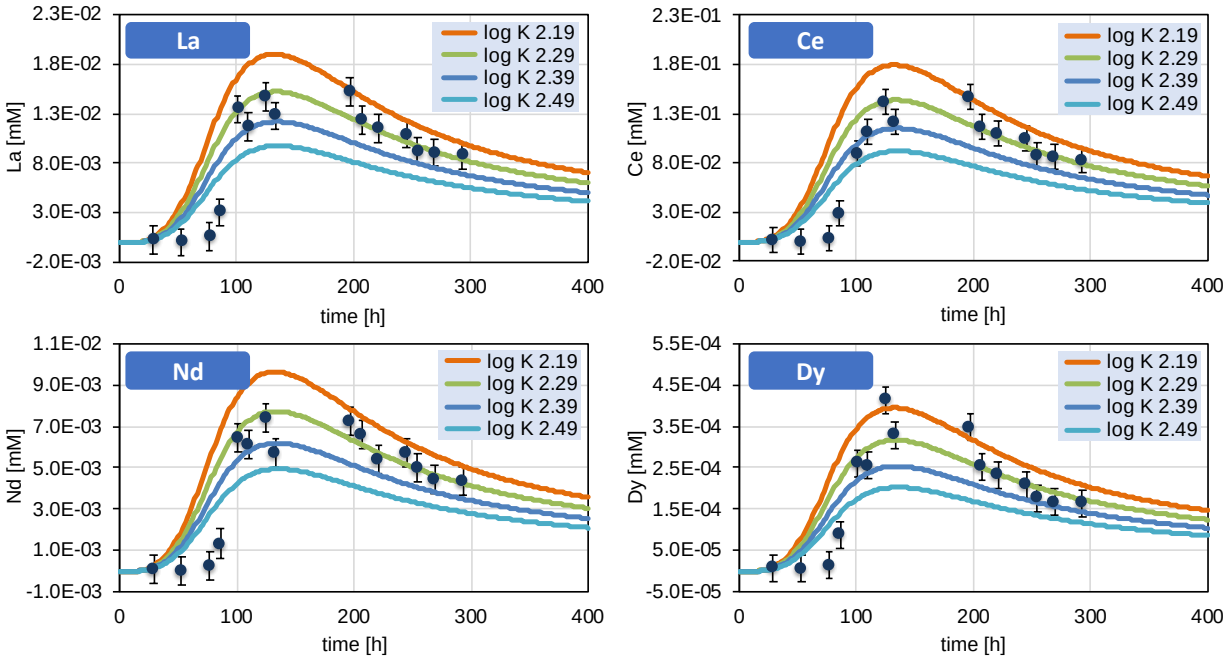

Fig 5.24 Calculated and measured REE concentrations in the outflow solution of the barium chloride column.

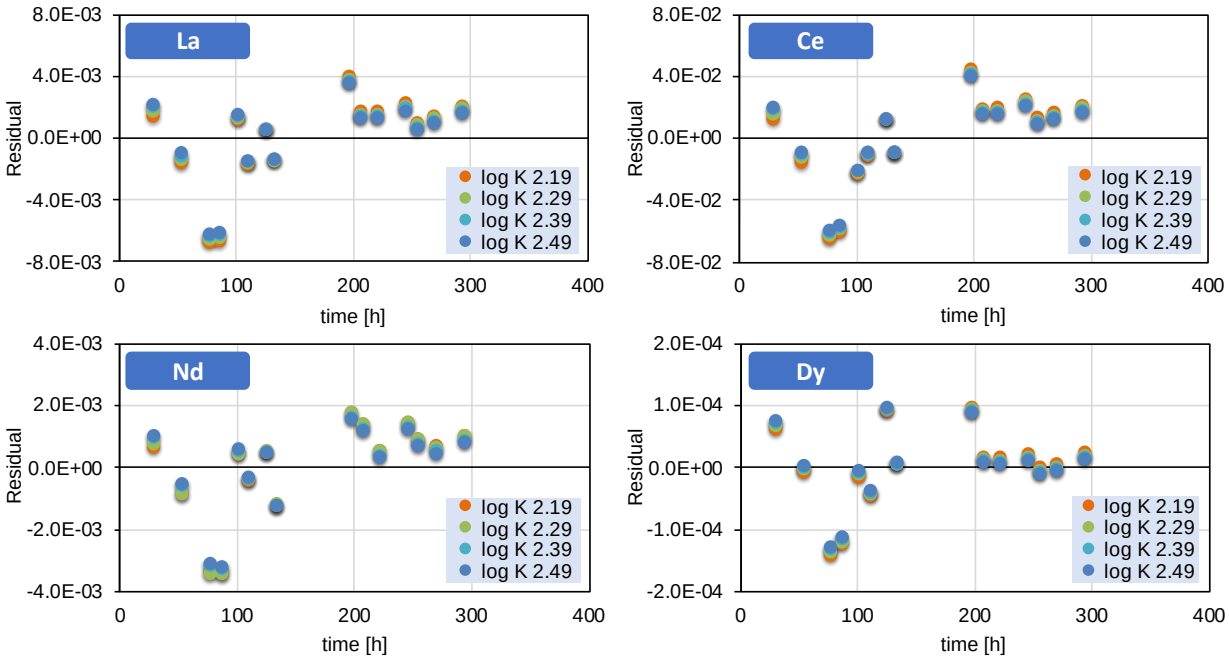

Fig 5.25 Residuals of the calculated and measured REE breakthrough curves in the barium chloride column.

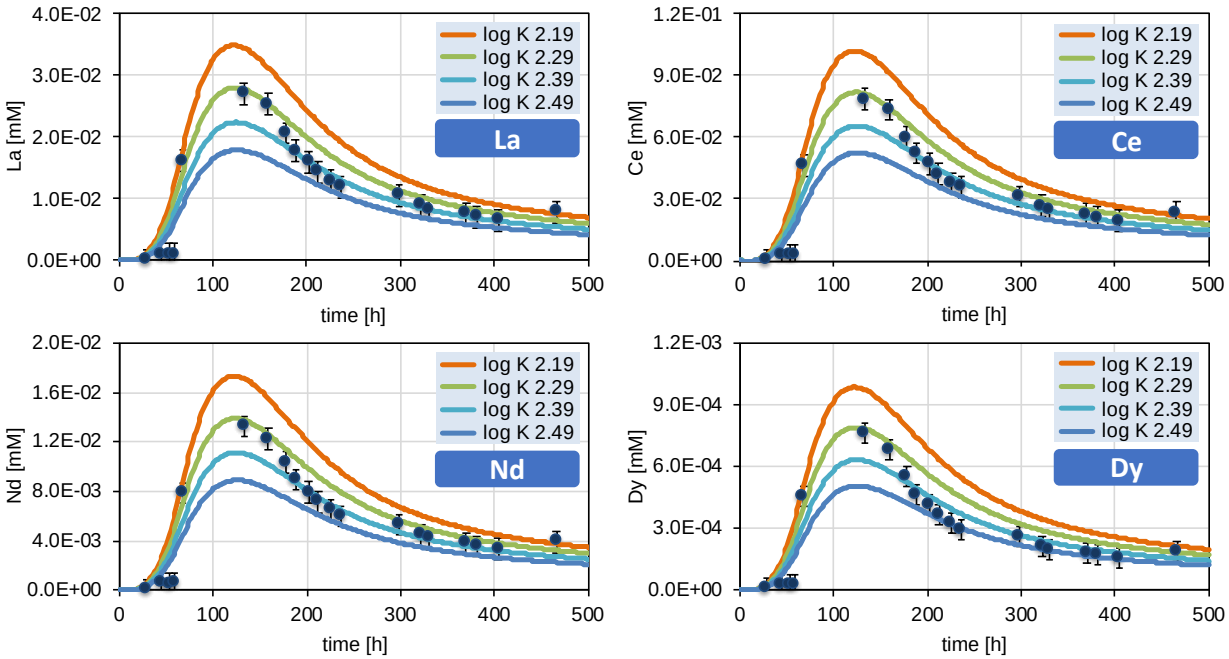

Fig 5.26 Calculated and measured REE concentrations in the outflow solution of the ammonium chloride column.

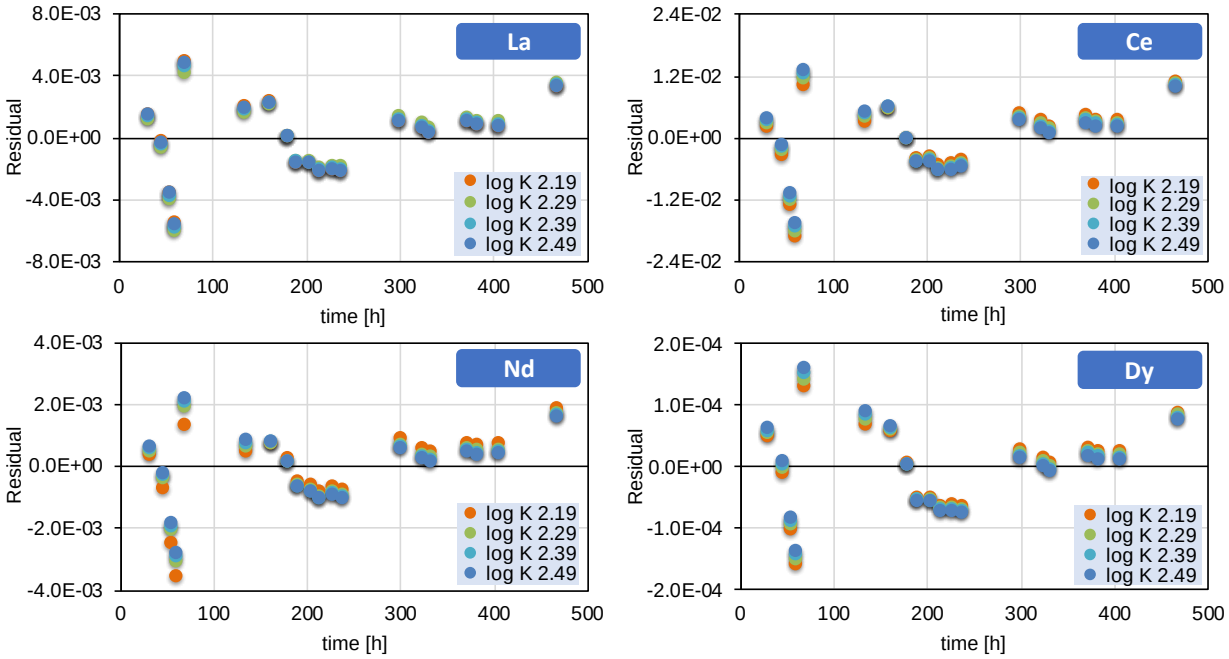

Fig 5.27 Residuals of the calculated and measured REE breakthrough curves in the ammonium chloride column.

The model does not perfectly represent the REE breakthrough curves in the columns. This is because the column experiments, unlike the batch tests, may be subject to kinetic processes as well as thermodynamic mechanisms and subject to preferential flow pathways that are not captured by the dual porosity hydraulic model.

The log K that best represented all the REE breakthrough curves was:

(5.57) $REE^{3+} + 3X^{-} = REEX_3$ $\log K = 2.29 \pm 0.5$

The best fit model was supported by the residual plots which showed the lowest values for the log K 2.29 simulation (Fig 5.25 and Fig 5.27) and by the R^2 values (Table 5.7) which were the highest for this model.

5.2.3 Literature REE Equilibrium Exchange Constants

There is one only literature study (Tertre *et al.,* 2006a) that has determined equilibrium constants for REE exchange reactions with kaolinite (i.e. the main exchanger in the study material; Table 1.1). Moreover, this study only determined a log K value for one of the REE.

The experimental Eu dataset was obtained from batch sorption experiments with the pure mineral kaolinite and the Eu exchange reaction was modelled with the diffuse double layer surface complexation model (see full description of the model in § 2.5.3.2).

Tertre *et al.* (2006a) determined the equilibrium constant:

(5.58) $3NaX + Eu^{3+} \leftrightarrow EuX_3 + 3Na^{+}$ $\log K = 11.0 \pm 0.4$

for the Na/Eu exchange reaction on a pure kaolinite mineral.

In this study, REE exchange reactions with the Madagascar IAD in the batch reactor dataset could be represented by a single equilibrium constant:

(5.59) $3NaX + REE^{3+} \leftrightarrow REEX_3 + 3Na^{+}$ $\log K = 2.29 \pm 0.3$ (SD)

or individual constants for each REE (which offered a very slight improvement).

Here, the equilibrium constant for all the REE was nine orders of magnitude smaller than the literature constant. However, thermodynamic equilibrium constants are fundamental quantities that should be independent of any site or application.

A possible reason for the difference could be related to the different modelling approaches used. This study considered only the ion exchange model to describe REE exchange because:

- The Madagascar IAD was characterised on the basis that the deposit contains ≥ 50 % ion-exchangeable REE, which are adsorbed onto clay mineral surfaces (Chi et al., 2005; Wu et al., 1990, 1995), and
- The kaolinite fraction makes up 85% of the sample material, thus it is the main ion exchanger in the deposit.

The different materials could also account for the order of magnitude difference between the equilibrium constants because the Madagascar IAD is a complex material comprising different minerals while the literature study used a pure mineral phase.

Another important consideration is that the REE exchange constants estimated in this study have only been fitted to a dataset from a single sample from the Madagascar IAD.

5.3 Fundamental Outcomes

Modelling of CEC experiments indicated that:

[1] The major exchangeable cation on the Madagascar IAD is Al^{3+} (in addition to its occurrence in the clay's mineral structure).

[2] The pH drop from near neutral to pH 4 in the non-buffered chloride solutions was the result of high concentrations of exchangeable Al^{3+} being mobilised into the aqueous phase.

Modelling of the batch reaction dataset revealed that a single thermodynamic equilibrium constant for the reaction:

(5.60) $\log K = 3NaX + REE^{3+} \leftrightarrow REEX_3 + 3Na^{+}$

where the log K

- $\log K = 2.29 \pm 0.3$ (SD) $\Rightarrow$ best fit for REE dataset in batch reaction tests
- $\log K = 2.29 \pm 0.5$ (SD) $\Rightarrow$ best fit for REE dataset in all soil columns

was able to describe all REE exchange reactions with the **Madagascar IAD**.

In addition, exchange constants were calculated for each individual REE to determine whether a better description of the REE dataset could be achieved. The individual log K dataset

only varied after 2 decimal places and the difference between the two models in terms of the objective function was:

- objective function = 5.71×10^{-11} $\Rightarrow$ for the different log K model
- objective function = 5.72×10^{-11} $\Rightarrow$ for the single log K model

Tertre *et al.* (2006a) was the only study to report a REE exchange constant (for Eu):

- log K = 11.0 ± 0.4 on pure kaolinite

The significant order of magnitude differences could be explained by the different modelling approaches used or by the different complexities of the materials. The exact reason for the order of magnitude variance is not known.

An important consideration for the REE exchange constants derived from equilibrium modelling is that these log K have only been fitted to a dataset from one sample from the Madagascar IAD. Therefore, these constants cannot be considered the equilibrium constants for all IAD-REE exchange reactions.

CHAPTER 6

ENVIRONMENTALLY FOCUSED MINING APPLICATION

One of the objectives of this study was to investigate whether a more environmentally sustainable mining approach, such as ISR, could be used to recover REE from the Madagascar IAD. In this regard, generic water flow and solute transport simulations were undertaken in HYDRUS-1D using existing site and literature data, to develop a conceptual model for ISR of the Madagascar IAD.

6.1 HYDRUS 1-D Model Description

HYDRUS-1D version 4.16 (Šimůnek *et al.,* 2008) is a public domain software package that simulates the one-dimensional movement of water, heat and solutes in the unsaturated zone between the soil surface and the groundwater table. In addition to the HYDRUS code, the software package includes an interactive graphics-based user interface module. This module consists of a project manager with a unit for pre processing and post processing.

The programme uses finite elements to numerically solve the Richards equation for saturated-unsaturated water flow and Fickian-based advection dispersion equations for heat and solute transport. The transport equations also include provisions for non-linear and/or non-equilibrium reaction between the solid and aqueous phases, linear equilibrium reactions between the aqueous and gaseous phases and zero-order reactions[27] (Šimůnek *et al.,* 2006).

One-dimensional uniform water movement in a partially saturated rigid porous medium is described by a modified form of the Richards equation:

$$\frac{\delta\theta}{\delta t} = \frac{\delta}{\delta x}\left[K\left(\frac{\delta h}{\delta x} + \cos\alpha\right)\right] - S \qquad (6.1)$$

where h is the water pressure head [L], θ is the volumetric water content [L^3L^{-3}], t is time [T], x is the spatial coordinate [L], S is the sink term [$L^3L^{-3}T^{-1}$], α is the angle between the flow direction and the vertical axis, and K is the unsaturated hydraulic conductivity [LT^{-1}].

The unsaturated hydraulic conductivity is defined as (Šimůnek *et al.,* 2005):

$$K(h,x) = K_s(x)K_r(h,x) \qquad (6.2)$$

[27] A zero-order reaction has a rate that is independent of the concentration of the reactant(s).

where K_s is the saturated hydraulic conductivity [LT^{-1}] and K_r is the relative hydraulic conductivity.

The sink term (S), defined as the volume of water removed from the soil per unit of time due to plant water uptake, can be described as

(6.3) $S(h) = \alpha(h) S_p$

where S_p is the potential water uptake [T^{-1}] and α(h) the given dimensionless function of the soil water pressure head ($0 \leq \alpha \leq 1$).

A few capabilities of the HYDRUS-1D model include:

- Dual-porosity water flow with solute transport and two-site sorption in the mobile zone;
- Dual-permeability type water flow and solute transport, and
- Coupled water, vapour and energy transport.

The programme can be used to analyse water and solute movement in unsaturated, partially saturated or fully saturated porous media.

The unsaturated soil hydraulic properties (the constitutive relationships) are described using Brooks & Corey (1964), Durner (1994), Kosugi (1996) and van Genuchten (1980) type analytical functions. Modified van Genuchten type functions that improve the description of the hydraulic properties near saturation were implemented by Durner (1994). Hysteresis can also be optionally considered (Šimůnek *et al.,* 2005).

The HYDRUS 1-D software package also includes the HP1 module. HYDRUS 1-D version 2 (Šimůnek *et al.,* 1998) was coupled with PHREEQC version 2 (Parkhurst & Appelo, 1999) to form the comprehensive simulation tool, HP1 (Jacques *et al*., 2003, 2006; Jacques & Šimůnek, 2005; Šimůnek *et al.,* 2006, 2008). HP1 is a significant expansion of the individual codes due to the preservation of most of their original features and capabilities.

HP1 still uses the Richards equation for variably-saturated water and convection–dispersion type equations for heat and solute transport. However, the code can now simulate a broad range of low temperature biogeochemical reactions in groundwater systems, including interactions with exchangers, minerals and sorption surfaces based on equilibrium, kinetic or mixed equilibrium-kinetic reactions (see Fig. 6.1).

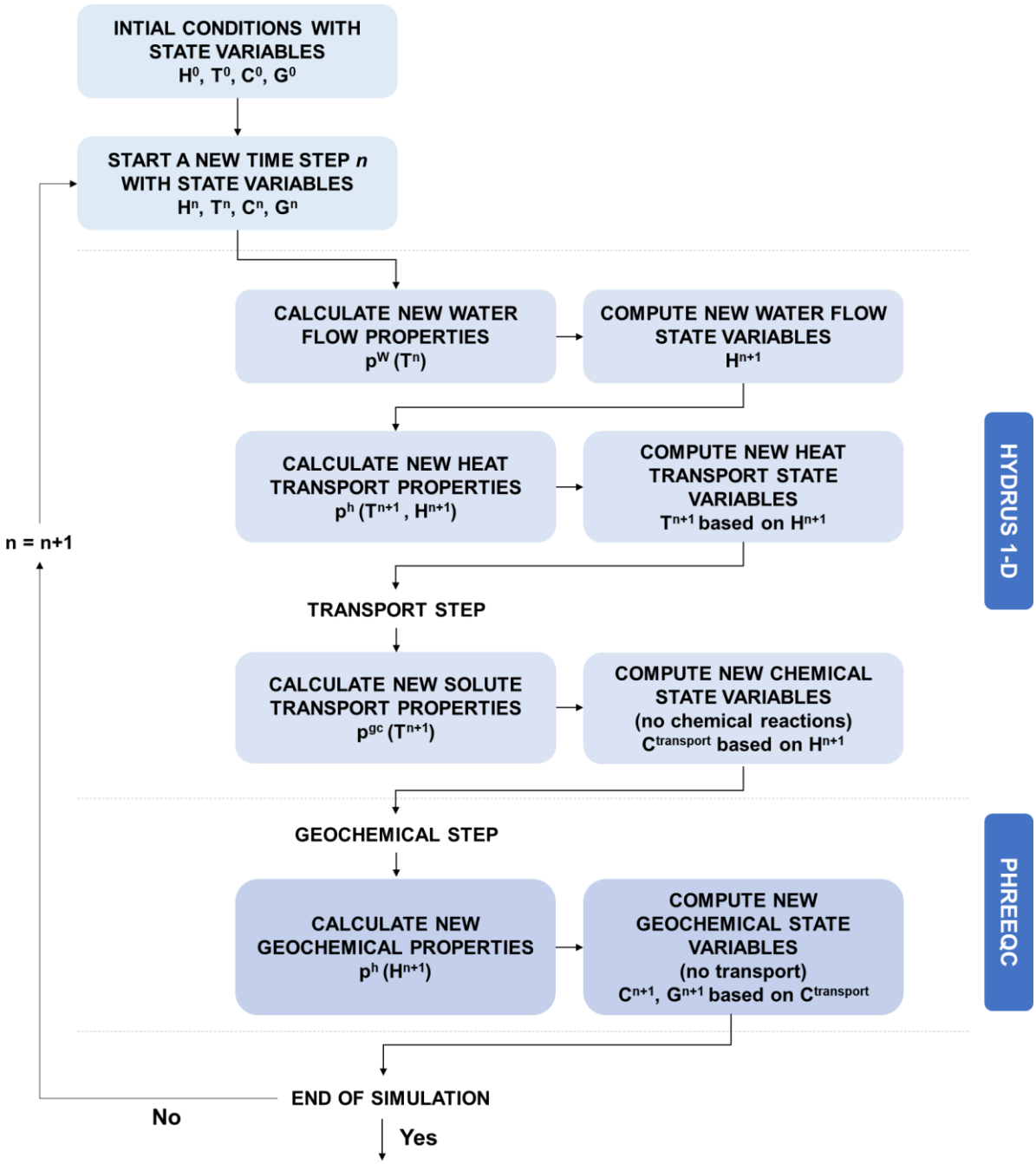

Fig. 6.1 Schematic of the modelling approach of the coupled HP1 model (from Jacques & Šimůnek, 2005).

6.2 Conceptual Model: Flow and Transport through the Madagascar Laterite

A number of generic properties about the Madagascar study area have been described in a technical report of the site (SRK, 2013) and in a hydrogeological mapping study of north-central Madagascar (Davies, 2009). In this research, these properties were considered applicable to the entire site. They include:

- Elevation ranges from 0 – 713 m;
- Very hilly, heterogeneous terrain;
- Average annual rainfall is 2000 mm;

- Average annual temperature is 25 °C, and
- Depth of water table varies between 1 -13 m.

A conceptual model based on these generic properties was used to represent the infiltration, flow and transport processes occurring at the Madagascar site, under natural hydraulic conditions and under in situ mining conditions (Fig. 6.2).

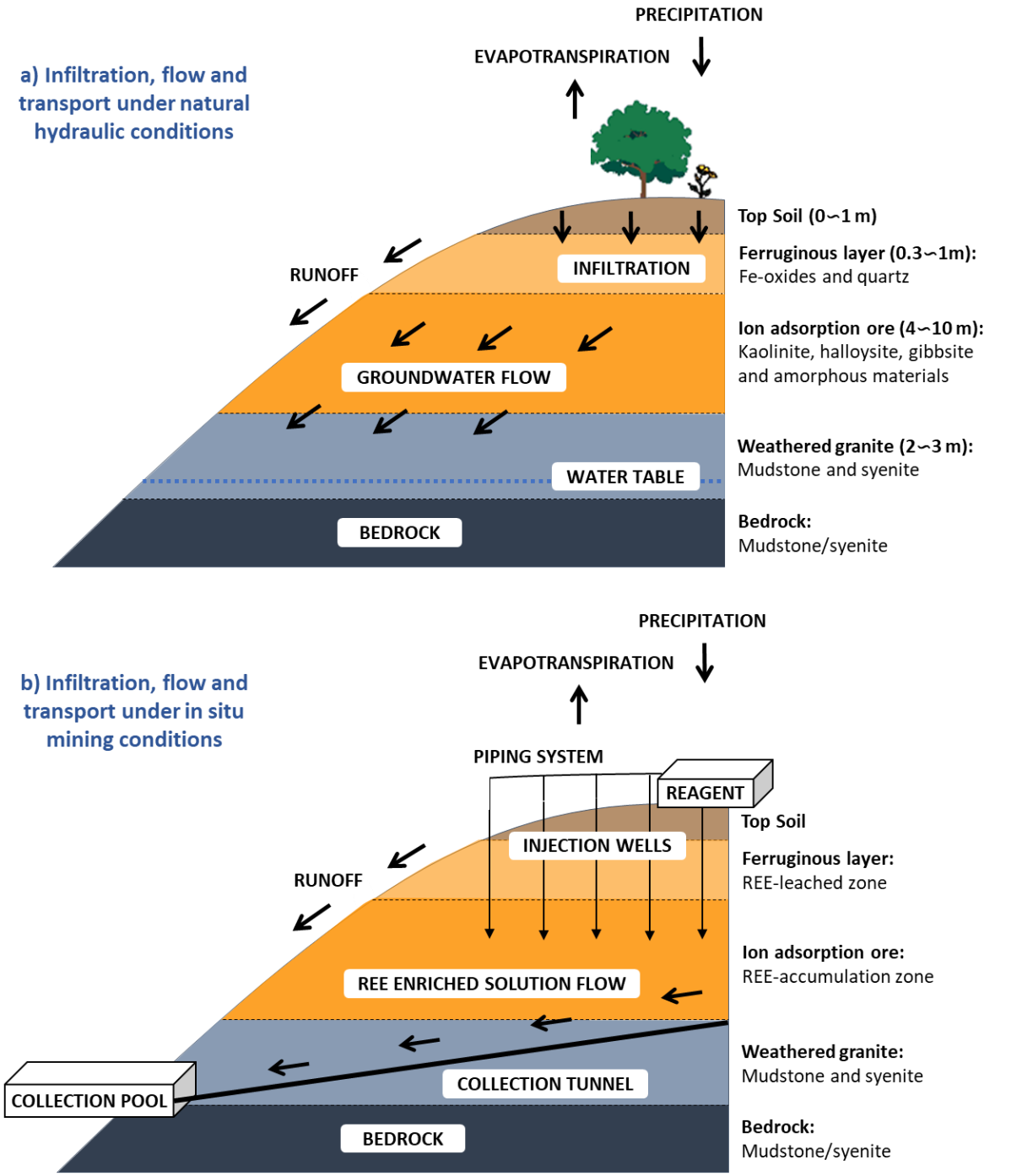

Fig. 6.2 Conceptual model of the infiltration, flow and transport processes at the Madagascar site. *Left:* under natural hydraulic conditions. *Right:* under in situ mining conditions.

The conceptual model developed for in situ mining processes, uses the hilly terrain at the Madagascar site to consider a hillslope wellfield operation. In addition, the entire laterite section was considered to be well above the water table, consequently HYDRUS-1D was used to simulate water flow and solute transport through unsaturated porous media.

6.3 Modelling Approach

The HYDRUS-1D and HP1 codes were used to define preliminary hydraulic properties of the Madagascar IAD and to simulate the flow and transport processes shown in the ISR conceptual model (Fig. 6.2). The modelling approach involved consideration of:

- Water flow
  - ⇒ Simulate the movement of water through a generic laterite profile with varying depths.
  - ⇒ Determine the effect of the single and dual porosity flow models on water infiltration.
- Water flow and solute transport
  - ⇒ Simulate the movement of water and REE through a generic laterite profile using an environmentally viable reactive solution.

The modelling procedure and the results will be described in more detail in the following sections. The input parameters for the HYDRUS-1D models are shown in Appendix C.

6.3.1 Water Flow

HYDRUS-1D requires a number of input parameters before water flow through the Madagascar IAD can be considered. These include the soil hydraulic properties:

- residual soil water content θ_r
- saturated water content θ_s
- parameter α in the soil water retention function [L^{-1}]
- parameter n in the soil water retention function
- saturated hydraulic conductivity K_s [LT^{-1}]
- tortuosity parameter in the conductivity function l

Since the hydraulic properties of the Madagascar soil could not be determined in this study, the values had to be estimated. Hence, these simulations represent generalised infiltration conditions through the laterite profile.

SRK (2013) provide a broad description of each of the layers within the Madagascar weathered profile. The layers include the top soil, ferruginuous layer, ion adsorption ore, weathered granite and the bedrock layer.

Based on this information and the literature values for the hydraulic properties of the different soil textural classes (Carsel & Parrish, 1988), the Madagascar soil hydraulic properties were defined on a preliminary basis. These parameters are presented in Table 6.1.

Table 6.1 The soil hydraulic parameters properties used in the HYDRUS-1D model.

Soil layer	Texture	θ_r [$m^3\ m^{-3}$]	θ_s [$m^3\ m^{-3}$]	α [m^{-1}]	n	l	Ks [$m\ d^{-1}$]
Top soil	Loamy Sand	0.057	0.41	12.4	2.28	0.5	3.502
Ferruginous layer	Sandy loam	0.065	0.41	7.5	1.89	0.5	1.061
Ion adsorption ore	Sandy clay loam	0.1	0.39	5.9	1.48	0.5	0.3144
Weathered granite	Clay loam	0.095	0.41	1.9	1.31	0.5	0.0624
Bedrock	Silty Clay Loam	0.089	0.43	1	1.23	0.5	0.0168

The remaining inputs to simulate water flow are the:

- Geometry information
  - ⇒ Number of soil layers and soil type for each and total depth of soil profile.
- Time information
  - ⇒ Time discretisation and the time-variable boundary conditions.
- Soil hydraulic model
  - ⇒ Soil hydraulic model (single porosity, dual porosity/dual permeability) and hysteresis.
- Water flow boundary conditions (BC).
  - ⇒ At the upper and lower boundaries.

6.3.1.1 Model Conditions

Soil water movement in the soil profile was described in HYDRUS-1D as:

$$\frac{\delta\theta(h,t)}{\delta t} = \frac{\delta}{\delta z}\left[K(h)\left(\frac{\delta h}{\delta z} + 1\right)\right] \quad (6.4)$$

where z is the vertical coordinate with the origin at the soil surface (positive upward). S was not considered because no plants are considered in this system.

Three five-layered soil profiles of differing depths (6 m, 10 m and 30 m) were used as input data for HYDRUS-1D. These thicknesses were chosen in accordance with the findings of Sanematsu & Watanabe, (2016), that suggest the thickness of laterite weathering profiles generally ranges from 6 to 10 m but can be as much as 30 m.

According to various literature sources, standard application of the in-situ mining process (outlined in § 2.2.4) can take up to 400 days (Papangelakis & Moldoveanu, 2014; Vahidi *et al.,* 2016; Yang *et al.,* 2013). Therefore, 400 days was used as the total simulation time.

The single porosity van Genuchten-Mualem model was first used for hydraulic model simulations, and then the dual porosity flow model (based on mass transport differences in the soil water pressure head) was implemented, to account for the effect of preferential flow (which was observed in the column breakthrough curves in § 3.3).

The dual porosity formulation for water flow is based on a mixed formation of the Richards equation to describe water flow in the macropores (mobile water region) and a mass balance equation to describe moisture dynamics in the matrix (immobile water region):

$$\frac{\delta\theta_m}{\delta t} = \frac{\delta}{\delta z}\left[K(h)\left(\frac{\delta h}{\delta z} + 1\right)\right] - S_m - T_w \tag{6.5}$$

$$\frac{\delta\theta_m}{\delta t} = S_{im} + T_w \tag{6.6}$$

where the subscripts m and im refer to the mobile and immobile water regions, respectively, $\theta = \theta_m + \theta_{im}$ is the volumetric moisture content [-], S_{im} and S_m are sink terms for both regions [T^{-1}], and T_w is the transfer rate for water exchange between macropores and matrix [T^{-1}].

In the dual porosity flow model based on mass transfer driven by differences in soil water pressure head, the exchange rate of water between the macropores and matrix regions, T_w, is assumed to be proportional to the difference in pressure heads between the two pore regions (Gerke & van Genuchten, 1993; Šimůnek *et al.,* 2003):

$$T_\omega = (h_m - h_{im}) \tag{6.7}$$

where ω is a first-order mass transfer coefficient [$L^{-1}\ T^{-1}$].

Pressure heads are needed for both pore regions in the dual porosity model. Thus, soil hydraulic properties are described by six parameters for macropores (θ_r, θ_s α, n, K_s, l), four parameters for the matrix ($\theta_{r\text{-}im}$, $\theta_{s\text{-}im}$, α_{im}, n_{im}), and a parameter (ω) for mass transfer between the two zones (Ma *et al.,* 2015; Šimůnek *et al.,* 2003).

The default HYDRUS values for the soil textural classes (Carsel & Parrish, 1988) were used for the additional water flow parameters. These are shown in Table 6.2.

Table 6.2 The additional soil hydraulic parameters for the dual porosity model.

Soil layer	Texture	$\theta_{r\text{-}im}$ [$m^3\ m^{-3}$]	$\theta_{s\text{-}im}$ [$m^3\ m^{-3}$]	α_{im} [m^{-1}]	n_{im}
Top soil	Loamy Sand	0	0.1	1.5	1.5
Ferruginous layer	Sandy loam	0	0.1	1.5	1.5
Ion adsorption ore	Sandy clay loam	0	0.1	1.5	1.5
Weathered granite	Clay loam	0	0.1	1.5	1.5
Bedrock	Silty Clay Loam	0	0.1	1.5	1.5

The hydraulic parameters for the macropores are shown in Table 6.1. The boundary conditions used in this model are the constant pressure head for the upper BC and free drainage as the lower BC:

$$\frac{\delta h}{\delta z} = 0 \qquad (6.8)$$

The inputs for the water infiltration simulations at different soil depths are shown in Table 6.3.

Table 6.3 Summary of the inputs for the water flow simulations.

Input	Value
Number of Soil Materials	5
Depth of the Soil Profile [m]	z = 6, 10, 30
Boundary Condition (top)	Constant Pressure Head
Boundary Condition (bottom)	Free Drainage
Hysteresis	none
Hydraulic model	van Genuchten-Mualem and Dual-porosity (head mass transfer)
Total Model Time [days]	400

HYDRUS 1-D produces a number of graphs to aid in the visualisation of the simulation results. Water content simulations with the single and dual-porosity models in a 6 m, 10 m and 30 m generic Madagascar laterite profile are shown in Fig. 6.3. In each profile, water content increased with increasing depth from 0.09 m^3m^{-3} at 0 m to 0.4 m^3m^{-3} at 6 m, 10 m and 30 m.

In addition, distinct plateaus in the water content trend are observed between each of the different soil layers (Fig. 6.3). Water content was also observed to decrease (shift to the left) with increasing simulation time. The residence time of infiltrating water to reach the bottom of the profile was < 40 days at 6 m, 10 m and 30 m.

The soil water retention properties in a 6 m, 10 m and 30 m generic Madagascar laterite profile are shown in Fig. 6.4, using the single and dual-porosity flow models. The soil water retention was clearly observed to increasing with depth (as in Fig. 6.3). The simulations were not influenced by the use of the different porosity models.

Fig. 6.5 shows cumulative infiltration simulated with HYDRUS 1-D over the 400 days, in 6 m, 10 m and 30 m soil profiles using the single and dual-porosity flow models. Cumulative infiltration appears to have decreased with soil profile depth from 0.0035 m in the 6 m profile to 0.013 m in the 30 m profile, after 400 days.

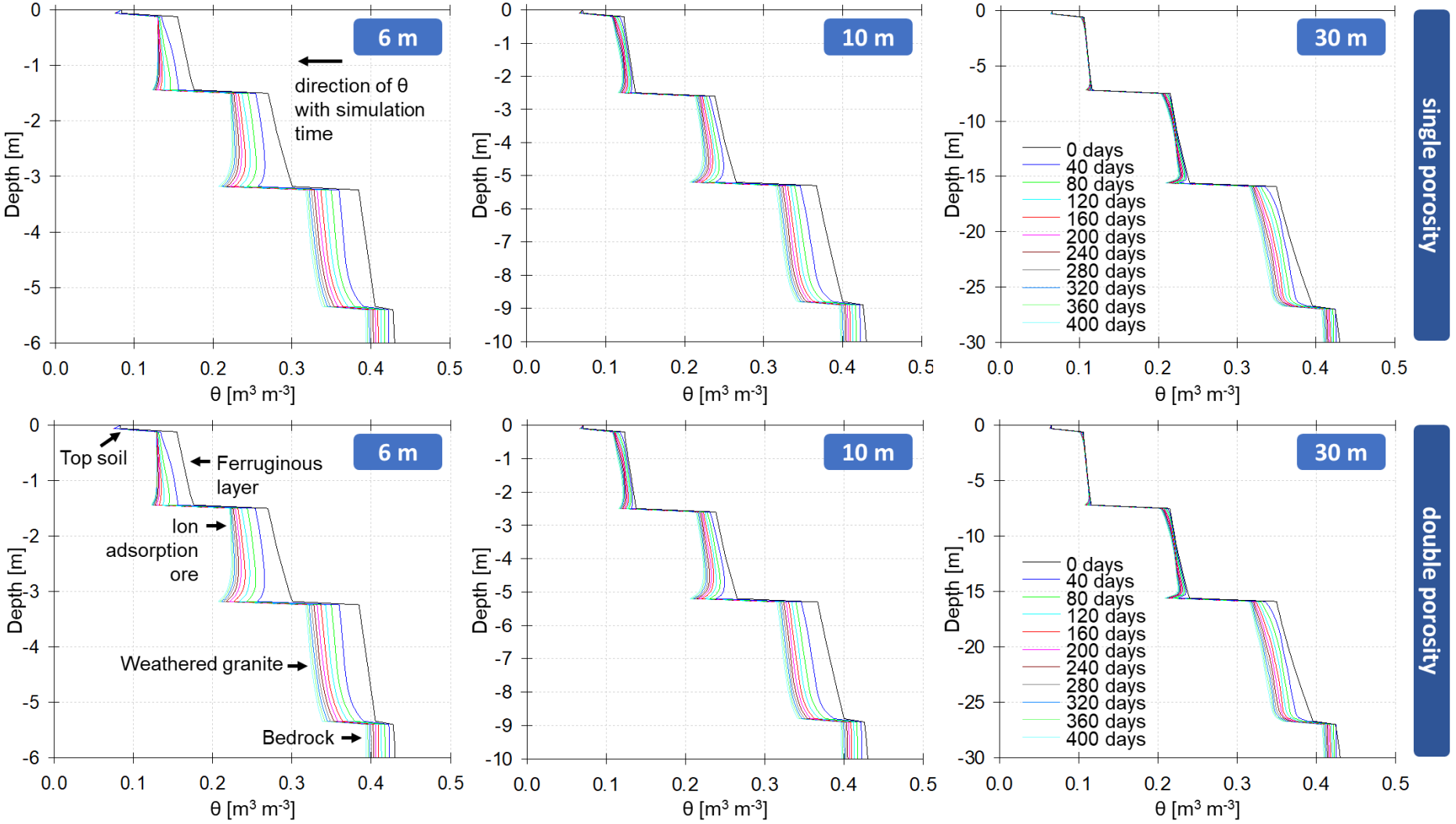

Fig. 6.3 Comparison of water contents [m^3m^{-3}] predicted using the single and dual-porosity flow models in a 6 m, 10 m and 30 m soil profile.

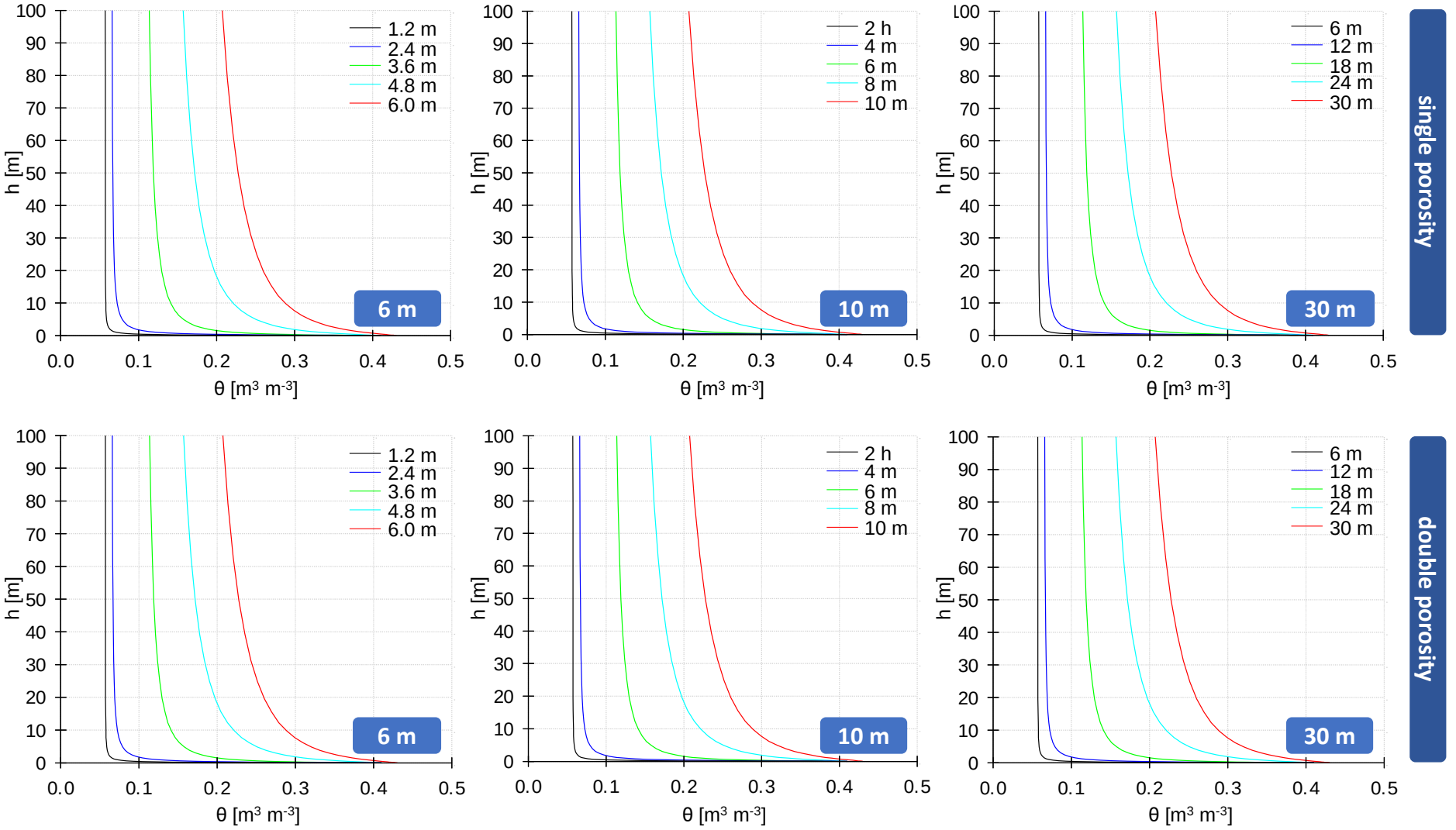

Fig. 6.4 Soil water retention simulated using the single and dual-porosity flow models in a 6 m, 10 m and 30 m soil profile. H is hydraulic head [m].

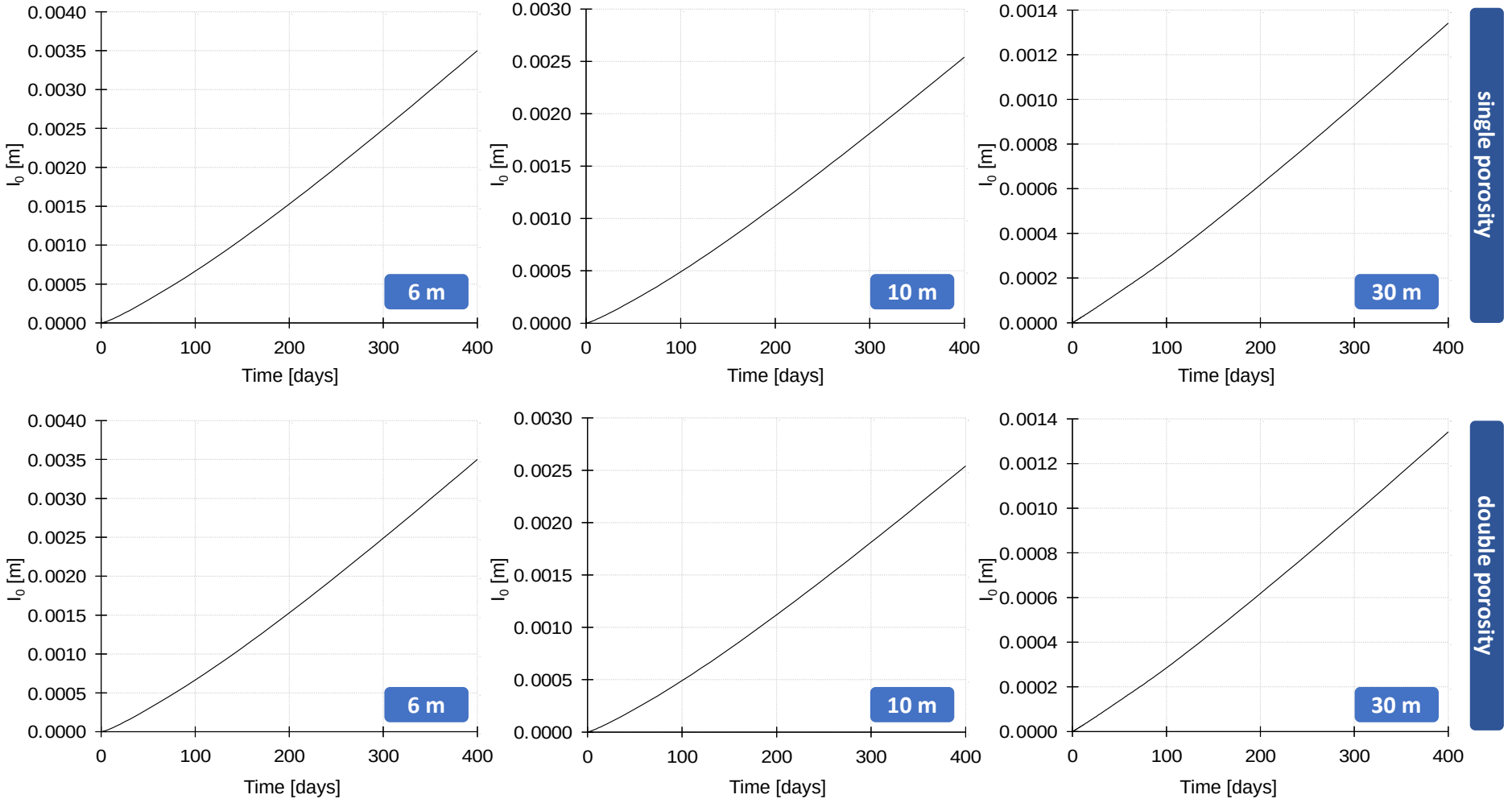

Fig. 6.5 Cumulative I_0 infiltration rates [m] simulated using the single and dual-porosity flow models in a 6 m, 10m and 30 m soil profile.

6.3.2 Water Flow and Solute Transport

In addition to the input parameters outlined in § 6.3.1.1 HP1 requires a number of other parameters in order to consider solute transport and steady state water flow through the Madagascar laterite. These include the soil specific parameters:

- bulk density ρ_b
- longitudinal dispersivity a_l
- dimensionless fraction of adsorption sites
- immobile water content[28]

Longitudinal dispersivity is usually determined in the field (Ružičić *et al*., 2013). This was not possible at the Madagascar site and literature standards could not be found, therefore a_l was adjusted to give physically realistic model results and was finally assigned a value of 1 m for the entire profile.

The bulk density of the ion adsorption layer was determined in this study. For the four other layers in the laterite profile, literature values were taken from the standard soil texture classes (Carsel & Parrish, 1988). The soil specific parameters are shown in Table 6.4.

Table 6.4 The soil specific parameters used in the HYDRUS-1D simulation.

Soil layer	Texture	ρ_b [g/cm^3]	a_l [m]	MassTr	Thlm = 0
Top soil	Loamy Sand	1.43	1	0	0
Ferruginous layer	Sandy loam	1.46	1	0	0
Ion adsorption ore	Sandy clay loam	1.30	1	0	0
Weathered granite	Clay loam	1.39	1	0	0
Bedrock	Silty Clay Loam	1.30	1	0	0

The remaining parameters that simulate solute transport are the:

- Solute transport model
  - ⇒ Solute transport model, time weighting scheme, space weighting scheme, iteration criteria (for nonlinear problems), and number of solutes.
- HP1 components database pathway
  - ⇒ Define the solutes.
- HP1 definition

[28] The immobile water content is set to = 0 when physical non-equilibrium is not considered.

⇒ Solution composition, geochemical model and additional outputs.

- Solute specific
  - ⇒ Molecular diffusion coefficient in soil air and molecular diffusion coefficient in free water.
- Solute transport boundary conditions
  - ⇒ At the upper and lower boundaries and the initial conditions.

6.3.2.1 Model Conditions

Steady state water flow was simulated with the van Genuchten-Mualem hydraulic model and a constant pressure head for the upper BC. All the lower BC options (e.g. horizontal drains) were simulated, but a freely draining soil profile was considered the most realistic in this situation, where the water table lies far below the ore body of interest (Šimůnek *et al.,* 2008).

Solute transport was simulated with the equilibrium solute transport model with Galerkin finite elements as the space weight scheme and Crank-Nicholson as the time weight scheme. Three five-layered soil profiles each with typical IAD profile depths (6 m, 10 m and 30 m) were considered in these simulations. The profiles were discretised into 41 finite elements.

The soil profile initially contains groundwater in equilibrium with the cation exchanger[29]. Seven solutes were included in the model (Na, Cl, Total O, Total H, K, Al and Ca).The profile was flushed with a 1 M NaCl solution. Both solutions were prepared under oxidising conditions (in equilibrium with the pO_2 in the atmosphere). The total simulation time was 400 days.

The amount of exchange sites (X) was 10.3 meq/100g of dry soil. This value was obtained from the CEC experiment with a concentrated barium chloride solution (§ 4.1). The log K constants for the exchange reactions are defined in the WATEQ4F database and therefore do not have to be specified in the input.

The solute parameters molecular diffusion coefficient in soil air and in free water were both set to equal zero. A concentration flux was used as an upper boundary condition and zero concentration gradient was assumed as a lower boundary condition with liquid phase concentrations as an initial condition.

Table 6.5 summarises the inputs for the steady state water flow and solute transport simulations at different soil depths.

[29] This initial soil solution was based on a groundwater sample collected by project colleagues from pit 2 during the field expedition.

Table 6.5 Inputs for the water flow and solute transport simulations.

Input	Value
Number of Soil Materials	5
Depth of the Soil Profile [m]	z = 6, 10, 30
Boundary Condition (top)	Constant Pressure Head
Boundary Condition (bottom)	Free Drainage
Hysteresis	none
Hydraulic model	van Genuchten-Mualem
Total Model Time [days]	400
Number of Solutes	7
Time Weighting Scheme	Crank-Nicholson Scheme
Space Weighting Scheme	Galerkin Finite Elements
Nonequilibrium Solute Transport Models	Equilibrium Model

Solute transport simulations with a NaCl (seawater) solution were undertaken because it is considered the most environmentally acceptable reagent to mobilise the REE. Standard applications of ISR commonly use $(NH_4)_2SO_4$ (Yang *et al.,* 2013). A constant pressure head of 0 m was assigned to the top and bottom boundary conditions in the simulations.

Fig. 6.6 shows the concentration of Na and Cl varying with simulation time in 6 m, 10 m and 30 m generic Madagascar soil profiles. The concentration of Cl being flushed from the soil decreases with the increasing depth profiles. After 400 days 1 mol/L Cl was still being flushed out at 6 m profile but at 30 m all the Cl was completely gone from the profile.

The concentration of Na that reached the bottom of the profile and was being flushed out at the end of the simulation, decreased with depth. At 400 days, the concentration of Na decreased from ~0.4 mol/L in the 6 m profile to 0.0 mol/L in the 30 m profile (Fig. 6.6). In the 30 m profile, all the Na was entirely flushed from the soil after transport through 20 m.

The time taken for 1 M NaCl solution to reach the bottom of three generic soil profiles at 6 m, 10 m and 30 m are shown in Fig. 6.7. The time taken for Na and Cl to reach the bottom of the profiles increased with depth. In the 30 m profiles, most of the element concentrations were flushed out at the bottom of the soil.

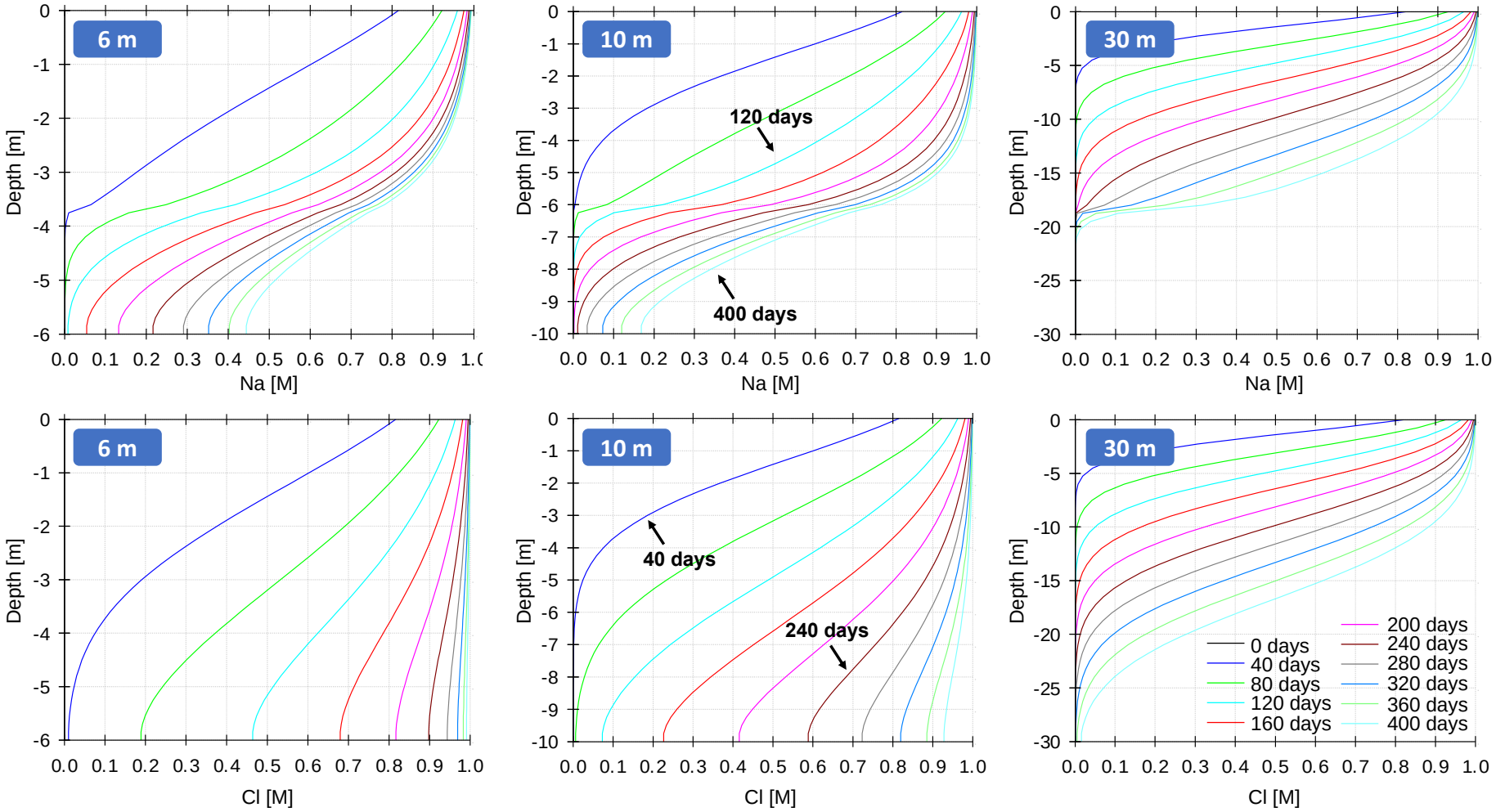

Fig. 6.6 Solute transport of 1 M NaCl through a 6 m, 10 m and 30 m soil profile.

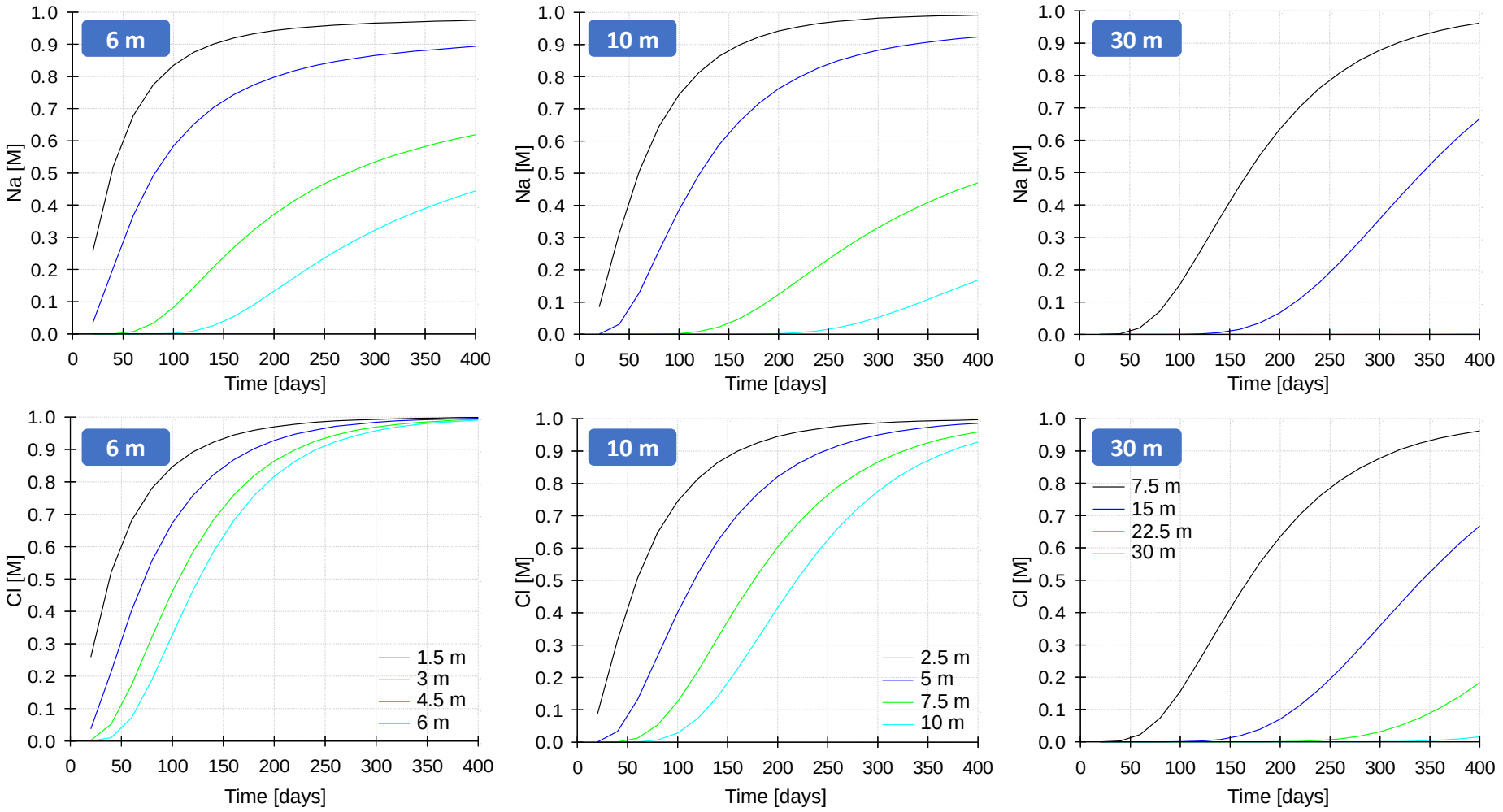

Fig. 6.7 Time taken for transport of 1 M NaCl to reach the bottom of a 6 m, 10 m and 30 m soil profile.

A number of additional simulations were performed in HYDRUS 1-D that determined the effect of increasing and decreasing ionic strength of the NaCl reactive solution by an order of magnitude. This was important to determine the optimum ionic strength to recover the REE during mining with ISR and to see how infiltration of the solution was affected.

The model conditions for water flow and solute transport are shown in Table 6.5. Six simulations were performed in which three five-layered soils and two ionic strength solutions were considered. The inflowing NaCl solutions had ionic strengths of 1×10^{-3} M and 2 M. The initial soil conditions comprised a groundwater solution in equilibrium with the exchanger.

Seven solutes were included in the simulations. These were Na, Cl, Total O, Total H, K, Al and Ca. The amount of exchange sites totalled 10.3 meq/100g. The exchange constants for the cation exchange reactions were already defined in the WATEQ4F database. The total simulation time was 400 days.

Fig. 6.8 - Fig. 6.11 show the transport of 1×10^{-3} M and 2 M NaCl solutions and their travel time through three soils at 6 m, 10, m and 30 m. In the 1×10^{-3} M simulations, the Na was entirely flushed out at 400 days (Fig. 6.8 and Fig. 6.9). The amount of Cl still being flushed from the soils at the end of the simulation increases with soil depth.

In the 2 M NaCl simulations, most of the Cl (~ 2M) and some Na (0.6 – 1.2 M) was still bring flushed from the profile at 400 days in the 6 m and 10 m soils (Fig. 6.9 and Fig. 6.11). However, in the 30 m soil the elements were entirely flushed out of the profile within 400 days. The time taken for Na and Cl to reach the bottom of the soils was independent of ionic strength.

A higher ionic strength solution is considered to be more effective to mobilise the exchangeable REE into solution (Moldoveanu & Papangelakis, 2012). These simulations indicate that 1 M ionic strength (Fig. 6.6) is adequate for ISR. Increasing or decreasing the ionic strength by an order of magnitude did not illustrate any significant infiltration differences.

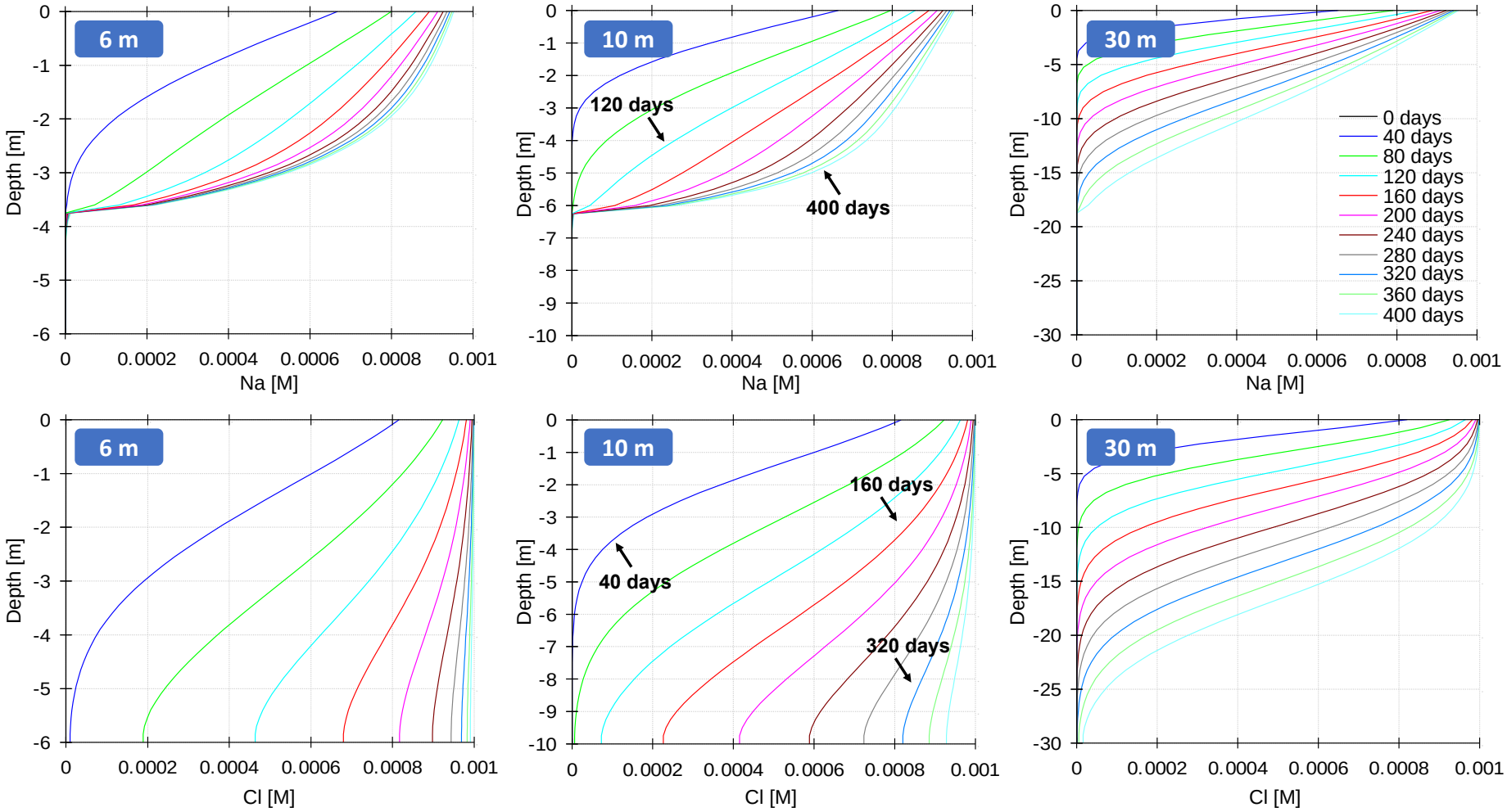

Fig. 6.8 Solute transport of 1 x 10^{-3} M NaCl through a 6 m, 10 m and 30 m soil profile.

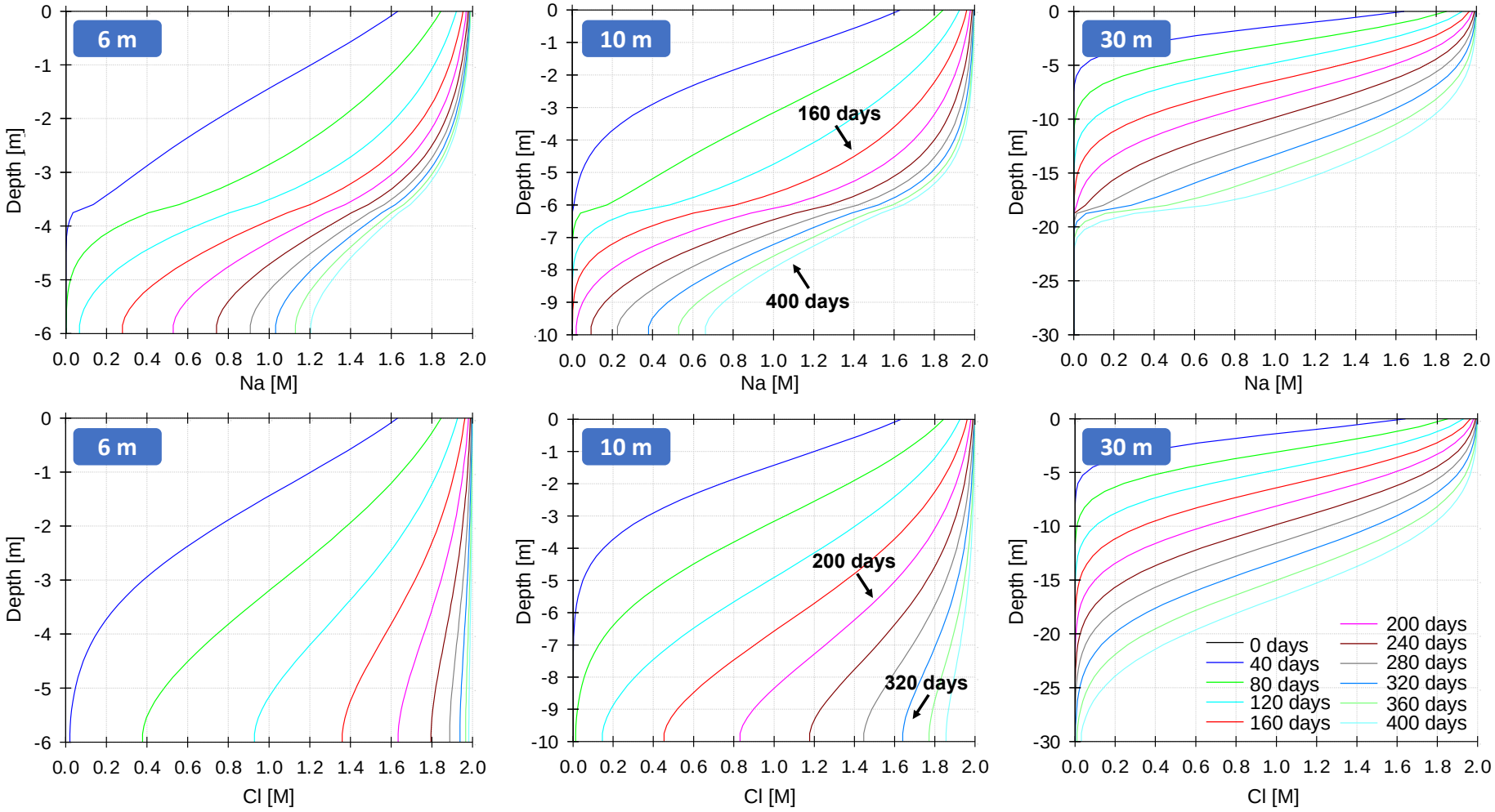

Fig. 6.9 Solute transport of 2 M NaCl through a 6 m, 10 m and 30 m soil profile.

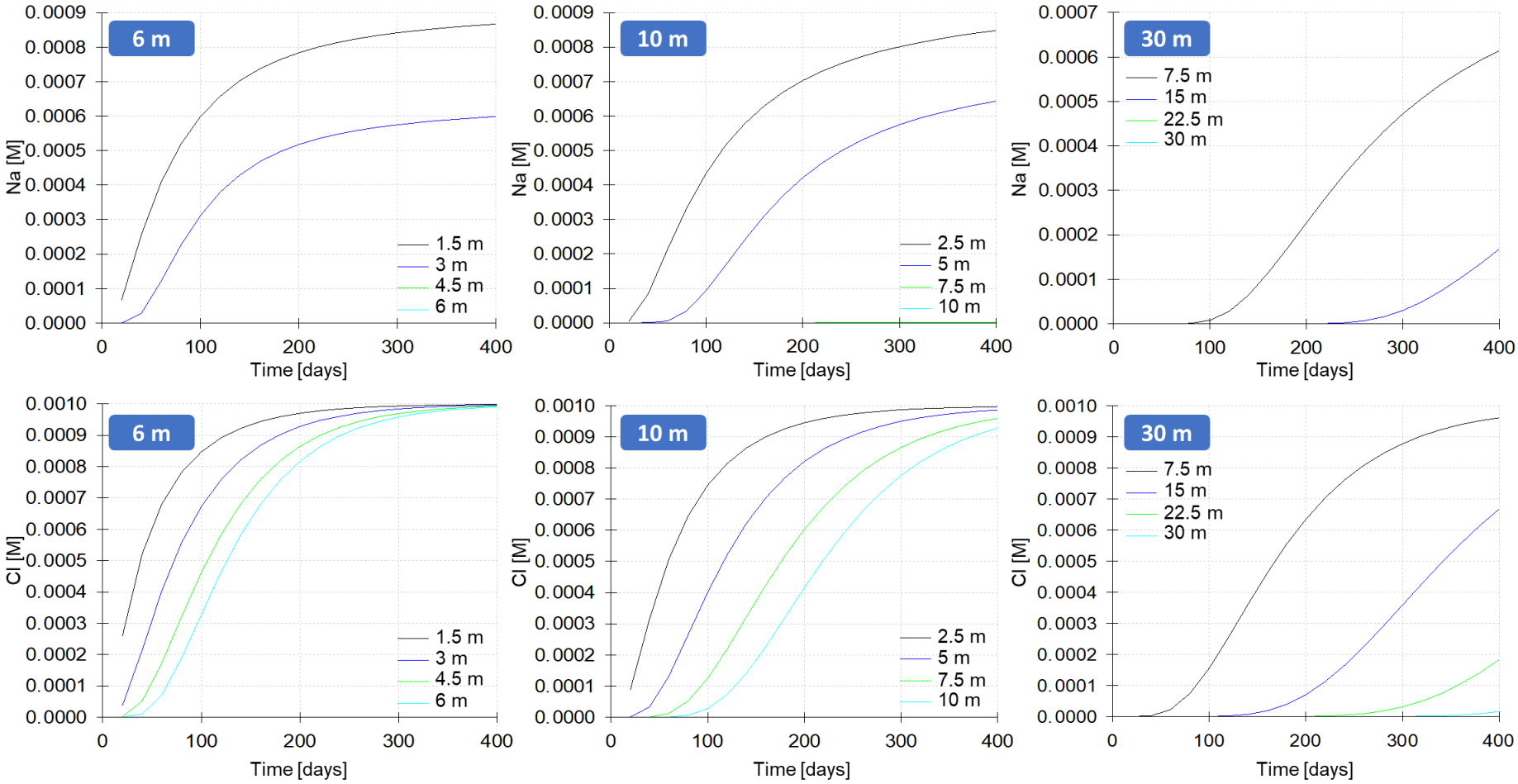

Fig. 6.10 Time taken for transport of 1 x 10^{-3} M NaCl to reach the bottom of a 6 m, 10 m and 30 m soil profile.

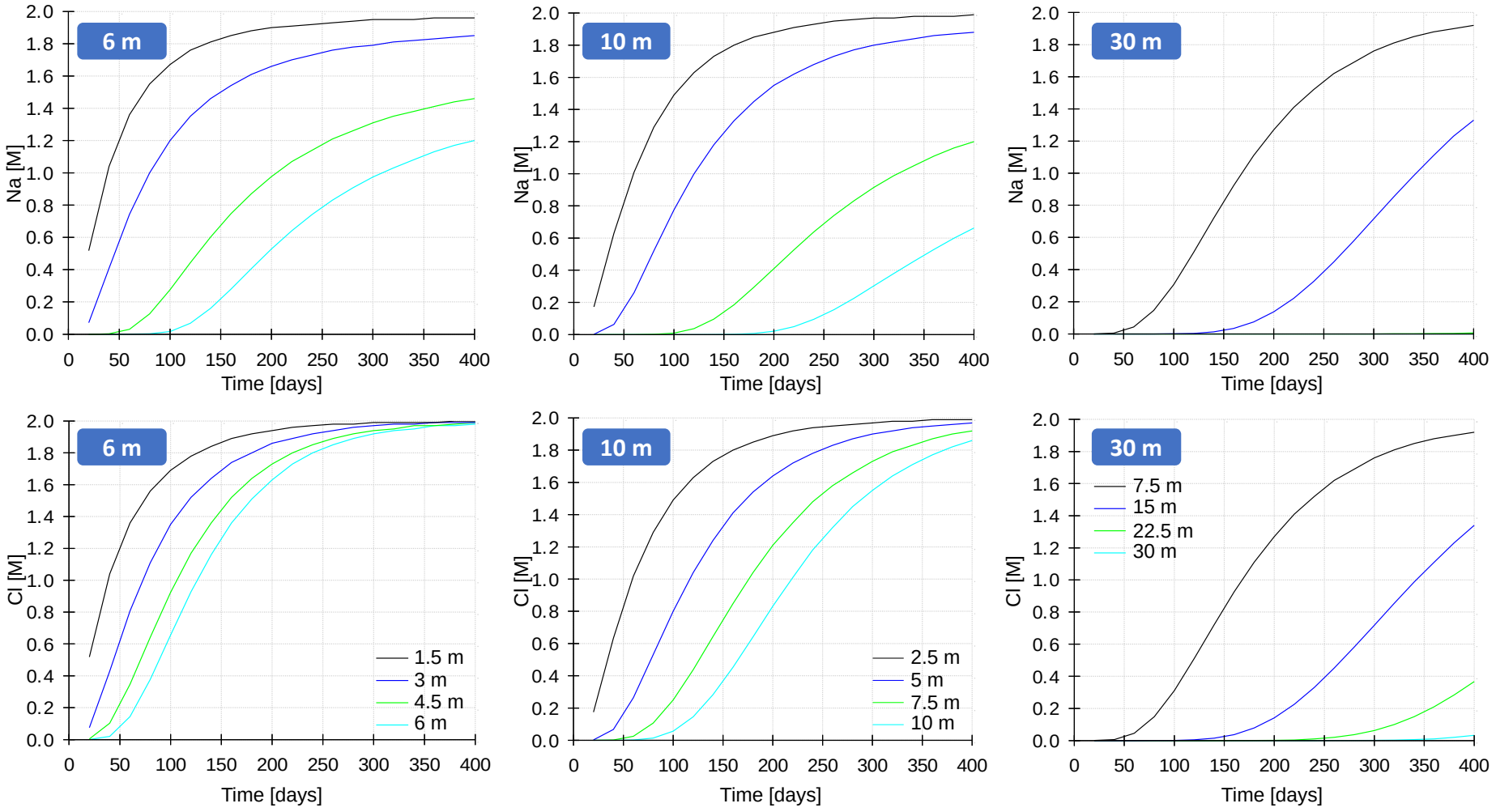

Fig. 6.11 Time taken for transport of 2 M NaCl to reach the bottom of a 6 m, 10 m and 30 m soil profile.

The following simulations include REE exchange reactions. These were undertaken to better understand REE transport thorough laterite soils. The model conditions are shown in Table 6.5 for steady state water flow and solute transport simulations. This includes free drainage as the lower boundary condition. Three five-layered soil profiles were considered.

The inflowing NaCl solution in each profile had a concentration of 1 M. For the initial soil conditions, a groundwater solution was put in equilibrium with the cation exchangers. Twenty solutes were included in the simulations, they were Na, Cl, Total O, Total H, K, Al, Ca, Y, La, Ce, Pr, Eu, Sm, Gd, Tb, Dy, Ho, Er, Yb and Lu[30]. The total simulation time was 400 days.

The amount of exchange sites totalled 10.3 meq/100g in each soil layer. The exchange composition comprised 0.24 meq/100g $REEX_3$ exchange species (for individual REE equivalent fractions see Table 5.1) and 10.06 meq/100g NaX exchange species. Exchange constants for the REE which were taken from this research (log K = 2.29).

Fig. 6.12 and Fig. 6.13 show reactive transport behaviour of La, Ce, Nd and Dy through three soil profiles. The 30 m profiles best illustrate the REE peaks being mobilised downwards through the soil. The REE were transported at similar rates. The breakthroughs at each time step (i.e. every 40 days) successively increase until peak concentration is reached at 400 days.

The time taken to recover the majority of the exchangeable REE concentrations by flushing with NaCl varies. For example in the 10 m profiles, 160 days was needed for most of La to be recovered, 120 days was needed for Ce and Nd, whereas Dy needed only 80 days to recover the majority of their concentrations.

The time required for REE recovery could be related to the concentration on the exchange surface. Ce has the highest concentration on the exchanger, and therefore takes more time to be transported through the profile. Dy was one of the least concentrated REE and thus required less time for the recovery of most of its exchangeable concentration.

A comparison of REE peak concentrations indicates that in the 30 m weathered profiles greater REE concentrations were observed and therefore more REE could be recovered than in the 6 m and 10 m profiles. For example, the peak concentration for Ce was > 0.008 mM in the 30 m profile but was < 0.004 mM in the 6 m profile.

[30] Tm was excluded because 20 is the maximum number of elements allowed in HYDRUS 1-D and it has the lowest equivalent fraction in the CEC of the Madagascar IAD (Table 5.1).

The simulations of REE transport through different depth soil profiles indicate that the best depth for REE recovery was between 10 m and 30 m. This was where the depth was sufficient to recover the richest horizons (within 400 days) but not so deep as to require unfeasibly long transport times (e.g. slow peak velocities).

The similarities in the reactive transport behaviour of all the REE in the HYDRUS-1D simulations and in the TRN simulations indicates that there is no fractionation of the REE pattern. This finding supports the results of the log K estimation i.e. that one log K can describe all REE exchange reactions with the Madagascar IAD. The coherent REE behaviour also supports the use of HYDRUS 1-D to test the applicability of ISR for IAD.

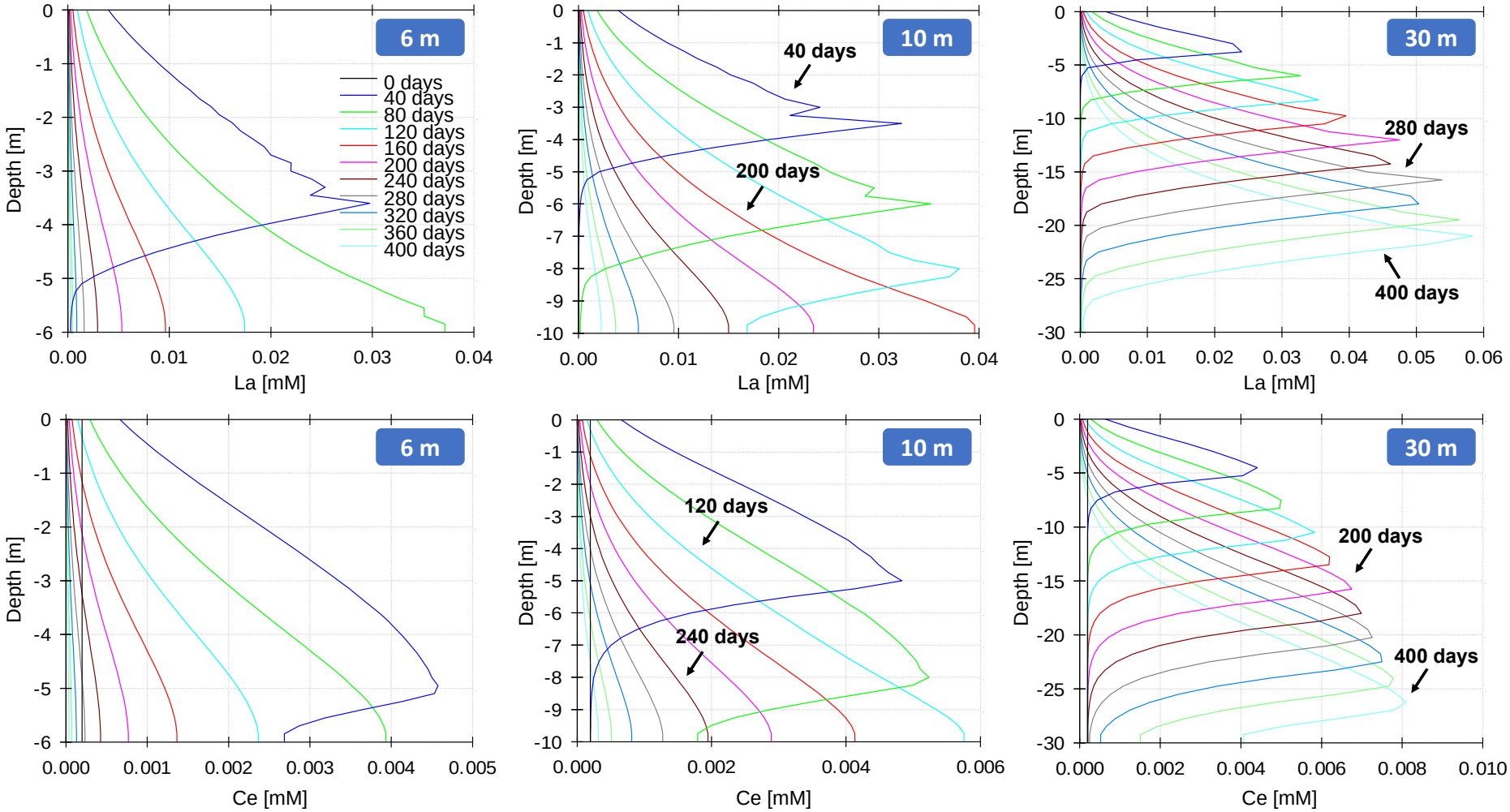

Fig. 6.12 Solute transport of La and Ce through a 6 m, 10 m and 30 m soil profile.

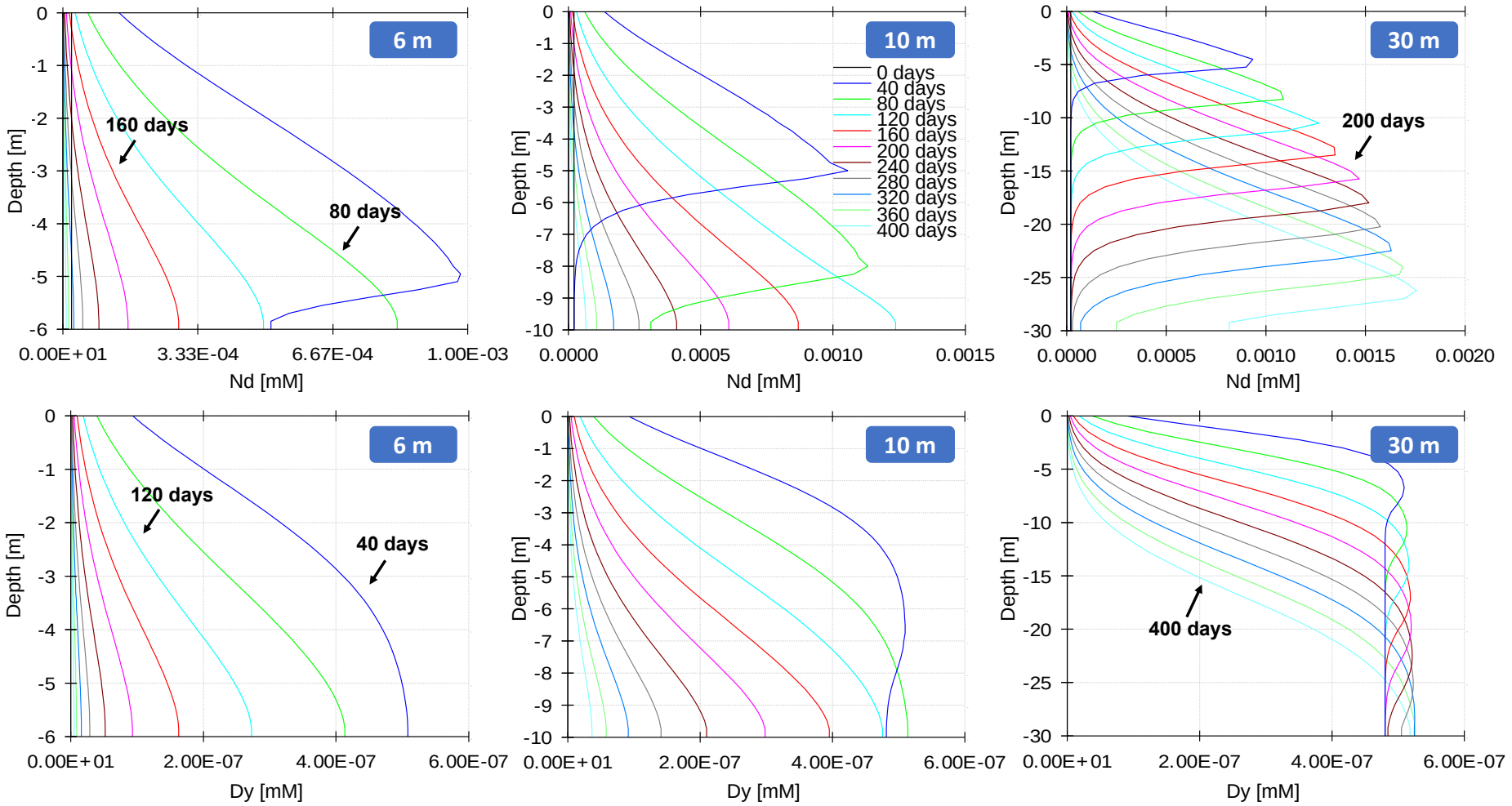

Fig. 6.13 Solute transport of Nd and Dy through a 6 m, 10 m and 30 m soil profile.

6.4 Further Site Investigation

Various generic simulations of water flow and solute transport through a laterite profile have been undertaken in this research. Future studies should determine site specific parameters in order to evaluate the hydrological properties of the deposit and move to the next stage of ISR assessment and design. This should involve field tests and pilot plant operations.

Exploration drilling and geophysical surveying should be undertaken to construct cross-sections of the deposit in order to define the extent of groundwater saturation and to identify confining layers. The existing information in hydrogeological mapping study of north-central Madagascar (Davies, 2009) should then be compared to the results of the exploration drilling.

Any distinct lithologies, facies or tectonic domains (e.g. Ambohimirahavavy igneous complex) within the study area should be delineated and within these sections test wells should be installed. Test wells could also be installed outside the mineralised area to help define the flow direction and velocity related to the groundwater gradient.

Core samples of the ore-bearing horizon should be recovered from each of the test wells. In addition, geophysical well logging surveys should be conducted in each pilot hole. This should include natural gamma, electric (self potential and resistivity), borehole flow distribution, calliper and deviation logs.

Representative drill core samples should be recovered from all lithological rock types across the entire ore-bearing horizon and also from both upper and lower water-confining layers. The whole core and disaggregated samples can be studied in the laboratory to determine hydraulic properties such as porosity and permeability.

Following determination of the hydrological properties using the methods described above, a feasibility study should be compiled which takes into account:

- the thickness of the ore horizon;
- depth of the ore body;
- the hydrostatic level of the water table, and
- the permeability of the ore and productivity of the ore.

If it is decided that the hydrological properties of the deposit make it suitable for ISR, the deposit should be subject to further detailed exploratory tests.

6.5 Key Outcomes

In accordance with the industrial driver for this research, a conceptual model of the geochemical reactive transport processes for ISR for the Madagascar IAD was developed, using existing literature and site data. Generic simulations of ISR processes based on the conceptual model were undertaken in HYDRUS-1D.

The simulations illustrate:

- Soil water flow and infiltration properties of generic laterite profiles using the single and dual porosity flow models;
- Solute transport of an environmentally acceptable reactive solution (NaCl) with different ionic strengths through generic laterite profiles, and
- Solute transport of the REE through generic laterite profiles with different depths following REE-Na exchange reactions.

The simulations indicate that:

- Use of the different porosity flow models did not influence soil water flow;
- The residence time of infiltrating water to reach the bottom of the profile was less than 40 days in all the different profile depths (6 m, 10 m, 30 m);
- The order of magnitude changes to ionic strength did not significantly change NaCl transport through the soil, thus a 1 M NaCl solution was considered adequate for use in simulations of REE cation exchange processes and in ISR applications;
- The REE were transported at similar rates through the soils;
- The time needed to recover the majority of the exchangeable La concentration by flushing with NaCl was 160 days, for Dy this was only 80 days. This may be related to their concentrations on the exchange surface, and
- REE peak concentration decreased with increased profile depth from 6 m to 30 m. Therefore, the best depth for REE recovery using ISR was between 6 m and 10 m.
- The REE behave coherently in both the HYDRUS-1D and TRN simulations, this suggests that HYDRUS-1D can be used to test the applicability of ISR for IAD.

Following these simulations, future work to assess the potential for ISR at the Madagascar study area requires additional site investigation to determine the hydrological properties of the Madagascar deposit. This should involve: exploration drilling, geophysical surveying, installation of test wells and analysis of whole drill core samples.

CHAPTER 7

CONCLUSIONS

The importance of the REE stems from their physicochemical similarities (i.e. mineral site coordination, charge and ionic radius) which have made them essential in many aspects of modern technology. Because of their numerous applications and the control that China over their supply, these trace metals are considered to be 'critical'.

IAD are a REE-bearing deposit of particular significance, due to the chemical ease with which recovery of the ion exchangeable REE adsorbed onto clay mineral surfaces is possible. Since IAD are only commercially processed in China, where mining has led to environmental degradation. This study considered an IAD under active exploration in Madagascar.

Alternative environmentally focused mining approaches should be considered to recover REE from IAD (e.g. in Madagascar) but, prior to this, the mechanism of REE mobilisation during mining must be understood, and be modelled. There are a number of literature studies investigating REE sorption processes with common IAD minerals.

REE-kaolinite interactions are the most widely studied, where cation exchange at interlayer sites is the dominating sorption mechanism. The model which considers ion exchange requires thermodynamic equilibrium constants to model exchange reactions. However, there are no exchange constants for all the REE in any literature or database source.

In accordance with the challenges outlined above, the research aim was to develop a numerical modelling approach to simulate the mobilisation of the REE from IAD during mining. The principal objectives were therefore to determine thermodynamic equilibrium constants for REE exchange reactions with the Madagascar IAD minerals, test these constants using data and reactive transport modelling of flow-through laboratory column experiments, and implement these processes in a reactive transport model at site scale.

7.1 Analytical Outcomes

Three types of experiments were carried out to provide model inputs for reactive transport and equilibrium simulations. CEC tests were performed to determine the exchange composition of the Madagascar IAD. Batch tests were undertaken to provide a REE dataset from which REE exchange constants were estimated. Soil column experiments were performed to verify the estimated REE exchange constants.

The CEC of Madagascar IAD was obtained with different salt solutions. Each gave an average CEC of 10 meq/100g of dry soil. This is within the literature standard of 3 – 15 meq/100g for pure kaolinite (Brady & Weil, 2002). The CEC of 10.34 ± 0.07 meq per 100g obtained with the barium salt was used as the model input. This was because this salt solution had been used in each type of experiment.

The major exchangeable cation on the Madagascar IAD was Al^{3+}, where it occupied more than 70% of exchange sites. This was in addition to its occurrence in the deposit's mineral structure. The resultant pH drop from near neutral to pH 4 when the sample material was put in contact with a salt solution could be explained by significant concentrations of exchangeable Al^{3+} being mobilised into the aqueous phase.

In the batch equilibrium tests, all the REE (incl. Sm and Eu) behaved coherently when mobilised into the aqueous phase by a concentrated salt solution at 9 SLR conditions, where increasing exchangeable REE concentrations in solution increased as a function of SLR. Spectral interference due to the presence of high barium concentrations during ICP-MS analysis was the only reason for the different Sm and Eu trends.

Cation exchange reactions were also observed in the soil column experiments by the retardation of the injected cation (Ba^{2+} or NH_4^+) breakthrough curve. Retardation of the breakthrough point occurred as a result of the injected cation exchanging for the REE^{3+}, Al^{3+} and the other trace elements in the column.

7.2 Modelling Outcomes

Equilibrium calculations were performed in PHREEQC to model REE-IAD exchange in the batch tests and to estimate equilibrium constants for these reactions. Reactive transport calculations were then undertaken in TRN to model REE breakthrough curves with the exchange constants derived by modelling the batch equilibrium experiments.

This research shows the cation exchange reactions are able to adequately describe the mobilisation of the REE from the Madagascar IAD with the exchange reaction:

(7.1) $3NaX + REE^{3+} \leftrightarrow REEX_3 + 3Na^+$ log K

which is split into

(7.2) $REE^{3+} + 3X^- = REEX_3$ log K = 2.29

(7.3) $Na^+ + X^- = NaX$ $\log K = 0.0$[31]

A single thermodynamic equilibrium constant of

- log K = 2.29 ± 0.3 (standard deviation) ⇒ best fit for REE dataset in batch tests
- log K = 2.29 ± 0.5 (standard deviation) ⇒ best fit for REE dataset in all soil columns

was able to describe all REE exchange reactions with the **Madagascar IAD**.

Exchange constants were also calculated for each individual REE to determine whether the REE dataset could be better represented. The individual log K dataset only varied after 2 decimal places and the objective function difference between the two models was:

- objective function = 5.71×10^{-11} ⇒ for the different log K model
- objective function = 5.72×10^{-11} ⇒ for the single log K model

There is only one literature study that reported a REE exchange constant of log K = 11.0 ± 0.4 for the Na/Eu reaction on pure kaolinite (Tertre *et al.*, 2006a). The literature value was determined using the diffuse double layer surface complexation model. The literature log K could not describe REE exchange reactions with the Madagascar IAD.

The order of magnitude differences could be explained by the different complexities of the materials or the different modelling approaches used. Furthermore only one constant was determined by Tertre *et al.* (2006a). In this study the REE exchange behaviour is coherent and can be described by a single constant but that may not be the case for the literature study.

However, because thermodynamic equilibrium constants are fundamental quantities they should not be affected by any of the explanations given in the previous paragraph. The exact reason for the order of magnitude variance is not known. But, it is important to note that the REE exchange constants derived from equilibrium modelling have only been fitted to a dataset from one sample from the Madagascar IAD. Therefore, these constants cannot be considered the equilibrium constants for all IAD-REE exchange reactions.

7.2.1 Environmentally Focused Modelling Application

Once REE exchange reactions with the Madagascar IAD could be accurately characterised, generic simulations based on a conceptual model of ISR processes at the study

[31] The exchange constant is from the WATEQ4F database.

area were undertaken. These simulations varied: soil profile depth, the ionic strength of the environmentally viable flushing solution and the soil hydraulic model.

The residence time for infiltrating water to reach the bottom of the profile was relatively fast (< 40 days), and this was independent of the increasing soil depth profiles (6 m, 10 m, 30 m). Changing the ionic strength of the flushing solution (1 x 10^{-3} M, 1 M and 2 M) did not significantly effect NaCl infiltration properties.

REE peak concentration increased with increased profile depth from 6 m to 30 m. Therefore, the best depth for REE recovery using ISR was indicated to be between 10 m and 30 m where the depth was not so deep as to require impractically long transport times to the point where recovery takes place i.e. with horizontal drains.

7.3 Future work

HYDRUS-1D has been used to generic ISR processes through the Madagascar soil profile. Development of a site specific model would require knowledge of the soil hydraulic properties (e.g. porosity) determined from whole core samples, as well as the installation of pilot wells and geophysical surveying. A 2D/3D flow and transport model could then be developed to move to the next stage of ISR assessment.

In order to determine whether the REE exchange constants obtained in this study are actually thermodynamic equilibrium constants, the constants should be applied to another IAD system and/or different samples from the Madagascar IAD. The literature REE equilibrium constants (Tertre *et al.,* 2006a) could also be applied to different IAD to determine their efficacy in describing REE exchange reactions.

Future work could also consider whether cation exchange is sensitive to the type of clay mineral. This would require the additional REE-batch datasets in which clays other than kaolinite are dominant in the sample material. This study successfully used exchange constants from WATEQ4F.dat which according to Tournassat *et al.* (2007) were determined for montmorillonite. This indicated that cation exchange was insensitive to the clay mineral.

BIBLIOGRAPHY

Aagaard, P., & Helgeson, H.C. (1982). Thermodynamic and kinetic constraints on reaction rates among minerals and aqueous solutions; I, Theoretical considerations. *American journal of Science*, 282 (3), 237-285.

Abaka-Wood, G.B., Addai-Mensah, J., & Skinner, W. (2016). Magnetic separation of monaazite from mixed minerals. *Chemical Engineering-Regeneration, Recovery and Reinvention*, 596.

Aide, M.T., & Aide, C (2012). Rare Earth Elements: Their Importance in Understanding Soil Genesis. *ISRN Soil Science.*

Aja, S. U. (1998). The Sorption of the Rare Earth Element, Nd, onto Kaolinite at 25 C. *Clays and Clay Minerals*, 46, 103-109.

Allaby, M. (2008). *A Dictionary of Earth Sciences*. Oxford: Oxford University Press.

Anders, E., & Grevesse N. (1989). Abundances of the elements: Meteoritic and solar. *Geochimica et Cosmochimica Acta,* 53, 197-214.

Anderson, P.R., & Christensen, T.H. (1988). Distribution coefficients of Cd, Co, Ni, and Zn in soils. *Journal of soil science*, 39 (1), 15-22.

Appelo, C.A.J. (1994). Cation and proton exchange, pH variations, and carbonate reactions in a freshening aquifer. *Water Resources Research*, 30 (10), 2793-2805.

Appelo, C.A.J., & Postma, D. (2005). *Geochemistry, groundwater and pollution*. Leiden: A.A. Balekma Publishers.

Arbogast, T., Douglas, Jr, J., & Hornung, U. (1990). Derivation of the double porosity model of single phase flow via homogenization theory. *SIAM Journal on Mathematical Analysis*, 21 (4), 823-836.

Aubert, D., Stille, P., & Probst, A. (2001). REE fractionation during granite weathering and removal by waters and suspended loads: Sr and Nd isotopic evidence. *Geochimica et Cosmochimica Acta*, 65 (3), 387-406.

Baczewski, L.T., Givord, D., Alameda, J.M., Dieny, B., Nozieres, J.P., Rebouillat, J.P., & Prejean, J.J. (1993). Magnetism in rare-earth-transition metal systems. Magnetization reversal and ultra-high susceptibility in sandwiched thin films based on rare-earth and cobalt alloys. *Acta Physica Polonica Series A*, 83, 629-629.

Ball, J.W., & Nordstrom, D.K. (1991). *User's manual for WATEQ4F, with revised thermodynamic data base and test cases for calculating speciation of major, trace, and redox elements in natural waters.* USGS.

Bao, Z., & Zhao, Z. (2008). Geochemistry of mineralisation with exchangeable REY in the weathering crusts of granitic rocks in South China. *Ore Geology Reviews*, 33, 519-535.

Barteková, E., & Kemp, R. (2016). National strategies for securing a stable supply of rare earths in different world regions. *Resources Policy*, 49, 153-164.

Bau, M. (1999). Scavenging of dissolved yttrium and rare earths by precipitating iron oxyhydroxide: experimental evidence for Ce oxidation, Y-Ho fractionation, and lanthanide tetrad effect. *Geochimica et Cosmochimica Acta*, 63 (1), 67-77.

Bear, F.E. (1965). Chemistry of the Soil. Reinhold Publishing: New York.

Bear, J. (1972). Dynamics of fluids in porous materials. *Society of Petroleum Engineers: Dallas, TX, USA*.

Berger, A., & Frei, R. (2014). The fate of chromium during tropical weathering: A laterite profile from Central Madagascar. *Geoderma*, 213, 521-532.

Bonnot-Courtois, C.J.R.N., & Jaffrezic-Renault, N. (1982). Etude des échanges entre terres rares et cations interfoliaires de deux argiles. *Clay Mineralogy*, 17 (4), 409-420.

Borges, J.B., Huh, Y., Moon, S., & Noh, H. (2008). Provenance and weathering control on river bed sediments of the eastern Tibetan Plateau and the Russian Far East. *Chemical Geology*, 254 (1), 52-72.

Bradbury, M.H., & Baeyens, B. (2002). Sorption of Eu on Na-and Ca-montmorillonites: experimental investigations and modelling with cation exchange and surface complexation. *Geochimica et Cosmochimica Acta*, 66 (13), 2325-2334.

Bradbury, M.H., & Baeyens, B. (2005). Modelling the sorption of Mn (II), Co (II), Ni (II), Zn (II), Cd (II), Eu (III), Am (III), Sn (IV), Th (IV), Np (V) and U (VI) on montmorillonite: Linear free energy relationships and estimates of surface binding constants for some selected heavy metals and actinides. *Geochimica et Cosmochimica Acta*, 69 (4), 875-892.

Bradbury, M. H., & Baeyens, B. (2009). Sorption modelling on illite. Part II: Actinide sorption and linear free energy relationships. *Geochimica et Cosmochimica Acta*, 73 (4), 1004-1013.

Bradbury, M.H., & Baeyens, B. (2011). Predictive sorption modelling of Ni (II), Co (II), Eu (IIII), Th (IV) and U (VI) on MX-80 bentonite and Opalinus Clay: A “bottom-up” approach. *Applied Clay Science*, 52 (1), 27-33.

Bradbury, M. H., Baeyens, B., Geckeis, H., & Rabung, T. (2005). Sorption of Eu (III)/Cm (III) on Ca-montmorillonite and Na-illite. Part 2: Surface complexation modelling. *Geochimica et Cosmochimica Acta*, 69 (23), 5403-5412.

Brady, P.V. (1994). Alumina surface chemistry at 25, 40, and 60 C. *Geochimica et cosmochimica acta*, 58 (3), 1213-1217.

Brady, P.V., Cygan, R.T., & Nagy, K.L. (1996). Molecular controls on kaolinite surface charge. *Journal of Colloid and Interface Science*, 183 (2), 356-364.

Brady, N.C., & Weil, R. R. (2002). *The Nature and Properties of Soil*. New Jersey, USA: Prentice Hall.

Braun, J.J., Viers, J., Dupré, B., Polve, M., Ndam, J., & Muller, J.P. (1998). Solid/liquid REE fractionation in the lateritic system of Goyoum, East Cameroon: the implication for the present dynamics of the soil covers of the humid tropical regions. *Geochimica et Cosmochimica Acta*, 62 (2), 273-299.

Brooks, R.H., & Corey, A.T. (1964). Hydraulic properties of porous media and their relation to drainage design. *Transactions of the ASAE*, 7 (1), 26-28.

Byrne, R.H., & Kim, K.H. (1990). Rare earth element scavenging in seawater. *Geochimica et Cosmochimica Acta*, 54 (10), 2645-2656.

Buijs, B., & Sievers, H. (2011). Critical thinking about critical minerals: Assessing risks related to resource security. *Polinares EU Policy on Natural Resources. The Hague: Clingendael International Energy Programme*.

Camobreco, V.J., Richards, B.K., Steenhuis, T.S., Peverly, J.H., & McBride, M.B. (1996). Movement of heavy metals through undisturbed and homogenized soil columns. *Soil Science*, 161 (11), 740-750.

Cantrell, K. J., & Byrne, R. H. (1987). Rare earth element complexation by carbonate and oxalate ions. *Geochimica et Cosmochimica Acta*, 51 (3), 597-605.

Cao, X., Yin, M., & Wang, X. (2001). Elimination of the spectral interference from polyatomic ions with rare earth elements in inductively coupled plasma mass spectrometry by combining algebraic correction with chromatographic separation. *Spectrochimica Acta Part B: Atomic Spectroscopy*, 56 (4), 431-441.

Carsel, R.F., & Parrish, R.S. (1988). Developing joint probability distributions of soil water retention characteristics. *Water resources research*, 24 (5), 755-769.

Carter, M.R. (Eds). (1993). Soil sampling and methods of analysis. CRC Press.

Chi, R., & Tian, J. (2008). *Weathered crust elution-deposited Rare Earth Ores*. China: Nova Science Publishing Inc.

Chi, R.A., Tian, J., Li, Z.J., Peng, C., Wu, Y.X., Li, S.R., Wang, C.W., & Zhou, Z.A. (2005). Existing State and Partitioning of Rare Earth on Weathered Ores. *Journal of rare earths*, 23 (6), 756.

Chi, R. A., Dai, Z. X., Xu, Z. G., Wu, Y. X., & Wang, C. W. (2006). Correlation analysis on partition of rare earth in ion-exchangeable phase from weathered crust ores. *Transactions of Nonferrous Metals Society of China*, 16 (6), 1421-1425.

Clark, A.M. (1984). Mineralogy of the rare earth elements. In *Developments in geochemistry* Elsevier.

Coppin, F., Berger, G., Bauer, A., Castet, S., & Loubet, M. (2002). Sorption of lanthanides on smectite and kaolinite. *Chemical Geology*, 182, 57-68.

Coppin, F., Castet, S., Berger, G., & Loubet, M. (2003). Microscopic reversibility of Sm and Yb sorption onto smectite and kaolinite: Experimental evidence. *Geochimica et Cosmochimica*, 67, 14, 2515-2527.

Cornell, R.M., & Schwertmann, U. (2003). The iron oxides: structure, properties, reactions, occurrences and uses. John Wiley & Sons.

Dams, R.F., Goossens, J., & Moens, L. (1995). Spectral and non-spectral interferences in inductively coupled plasma mass-spectrometry. *Microchimica Acta*, 119 (3-4), 277-286.

Darcy, H. (1856). *Les fontaines publiques de la ville de Dijon: exposition et application.* Paris.

Davies, C.W. (1962). *Ion Association*. London: Butterworths.

Davis, J.A., James, R.O., & Leckie, J.O. (1978). Surface ionization and complexation at the oxide/water interface: I. Computation of electrical double layer properties in simple electrolytes. *Journal of colloid and interface science*, 63 (3), 480-499.

Del Nero, M., Froideval, A., Gaillard, C., Mignot, G., Barillon, R., Munier, I., & Ozgümüs, A. (2004). Mechanisms of uranyl sorption. *Geological Society, London, Special Publications*, 236 (1), 545-560.

Ding, J. (2012). Historical review of the ionic rare earth mining: In honor of the 60 anniversary of GNMRI [J]. *Nonferrous Metals Science and Engineering*, 3 (4), 14-19.

Doherty, J. (1994). PEST: a unique computer program for model-independent parameter optimisation. *Water Down Under 94: Groundwater/Surface Hydrology Common Interest Papers*, 551.

Dontsova, K.M., Yost, S.L., Šimunek, J., Pennington, J.C., & Williford, C.W. (2006). Dissolution and transport of TNT, RDX, and Composition B in saturated soil columns. *Journal of Environmental Quality*, 35 (6), 2043-2054.

Durner, W. (1994). Hydraulic conductivity estimation for soils with heterogeneous pore structure. *Water resources research*, 30 (2), 211-223.

Dzombak, D.A., & Morel, F.M.M. (1990). *Surface complexation modeling: hydrous ferric oxide*. New York: John Wiley & Sons.

European Commission. (2014). Report on critical raw materials for the EU-Report of the Ad hoc Working Group on defining critical raw materials. *European Commission*.

Fletcher, P., & Sposito, G. (1989). Chemical modeling of clay/electrolyte interactions of montmorillonite. *Clay Minerals*, 24 (2), 375-391.

Freundlich, H. (1909). Kolloidchemie. *Akademischer Verlagsgeselschaft, Leipzig*.
Fryer, B.J. (1977). Trace element geochemistry of the Sokoman Iron Formation. *Canadian Journal of Earth Sciences*, 14 (7), 1598-1610.

Gerke, H.H., & Van Genuchten, M.T. (1993). A dual-porosity model for simulating the preferential movement of water and solutes in structured porous media. *Water resources research*, 29 (2), 305-319.

Gidigasu, M.D. (1972). Mode of formation and geotechnical characteristics of laterite materials of Ghana in relation to soil forming factors. *Engineering Geology*, 6 (2), 79-150.

Giles, C. H., Smith, D., & Huitson, A. (1974). A general treatment and classification of the solute adsorption isotherm. I. Theoretical. *Journal of colloid and interface science*, 47 (3), 755-765.

Glass, R.J., Oosting, G.H., & Steenhuis, T.S. (1989). Preferential solute transport in layered homogeneous sands as a consequence of wetting front instability. *Journal of Hydrology (Amsterdam)*, 110 (1), 87-105.

Golev, A., Scott, M., Erskine, P.D., Ali, S.H., & Ballantyne, G. R. (2014). Rare earths supply chains: Current status, constraints and opportunities. *Resources Policy*, 41, 52-59.

Goodenough, K.M., Wall, F., & Merriman, D. (2018). The rare earth elements: demand, global resources, and challenges for resourcing future generations. *Natural Resources Research*, 27 (2), 201-216.

Graf, J.L. (1978). Rare earth elements, iron formations and sea water. *Geochimica et Cosmochimica Acta*, 42 (12), 1845-1850.

Gray, A.L., & Williams, J.G. (1987). Communication. Oxide and doubly charged ion response of a commercial inductively coupled plasma mass spectrometry instrument. *Journal of Analytical Atomic Spectrometry*, *2* (1), 81-82.

Grim, E. (1968). *Clay Mineralogy*. New York: McGraw-Hill.

Guo, W. (2012). The rare earth development can no longer overdraw ecological cost. China Environment News.

Gupta, C.K., & Krishnamurthy, N. (1992). Extractive metallurgy of rare earths. *International Materials Reviews*, 37 (1), 197-248.

Gupta, C.K., & Krishnamurthy, N. (2005). *Extractive metallurgy of rare earths*. New York: CRC Press.

Han, W.S., McPherson, B.J., Lichtner, P.C., & Wang, F.P. (2010). Evaluation of trapping mechanisms in geologic CO2 sequestration: Case study of SACROC northern platform, a 35-year CO2 injection site. *American Journal of Science*, 310 (4), 282-324.

Harper, L.A. (2005). *Ammonia: measurement issues*. U.S. Department of Agriculture: Agricultural Research Service, Lincoln, Nebraska.

Hatch, G.P. (2012). Dynamics in the global market for rare earths. *Elements*, 8 (5), 341-346.

Hayes, K.F., Redden, G., Ela, W., & Leckie, J.O. (1991). Surface complexation models: an evaluation of model parameter estimation using FITEQL and oxide mineral titration data. *Journal of colloid and interface science*, 142 (2), 448-469.

Helfferich, F.G. (1995). *Ion exchange*. Courier Corporation.

Helgeson, H.C. (1968). Evaluation of irreversible reactions in geochemical processes involving minerals and aqueous solutions—I. Thermodynamic relations. *Geochimica et Cosmochimica Acta*, 32 (8), 853-877.

Hendershot, W.H., & Duquette, M. (1986). A simple barium chloride method for determining cation exchange capacity and exchangeable cations. Soil Science Society of America Journal, 50 (3), 605-608.

Henderson, P. (1984). *Rare Earth Element Geochemistry*. Amsterdam: Elsevier.

Hillel, D., & Hatfield, J.L. (Eds.). (2005). *Encyclopedia of Soils in the Environment* (Vol. 3). Amsterdam: Elsevier.

Hillier, S. (2003). Clay Mineralogy, in Middleton, G.V., Church, M.J., Coniglio, M., Hardie, L.A., & Longstaffe, F.J. (Eds.) *Encyclopaedia of sediments and sedimentary rocks*. Kluwer Academic Publishers.

Ho, Y.S. (2004). Selection of optimum sorption isotherm. *Carbon*, 42 (10), 2115-2116.

Huittinen, N., Rabung, T., Andrieux, P., Lehto, J., & Geckeis, H. (2010). A comparative batch sorption and time-resolved laser fluorescence spectroscopy study on the sorption of Eu (III) and Cm (III) on synthetic and natural kaolinite. *Radiochimica Acta International journal for chemical aspects of nuclear science and technology*, 98 (9-11), 613-620.

Hunter, R.J. (1981). *Zeta Potential in Colloid Science*. New York: Academic Press.

Humphries, M. (2013). Rare earth elements: The global supply chain. Technical report, Congressional Research Service.

Jacques, D., & Šimůnek, J. (2005). *User manual of the multicompenent variably-saturated flow and transport model hp1* (No. BLG--998). SCK-CEN.

Jacques, D., Šimůnek, J., Mallants, D., & van Genuchten, M.T. (2003). The HYDRUS-PHREEQC multicomponent transport model for variably-saturated porous media: Code verification and application. *MODFLOW and More*, 23-27.

Jacques, D., Šimůnek, J., Mallants, D., & Van Genuchten, M.T. (2006). Operator-splitting errors in coupled reactive transport codes for transient variably saturated flow and contaminant transport in layered soil profiles. *Journal of contaminant hydrology*, 88 (3-4), 197-218.

Jarvis, K.E. (1988). Inductively coupled plasma mass spectrometry: a new technique for the rapid or ultra-trace level determination of the rare-earth elements in geological materials. *Chemical Geology*, 68 (1-2), 31-39.

Jarvis, K.E. (1989). Determination of rare earth elements in geological samples by inductively coupled plasma mass spectrometry. *Journal of Analytical Atomic Spectrometry*, 4 (7), 563-570.

Jarvis, N. J. (1998). Modeling the impact of preferential flow on nonpoint source pollution. *Physical Nonequilibrium in Soils: Modeling and Application, Ann Arbor Press, Chelsea,* MI, 195-221.

Jarvis, K.E., Gray, A.L., & Houk, R.S. (1991). *Handbook of inductively coupled plasma mass spectrometry*. Chapman and Hall.

Jarvis, K.E., Gray, A.L., & McCurdy, E. (1989). Avoidance of spectral interference on europium in inductively coupled plasma mass spectrometry by sensitive measurement of the doubly charged ion. *Journal of Analytical Atomic Spectrometry*, 4 (8), 743-747.

Jenne, E.A. (1968). Controls on Mn, Fe, Co, Ni, Cu and Zn concentrations in soils and waters: the significant role of hydrous Mn and Fe oxides. *Trace Inorganics in Water – Advances in Chemistry,* 73, 337-387.

Johnson, J., Anderson, G., & Parkhurst, D. (2000). Database “thermo. com. V8. R6. 230,” Rev. 1-11. *Lawrence Livermore National Laboratory.* Livermore, California.

Jordens, A., Cheng, Y.P., & Waters, K.E. (2013). A review of the beneficiation of rare earth element bearing minerals. *Minerals Engineering,* 41, 97-114.

Jun, T., Jingqun, Y., Guohua, R., Mintao, J., & Ruan, C. (2011). Extraction of rare earths from the leach liquor of the weathered crust elution-deposited rare earth ore with non-precipitation. *International Journal of Mineral Processing*, 98 (3-4), 125-131.

Jun, T., Ru-an, C., & Jing-qun, Y. (2010). Leaching process of rare earths from weathered crust elution-deposited rare earth ore. *Transactions of Nonferrous Metals Society of China*, 20, 892-89.

Kalka, H. (2018). *TRN version 2.2.5*.Umwelt- und Ingenieurtechnik GmbH Dresden.

Kautenburger, R. & Beck, H.P. (2010). Influence of geochemical parameters on the sorption and desorption behaviour of europium and gadolinium onto kaolinite. *Journal of Environmental Monitoring*, 12 (6), 1295 - 1301.

Kawabe, I., Ohta, A., Ishii, S., Tokumura, M., & Miyauchi, K. (1999). REE partitioning between Fe-Mn oxyhydroxide precipitates and weakly acid NaCl solutions: Convex tetrad effect and fractionation of Y and Sc from heavy lanthanides. *Geochemical Journal*, 33 (3), 167-179.

Kent, A.J. (2005). Production of barium and light rare earth element oxides during LA-ICP-MS microanalysis. *Journal of Analytical Atomic Spectrometry*, 20 (11), 1256-1262.

Kinniburgh, D.G. (1986). General purpose adsorption isotherms. *Environmental Science & Technology*, 20 (9), 895-904.

Koeppenkastrop, D., Decarlo, E.H., & Roth, M. (1991). A method to investigate the interaction of rare earth elements in aqueous solution with metal oxides. *Journal of radioanalytical and nuclear chemistry*, 152 (2), 337-346.

Koeppenkastrop, D., & Decarlo, E.H. (1992). Sorption of rare-earth elements from seawater onto synthetic mineral particles: An experimental approach. *Chemical geology*, 95 (3-4), 251-263.

Kookana, R.S., & Naidu, R. (1998). Effect of soil solution composition on cadmium transport through variable charge soils. *Geoderma*, 84 (1), 235-248.

Kosugi, K.I. (1996). Lognormal distribution model for unsaturated soil hydraulic properties. *Water Resources Research*, 32 (9), 2697-2703.

Kulik, D.A., Aja, S.U., Sinitsyn, V.A., & Wood, S.A. (2000). Acid–base surface chemistry and sorption of some lanthanides on K+-saturated Marblehead illite: II. A multisite–surface complexation modeling. *Geochimica et Cosmochimica Acta*, 64 (2), 195-213.

Kung, K.S. (1990). Preferential flow in a sandy vadose zone: 2. Mechanism and implications. *Geoderma*, 46 (1-3), 59-71.

Kurbatov, M.H., Wood, GB., & Kurbatov, J.D. (1951). Isothermal adsorption of cobalt from dilute solutions. *The Journal of Physical Chemistry*, 55 (7), 1170-1182.

Lagaly, G. (1981). Characterization of clays by organic compounds. *Clay Mineralogy,* 16 (1), 1.

Langmuir, D. (1997). *Aqueous environmental*. Prentice Hall.

Langmuir, I. (1918). The adsorption of gases on plane surfaces of glass, mica and platinum. *Journal of the American Chemical society*, 40 (9), 1361-1403.

Le Couteur, P.C. (2011). *Geological Report on the Chambe Basin Area of Exclusive Prospecting License EPL0325/11 Mulanje Massif, Southern Malawi, East Africa*.

Li, C. (2011). The generalization and application of new technology on lixiviating mineral at the original place for ionic rare earths [J]. *Nonferrous Metals Science and Engineering*, 1, 016.

Li, Y.X., Zhang, L., & Zhou, X.M. (2010). Resource and environment protected exploitation model for ion-type rare earth deposit in southern of China. *Chinese Rare Earths*, 2, 023.

Lichtner, P.C. (1988). The quasi-stationary state approximation to coupled mass transport and fluid-rock interaction in a porous medium. *Geochimica et Cosmochimica Acta*, 52 (1), 143-165.

Limousin, G., Gaudet, J.P., Charlet, L., Szenknect, S., Barthes, V., & Krimissa, M. (2007). Sorption isotherms: a review on physical bases, modeling and measurement. *Applied geochemistry*, 22 (2), 249-275.

Oyelami, C.A., & Van Rooy, J.L. (2016). A review of the use of lateritic soils in the construction/development of sustainable housing in Africa: A geological perspective. *Journal of African Earth Sciences*, 119, 226-237.

Ma, C., & Eggleton, R.A. (1999). Cation exchange capacity of kaolinite. *Clays and Clay minerals*, 47 (2), 174-180.

Ma, C.A., Cai, Q. X., Wang, H., Shao, M.A., Fan, J., Shi, Z., & Wang, F. (2015). Modeling of water flow in reclaimed mine spoil with embedded lignitic fragments using Hydrus-1D. *Mine Water and the Environment*, 34 (2), 197-203.

Maji, S.K., Pal, A., Pal, T., & Adak, A. (2007). Adsorption thermodynamics of arsenic on laterite soil. *Journal of Surface Science and Technology*, 23 (3/4), 161.

Mancheri, N.A. (2015). World trade in rare earths, Chinese export restrictions, and implications. *Resources Policy*, 46, 262-271.

Marmier, N., Dumonceau, J., Chupeau, J., & Fromage, F. (1994). Modeling of Yb (III) sorption on kaolinite by using single oxide surface complexation models. *MRS Online Proceedings Library Archive*, 353.

Marmier, N., Dumonceau, J., & Fromage, F. (1997). Surface complexation modeling of Yb (III) sorption and desorption on hematite and alumina. *Journal of contaminant hydrology*, 26 (1-4), 159-167.

Masipan, T., Chotpantarat, S., & Boonkaewwan, S. (2016). Experimental and modelling investigations of tracer transport in variably saturated agricultural soil of Thailand: Column study. *Sustainable Environment Research*, 26 (2), 97-101.

Massari, S., & Ruberti, M. (2013). Rare earth elements as critical raw materials: Focus on international markets and future strategies. *Resources Policy*, 38 (1), 36-43.

Mayer, K.U., Frind, E.O., & Blowes, D.W. (2002). Multicomponent reactive transport modeling in variably saturated porous media using a generalized formulation for kinetically controlled reactions. *Water Resources Research*, 38 (9), 13-1.

McBride, M.B. (1976). Origin and position of exchange sites in kaolinite: an ESR study. *Clays and clay minerals*, 24 (2), 88-92.

McBride, M.B. (1994). *Environmental Chemistry of Soils.* Oxford University Press, New York.

McLennan, S., & Taylor, S.R. (2012). Geology, Geochemistry and Natural Abundances of the Rare Earth Elements in Atwood, D.A. (Eds). *The Rare Earth Elements: Fundamentals and Applications*. West Sussex: John Wiley & Sons, Ltd.

Mentani, T., Ohmura, T., Watanabe, Y., & Urabe, T. (2010). So-called ion-adsorption type REE deposits found in weathered crust of ilmenite-series granite in northern Vietnam. *GSA Denver Annual Meeting*.

Meeussen, J.C.L., van der Sloot, H.A., Dijkstra, J.J., & Kosson, D.S. (2009). *Review of thermodynamic and adsorption databases*. Energy Research Centre of the Netherlands and Vanderbilt University/CRESP.

Miranda-Trevino, J.C., & Coles, C.A. (2003). Kaolinite properties, structure and influence of metal retention on pH. *Applied Clay Science*, 23 (1), 133-139.

Moldoveanu, G., & Papangelakis, V.G. (2012). Recovery of rare earth elements adsorbed on clay minerals: I. Desorption mechanism. *Hydrometallurgy*, 117-118, 71-78.

Möller, P. (1989). Rare earth mineral deposits and their industrial importance. In *Lanthanides, tantalum and niobium*. Springer, Berlin, Heidelberg.

Mudd, G. M. (2001). Critical review of acid in situ leach uranium mining: 1. USA and Australia. *Environmental Geology*, 41, 390-403.

Murata, K.J., Dutra, C.V., Da Costa, M.T., & Branco, J.J.R. (1959). Composition of monazites from pegmatites in eastern Minas Gerais, Brazil. *Geochimica et Cosmochimica Acta*, 16 (1-3), 1-14.

Navarro, J., & Zhao, F. (2014). Life-cycle assessment of the production of rare-earth elements for energy applications: a review. *Frontiers in Energy Research*, 2, 45.

Neumann, H., Jensen, B.B., & Brunfelt, A.O. (1966). Distribution patterns of rare earth elements in minerals. *Rev. nor. geológ*, 50, 357-373.

Nicolai, J., Märten, H., & Kalka, H. (2017). In-Situ Recovery of Technology Metals. Umwelt- und Ingenieurtechnik GmbH Dresden.

Nordstrom, D.K., & Munoz, J.I. (1994). *Geotechnical Thermodynamics*. Blackwell Scientific Publications.

Palmer, M.A., Berhhardt, E.S., Schlesinger, W.H., Eshleman, K.N., Foufoula-Georgiou, E., Hendryx, M.S., Lemly, A.D., Likens, G.E., Loucks, O.L., Power, M.E., White, P.S., & Wilcock, P.R. (2010). Mountaintop Mining Consequences, *Science*, 327, 148-149.

Pansu, M., & Gautheyrou, J. (2007). *Handbook of soil analysis: mineralogical, organic and inorganic methods*. Springer Science & Business Media.

Papangelakis, V.G., & Moldoveanu, G. (2014). Recovery of Rare Earth Elements from Clay Minerals. *European Rare Earth Resource Conference*. Available at http://www.eurare.eu/docs/eres2014/fifthSession/VladimirosPapangelakis.pdf [Accessed 9th October 2015].

Parfitt, R.L., Fraser, A.R., & Farmer, V.C. (1977). Adsorption on hydrous oxides. III. Fulvic acid and humic acid on goethite, gibbsite and imogolite. *Journal of Soil Science*, 28 (2), 289-296.

Parkhurst, D.L. (1990). Ion-association models and mean activity coefficients of various salts*. American Chemical Society*, 3, 30-43.

Parkhurst, D.L., & Appelo, C.A.J. (2013). *Description of input and examples for PHREEQC version 3: a computer program for speciation, batch-reaction, one-dimensional transport, and inverse geochemical calculations*. US Geological Survey.

Parkhurst, D.L., & Appelo, C.A.J. (1999). User's guide to PHREEQC (Version 2): A computer program for speciation, batch-reaction, one-dimensional transport, and inverse geochemical calculations. Colorado: U.S. Geological Survey.

Paulick, H., & Machacek, E. (2017). The global rare earth element exploration boom: An analysis of resources outside of China and discussion of development perspectives. *Resources Policy*, 52, 134-153.

Payne, T.E., Brendler, V., Ochs, M., Baeyens, B., Brown, P.L., Davis, J.A., Eckberg, C., Kulik, D.A., Lutzenkirchen, J., Missana, T., Tachi, Y., Van Loon, L.R., & Altmann, S. (2013). Guidelines for thermodynamic sorption modelling in the context of radioactive waste disposal. *Environmental modelling & software*, 42, 143-156.

Piper, D. Z. (1974). Rare earth elements in the sedimentary cycle: a summary. *Chemical Geology*, 14 (4), 285-304.

Platt, A.W.G. (2012). Variable Valency in Atwood, D.A. (Eds). *The Rare Earth Elements: Fundamentals and Applications*. West Sussex: John Wiley & Sons, Ltd.

Plummer, C.C., McGeary, D., & Carlson, D.H. (1991). *Physical geology.* Wm. C. Brown.

Prommer, H., Barry, D.A. & Zheng, C. (2003). MODFLOW/MT3DMS-Based Reactive Transport Modeling. *Groundwater*, 41 (2), 247–257.

Quinn, K.A., Byrne, R.H., & Schijf, J. (2006a). Sorption of yttrium and rare earth elements by amorphous ferric hydroxide: influence of pH and ionic strength. *Marine Chemistry*, 99 (1-4), 128-150.

Quinn, K.A., Byrne, R.H., & Schijf, J. (2006b). Sorption of yttrium and rare earth elements by amorphous ferric hydroxide: influence of solution complexation with carbonate. *Geochimica et Cosmochimica Acta*, 70 (16), 4151-4165.

Rabung, T., Geckeis, H., Kim, J.I., & Beck, H.P. (1998). Sorption of Eu (III) on a natural hematite: application of a surface complexation model. *Journal of colloid and interface science*, 208 (1), 153-161.

Rabung, T., Stumpf, T., Geckeis, H., Klenze, R., & Kim, J.I. (2000). Sorption of Am(III) and Eu(III) onto γ-Al2O3: experiment and modelling. *Radiochimica Acta*, 88, 711-716.

Rand, B., & Melton, I.E. (1977). Particle interactions in aqueous kaolinite suspensions, I. Effect of pH and electrolyte upon the mode of particle interaction in homoionic sodium kaolinite suspensions. *Journal of Colloid and Interface Science,* 60, 308-320.

Rocha, A., Schissel, D., Sprecher, A., de Tarso, P., & Goode, J. (2013). Process development for the Serra Verde weathered crust elution-deposited rare earth deposit in Brazil. *Proceedings of the 52rd Conference of Metallurgists*.

Roskill. (2007). *The economics of rare earths and yttrium*. Roskill Information Services Limited.

Ružičić, S., Kovac, Z., Mileusnic, M., & Posavec, K. (2013). Longitudinal dispersivity determination using conservative tracer in the field. In *4th International Conference HYDRUS Software Applications to Subsurface Flow and Contaminant Transport Problems*.

Saalfeld, H., & Wedde, M. (1974). Refinement of the crystal structure of gibbsite, Al(OH)3. *Zeitschrift für Kristallographie-Crystalline Materials*, 139 (1-6), 129-135.

Sanematsu, K., Kon, Y., & Imai, A. (2015). Influence of phosphate on mobility and adsorption of REEs during weathering of granites in Thailand. *Journal of Asian Earth Sciences*, 111, 14–30.

Sanematsu, K., Kon, Y., Imai, A., Watanabe, K., & Watanabe, Y. (2013). Geochemical and mineralogical characteristics of ion-adsorption type REE mineralization in Phuket, Thailand. *Mineralium Deposita*, 48, 437–451.

Sanematsu, K., Murakami, H., Watanabe, Y., Duangsurigna, S., & Siphandone, V. (2009). Enrichment of rare earth elements (REE) in granitic rocks and their weathered crusts in central and southern Laos. *Bulletin of the Geological Survey of Japan*, 60 (11-12), 527-558.

Sanematsu, K., & Watanabe, Y. (2016). Characteristics and genesis of ion adsorption-type rare earth element deposits. *Reviews in Economic Geology*, 18, 55-79.

Sarangi, A.K., & Beri, K.K. (2000). Uranium mining by in-situ leaching. In *Proceedings of the International conference on "Technology management for mining processing and environment", Kharagpur*.

Saxena, R.K., Jarvis, N.J., & Bergström, L. (1994). Interpreting non-steady state tracer breakthrough experiments in sand and clay soils using a dual-porosity model. *Journal of Hydrology*, 162 (3-4), 279-298.

Schoeller, W.R., & Powell, A.R. (1955). The Analysis of Minerals and Ores of the Rarer Elements. London; Charles Griffin and Company.

Schüler, D., Buchert, M., Liu, R., Dittrich, S., & Merz, C. (2011). Study on rare earths and their recycling. Final Report for the Greens/EFA Group in the European Parliament. *Öko-Institut eV Darmstadt*.

Selim, H.M. (2012). Competitive sorption of heavy metals in soils: experimental evidence. *Competitive Sorption and Transport of Heavy Metals in Soils and Geological Media*.

Seyfried, M.S., & Rao, P.S.C. (1987). Solute Transport in Undisturbed Columns of an Aggregated Tropical Soil: Preferential Flow Effects 1. *Soil Science Society of America Journal*, 51 (6), 1434-1444.

Shabani, M.B., Akagi, T., Shimizu, H., & Masuda, A. (1990). Rapid and accurate determination of sub-parts per trillion lanthanides and yttrium in seawater by development

of solvent extraction and back extraction using inductively coupled plasma mass spectrometry. *Analytical Chemistry*, 62, 2709.

Singh, S.K., Subramanian, V., & Gibbs, R.J. (1984). Hydrous Fe and Mn oxides—scavengers of heavy metals in the aquatic environment. *Critical Reviews in Environmental Control*, 14 (1), 33-90.

Simandl, G.J. (2014). Geology and market-dependent significance of rare earth element resources. *Mineralium Deposita*, 49 (8), 889-904.

Šimůnek, J., Jarvis, N. J., Van Genuchten, M. T., & Gärdenäs, A. (2003). Review and comparison of models for describing non-equilibrium and preferential flow and transport in the vadose zone. *Journal of hydrology*, 272 (1-4), 14-35.

Šimůnek, J., Sejna, M., Van Genuchten, M.T., Šimůnek, J., Šejna, M., Jacques, D., & Sakai, M. (1998). HYDRUS-1D. *Simulating the one-dimensional movement of water, heat, and multiple solutes in variably-saturated media, version 2*.

Šimůnek, J., Van Genuchten, M.T., & Sejna, M. (2005). The HYDRUS-1D software package for simulating the one-dimensional movement of water, heat, and multiple solutes in variably-saturated media. *University of California-Riverside Research Reports*, 3, 1-240.

Šimůnek, J., Jacques, D., & Van Genuchten, M.T (2006). Multicomponent geochemical transport modeling using the HYDRUS-1D computer software package. In *American Water Resources Association Conference Proceedings*.

Šimůnek, J., Šejna, M., Saito, H., Sakai, M., & Van Genuchten, M.T. (2008). The HYDRUS-1D software package for simulating the movement of water, heat, and multiple solutes in variably saturated media, version 4.0: HYDRUS Software Series 3. *Department of Environmental Sciences, University of California Riverside, Riverside, California, USA*, *315*.

Smith, K.S. (1999). Metal sorption on mineral surfaces: an overview with examples relating to mineral deposits. *The Environmental Geochemistry of Mineral Deposits. Part A: Processes, Techniques, and Health Issues*, 6, 161-182.

Sposito, G. (1983). On the surface complexation model of the oxide-aqueous solution interface. *Journal of Colloid and Interface Science*, 91 (2), 329-340.

SRK (2013). *A Competent Persons Report on the Tantalus Project, Northern Madagascar*. Available at http://www.tre-ag.com/~/media/Files/T/Tantalus-Rare-Earths/Attachments/pdf/2013_01_21_ES7520_SRKES_Tantalus%20CPR_Final_English.pdf [Accessed 14th March 2016].

Steefel, C.I., DePaolo, D.J., & Lichtner, P.C. (2005). Reactive transport modeling: An essential tool and a new research approach for the Earth sciences. *Earth and Planetary Science Letters*, 240 (3-4), 539-558.

Steefel, C.I., & Maher, K. (2009). Fluid-rock interaction: A reactive transport approach. *Reviews in Mineralogy and Geochemistry*, 70 (1), 485-532.

Steenhuis, T.S., Parlange, J.Y., & Aburime, S.A. (1995). Preferential flow in structured and sandy soils: consequences for modeling and monitoring. *Handbook of vadose zone characterization and monitoring*, 61-77.

Stumm, W., & Morgan, J.J. (2012). *Aquatic chemistry: chemical equilibria and rates in natural waters*. West Sussex: John Wiley & Sons.

Stumpf, T., Bauer, A., Coppin, F., Fanghänel, T., & Kim, J.I. (2002). Inner-sphere, outer-sphere and ternary surface complexes: a TRLFS study of the sorptionn process of Eu (III) onto smectite and kaolinite. *Radiochimica Acta*, 90 (6), 345-349.

Tang, J., & Johannesson, K.H. (2003). Speciation of rare earth elements in natural terrestrial waters: assessing the role of dissolved organic matter from the modeling approach. *Geochimica et Cosmochimica Acta*, 67 (13), 2321-2339.

Tang, J., & Johannesson, K.H. (2005). Adsorption of rare earth elements onto Carrizo sand: experimental investigations and modelling with surface complexation. *Geochimica et Cosmochimica Acta*, 69 (22), 5247-5261.

Ter-Mikirtychev, V., & Ter-Mikirtychev, V. (2014). Optical properties and optical spectroscopy of rare earth ions in solids. *Fundamentals of Fiber Lasers and Fiber Amplifiers*, 7-26.

Tertre, E., Berger, G., Castet, S., Loubet, M., & Giffaut, E. (2005). Experimental sorption of Ni^{2+}, Cs^{+} and Ln^{3+} onto a montmorillonite up to 150 °C. *Geochimica et Cosmochimica Acta*, 69, 4937-4948.

Tertre, E., Berger, G., Simoni, E., Castet, E., Loubet, M., & Catalette, H. (2006a). Europium retention onto clay minerals from 25 to 150 °C: Experimental measurements, spectroscopic features and sorption modelling. *Geochimica et Cosmochimica Acta*, 70, 4563-4578.

Tertre, E., Castet, S., Berger, G., Loubet, M., & Giffaut, E. (2006b). Surface chemistry of kaolinite and Na-montmorillonite in aqueous electrolyte solutions at 25 and 60 C: experimental and modeling study. *Geochimica et Cosmochimica Acta*, 70 (18), 4579-4599.

Tertre, E., Hofmann, A., & Berger, G. (2008). Rare earth element sorption by basaltic rock: experimental data and modeling results using the “Generalised Composite approach”. *Geochimica et Cosmochimica Acta*, 72 (4), 1043-1056.

Thompson, J.B. (1959). Local equilibrium in metasomatic processes. *Researches in geochemistry*.

Tian, J., Tang, X., Yin, J., Luo, X., Rao, G., & Jiang, M. (2013). Process optimization on leaching of a lean weathered crust elution-deposited rare earth ores. *International Journal of Mineral Processing*, 119, 83-88.

Tombácz, E., Nyilas, T., Libor, Z., & Csanaki, C. (2004). Surface charge heterogeneity and aggregation of clay lamellae in aqueous suspensions. In *From Colloids to Nanotechnology*. Berlin; Springer.

Tostevin, R., Shields, G.A., Tarbuck, G.M., He, T., Clarkson, M.O., & Wood, R. A. (2016). Effective use of cerium anomalies as a redox proxy in carbonate-dominated marine settings. *Chemical Geology*, 438, 146-162.

Tournassat, C., Gailhanou, H., Crouzet, C., Braibant, G., Gautier, A., Lassin, A., Blanc, P., & Gaucher, E. C. (2007). Two cation exchange models for direct and inverse modelling of solution major cation composition in equilibrium with illite surfaces. *Geochimica et Cosmochimica Acta*, 71 (5), 1098-1114.

Truesdell, A.H., & Jones, B.F. (1974). WATEQ, a computer program for calculating chemical equilibria of natural waters. *Journal of Research of the US Geological Survey*, 2, 233-248.

Tunega, D. (2012). Theoretical study of properties of goethite (α-FeOOH) at ambient and high-pressure conditions. *The Journal of Physical Chemistry C*, 116 (11), 6703-6713.

Uddin, M.K. (2017). A review on the adsorption of heavy metals by clay minerals, with special focus on the past decade. *Chemical Engineering Journal*, 308, 438-462.

USGS. (1996). Minerals Information. Rare Earths. Statistics and Information. https://minerals.usgs.gov/minerals/pubs/commodity/rare_earths/rareemcs96.pdf [Accessed 10th January 2019].

USGS. (2011). Minerals Information. Rare Earths. Statistics and Information. https://minerals.usgs.gov/minerals/pubs/commodity/rare_earths/mcs-2011-raree.pdf [Accessed 10th January 2019].

USGS. (2018). Minerals Information. Rare Earths. Statistics and Information. https://minerals.usgs.gov/minerals/pubs/commodity/rare_earths/mcs-2018-raree.pdf [Accessed 10th January 2019].

Vahidi, E., Navarro, J., & Zhao, F. (2016). An initial life cycle assessment of rare earth oxides production from ion-adsorption clays. *Resources, Conservation and Recycling*, 113, 1-11

Van Genuchten, M.T. (1980). A closed-form equation for predicting the hydraulic conductivity of unsaturated soils 1. *Soil science society of America journal*, 44 (5), 892-898.

Van Olphen, H. (1977). *An introduction to clay colloid chemistry: for clay technologists, geologists, and soil scientists*.

Van Kranendonk, M.J., Webb, G.E., & Kamber, B.S. (2003). Geological and trace element evidence for a marine sedimentary environment of deposition and biogenicity of 3.45 Ga stromatolitic carbonates in the Pilbara Craton, and support for a reducing Archaean ocean. *Geobiology*, 1 (2), 91-108.

Verma, P.K., & Mohapatra, P.K. (2016). Effect of different complexing ligands on europium uptake from aqueous phase by kaolinite: batch sorption and fluorescence studies. *Royal Society of Chemistry*, 6, 84464- 84471.

Voβenkaul, D., Stoltz, N.B., Meyer, F.M., & Friedrich, B. (2015). Extraction of Rare Earth Elements from non-Chinese Ion Adsorption Clays. *Processing of EMC 2015*. Available at http://www.metallurgie.rwth-aachen.de/new/images/pages/publikationen/vo_enkaeul_extr_id_8872.pdf [Accessed 12th April 2016].

Xiangke, W., Wenming, D., Yingchun, G., Changhui, W., & Zuyi, T. (2001). Sorption characteristics of radioeuropium on bentonite and kaolinite. *Journal of radioanalytical and Nuclear Chemistry*, 250 (2), 267-270.

Wall, F. (2014). Rare earth elements. *Critical metals handbook*, 312-339.

Walter, A.L., Frind, E.O., Blowes, D.W., Ptacek, C.J., & Molson, J.W. (1994). Modeling of multicomponent reactive transport in groundwater: 1. model development and evaluation. *Water Resources Research*, 30 (11), 3137-3148.

Walters, A., Lusty, P., & Hill, A. (2011). *Rare Earth Elements: Mineral Profile*. British Geological Survey, United Kingdom.

Williams, D.J.A., & Williams, K.P. (1978). Electrophoresis and zeta potential of kaolinite. *Journal of Colloid and Interface Science*, 65 (1), 79-87.

Wilson, B. M. (2007). *Igneous petrogenesis a global tectonic approach*. Springer Science & Business Media.

Wu, C.Y., Huang, D.H., & Guo, Z.G. (1990). REE geochemistry in the weathered crust of granites, Longnan area, Jiangxi Province. *Acta Geologica Sinica,* 3 (2), 193-209.

Wu, C., Yuan, Z., & Bai, G. (1995). Rare earth deposits in China. *Mineralogical Society Series*, 7, 281-310.

Wübbeke, J. (2013). Rare earth elements in China: Policies and narratives of reinventing an industry. *Resources Policy*, 38 (3), 384-394.

Yang, X.J., Lin, A., Li, X-L., Wu, Y., Zhou, W., & Chen, Z. (2013). China's ion-adsorption rare earth resources, mining consequences and preservation. *Environmental Development*, 8, 131-136

Yu, Q., Qiu, D., Ma, R., & Zhou, Z. (1990). The techniques for extraction of rare earths from the ionic type rare earth ores and their possible improvements. *Mining and Metallurgical Engineering (China)*, 10 (1), 42-45.

Zagorodni, A.A. (2006). *Ion exchange materials: properties and applications*. Elsevier.

Zhang, Z.H. (1990). A study on weathering crust ion adsorption type REE deposits, south China. *Contributions to Geology and Mineral Resources Research*, 5 (1), 57.

Zhao, J., Tang, X. Z., & Wu, C. (2001). Status quo of mining and recovering technologies for ion-absorbed rare earth deposits in China. *Yunnan metallurgy*, 30 (1), 11-14.

Zhu, Y., Zhou, L., & Li, Q. (2011). Water pollution prevention method for in-situ leach mining of ion-absorbed rare-earth mineral. *Nonferrous Metals (Mineral Processing Section)*, 6, 46-49.

Appendix A

Literature Data

A.1 Global Ion Adsorption Deposits

Location	Sample	Depth [m]	La [ppm]	Ce [ppm]	Pr [ppm]	Nd [ppm]	Sm [ppm]	Eu [ppm]	Gd [ppm]	Tb [ppm]	Dy [ppm]	Ho [ppm]	Er [ppm]	Tm [ppm]	Yb [ppm]	Lu [ppm]	Y [ppm]
Pit 3, Madagascar	0578	0.3	3.61	62.28	0.47	1.35	0.17	0.02	0.23	0.02	0.08	0.01	0.03	0.00	0.02	0.00	0.42
	0579	0.5	4.64	47.74	0.79	2.42	0.33	0.04	0.32	0.03	0.16	0.03	0.07	0.01	0.04	0.01	0.70
	0581	0.8	4.72	43.80	0.87	2.71	0.39	0.05	0.35	0.04	0.18	0.03	0.08	0.01	0.06	0.01	0.79
	0582	1.0	4.51	46.76	0.86	2.73	0.41	0.05	0.37	0.04	0.19	0.03	0.08	0.01	0.06	0.01	0.76
	0583	1.3	4.08	48.52	0.78	2.47	0.38	0.05	0.34	0.04	0.17	0.03	0.07	0.01	0.05	0.01	0.67
	0584	1.5	3.62	47.14	0.67	2.14	0.33	0.04	0.30	0.03	0.15	0.03	0.06	0.01	0.04	0.00	0.55
	0586	1.8	2.63	31.50	0.48	1.54	0.24	0.03	0.22	0.03	0.11	0.02	0.04	0.01	0.03	0.00	0.39
	0587	2.0	2.08	25.92	0.37	1.21	0.18	0.02	0.17	0.02	0.08	0.01	0.03	0.00	0.02	0.00	0.29
	0588	2.3	2.45	33.97	0.44	1.39	0.22	0.03	0.20	0.02	0.10	0.02	0.04	0.00	0.03	0.00	0.32
	0589	2.5	2.56	38.20	0.46	1.43	0.23	0.03	0.21	0.02	0.09	0.02	0.04	0.00	0.03	0.00	0.32
	0590	2.8	2.98	42.28	0.53	1.67	0.25	0.03	0.23	0.02	0.10	0.02	0.04	0.01	0.03	0.00	0.34
	0591	3.0	2.78	32.40	0.48	1.49	0.20	0.02	0.17	0.02	0.07	0.01	0.03	0.00	0.02	0.00	0.25
	0592	3.3	6.37	64.80	1.09	3.42	0.45	0.05	0.38	0.04	0.16	0.03	0.06	0.01	0.05	0.01	0.52
	0594	3.5	8.86	86.01	1.53	4.76	0.63	0.07	0.52	0.05	0.22	0.03	0.08	0.01	0.06	0.01	0.71
	0595	3.8	8.19	73.03	1.41	4.43	0.58	0.07	0.46	0.05	0.19	0.03	0.07	0.01	0.06	0.01	0.62
	0596	4.0	6.92	60.35	1.19	3.76	0.49	0.06	0.39	0.04	0.17	0.03	0.06	0.01	0.05	0.01	0.53
	0597	4.3	1.36	11.77	0.25	0.77	0.11	0.01	0.08	0.01	0.03	0.01	0.01	0.00	0.01	0.00	0.11
Longnan County, China	LN-1	0.5	21.4	47.2	5.17	17.6	4.14	0.50	4.35	0.75	4.94	0.99	3.05	0.49	3.55	0.52	-
	LN-2	2	25.7	38.2	9.13	46.4	25.1	0.42	28.5	4.27	24.6	4.92	15.0	2.51	17.9	2.79	-
	LN-3	3.5	34.4	27.0	11.1	57.3	45.1	0.40	90.1	17.8	118	23.7	70.1	11.5	75.5	11.36	-
	LN-4	5	16.5	19.8	6.14	30.8	22.7	0.26	55.0	12.6	87.8	17.6	53.2	8.31	58.1	8.52	-
	LN-5	6.5	15.7	29.6	5.92	30.2	20.9	0.18	45.3	10.2	74.0	15.3	45.1	7.02	47.3	7.19	-
	LN-8	8	8.11	17.8	3.63	16.8	12.0	0.09	24.9	5.47	40.0	8.27	25.8	4.12	29.1	4.41	-
	LN-9	9.5	8.86	14.3	2.65	13.9	8.50	0.10	15.1	3.27	24.0	4.90	15.0	2.60	16.2	2.55	-

Location	Sample	Depth [m]	La [ppm]	Ce [ppm]	Pr [ppm]	Nd [ppm]	Sm [ppm]	Eu [ppm]	Gd [ppm]	Tb [ppm]	Dy [ppm]	Ho [ppm]	Er [ppm]	Tm [ppm]	Yb [ppm]	Lu [ppm]	Y [ppm]
Phuket, Thailand	B1	0.5	83.8	253	16.9	53.6	7.84	0.60	6.68	0.62	3.24	0.59	1.77	0.25	1.76	0.25	-
	B2	1.4	113	301	24.4	78.2	10.8	0.76	8.95	0.82	4.22	0.73	2.29	0.31	2.21	0.32	-
	B3	2.1	119	183	29.3	97.9	15.2	1.07	11.5	1.10	5.66	1.00	3.05	0.42	2.91	0.43	-
	B4	2.8	86.6	300	21.0	69.0	10.9	0.76	8.20	0.76	4.08	0.71	2.34	0.34	2.55	0.42	-
	B5	3.5	77.3	174	17.5	57.4	8.47	0.61	6.36	0.57	2.88	0.52	1.69	0.23	1.70	0.25	-
	B6	4.2	57.5	279	14.1	47.2	6.65	0.54	5.28	0.50	2.66	0.55	1.98	0.34	2.76	0.46	-
Attapu	P716B	0.5	172	249	33.7	112	19.3	4.39	15.7	2.58	13.4	2.42	6.48	0.84	4.95	0.71	-
	P724C	1	57.7	102	10.6	29.7	5.1	1.08	3.8	0.4	2.0	0.3	0.9	0.14	0.9	0.14	-
	P725A	1.5	152	311	23.5	62.6	7.88	1.32	3.5	0.52	2.58	0.44	1.16	0.15	0.93	0.15	-
	P726B	2	88.1	156	17.5	60.2	8.93	1.93	6.88	0.98	5.14	0.95	2.72	0.39	2.46	0.38	-
	P781C	2.5	59.7	105	9.32	30	3.74	0.91	1.84	0.25	1.23	0.22	0.6	0.09	0.58	0.09	-
	P782B	3	39.8	90.8	6.68	20	2.81	0.84	1.2	0.2	1.18	0.23	0.67	0.1	0.69	0.11	-
	P783B	3.5	94.1	140	15.4	46.9	6.32	2.14	4.04	0.56	2.85	0.53	1.43	0.21	1.33	0.21	-
	P783C	4	30.8	41.4	4.82	15	1.98	1.21	1.46	0.2	0.97	0.19	0.54	0.08	0.64	0.11	-

Table A.1 REE distribution patterns (ppm) from four weathered profiles. Data representing the Attapu IAD is taken from Sanematsu *et al*. (2009). Data used for the Longnan County IAD is from Bao & Zhao (2008). Data representing the Phuket IAD was taken from Sanematsu *et al*. (2013). $NH_4(SO_4)_2$ leach pit 3 transect data determined at Brighton University represented the REE distribution in the Madagascar IAD.

Appendix B

Analytical Data

B.1 CEC Test Dataset

Reagent	Repeat Tests	Na [mM]	Mg [mM]	Al [mM]	Si [mM]	K [mM]	Ca [mM]	Sc [mM]	Mn [mM]	Ni [mM]	Cu [mM]	Zn [mM]	Y [mM]	La [mM]
barium chloride	1	0.47	0.21	2.28	1.00E-03	7.98E-02	3.17E-01	3.09E-05	2.84E-03	1.42E-05	1.24E-01	7.05E-01	1.29E-03	5.49E-03
	2	0.52	0.21	2.28	1.00E-03	8.13E-02	3.22E-01	3.09E-05	7.52E-05	1.37E-05	1.15E-01	7.22E-01	1.33E-03	5.46E-03
ammonium chloride	1	0.05	0.15	3.09	5.55E-02	5.52E-02	8.81E-02	2.22E-05	3.73E-03	2.21E-04	5.02E-04	5.98E-04	5.30E-04	3.98E-03
	2	0.05	0.15	3.09	5.45E-02	5.50E-02	9.08E-02	2.22E-05	3.99E-03	2.20E-04	5.21E-04	6.10E-04	5.43E-04	4.09E-03
ammonium acetate	1	0.09	0.16	0.03	1.32E-01	4.42E-02	2.55E-01	2.22E-05	2.24E-03	2.64E-04	6.34E-04	5.37E-04	2.50E-04	2.51E-03
	2	0.08	0.14	0.03	1.27E-01	4.09E-02	2.50E-01	2.22E-05	1.57E-03	2.59E-04	6.03E-04	5.39E-04	2.41E-04	2.81E-03

Continued…

Reagent	Repeat Tests	Ce [mM]	Pr [mM]	Nd [mM]	Eu [mM]	Sm [mM]	Gd [mM]	Tb [mM]	Dy [mM]	Ho [mM]	Er [mM]	Tm [mM]	Yb [mM]	Lu [mM]
barium chloride	1	3.11E-02	5.65E-04	3.29E-03	1.15E-02	2.81E-02	5.05E-05	1.56E-05	7.75E-05	9.22E-06	2.49E-05	5.92E-06	5.78E-06	6.06E-06
	2	3.21E-02	5.60E-04	3.34E-03	1.14E-02	2.84E-02	5.10E-05	1.52E-05	7.74E-05	9.00E-06	2.44E-05	5.80E-06	6.00E-06	6.20E-06
ammonium chloride	1	4.04E-02	7.08E-04	2.20E-03	2.85E-04	3.74E-05	1.74E-03	2.89E-05	9.66E-05	1.49E-05	4.05E-05	5.92E-06	2.58E-05	5.72E-06
	2	4.01E-02	7.31E-04	2.27E-03	2.88E-04	3.91E-05	1.75E-03	2.90E-05	9.85E-05	1.50E-05	4.22E-05	5.92E-06	2.81E-05	5.72E-06
ammonium acetate	1	2.30E-02	3.95E-04	1.73E-03	1.53E-04	2.30E-05	1.15E-03	1.52E-05	4.44E-05	6.05E-06	1.72E-05	5.92E-06	7.17E-06	5.72E-06
	2	2.48E-02	4.21E-04	1.83E-03	1.59E-04	2.34E-05	1.13E-03	1.59E-05	4.31E-05	6.03E-06	1.75E-05	5.92E-06	6.70E-06	5.72E-06

Table B.1 Element concentrations used to calculate the CEC of the Madagascar IAD.

B.2 Batch Reaction Dataset

	SLR [g/mL]	Na [mM]	Mg [mM]	Al [mM]	Si [mM]	Ca [mM]	Ba [mM]	K [mM]	Cu [mM]	Zn [mM]	Mn [mM]
Batch 1	0.11	0.51	0.19	2.43	<0.04	0.26	851.98	0.01	0.11	0.66	0.00
	0.18	0.42	0.24	3.62	<0.04	0.27	3291.41	0.00	0.11	0.63	0.00
	0.25	0.37	0.25	3.61	<0.04	0.22	652.46	0.00	0.11	0.63	0.00
	0.33	0.60	0.40	4.86	<0.04	0.69	667.75	0.02	0.11	0.66	0.01
	0.43	0.41	0.38	6.41	<0.04	0.26	562.16	0.01	0.11	0.61	0.01
	0.54	0.47	0.53	8.97	<0.04	0.29	540.32	0.02	0.10	0.54	0.01
	0.67	0.51	0.65	11.08	<0.04	0.31	509.00	0.02	0.09	0.54	0.01
	0.82	0.50	0.72	12.27	<0.04	0.31	427.45	0.02	0.09	0.51	0.02
	1.00	0.57	0.86	14.68	<0.04	0.30	476.96	0.09	0.09	0.50	0.02
Batch 2	0.11	0.38	0.21	2.94	<0.04	0.23	635.71	0.01	0.12	0.69	0.00
	0.18	0.40	0.24	3.58	<0.04	0.26	4995.38	0.01	0.11	0.65	0.00
	0.25	0.40	0.31	4.97	<0.04	0.26	3488.02	0.01	0.11	0.63	0.01
	0.33	0.44	0.39	6.45	<0.04	0.30	1390.84	0.01	0.11	0.61	0.01
	0.43	0.58	0.49	8.08	<0.04	0.29	2592.35	0.02	0.10	0.59	0.01
	0.54	0.71	0.54	8.93	<0.04	0.33	496.62	0.02	0.09	0.53	0.01
	0.67	0.70	0.60	9.93	<0.04	0.39	509.73	0.02	0.09	0.51	0.01
	0.82	0.59	0.75	12.79	<0.04	0.32	2046.21	0.02	0.09	0.54	0.01
	1.00	0.66	0.87	14.53	<0.04	0.36	374.29	0.03	0.09	0.50	0.02
Batch 3	0.11	0.63	0.33	2.88	<0.04	0.77	701.25	0.02	0.12	0.70	0.00
	0.18	0.66	0.38	3.97	<0.04	0.78	630.61	0.02	0.12	0.71	0.00
	0.25	0.67	0.43	4.71	<0.04	0.77	615.32	0.03	0.12	0.69	0.01
	0.33	0.98	0.56	6.97	<0.04	0.91	2359.33	0.03	0.12	0.68	0.01
	0.43	0.84	0.61	8.26	<0.04	0.83	571.63	0.03	0.12	0.66	0.01
	0.54	0.81	0.67	9.12	<0.04	0.79	461.67	0.03	0.11	0.65	0.01
	0.67	0.81	0.79	11.56	<0.04	0.81	382.30	0.03	0.11	0.63	0.01
	0.82	0.78	0.85	13.16	<0.04	0.73	511.19	0.03	0.10	0.59	0.01
	1.00	0.77	0.91	13.79	<0.04	0.72	391.04	0.08	0.09	0.53	0.02

Continued…

	SLR [g/mL]	Sc [mM]	Ti [mM]	Fe [mM]	Co [mM]	Ni [mM]	Y [mM]	La [mM]	Ce [mM]	Pr [mM]	Nd [mM]
Batch 1	0.11	2.25E-05	2.38E-05	1.79E-03	1.70E-05	1.70E-05	1.29E-03	6.22E-03	3.68E-02	6.65E-04	3.81E-03
	0.18	1.57E-05	2.30E-05	1.79E-03	1.70E-05	1.70E-05	1.51E-03	7.85E-03	5.29E-02	9.37E-04	5.59E-03
	0.25	1.59E-05	2.61E-05	1.79E-03	1.70E-05	1.70E-05	1.54E-03	7.78E-03	5.40E-02	9.94E-04	5.56E-03
	0.33	1.73E-05	2.86E-05	1.79E-03	1.99E-05	1.70E-05	1.97E-03	1.00E-02	7.28E-02	1.31E-03	7.28E-03
	0.43	1.61E-05	3.66E-05	1.79E-03	2.49E-05	1.70E-05	2.23E-03	1.20E-02	9.35E-02	1.71E-03	1.01E-02
	0.54	2.67E-05	4.35E-05	1.79E-03	6.74E-05	1.70E-05	2.72E-03	1.53E-02	1.29E-01	2.38E-03	1.38E-02
	0.67	2.29E-05	1.90E-04	1.79E-03	6.65E-05	1.70E-05	3.27E-03	1.82E-02	1.57E-01	2.83E-03	1.68E-02
	0.82	3.63E-05	4.53E-05	1.79E-03	5.67E-05	1.70E-05	3.39E-03	2.00E-02	1.74E-01	3.19E-03	1.89E-02
	1.00	4.27E-05	6.89E-05	1.79E-03	9.25E-05	1.70E-05	3.94E-03	2.35E-02	2.07E-01	3.79E-03	2.23E-02
Batch 2	0.11	1.18E-05	3.05E-05	1.79E-03	1.70E-05	1.70E-05	1.45E-03	6.53E-03	4.05E-02	7.52E-04	3.97E-03
	0.18	1.45E-05	4.58E-05	1.79E-03	1.70E-05	1.70E-05	1.52E-03	7.34E-03	4.93E-02	9.08E-04	5.03E-03
	0.25	1.92E-05	7.06E-05	1.79E-03	2.36E-05	1.70E-05	1.86E-03	9.43E-03	7.02E-02	1.25E-03	7.14E-03
	0.33	2.22E-05	4.80E-05	1.79E-03	2.41E-05	1.70E-05	2.25E-03	1.14E-02	8.99E-02	1.63E-03	9.36E-03
	0.43	3.07E-05	5.49E-05	1.79E-03	4.75E-05	1.70E-05	2.42E-03	1.36E-02	1.12E-01	2.06E-03	1.13E-02
	0.54	3.67E-05	6.06E-05	1.79E-03	3.85E-05	1.70E-05	2.67E-03	1.47E-02	1.23E-01	2.29E-03	1.40E-02
	0.67	4.23E-05	5.52E-05	1.79E-03	6.53E-05	1.70E-05	2.83E-03	1.63E-02	1.41E-01	2.57E-03	1.48E-02
	0.82	4.54E-05	5.87E-05	1.79E-03	7.94E-05	1.70E-05	3.58E-03	2.04E-02	1.78E-01	3.24E-03	1.91E-02
	1.00	5.36E-05	7.23E-05	1.79E-03	8.37E-05	1.70E-05	3.78E-03	2.25E-02	2.00E-01	3.63E-03	2.08E-02
Batch 3	0.11	2.38E-05	6.33E-05	1.79E-03	1.70E-05	1.70E-05	1.41E-03	6.65E-03	4.16E-02	7.59E-04	3.94E-03
	0.18	2.06E-05	5.62E-05	1.79E-03	1.70E-05	1.70E-05	1.65E-03	8.21E-03	5.50E-02	1.01E-03	5.66E-03
	0.25	2.22E-05	5.77E-05	1.79E-03	2.36E-05	1.99E-05	1.86E-03	9.29E-03	6.73E-02	1.23E-03	7.35E-03
	0.33	3.18E-05	6.79E-05	1.79E-03	3.22E-05	1.70E-05	2.41E-03	1.23E-02	9.71E-02	1.78E-03	1.04E-02
	0.43	3.40E-05	5.10E-05	1.79E-03	1.16E-04	1.70E-05	2.68E-03	1.39E-02	1.14E-01	2.06E-03	1.19E-02
	0.54	4.76E-05	6.91E-05	1.79E-03	4.19E-05	1.70E-05	2.91E-03	1.53E-02	1.31E-01	2.35E-03	1.40E-02
	0.67	4.05E-05	7.60E-05	1.79E-03	4.02E-05	1.70E-05	3.34E-03	1.87E-02	1.61E-01	2.95E-03	1.76E-02
	0.82	5.23E-05	8.11E-05	1.79E-03	5.06E-05	1.70E-05	3.48E-03	2.06E-02	1.78E-01	3.25E-03	1.84E-02
	1.00	5.78E-05	7.12E-05	1.79E-03	1.16E-04	1.70E-05	3.70E-03	2.16E-02	1.91E-01	3.52E-03	2.16E-02

Continued…

	SLR [g/mL]	Eu [mM]	Sm [mM]	Gd [mM]	Tb [mM]	Dy [mM]	Ho [mM]	Er [mM]	Tm [mM]	Yb [mM]	Lu [mM]
	0.11	1.19E-02	2.93E-02	1.12E-04	1.59E-05	9.05E-05	9.82E-06	2.64E-05	1.18E-06	1.48E-05	7.20E-06
	0.18	1.14E-02	2.78E-02	1.71E-04	2.24E-05	1.35E-04	1.51E-05	4.07E-05	2.96E-06	1.73E-05	8.46E-06
	0.25	1.12E-02	2.74E-02	1.63E-04	2.40E-05	1.26E-04	1.59E-05	4.20E-05	4.74E-06	1.55E-05	8.57E-06
	0.33	1.16E-02	2.87E-02	2.54E-04	3.39E-05	1.80E-04	2.12E-05	5.98E-05	6.57E-06	3.29E-05	9.89E-06
Batch 1	0.43	1.07E-02	2.69E-02	3.26E-04	4.10E-05	2.25E-04	2.74E-05	6.58E-05	6.69E-06	4.17E-05	1.17E-05
	0.54	9.08E-03	2.33E-02	5.01E-04	5.87E-05	3.00E-04	3.64E-05	8.91E-05	1.04E-05	1.07E-05	1.26E-05
	0.67	9.08E-03	2.29E-02	6.21E-04	6.92E-05	4.10E-04	4.48E-05	1.12E-04	1.32E-05	9.53E-05	1.42E-05
	0.82	8.69E-03	2.17E-02	6.87E-04	7.55E-05	4.28E-04	5.03E-05	1.21E-04	1.43E-05	1.02E-04	1.54E-05
	1.00	8.42E-03	2.17E-02	8.33E-04	9.12E-05	5.05E-04	5.83E-05	1.43E-04	1.67E-05	1.28E-04	1.78E-05
	0.11	1.14E-02	2.85E-02	1.14E-04	1.86E-05	9.85E-05	1.25E-05	3.32E-05	1.18E-06	8.67E-06	7.54E-06
	0.18	1.07E-02	2.61E-02	1.44E-04	2.37E-05	1.18E-04	1.46E-05	3.72E-05	2.96E-06	1.50E-05	8.63E-06
	0.25	1.04E-02	2.57E-02	2.33E-04	3.09E-05	1.74E-04	2.03E-05	5.52E-05	4.74E-06	2.25E-05	9.43E-06
	0.33	1.00E-02	2.50E-02	3.21E-04	4.34E-05	2.18E-04	2.62E-05	6.52E-05	7.04E-06	3.25E-05	1.06E-05
Batch 2	0.43	9.67E-03	2.36E-02	4.41E-04	5.06E-05	2.81E-04	3.32E-05	8.19E-05	8.64E-06	5.75E-05	1.23E-05
	0.54	8.88E-03	2.23E-02	4.93E-04	5.88E-05	3.19E-04	3.46E-05	8.97E-05	1.03E-05	6.36E-05	1.17E-05
	0.67	8.16E-03	2.02E-02	5.71E-04	6.42E-05	3.39E-04	4.10E-05	1.03E-04	1.08E-05	7.45E-05	1.21E-05
	0.82	8.82E-03	2.23E-02	7.63E-04	8.31E-05	4.22E-04	5.15E-05	1.28E-04	1.41E-05	1.06E-04	1.71E-05
	1.00	8.23E-03	2.11E-02	8.71E-04	9.12E-05	4.83E-04	5.98E-05	1.46E-04	1.81E-05	1.29E-04	1.83E-05
	0.11	1.18E-02	2.93E-02	1.11E-04	1.91E-05	1.02E-04	1.24E-05	3.46E-05	1.18E-06	8.67E-06	7.72E-06
	0.18	1.18E-02	2.93E-02	1.63E-04	2.58E-05	1.36E-04	1.53E-05	4.35E-05	2.96E-06	1.50E-05	7.77E-06
	0.25	1.13E-02	2.83E-02	2.28E-04	3.15E-05	1.56E-04	1.93E-05	5.40E-05	4.74E-06	2.43E-05	1.00E-05
	0.33	1.11E-02	2.75E-02	3.61E-04	4.47E-05	2.42E-04	2.80E-05	7.23E-05	8.17E-06	4.11E-05	1.11E-05
Batch 3	0.43	1.07E-02	2.66E-02	4.45E-04	5.50E-05	2.66E-04	3.50E-05	8.07E-05	8.46E-06	5.75E-05	1.24E-05
	0.54	1.05E-02	2.60E-02	5.20E-04	5.88E-05	3.07E-04	3.68E-05	8.97E-05	1.15E-05	6.47E-05	1.28E-05
	0.67	1.03E-02	2.60E-02	6.74E-04	7.36E-05	4.10E-04	4.65E-05	1.15E-04	1.28E-05	9.07E-05	1.57E-05
	0.82	9.74E-03	2.49E-02	7.50E-04	8.31E-05	4.28E-04	5.40E-05	1.27E-04	1.40E-05	1.06E-04	1.69E-05
	1.00	8.49E-03	2.19E-02	8.46E-04	9.12E-05	4.52E-04	5.81E-05	1.33E-04	1.63E-05	1.18E-04	1.75E-05

Continued…

	SLR [g/mL]	Chloride [mM]	Nitrate [mM]	Phosphate [mM]	Sulphate [mM]	Carbonate [mM]
	0.11	1.08	<8.06E-05	<1.05E-04	<1.04E-04	<1.67E-05
	0.18	1.05	<8.06E-05	<1.05E-04	<1.04E-04	<1.67E-05
	0.25	1.05	<8.06E-05	<1.05E-04	<1.04E-04	<1.67E-05
	0.33	1.09	1.39E-04	<1.05E-04	<1.04E-04	<1.67E-05
Batch 1	0.43	0.97	<8.06E-05	<1.05E-04	<1.04E-04	-
	0.54	0.96	<8.06E-05	<1.05E-04	<1.04E-04	<1.67E-05
	0.67	0.89	<8.06E-05	<1.05E-04	<1.04E-04	<1.67E-05
	0.82	0.86	<8.06E-05	<1.05E-04	<1.04E-04	<1.67E-05
	1.00	0.86	<8.06E-05	<1.05E-04	<1.04E-04	-
	0.11	1.03	<8.06E-05	<1.05E-04	<1.04E-04	<1.67E-05
	0.18	1.03	<8.06E-05	<1.05E-04	<1.04E-04	<1.67E-05
	0.25	0.99	<8.06E-05	<1.05E-04	<1.04E-04	<1.67E-05
	0.33	0.96	<8.06E-05	<1.05E-04	<1.04E-04	<1.67E-05
Batch 2	0.43	0.89	<8.06E-05	<1.05E-04	<1.04E-04	<1.67E-05
	0.54	0.88	<8.06E-05	<1.05E-04	<1.04E-04	-
	0.67	0.76	<8.06E-05	<1.05E-04	<1.04E-04	-
	0.82	0.85	<8.06E-05	<1.05E-04	<1.04E-04	-
	1.00	0.82	<8.06E-05	<1.05E-04	<1.04E-04	-
	0.11	1.08	1.60E-04	<1.05E-04	<1.04E-04	<1.67E-05
	0.18	1.08	1.53E-04	<1.05E-04	<1.04E-04	<1.67E-05
	0.25	1.07	1.48E-04	<1.05E-04	<1.04E-04	<1.67E-05
	0.33	0.98	1.61E-04	<1.05E-04	<1.04E-04	<1.67E-05
Batch 3	0.43	1.02	1.37E-04	<1.05E-04	<1.04E-04	<1.67E-05
	0.54	0.97	1.26E-04	<1.05E-04	<1.04E-04	<1.67E-05
	0.67	0.95	1.21E-04	<1.05E-04	<1.04E-04	<1.67E-05
	0.82	0.87	1.10E-04	<1.05E-04	<1.04E-04	-
	1.00	0.83	1.11E-04	<1.05E-04	<1.04E-04	-

Table B.2 All element concentrations mobilised into solution during the batch tests at 9 SLR conditions (in triplicate).

B.3 Soil Column Dataset

	No.	Start of Collection [date/h]	End of Collection [date/h]	Solution	Na [mM]	Mg [mM]	Al [mM]	Si [mM]	K [mM]	Ca [mM]	Mn [mM]	Fe [mM]	Co [mM]	Ni [mM]	Cu [mM]	Zn [mM]	Ba [mM]	Y [mM]
Column 1	1	12.07.17 / 10:00	13.07.17 / 07:00	DI water	0.04	0.01	0.00	0.04	0.24	0.05	1.82E-04	1.79E-04	1.70E-04	1.70E-04	1.57E-04	3.50E-03	0.04	1.12E-05
	2	13.07.17 / 07:00	13.07.17 / 16:00	DI water	0.04	0.01	0.00	0.04	0.14	0.03	1.82E-04	1.79E-04	1.70E-04	1.70E-04	1.57E-04	3.24E-03	0.02	1.12E-05
	3	13.07.17 / 16:00	14.07.17 / 07:00	DI water	0.15	0.02	0.02	0.04	0.06	0.05	2.84E-04	1.79E-04	1.70E-04	1.70E-04	1.57E-04	7.81E-03	0.02	1.12E-05
	4	14.07.17 / 07:00	17.07.17 / 07:00	DI water	0.04	0.01	0.01	0.04	0.04	0.02	2.08E-04	1.79E-04	1.70E-04	1.70E-04	1.57E-04	8.85E-04	0.01	1.12E-05
	5	17.07.17 / 07:00	18.07.17 / 07:00	DI water	0.04	0.01	0.01	0.04	0.04	0.02	2.37E-04	1.79E-04	1.70E-04	1.70E-04	1.57E-04	8.82E-04	0.02	1.12E-05
	6	18.07.17 / 07:00	19.07.17 / 07:30	DI water	0.04	0.01	0.01	0.04	0.04	0.02	2.04E-04	1.79E-04	1.70E-04	1.70E-04	1.57E-04	9.63E-04	0.03	1.12E-05
	7	19.07.17 / 07:30	19.07.17 / 15:00	DI water	0.04	0.01	0.01	0.04	0.04	0.03	2.20E-04	1.79E-04	1.70E-04	1.70E-04	1.57E-04	9.39E-04	0.06	1.12E-05
	8	19.07.17 / 15:00	20.07.17 / 07:00	DI water	0.04	0.01	0.02	0.04	0.04	0.02	2.00E-04	1.79E-04	1.70E-04	1.70E-04	1.57E-04	8.66E-04	0.03	1.12E-05
	9	20.07.17 / 07:00	21.07.17 / 07:00	DI water	0.13	0.01	0.39	0.04	0.04	0.02	2.60E-04	1.79E-04	1.70E-04	1.70E-04	1.57E-04	1.56E-03	0.11	1.12E-05
	10	21.07.17 / 07:00	21.07.17 / 17:00	DI water	0.04	0.01	0.01	0.04	0.04	0.02	1.82E-04	1.79E-04	1.70E-04	1.70E-04	1.57E-04	8.93E-04	0.03	1.12E-05
	11	21.07.17 / 17:00	24.07.17 / 07:00	0.05 M $BaCl_2$	0.05	0.07	0.02	0.04	0.05	0.02	1.71E-03	1.79E-04	1.70E-04	1.70E-04	1.57E-04	1.37E-03	0.07	5.20E-05
	12	24.07.17 / 07:00	25.07.17 / 07:00	0.05 M $BaCl_2$	0.15	0.01	0.03	0.04	0.05	0.03	2.40E-04	1.79E-04	1.70E-04	1.70E-04	1.57E-04	5.20E-03	0.03	1.12E-05
	13	25.07.17 / 07:00	26.07.17 / 07:00	0.05 M $BaCl_2$	0.37	0.16	0.74	0.05	0.04	0.06	5.15E-03	1.79E-04	1.70E-04	1.70E-04	1.57E-04	6.09E-03	0.16	1.28E-04
	14	26.07.17 / 07:00	26.07.17 / 16:00	0.05 M $BaCl_2$	1.35	2.91	5.15	0.09	0.05	0.28	7.21E-02	1.79E-04	1.70E-04	2.54E-04	1.57E-04	2.49E-02	0.04	6.40E-04
	15	26.07.17 / 16:00	27.07.17 / 07:00	0.05 M $BaCl_2$	0.78	5.31	10.90	0.15	0.05	0.47	1.37E-01	1.79E-04	1.70E-04	4.86E-04	1.57E-04	1.62E-02	0.40	1.74E-03
	16	27.07.17 / 07:00	27.07.17 / 16:00	0.05 M $BaCl_2$	0.30	3.82	13.56	0.13	0.05	0.43	1.00E-01	1.79E-04	1.70E-04	4.69E-04	1.57E-04	1.10E-02	1.17	2.13E-03
	17	27.07.17 / 16:00	28.07.17 / 07:00	0.05 M $BaCl_2$	0.06	2.49	18.20	0.12	0.05	0.39	7.17E-02	1.79E-04	1.70E-04	4.50E-04	1.57E-04	1.20E-02	4.22	2.88E-03
	18	27.07.17 / 07:00	28.07.17 / 15:00	0.05 M $BaCl_2$	0.12	1.14	13.97	0.11	0.05	0.24	4.39E-02	1.79E-04	1.70E-04	3.07E-04	1.57E-04	1.46E-02	5.60	2.35E-03
	19	27.07.17 / 15:00	31.07.17 / 07:00	0.05 M $BaCl_2$	0.04	0.51	15.12	0.10	0.07	0.16	2.62E-02	1.79E-04	1.70E-04	2.18E-04	1.57E-04	2.19E-02	14.20	2.94E-03
	20	31.07.17 / 07:00	31.07.17 / 17:00	0.05 M $BaCl_2$	0.04	0.13	12.16	0.08	0.07	0.09	8.25E-03	1.79E-04	1.70E-04	1.70E-04	1.57E-04	2.58E-02	18.64	2.35E-03
	21	31.07.17 / 17:00	01.08.17 / 07:00	0.05 M $BaCl_2$	0.04	0.08	11.82	0.08	0.07	0.10	6.41E-03	1.79E-04	1.70E-04	1.70E-04	1.57E-04	3.40E-02	21.92	2.38E-03

	No.	Start of Collection [date/h]	End of Collection [date/h]	Solution	Na [mM]	Mg [mM]	Al [mM]	Si [mM]	K [mM]	Ca [mM]	Mn [mM]	Fe [mM]	Co [mM]	Ni [mM]	Cu [mM]	Zn [mM]	Ba [mM]	Y [mM]
	22	01.08.17 / 07:00	02.08.17 / 07:00	0.05 M $BaCl_2$	0.04	0.09	10.79	0.08	0.07	0.07	6.57E-03	1.79E-04	1.70E-04	1.70E-04	1.57E-04	3.23E-02	24.90	2.29E-03
	23	02.08.17 / 16:30	02.08.17 / 16:30	0.05 M $BaCl_2$	0.04	0.03	8.93	0.08	0.07	0.04	4.02E-03	1.79E-04	1.70E-04	1.70E-04	1.57E-04	3.24E-02	25.41	1.99E-03
	24	02.08.17 / 07:00	03.08.17 / 07:00	0.05 M $BaCl_2$	0.04	0.02	8.89	0.08	0.07	0.04	3.66E-03	1.79E-04	1.70E-04	1.70E-04	1.57E-04	3.35E-02	27.67	2.00E-03
	25	03.08.17 / 07:00	04.08.17 / 07:00	0.05 M $BaCl_2$	0.04	0.16	5.00	0.09	0.08	0.09	7.44E-03	1.79E-04	1.70E-04	1.70E-04	1.57E-04	4.07E-02	29.78	2.06E-03
	1	12.07.17 / 10:00	13.07.17 / 07:00	DI water	0.04	0.00	0.00	0.04	0.28	0.02	1.98E-04	1.79E-04	1.70E-04	1.70E-04	1.57E-04	1.85E-03	0.01	1.12E-05
	2	13.07.17 / 07:00	13.07.17 / 16:00	DI water	0.06	0.02	0.00	0.04	0.16	0.04	5.02E-04	1.79E-04	1.70E-04	1.70E-04	1.57E-04	2.60E-03	0.01	1.12E-05
	3	13.07.17 / 16:00	14.07.17 / 07:00	DI water	0.23	0.02	0.02	0.05	0.13	0.05	4.40E-04	1.79E-04	1.70E-04	1.70E-04	1.57E-04	8.37E-03	0.04	1.12E-05
	4	14.07.17 / 07:00	17.07.17 / 07:00	DI water	0.06	0.01	0.01	0.04	0.12	0.02	2.99E-04	1.79E-04	1.70E-04	1.70E-04	1.57E-04	1.93E-03	0.01	1.12E-05
	5	17.07.17 / 07:00	18.07.17 / 07:00	DI water	0.06	0.01	0.01	0.04	0.17	0.04	3.29E-04	1.79E-04	1.70E-04	1.70E-04	1.57E-04	1.97E-03	0.19	1.37E-05
	6	18.07.17 / 07:00	19.07.17 / 07:30	DI water	0.07	0.01	0.01	0.04	0.19	0.03	3.97E-04	1.79E-04	1.70E-04	1.70E-04	1.57E-04	2.05E-03	0.01	1.93E-05
	7	19.07.17 / 07:30	19.07.17 / 15:00	DI water	0.07	0.02	0.01	0.04	0.16	0.04	3.77E-04	1.79E-04	1.70E-04	1.70E-04	1.57E-04	2.03E-03	0.03	1.12E-05
	8	19.07.17 / 15:00	20.07.17 / 07:00	DI water	0.06	0.01	0.02	0.04	0.17	0.02	4.06E-04	1.79E-04	1.70E-04	1.70E-04	1.57E-04	1.77E-03	0.04	1.12E-05
	9	20.07.17 / 07:00	21.07.17 / 07:00	DI water	0.18	0.01	0.39	0.05	0.16	0.02	5.13E-04	1.79E-04	1.70E-04	1.70E-04	1.57E-04	2.86E-03	0.40	5.46E-05
Column 2	10	21.07.17 / 07:00	21.07.17 / 17:00	DI water	0.06	0.01	0.01	0.04	0.17	0.02	3.29E-04	1.79E-04	1.70E-04	1.70E-04	1.57E-04	1.64E-03	0.03	1.12E-05
	11	21.07.17 / 17:00	24.07.17 / 07:00	0.05 M $BaCl_2$	0.06	0.01	0.02	0.04	0.18	0.02	3.29E-04	1.79E-04	1.70E-04	1.70E-04	1.57E-04	2.49E-03	0.02	1.12E-05
	12	24.07.17 / 07:00	25.07.17 / 07:00	0.05 M $BaCl_2$	0.22	0.01	0.03	0.06	0.31	0.02	5.48E-04	1.79E-04	1.70E-04	1.70E-04	1.57E-04	4.14E-03	0.03	1.12E-05
	13	25.07.17 / 07:00	26.07.17 / 07:00	0.05 M $BaCl_2$	0.55	0.46	0.74	0.06	0.20	0.06	8.85E-03	1.79E-04	4.73E-05	1.70E-04	1.57E-04	5.77E-03	0.06	9.21E-05
	14	26.07.17 / 07:00	26.07.17 / 16:00	0.05 M $BaCl_2$	1.78	2.78	5.15	0.14	0.18	0.28	5.61E-02	1.79E-04	2.32E-04	1.70E-04	1.57E-04	6.67E-03	0.32	7.90E-04
	15	26.07.17 / 16:00	27.07.17 / 07:00	0.05 M $BaCl_2$	1.30	4.61	10.90	0.18	0.18	0.41	9.63E-02	1.79E-04	3.89E-04	1.70E-04	1.57E-04	1.13E-02	0.98	1.74E-03
	16	27.07.17 / 07:00	27.07.17 / 16:00	0.05 M $BaCl_2$	0.48	3.64	13.56	0.18	0.16	0.31	7.75E-02	1.79E-04	3.89E-04	1.70E-04	1.57E-04	1.09E-02	1.20	2.31E-03
	17	27.07.17 / 16:00	28.07.17 / 07:00	0.05 M $BaCl_2$	0.25	2.63	18.20	0.15	0.16	0.30	5.46E-02	1.79E-04	3.27E-04	1.70E-04	1.57E-04	1.02E-02	4.75	2.63E-03
	18	27.07.17 / 07:00	28.07.17 / 15:00	0.05 M $BaCl_2$	0.32	1.42	13.97	0.15	0.17	0.29	3.00E-02	1.79E-04	2.43E-04	1.70E-04	1.57E-04	1.65E-02	6.99	2.55E-03
	19	27.07.17 / 15:00	31.07.17 / 07:00	0.05 M $BaCl_2$	0.04	0.85	15.12	0.11	0.16	0.11	1.59E-02	1.79E-04	1.95E-04	1.70E-04	1.57E-04	1.96E-02	14.33	2.67E-03

No.	Start of Collection [date/h]	End of Collection [date/h]	Solution	Na [mM]	Mg [mM]	Al [mM]	Si [mM]	K [mM]	Ca [mM]	Mn [mM]	Fe [mM]	Co [mM]	Ni [mM]	Cu [mM]	Zn [mM]	Ba [mM]	Y [mM]
20	31.07.17 / 07:00	31.07.17 / 17:00	0.05 M $BaCl_2$	0.04	0.22	12.16	0.10	0.17	0.07	7.44E-03	1.79E-04	1.70E-04	1.70E-04	1.57E-04	2.39E-02	14.68	2.33E-03
21	31.07.17 / 17:00	01.08.17 / 07:00	0.05 M $BaCl_2$	0.24	0.25	11.82	0.12	0.16	0.18	7.21E-03	1.79E-04	1.70E-04	1.70E-04	1.57E-04	2.78E-02	15.84	2.25E-03
22	01.08.17 / 07:00	02.08.17 / 07:00	0.05 M $BaCl_2$	0.04	0.07	10.79	0.10	0.12	0.05	3.73E-03	1.79E-04	1.70E-04	1.70E-04	1.57E-04	2.89E-02	19.68	2.25E-03
23	02.08.17 / 16:30	02.08.17 / 16:30	0.05 M $BaCl_2$	0.04	0.03	8.93	0.08	0.11	0.03	2.71E-03	1.79E-04	1.70E-04	1.70E-04	1.57E-04	2.77E-02	18.13	1.84E-03
24	02.08.17 / 07:00	03.08.17 / 07:00	0.05 M $BaCl_2$	0.04	0.05	8.89	0.10	0.12	0.03	3.22E-03	1.79E-04	1.70E-04	1.70E-04	1.57E-04	2.98E-02	19.06	1.97E-03
25	03.08.17 / 07:00	04.08.17 / 07:00	0.05 M $BaCl_2$	0.10	0.02	5.00	0.11	0.10	0.03	1.68E-03	1.79E-04	1.70E-04	1.70E-04	1.57E-04	2.28E-02	28.01	1.14E-03

Continued…..

	No.	Start Collection [date/h]	End Collection [date/h]	Solution	La [mM]	Ce [mM]	Pr [mM]	Nd [mM]	Sm [mM]	Eu [mM]	Gd [mM]	Tb [mM]	Dy [mM]	Ho [mM]	Er [mM]	Tm [mM]	Yb [mM]	Lu [mM]
Column 1	1	12.07.17 / 10:00	13.07.17 / 07:00	DI water	7.20E-06	7.14E-06	7.10E-06	6.93E-06	6.58E-06	6.65E-06	2.13E-05	6.29E-06	6.15E-06	6.06E-06	5.98E-06	5.92E-06	5.78E-06	5.72E-06
	2	13.07.17 / 07:00	13.07.17 / 16:00	DI water	1.56E-05	2.15E-05	7.10E-06	6.93E-06	6.58E-06	6.65E-06	1.61E-05	6.29E-06	6.15E-06	6.06E-06	5.98E-06	5.92E-06	5.78E-06	5.72E-06
	3	13.07.17 / 16:00	14.07.17 / 07:00	DI water	1.06E-05	7.49E-05	7.10E-06	6.93E-06	1.05E-05	6.65E-06	1.21E-05	6.29E-06	6.15E-06	6.06E-06	5.98E-06	5.92E-06	5.78E-06	5.72E-06
	4	14.07.17 / 07:00	17.07.17 / 07:00	DI water	8.85E-06	1.05E-05	7.10E-06	6.93E-06	6.58E-06	6.65E-06	9.60E-06	6.29E-06	6.15E-06	6.06E-06	5.98E-06	5.92E-06	5.78E-06	5.72E-06
	5	17.07.17 / 07:00	18.07.17 / 07:00	DI water	7.20E-06	1.59E-05	7.10E-06	6.93E-06	5.31E-05	2.87E-05	7.82E-05	6.29E-06	6.15E-06	6.06E-06	5.98E-06	5.92E-06	5.78E-06	5.72E-06
	6	18.07.17 / 07:00	19.07.17 / 07:30	DI water	9.50E-06	1.71E-05	7.10E-06	6.93E-06	6.58E-06	6.65E-06	7.57E-06	6.29E-06	6.15E-06	6.06E-06	5.98E-06	5.92E-06	5.78E-06	5.72E-06
	7	19.07.17 / 07:30	19.07.17 / 15:00	DI water	1.23E-05	3.13E-05	7.10E-06	6.93E-06	1.01E-05	6.65E-06	1.07E-05	6.29E-06	6.15E-06	6.06E-06	5.98E-06	5.92E-06	5.78E-06	5.72E-06
	8	19.07.17 / 15:00	20.07.17 / 07:00	DI water	8.49E-06	1.49E-05	7.10E-06	6.93E-06	1.27E-05	6.65E-06	9.03E-06	6.29E-06	6.15E-06	6.06E-06	5.98E-06	5.92E-06	5.78E-06	5.72E-06
	9	20.07.17 / 07:00	21.07.17 / 07:00	DI water	1.26E-05	1.36E-04	7.10E-06	6.93E-06	1.18E-04	5.81E-05	8.20E-06	6.29E-06	6.15E-06	6.06E-06	5.98E-06	5.92E-06	5.78E-06	5.72E-06
	10	21.07.17 / 07:00	21.07.17 / 17:00	DI water	1.14E-05	3.15E-05	7.10E-06	6.93E-06	9.08E-06	6.65E-06	8.39E-06	6.29E-06	6.15E-06	6.06E-06	5.98E-06	5.92E-06	5.78E-06	5.72E-06
	11	21.07.17 / 17:00	24.07.17 / 07:00	0.05 M $BaCl_2$	2.51E-04	2.08E-03	3.92E-05	1.30E-04	6.58E-06	6.65E-06	3.68E-05	6.29E-06	6.71E-06	6.06E-06	5.98E-06	5.92E-06	5.78E-06	5.72E-06
	12	24.07.17 / 07:00	25.07.17 / 07:00	0.05 M $BaCl_2$	1.81E-05	8.35E-05	7.10E-06	6.93E-06	9.02E-06	6.65E-06	5.99E-06	6.29E-06	6.15E-06	6.06E-06	5.98E-06	5.92E-06	5.78E-06	5.72E-06
	13	25.07.17 / 07:00	26.07.17 / 07:00	0.05 M $BaCl_2$	6.12E-04	3.20E-03	7.88E-05	2.66E-04	4.90E-05	1.28E-05	5.77E-05	6.29E-06	1.32E-05	6.06E-06	5.98E-06	5.92E-06	5.78E-06	5.72E-06
	14	26.07.17 / 07:00	26.07.17 / 16:00	0.05 M $BaCl_2$	3.07E-03	2.85E-02	4.93E-04	1.34E-03	5.02E-04	1.45E-04	4.21E-04	2.07E-05	8.74E-05	1.40E-05	3.47E-05	5.92E-06	2.63E-05	5.72E-06
	15	26.07.17 / 16:00	27.07.17 / 07:00	0.05 M $BaCl_2$	1.35E-02	8.92E-02	1.44E-03	6.44E-03	1.04E-03	2.77E-04	1.31E-03	6.36E-05	2.60E-04	4.03E-05	1.02E-04	1.24E-05	7.11E-05	9.89E-06
	16	27.07.17 / 07:00	27.07.17 / 16:00	0.05 M $BaCl_2$	1.17E-02	1.11E-01	1.80E-03	6.11E-03	1.80E-03	5.75E-04	1.64E-03	7.87E-05	2.55E-04	5.00E-05	1.25E-04	1.52E-05	8.55E-05	1.24E-05
	17	27.07.17 / 16:00	28.07.17 / 07:00	0.05 M $BaCl_2$	1.47E-02	1.42E-01	2.51E-03	7.42E-03	2.51E-03	9.31E-04	2.30E-03	1.08E-04	4.14E-04	6.49E-05	1.58E-04	1.89E-05	1.05E-04	1.54E-05
	18	27.07.17 / 07:00	28.07.17 / 15:00	0.05 M $BaCl_2$	1.28E-02	1.22E-01	2.07E-03	5.75E-03	3.21E-03	1.34E-03	1.88E-03	8.75E-05	3.29E-04	5.24E-05	1.28E-04	1.53E-05	8.44E-05	1.24E-05
	19	27.07.17 / 15:00	31.07.17 / 07:00	0.05 M $BaCl_2$	1.52E-02	1.47E-01	2.65E-03	7.28E-03	4.34E-03	1.96E-03	2.17E-03	9.82E-05	3.47E-04	5.38E-05	1.32E-04	1.53E-05	8.03E-05	1.20E-05
	20	31.07.17 / 07:00	31.07.17 / 17:00	0.05 M $BaCl_2$	1.24E-02	1.17E-01	2.09E-03	6.63E-03	4.87E-03	2.31E-03	1.62E-03	7.11E-05	2.52E-04	3.92E-05	9.69E-05	1.14E-05	5.67E-05	8.69E-06
	21	31.07.17 / 17:00	01.08.17 / 07:00	0.05 M $BaCl_2$	1.15E-02	1.10E-01	2.04E-03	5.37E-03	5.30E-03	2.55E-03	1.51E-03	6.86E-05	2.32E-04	3.66E-05	8.97E-05	1.02E-05	5.07E-05	7.60E-06
	22	01.08.17 / 07:00	02.08.17 / 07:00	0.05 M $BaCl_2$	1.09E-02	1.05E-01	1.89E-03	5.71E-03	6.03E-03	3.01E-03	1.42E-03	6.17E-05	2.08E-04	3.19E-05	7.77E-05	8.82E-06	4.42E-05	6.92E-06

	No.	Start Collection [date/h]	End Collection [date/h]	Solution	La [mM]	Ce [mM]	Pr [mM]	Nd [mM]	Sm [mM]	Eu [mM]	Gd [mM]	Tb [mM]	Dy [mM]	Ho [mM]	Er [mM]	Tm [mM]	Yb [mM]	Lu [mM]
	23	02.08.17 / 16:30	02.08.17 / 16:30	0.05 M $BaCl_2$	9.21E-03	8.85E-02	1.67E-03	4.97E-03	5.65E-03	2.85E-03	1.23E-03	5.35E-05	1.76E-04	2.67E-05	6.70E-05	7.64E-06	3.88E-05	6.12E-06
	24	02.08.17 / 07:00	03.08.17 / 07:00	0.05 M $BaCl_2$	9.07E-03	8.64E-02	1.63E-03	4.43E-03	6.37E-03	3.21E-03	1.16E-03	5.00E-05	1.66E-04	2.49E-05	6.16E-05	7.04E-06	3.49E-05	5.83E-06
	25	03.08.17 / 07:00	04.08.17 / 07:00	0.05 M $BaCl_2$	8.78E-03	8.28E-02	1.60E-03	4.35E-03	4.63E-03	2.39E-03	1.14E-03	4.96E-05	1.64E-04	2.45E-05	5.95E-05	6.81E-06	3.59E-05	5.72E-06
Column 2	1	12.07.17 / 10:00	13.07.17 / 07:00	DI water	1.86E-05	5.85E-05	7.10E-06	8.39E-06	6.58E-06	6.65E-06	9.22E-06	6.29E-06	6.15E-06	6.06E-06	5.98E-06	5.92E-06	5.78E-06	5.72E-06
	2	13.07.17 / 07:00	13.07.17 / 16:00	DI water	1.71E-05	4.13E-05	7.10E-06	6.93E-06	6.58E-06	6.65E-06	7.76E-06	6.29E-06	6.15E-06	6.06E-06	5.98E-06	5.92E-06	5.78E-06	5.72E-06
	3	13.07.17 / 16:00	14.07.17 / 07:00	DI water	1.58E-05	1.07E-04	7.10E-06	6.93E-06	1.05E-05	6.65E-06	8.14E-06	6.29E-06	6.15E-06	6.06E-06	5.98E-06	5.92E-06	5.78E-06	5.72E-06
	4	14.07.17 / 07:00	17.07.17 / 07:00	DI water	1.33E-05	4.71E-05	7.10E-06	6.93E-06	6.58E-06	6.65E-06	7.76E-06	6.29E-06	6.15E-06	6.06E-06	5.98E-06	5.92E-06	5.78E-06	5.72E-06
	5	17.07.17 / 07:00	18.07.17 / 07:00	DI water	3.05E-05	7.92E-05	7.10E-06	1.14E-05	5.31E-05	2.87E-05	7.76E-06	6.29E-06	6.15E-06	6.06E-06	5.98E-06	5.92E-06	5.78E-06	5.72E-06
	6	18.07.17 / 07:00	19.07.17 / 07:30	DI water	3.88E-05	4.30E-05	7.10E-06	1.66E-05	6.58E-06	6.65E-06	9.35E-06	6.29E-06	6.15E-06	6.06E-06	5.98E-06	5.92E-06	5.78E-06	5.72E-06
	7	19.07.17 / 07:30	19.07.17 / 15:00	DI water	2.20E-05	8.92E-05	7.10E-06	1.15E-05	1.01E-05	6.65E-06	7.89E-06	6.29E-06	6.15E-06	6.06E-06	5.98E-06	5.92E-06	5.78E-06	5.72E-06
	8	19.07.17 / 15:00	20.07.17 / 07:00	DI water	2.65E-05	1.31E-04	7.10E-06	1.16E-05	1.27E-05	6.65E-06	8.97E-06	6.29E-06	6.15E-06	6.06E-06	5.98E-06	5.92E-06	5.78E-06	5.72E-06
	9	20.07.17 / 07:00	21.07.17 / 07:00	DI water	2.96E-04	2.60E-03	4.68E-05	1.64E-04	1.18E-04	5.81E-05	4.66E-05	6.29E-06	6.15E-06	6.06E-06	5.98E-06	5.92E-06	5.78E-06	5.72E-06
	10	21.07.17 / 07:00	21.07.17 / 17:00	DI water	2.12E-05	8.49E-05	7.10E-06	1.05E-05	9.08E-06	6.65E-06	6.36E-06	6.29E-06	6.15E-06	6.06E-06	5.98E-06	5.92E-06	5.78E-06	5.72E-06
	11	21.07.17 / 17:00	24.07.17 / 07:00	0.05 M $BaCl_2$	2.63E-05	1.26E-04	7.10E-06	1.37E-05	6.58E-06	6.65E-06	6.36E-06	6.29E-06	6.15E-06	6.06E-06	5.98E-06	5.92E-06	5.78E-06	5.72E-06
	12	24.07.17 / 07:00	25.07.17 / 07:00	0.05 M $BaCl_2$	2.98E-05	2.23E-04	7.10E-06	1.46E-05	9.02E-06	6.65E-06	9.22E-06	6.29E-06	6.15E-06	6.06E-06	5.98E-06	5.92E-06	5.78E-06	5.72E-06
	13	25.07.17 / 07:00	26.07.17 / 07:00	0.05 M $BaCl_2$	5.38E-04	4.77E-03	8.45E-05	2.72E-04	4.90E-05	1.28E-05	7.95E-06	6.29E-06	1.34E-05	6.06E-06	5.98E-06	5.92E-06	5.78E-06	5.72E-06
	14	26.07.17 / 07:00	26.07.17 / 16:00	0.05 M $BaCl_2$	4.66E-03	4.32E-02	7.59E-04	2.17E-03	5.02E-04	1.45E-04	7.19E-04	3.44E-05	1.30E-04	2.10E-05	5.12E-05	6.27E-06	3.63E-05	5.72E-06
	15	26.07.17 / 16:00	27.07.17 / 07:00	0.05 M $BaCl_2$	9.86E-03	9.56E-02	1.67E-03	4.82E-03	1.04E-03	2.77E-04	1.56E-03	7.49E-05	2.86E-04	4.56E-05	1.12E-04	1.36E-05	7.63E-05	1.08E-05
	16	27.07.17 / 07:00	27.07.17 / 16:00	0.05 M $BaCl_2$	1.27E-02	1.23E-01	2.22E-03	5.84E-03	1.80E-03	5.75E-04	2.09E-03	9.63E-05	3.61E-04	5.61E-05	1.42E-04	1.69E-05	8.96E-05	1.29E-05
	17	27.07.17 / 16:00	28.07.17 / 07:00	0.05 M $BaCl_2$	1.44E-02	1.41E-01	2.53E-03	7.07E-03	2.51E-03	9.31E-04	2.30E-03	1.05E-04	3.80E-04	6.03E-05	1.48E-04	1.73E-05	9.53E-05	1.38E-05
	18	27.07.17 / 07:00	28.07.17 / 15:00	0.05 M $BaCl_2$	1.35E-02	1.29E-01	2.51E-03	6.67E-03	3.21E-03	1.34E-03	2.17E-03	9.82E-05	3.46E-04	5.44E-05	1.35E-04	1.61E-05	8.38E-05	1.23E-05
	19	27.07.17 / 15:00	31.07.17 / 07:00	0.05 M $BaCl_2$	1.48E-02	1.44E-01	2.58E-03	7.97E-03	4.34E-03	1.96E-03	2.05E-03	9.25E-05	3.24E-04	5.04E-05	1.23E-04	1.44E-05	7.45E-05	1.10E-05
	20	31.07.17 / 07:00	31.07.17 / 17:00	0.05 M $BaCl_2$	1.23E-02	1.20E-01	2.13E-03	6.48E-03	4.87E-03	2.31E-03	1.68E-03	7.42E-05	2.54E-04	3.88E-05	9.51E-05	1.07E-05	5.58E-05	8.52E-06

No.	Start Collection [date/h]	End Collection [date/h]	Solution	La [mM]	Ce [mM]	Pr [mM]	Nd [mM]	Sm [mM]	Eu [mM]	Gd [mM]	Tb [mM]	Dy [mM]	Ho [mM]	Er [mM]	Tm [mM]	Yb [mM]	Lu [mM]
21	31.07.17 / 17:00	01.08.17 / 07:00	0.05 M $BaCl_2$	1.20E-02	1.16E-01	2.10E-03	6.43E-03	5.30E-03	2.55E-03	1.53E-04	7.11E-05	2.42E-04	3.77E-05	9.09E-05	1.07E-05	5.13E-05	8.00E-06
22	01.08.17 / 07:00	02.08.17 / 07:00	0.05 M $BaCl_2$	1.12E-02	1.08E-01	1.93E-03	5.62E-03	6.03E-03	3.01E-03	1.45E-03	6.24E-05	2.08E-04	3.20E-05	7.83E-05	8.58E-06	4.33E-05	7.09E-06
23	02.08.17 / 16:30	02.08.17 / 16:30	0.05 M $BaCl_2$	9.29E-03	8.99E-02	1.60E-03	4.96E-03	5.65E-03	2.85E-03	1.21E-03	5.23E-05	1.74E-04	2.68E-05	6.46E-05	7.04E-06	3.74E-05	6.06E-06
24	02.08.17 / 07:00	03.08.17 / 07:00	0.05 M $BaCl_2$	9.50E-03	8.99E-02	1.74E-03	4.71E-03	6.37E-03	3.21E-03	1.27E-03	5.46E-05	1.81E-04	2.76E-05	6.70E-05	7.75E-06	3.92E-05	6.17E-06
25	03.08.17 / 07:00	04.08.17 / 07:00	0.05 M $BaCl_2$	5.23E-03	5.06E-02	1.02E-03	3.04E-03	4.63E-03	2.39E-03	8.20E-04	3.54E-05	1.19E-04	1.84E-05	4.27E-05	5.92E-06	2.59E-05	5.72E-06

Continued…

	Sample	Start of Collection [date/h]	End of Collection [date/h]	Solution	Chloride [mM]	Nitrate [mM]	Phosphate [mM]	Sulphate [mM]
Column 1	1	12.07.17 / 10:00	13.07.17 / 07:00	DI water	0.12	0.01	0.01	0.02
	2	13.07.17 / 07:00	13.07.17 / 16:00	DI water	0.14	0.01	0.01	0.02
	3	13.07.17 / 16:00	14.07.17 / 07:00	DI water	0.18	0.01	0.01	0.02
	4	14.07.17 / 07:00	17.07.17 / 07:00	DI water	0.27	0.01	0.01	0.03
	5	17.07.17 / 07:00	18.07.17 / 07:00	DI water	0.45	0.01	0.01	0.02
	6	18.07.17 / 07:00	19.07.17 / 07:30	DI water	1.02	0.01	0.01	0.02
	7	19.07.17 / 07:30	19.07.17 / 15:00	DI water	1.31	0.01	0.01	0.02
	8	19.07.17 / 15:00	20.07.17 / 07:00	DI water	1.59	0.01	0.01	0.01
	9	20.07.17 / 07:00	21.07.17 / 07:00	DI water	1.84	0.01	0.01	0.01
	10	21.07.17 / 07:00	21.07.17 / 17:00	DI water	1.84	0.01	0.01	0.01
	11	21.07.17 / 17:00	24.07.17 / 07:00	0.05 M $BaCl_2$	1.84	0.01	0.01	0.01
	12	24.07.17 / 07:00	25.07.17 / 07:00	0.05 M $BaCl_2$	16.15	0.01	0.01	0.01
	13	25.07.17 / 07:00	26.07.17 / 07:00	0.05 M $BaCl_2$	19.19	0.01	0.01	0.03
	14	26.07.17 / 07:00	26.07.17 / 16:00	0.05 M $BaCl_2$	30.58	0.01	0.01	0.03
	15	26.07.17 / 16:00	27.07.17 / 07:00	0.05 M $BaCl_2$	47.67	0.01	0.01	0.01
	16	27.07.17 / 07:00	27.07.17 / 16:00	0.05 M $BaCl_2$	53.03	0.01	0.01	0.03
	17	27.07.17 / 16:00	28.07.17 / 07:00	0.05 M $BaCl_2$	55.85	0.01	0.01	0.03
	18	27.07.17 / 07:00	28.07.17 / 15:00	0.05 M $BaCl_2$	56.69	0.01	0.01	0.01
	19	27.07.17 / 15:00	31.07.17 / 07:00	0.05 M $BaCl_2$	62.34	0.01	0.01	0.02
	20	31.07.17 / 07:00	31.07.17 / 17:00	0.05 M $BaCl_2$	67.98	0.01	0.01	0.01
	21	31.07.17 / 17:00	01.08.17 / 07:00	0.05 M $BaCl_2$	75.03	0.01	0.01	0.01
	22	01.08.17 / 07:00	02.08.17 / 07:00	0.05 M $BaCl_2$	75.03	0.01	0.01	0.01
	23	02.08.17 / 16:30	02.08.17 / 16:30	0.05 M $BaCl_2$	75.03	0.01	0.01	0.02
	24	02.08.17 / 07:00	03.08.17 / 07:00	0.05 M $BaCl_2$	75.03	0.01	0.01	0.01
	25	03.08.17 / 07:00	04.08.17 / 07:00	0.05 M $BaCl_2$	77.00	0.01	0.01	0.01
Column 2	1	12.07.17 / 10:00	13.07.17 / 07:00	DI water	0.06	0.01	0.01	0.02
	2	13.07.17 / 07:00	13.07.17 / 16:00	DI water	0.13	0.01	0.01	0.02
	3	13.07.17 / 16:00	14.07.17 / 07:00	DI water	0.26	0.01	0.01	0.04
	4	14.07.17 / 07:00	17.07.17 / 07:00	DI water	0.32	0.01	0.01	0.03

Sample	Start of Collection [date/h]	End of Collection [date/h]	Solution	Chloride [mM]	Nitrate [mM]	Phosphate [mM]	Sulphate [mM]
5	17.07.17 / 07:00	18.07.17 / 07:00	DI water	0.51	0.01	0.01	0.03
6	18.07.17 / 07:00	19.07.17 / 07:30	DI water	0.56	0.01	0.01	0.03
7	19.07.17 / 07:30	19.07.17 / 15:00	DI water	1.39	0.00	0.01	0.01
8	19.07.17 / 15:00	20.07.17 / 07:00	DI water	1.69	1.01	0.01	0.01
9	20.07.17 / 07:00	21.07.17 / 07:00	DI water	2.00	0.01	0.01	0.01
10	21.07.17 / 07:00	21.07.17 / 17:00	DI water	3.02	0.01	0.01	0.00
11	21.07.17 / 17:00	24.07.17 / 07:00	0.05 M $BaCl_2$	4.85	0.01	0.01	0.00
12	24.07.17 / 07:00	25.07.17 / 07:00	0.05 M $BaCl_2$	5.64	0.01	0.01	0.02
13	25.07.17 / 07:00	26.07.17 / 07:00	0.05 M $BaCl_2$	15.06	0.01	0.01	0.04
14	26.07.17 / 07:00	26.07.17 / 16:00	0.05 M $BaCl_2$	24.60	0.02	0.01	0.01
15	26.07.17 / 16:00	27.07.17 / 07:00	0.05 M $BaCl_2$	48.80	0.02	0.01	0.01
16	27.07.17 / 07:00	27.07.17 / 16:00	0.05 M $BaCl_2$	58.39	0.01	0.01	0.01
17	27.07.17 / 16:00	28.07.17 / 07:00	0.05 M $BaCl_2$	64.03	0.02	0.01	0.01
18	27.07.17 / 07:00	28.07.17 / 15:00	0.05 M $BaCl_2$	65.72	0.03	0.01	0.01
19	27.07.17 / 15:00	31.07.17 / 07:00	0.05 M $BaCl_2$	68.54	0.02	0.01	0.01
20	31.07.17 / 07:00	31.07.17 / 17:00	0.05 M $BaCl_2$	71.36	0.02	0.01	0.01
21	31.07.17 / 17:00	01.08.17 / 07:00	0.05 M $BaCl_2$	72.49	0.02	0.01	0.01
22	01.08.17 / 07:00	02.08.17 / 07:00	0.05 M $BaCl_2$	73.05	0.01	0.01	0.01
23	02.08.17 / 16:30	02.08.17 / 16:30	0.05 M $BaCl_2$	75.31	0.01	0.01	0.01
24	02.08.17 / 07:00	03.08.17 / 07:00	0.05 M $BaCl_2$	78.13	0.01	0.01	0.01
25	03.08.17 / 07:00	04.08.17 / 07:00	0.05 M $BaCl_2$	78.98	0.01	0.01	0.01

Continued…

	No.	Start Collection [date/h]	End Collection [date/h]	Solution	Na [mM]	Mg [mM]	Al [mM]	Si [mM]	K [mM]	Ca [mM]	Mn [mM]	Fe [mM]	Co [mM]	Ni [mM]	Cu [mM]	Zn [mM]	Ba [mM]	Y [mM]
Column 1	1	23.08.17 / 17:00	24.08.17 / 15:30	DI water	0.08	0.02	0.07	0.07	0.02	0.06	7.14E-04	1.79E-04	1.70E-04	3.65E-03	1.57E-04	1.84E-03	2.75E-01	4.62E-05
	2	24.08.17 / 15:30	25.08.17 / 07:30	DI water	0.08	0.02	0.10	0.04	0.01	0.03	1.21E-03	1.79E-04	1.70E-04	4.86E-03	1.57E-04	2.48E-03	4.27E-01	4.71E-05
	3	25.08.17 / 07:30	25.08.17 / 16:00	DI water	0.12	0.02	0.07	0.04	0.01	0.03	7.88E-04	1.79E-04	1.70E-04	2.64E-03	1.57E-04	1.73E-03	2.96E-01	2.94E-05
	4	25.08.17 / 16:00	28.08.17 / 07:00	DI water	0.12	0.02	0.03	0.04	0.02	0.02	4.15E-04	1.79E-04	1.70E-04	8.84E-04	1.57E-04	1.03E-03	1.13E-01	1.21E-05
	5	28.08.17 / 07:00	28.08.17 / 16:30	DI water	0.14	0.03	0.01	0.05	0.04	0.03	2.95E-04	1.79E-04	1.70E-04	3.27E-04	1.57E-04	7.83E-04	4.25E-02	1.12E-05
	6	28.08.17 / 07:00	29.08.17 / 07:00	DI water	0.11	0.01	0.01	0.04	0.02	0.01	2.53E-04	1.79E-04	1.70E-04	1.70E-04	1.57E-04	5.43E-04	2.76E-02	1.12E-05
	7	29.08.17 / 07:00	30.08.17 / 07:00	DI water	0.11	0.01	0.01	0.04	0.01	0.01	2.26E-04	1.79E-04	1.70E-04	1.70E-04	1.57E-04	3.96E-04	2.18E-02	1.12E-05
	8	30.08.17 / 07:00	31.08.17 / 07:00	DI water	0.12	0.01	0.01	0.04	0.01	0.02	2.00E-04	1.79E-04	1.70E-04	1.70E-04	1.57E-04	4.01E-04	1.75E-02	1.12E-05
	9	31.08.17 / 07:00	01.09.17 / 08:00	0.1 M NH_4Cl	0.06	0.01	0.01	0.04	0.00	0.01	1.01E-04	1.79E-04	1.70E-04	1.70E-04	1.57E-04	3.01E-04	1.80E-02	1.12E-05
	10	01.09.17 / 08:00	01.09.17 / 15:30	0.1 M NH_4Cl	0.10	0.01	0.00	0.04	0.01	0.03	2.75E-04	1.79E-04	1.70E-04	1.70E-04	1.57E-04	3.62E-04	2.09E-02	1.12E-05
	11	01.09.17 / 15:30	04.09.17 / 07:00	0.1 M NH_4Cl	0.10	0.01	0.01	0.06	0.09	0.02	1.63E-04	1.79E-04	1.70E-04	2.40E-04	3.94E-04	4.88E-04	1.65E-02	1.12E-05
	12	04.09.17 / 07:00	05.09.17 / 07:00	0.1 M NH_4Cl	0.11	0.01	0.01	0.06	0.09	0.02	1.61E-04	1.79E-04	1.70E-04	2.06E-04	2.94E-04	4.45E-04	1.87E-02	1.12E-05
	13	05.09.17 / 07:00	06.09.17 / 07:00	0.1 M NH_4Cl	0.10	0.01	0.01	0.06	0.09	0.02	1.66E-04	1.79E-04	1.70E-04	2.01E-04	3.24E-04	3.95E-04	1.46E-02	1.12E-05
	14	06.09.17 / 07:00	06.09.17 / 16:00	0.1 M NH_4Cl	0.12	0.01	0.01	0.06	0.09	0.02	1.67E-04	1.79E-04	1.70E-04	2.15E-04	3.21E-04	4.95E-04	1.40E-02	1.12E-05
	15	06.09.17 / 16:00	07.09.17 / 07:30	0.1 M NH_4Cl	1.47	0.81	1.11	0.07	0.10	0.07	1.77E-02	1.79E-04	1.70E-04	2.44E-04	3.75E-04	8.47E-04	4.03E-02	1.70E-04
	16	07.09.17 / 07:30	07.09.17 / 17:00	0.1 M NH_4Cl	0.51	0.69	1.14	0.06	0.09	0.06	1.50E-02	1.79E-04	1.70E-04	2.66E-04	4.17E-04	5.80E-04	3.13E-02	1.55E-04
	17	07.09.17 / 17:00	08.09.17 / 07:30	0.1 M NH_4Cl	0.41	0.70	1.19	0.07	0.09	0.06	1.51E-02	1.79E-04	1.70E-04	2.45E-04	4.04E-04	6.65E-04	2.95E-02	1.65E-04
	18	08.09.17 / 07:30	08.09.17 / 17:00	0.1 M NH_4Cl	1.14	8.56	13.82	0.17	0.09	0.52	1.76E-01	1.79E-04	4.43E-04	6.55E-04	1.57E-04	1.93E-03	9.10E-02	2.58E-03
	19	08.09.17 / 17:00	11.09.17 / 10:00	0.1 M NH_4Cl	0.21	3.65	23.02	0.21	0.17	0.42	7.61E-02	1.79E-04	3.82E-04	6.37E-04	1.57E-04	1.62E-03	2.24E-01	4.33E-03

	No.	Start Collection [date/h]	End Collection [date/h]	Solution	Na [mM]	Mg [mM]	Al [mM]	Si [mM]	K [mM]	Ca [mM]	Mn [mM]	Fe [mM]	Co [mM]	Ni [mM]	Cu [mM]	Zn [mM]	Ba [mM]	Y [mM]
	20	11.09.17 / 10:00	12.09.17 / 12:00	0.1 M NH_4Cl	0.04	0.53	18.90	0.19	0.26	0.14	1.40E-02	1.79E-04	1.85E-04	3.09E-04	4.16E-04	1.64E-03	1.28E-01	3.91E-03
	21	12.09.17 / 12:00	13.09.17 / 07:10	0.1 M NH_4Cl	0.04	0.13	15.16	0.18	0.25	0.07	5.55E-03	1.79E-04	1.70E-04	2.76E-04	3.77E-04	1.50E-03	6.79E-02	3.01E-03
	22	13.09.17 / 07:10	13.09.17 / 17:10	0.1 M NH_4Cl	0.04	0.05	12.68	0.16	0.22	0.05	3.80E-03	1.79E-04	1.70E-04	2.76E-04	3.87E-04	1.46E-03	4.59E-02	2.49E-03
	23	13.09.17 / 17:10	14.09.17 / 07:10	0.1 M NH_4Cl	0.04	0.03	11.64	0.16	0.20	0.04	3.06E-03	1.79E-04	1.70E-04	4.31E-04	1.57E-04	1.42E-03	3.80E-02	2.22E-03
	24	14.09.17 / 07:10	14.09.17 / 17:10	0.1 M NH_4Cl	0.04	0.02	10.64	0.15	0.17	0.04	2.78E-03	1.79E-04	1.70E-04	2.63E-04	3.98E-04	1.44E-03	2.92E-02	1.92E-03
	25	14.09.17 / 17:10	15.09.17 / 07:10	0.1 M NH_4Cl	0.04	0.02	9.67	0.15	0.15	0.03	2.49E-03	1.79E-04	1.70E-04	4.37E-04	1.57E-04	1.29E-03	2.61E-02	1.71E-03
	26	15.09.17 / 07:10	15.09.17 / 17:10	0.1 M NH_4Cl	0.04	0.01	8.64	0.14	0.13	0.03	2.38E-03	1.79E-04	1.70E-04	2.63E-04	3.47E-04	1.26E-03	2.44E-02	1.55E-03
	27	15.09.17 / 17:10	18.09.17 / 07:10	0.1 M NH_4Cl	0.04	0.01	7.56	0.13	0.12	0.03	2.28E-03	1.79E-04	1.70E-04	4.00E-04	1.57E-04	1.35E-03	2.47E-02	1.34E-03
	28	18.09.17 / 07:10	19.09.17 / 07:10	0.1 M NH_4Cl	0.04	0.01	6.15	0.13	0.11	0.03	2.11E-03	1.79E-04	1.70E-04	2.89E-04	3.82E-04	1.43E-03	2.40E-02	1.12E-03
	29	19.09.17 / 07:10	19.09.17 / 15:10	0.1 M NH_4Cl	0.04	0.01	5.67	0.13	0.10	0.03	2.11E-03	1.79E-04	1.70E-04	2.78E-04	3.40E-04	1.56E-03	2.40E-02	1.04E-03
	30	19.09.17 / 15:10	21.09.17 / 07:10	0.1 M NH_4Cl	0.04	0.01	5.30	0.13	0.10	0.03	1.98E-03	1.79E-04	1.70E-04	2.53E-04	3.08E-04	2.00E-03	2.43E-02	9.46E-04
	31	21.09.17 / 07:10	21.09.17 / 18:10	0.1 M NH_4Cl	0.04	0.01	4.86	0.13	0.10	0.03	1.98E-03	1.79E-04	1.70E-04	2.56E-04	3.37E-04	1.32E-03	2.29E-02	8.68E-04
	32	21.09.17 / 18:10	22.09.17 / 17:10	0.1 M NH_4Cl	0.04	0.01	4.48	0.12	0.09	0.03	1.89E-03	1.79E-04	1.70E-04	4.10E-04	1.57E-04	1.25E-03	2.25E-02	7.92E-04
	33	22.09.17 / 17:10	25.09.17 / 07:10	0.1 M NH_4Cl	0.04	0.01	5.30	0.13	0.11	0.03	1.81E-03	1.79E-04	1.70E-04	2.34E-04	3.67E-04	1.53E-03	2.20E-02	9.66E-04
Column 2	1	23.08.17 / 17:00	24.08.17 / 15:30	DI water	0.05	0.02	0.01	0.04	0.05	0.02	4.73E-04	1.79E-04	1.70E-04	1.59E-03	1.57E-04	1.79E-03	6.18E-01	1.23E-05
	2	24.08.17 / 15:30	25.08.17 / 07:30	DI water	0.20	0.06	0.04	0.04	0.07	0.04	1.42E-03	1.79E-04	1.70E-04	2.27E-03	1.57E-04	1.97E-03	5.73E-01	1.74E-05
	3	25.08.17 / 07:30	25.08.17 / 16:00	DI water	0.19	0.06	0.03	0.04	0.05	0.03	1.37E-03	1.79E-04	1.70E-04	1.53E-03	1.57E-04	1.46E-03	3.87E-01	1.23E-05
	4	25.08.17 / 16:00	28.08.17 / 07:00	DI water	0.07	0.02	0.01	0.04	0.03	0.02	4.22E-04	1.79E-04	1.70E-04	4.50E-04	1.57E-04	9.36E-04	8.45E-02	1.12E-05
	5	28.08.17 / 07:00	28.08.17 / 16:30	DI water	0.16	0.04	0.01	0.04	0.08	0.04	6.24E-04	1.79E-04	1.70E-04	4.94E-04	1.57E-04	8.89E-04	9.68E-02	1.12E-05

No.	Start Collection [date/h]	End Collection [date/h]	Solution	Na [mM]	Mg [mM]	Al [mM]	Si [mM]	K [mM]	Ca [mM]	Mn [mM]	Fe [mM]	Co [mM]	Ni [mM]	Cu [mM]	Zn [mM]	Ba [mM]	Y [mM]
6	28.08.17 / 07:00	29.08.17 / 07:00	DI water	0.14	0.04	0.01	0.04	0.07	0.03	5.72E-04	1.79E-04	1.70E-04	4.29E-04	1.57E-04	1.16E-03	7.79E-02	1.12E-05
7	29.08.17 / 07:00	30.08.17 / 07:00	DI water	0.12	0.03	0.02	0.05	0.05	0.02	7.21E-04	1.79E-04	1.70E-04	2.96E-04	1.57E-04	1.33E-03	6.42E-02	1.12E-05
8	30.08.17 / 07:00	31.08.17 / 07:00	DI water	0.10	0.02	0.01	0.04	0.05	0.02	4.22E-04	1.79E-04	1.70E-04	2.78E-04	1.57E-04	1.34E-03	4.86E-02	1.12E-05
9	31.08.17 / 07:00	01.09.17 / 08:00	0.1 M NH_4Cl	0.05	0.01	0.01	0.04	0.03	0.03	1.65E-04	1.79E-04	1.70E-04	5.01E-04	1.57E-04	7.75E-04	2.25E-02	1.12E-05
10	01.09.17 / 08:00	01.09.17 / 15:30	0.1 M NH_4Cl	0.09	0.02	0.27	0.04	0.05	0.08	4.08E-04	1.79E-04	1.70E-04	1.70E-04	1.57E-04	6.44E-04	3.07E-02	6.20E-05
11	01.09.17 / 15:30	04.09.17 / 07:00	0.1 M NH_4Cl	0.09	0.02	0.01	0.04	0.06	0.03	3.28E-04	1.79E-04	1.70E-04	4.41E-04	1.57E-04	1.13E-03	3.47E-02	1.12E-05
12	04.09.17 / 07:00	05.09.17 / 07:00	0.1 M NH_4Cl	0.10	0.02	0.55	0.04	0.30	0.03	2.88E-04	1.79E-04	1.70E-04	1.70E-04	1.57E-04	9.93E-04	2.70E-02	4.80E-05
13	05.09.17 / 07:00	06.09.17 / 07:00	0.1 M NH_4Cl	0.09	0.01	0.01	0.04	0.06	0.03	2.68E-04	1.79E-04	1.70E-04	4.33E-04	1.57E-04	6.25E-04	2.45E-02	1.12E-05
14	06.09.17 / 07:00	06.09.17 / 16:00	0.1 M NH_4Cl	1.00	0.82	1.43	0.04	0.06	0.13	1.84E-02	1.79E-04	1.70E-04	1.20E-03	1.57E-04	7.25E-03	2.93E-01	2.61E-04
15	06.09.17 / 16:00	07.09.17 / 07:30	0.1 M NH_4Cl	2.07	7.98	26.76	0.21	0.09	0.70	1.63E-01	1.79E-04	6.14E-04	3.49E-03	1.57E-04	1.11E-02	5.67E-01	4.59E-03
16	07.09.17 / 07:30	07.09.17 / 17:00	0.1 M NH_4Cl	0.37	3.89	50.78	0.36	0.22	0.47	7.66E-02	1.79E-04	4.48E-04	9.37E-04	1.57E-04	3.35E-03	1.35E-01	8.80E-03
17	07.09.17 / 17:00	08.09.17 / 07:30	0.1 M NH_4Cl	0.07	1.05	23.68	0.12	0.08	0.06	2.00E-02	1.79E-04	1.70E-04	3.31E-04	1.57E-04	9.41E-04	4.57E-02	4.16E-03
18	08.09.17 / 07:30	08.09.17 / 17:00	0.1 M NH_4Cl	0.07	1.19	39.29	0.31	0.27	0.10	2.35E-02	1.79E-04	2.26E-04	4.38E-04	1.57E-04	1.58E-03	6.77E-02	6.93E-03
19	08.09.17 / 17:00	11.09.17 / 10:00	0.1 M NH_4Cl	0.03	0.62	31.91	0.25	0.26	0.03	1.31E-02	1.79E-04	1.70E-04	2.76E-04	1.57E-04	1.59E-03	5.13E-02	5.68E-03
20	11.09.17 / 10:00	12.09.17 / 12:00	0.1 M NH_4Cl	0.01	0.18	20.31	0.20	0.19	0.02	4.59E-03	1.79E-04	1.70E-04	1.79E-04	1.57E-04	1.46E-03	3.36E-02	3.69E-03
21	12.09.17 / 12:00	13.09.17 / 07:10	0.1 M NH_4Cl	0.01	0.08	15.94	0.18	0.14	0.02	2.95E-03	1.79E-04	1.70E-04	1.70E-04	1.57E-04	1.18E-03	3.23E-02	2.85E-03
22	13.09.17 / 07:10	13.09.17 / 17:10	0.1 M NH_4Cl	0.01	0.05	13.49	0.17	0.12	0.02	2.31E-03	1.79E-04	1.70E-04	1.70E-04	1.57E-04	9.41E-04	3.07E-02	2.40E-03
23	13.09.17 / 17:10	14.09.17 / 07:10	0.1 M NH_4Cl	0.01	0.04	11.75	0.16	0.09	0.02	1.93E-03	1.79E-04	1.70E-04	1.70E-04	1.57E-04	8.73E-04	2.93E-02	2.08E-03
24	14.09.17 / 07:10	14.09.17 / 17:10	0.1 M NH_4Cl	0.01	0.03	10.30	0.15	0.08	0.02	1.61E-03	1.79E-04	1.70E-04	3.85E-04	1.57E-04	8.40E-04	2.78E-02	1.82E-03

No.	Start Collection [date/h]	End Collection [date/h]	Solution	Na [mM]	Mg [mM]	Al [mM]	Si [mM]	K [mM]	Ca [mM]	Mn [mM]	Fe [mM]	Co [mM]	Ni [mM]	Cu [mM]	Zn [mM]	Ba [mM]	Y [mM]
25	14.09.17 / 17:10	15.09.17 / 07:10	0.1 M NH_4Cl	0.01	0.02	9.45	0.15	0.07	0.02	1.48E-03	1.79E-04	1.70E-04	1.70E-04	1.57E-04	8.00E-04	2.69E-02	1.65E-03
26	15.09.17 / 07:10	15.09.17 / 17:10	0.1 M NH_4Cl	0.01	0.02	8.23	0.13	0.07	0.02	1.31E-03	1.79E-04	1.70E-04	1.70E-04	1.57E-04	7.59E-04	2.41E-02	1.44E-03
27	15.09.17 / 17:10	18.09.17 / 07:10	0.1 M NH_4Cl	0.01	0.02	7.30	0.13	0.07	0.02	1.17E-03	1.79E-04	1.70E-04	1.70E-04	1.57E-04	1.00E-03	2.21E-02	1.25E-03
28	18.09.17 / 07:10	19.09.17 / 07:10	0.1 M NH_4Cl	0.01	0.02	5.63	0.11	0.07	0.02	1.13E-03	1.79E-04	1.70E-04	1.70E-04	1.57E-04	1.11E-03	1.84E-02	9.71E-04
29	19.09.17 / 07:10	19.09.17 / 15:10	0.1 M NH_4Cl	0.01	0.02	5.00	0.11	0.06	0.02	1.01E-03	1.79E-04	1.70E-04	1.70E-04	1.57E-04	8.46E-04	1.84E-02	8.45E-04
30	19.09.17 / 15:10	21.09.17 / 07:10	0.1 M NH_4Cl	0.01	0.01	4.52	0.11	0.06	0.02	9.59E-04	1.79E-04	1.70E-04	1.70E-04	1.57E-04	8.99E-04	1.78E-02	7.60E-04
31	21.09.17 / 07:10	21.09.17 / 18:10	0.1 M NH_4Cl	0.00	0.01	3.89	0.10	0.06	0.02	9.45E-04	1.79E-04	1.70E-04	6.32E-04	1.57E-04	9.85E-04	1.59E-02	6.49E-04
32	21.09.17 / 18:10	22.09.17 / 17:10	0.1 M NH_4Cl	0.00	0.01	3.31	0.09	0.05	0.02	9.14E-04	1.79E-04	1.70E-04	2.86E-04	1.57E-04	7.83E-04	1.59E-02	5.42E-04
33	22.09.17 / 17:10	25.09.17 / 07:10	0.1 M NH_4Cl	0.00	0.01	2.88	0.09	0.06	0.02	7.86E-04	1.79E-04	1.70E-04	4.07E-04	1.57E-04	9.30E-04	1.50E-02	4.66E-04

Continued…

		Start Collection [date/h]	End Collection [date/h]	Solution	La [mM]	Ce [mM]	Pr [mM]	Nd [mM]	Sm [mM]	Eu [mM]	Gd [mM]	Tb [mM]	Dy [mM]	Ho [mM]	Er [mM]	Tm [mM]	Yb [mM]	Lu [mM]
Column 1	1	23.08.17 / 17:00	24.08.17 / 15:30	DI water	1.25E-04	2.95E-04	1.87E-05	5.78E-05	8.25E-05	3.00E-05	6.36E-06	6.29E-06	6.15E-06	6.06E-06	5.98E-06	5.92E-06	5.78E-06	5.72E-06
	2	24.08.17 / 15:30	25.08.17 / 07:30	DI water	2.01E-04	5.10E-04	3.09E-05	1.06E-04	1.42E-04	5.19E-05	6.36E-06	6.29E-06	6.15E-06	6.06E-06	5.98E-06	5.92E-06	5.78E-06	5.72E-06
	3	25.08.17 / 07:30	25.08.17 / 16:00	DI water	1.32E-04	3.51E-04	2.02E-05	6.61E-05	9.91E-05	3.68E-05	6.36E-06	6.29E-06	6.15E-06	6.06E-06	5.98E-06	5.92E-06	5.78E-06	5.72E-06
	4	25.08.17 / 16:00	28.08.17 / 07:00	DI water	5.66E-05	1.34E-04	8.37E-06	2.66E-05	3.55E-05	1.37E-05	6.36E-06	6.29E-06	6.15E-06	6.06E-06	5.98E-06	5.92E-06	5.78E-06	5.72E-06
	5	28.08.17 / 07:00	28.08.17 / 16:30	DI water	2.15E-05	4.19E-05	7.10E-06	9.43E-06	1.39E-05	6.58E-06	6.36E-06	6.29E-06	6.15E-06	6.06E-06	5.98E-06	5.92E-06	5.78E-06	5.72E-06
	6	28.08.17 / 07:00	29.08.17 / 07:00	DI water	1.94E-05	3.54E-05	7.10E-06	8.32E-06	9.44E-06	6.58E-06	6.36E-06	6.29E-06	6.15E-06	6.06E-06	5.98E-06	5.92E-06	5.78E-06	5.72E-06
	7	29.08.17 / 07:00	30.08.17 / 07:00	DI water	3.56E-05	3.80E-05	7.10E-06	1.36E-05	7.52E-06	6.58E-06	6.36E-06	6.29E-06	6.15E-06	6.06E-06	5.98E-06	5.92E-06	5.78E-06	5.72E-06
	8	30.08.17 / 07:00	31.08.17 / 07:00	DI water	1.04E-05	1.58E-05	7.10E-06	6.93E-06	6.65E-06	6.58E-06	6.36E-06	6.29E-06	6.15E-06	6.06E-06	5.98E-06	5.92E-06	5.78E-06	5.72E-06
	9	31.08.17 / 07:00	01.09.17 / 08:00	0.1 M NH_4Cl	7.49E-06	1.24E-05	7.10E-06	6.93E-06	6.65E-06	6.58E-06	6.36E-06	6.29E-06	6.15E-06	6.06E-06	5.98E-06	5.92E-06	5.78E-06	5.72E-06
	10	01.09.17 / 08:00	01.09.17 / 15:30	0.1 M NH_4Cl	7.20E-06	9.49E-06	7.10E-06	6.93E-06	6.65E-06	6.58E-06	6.36E-06	6.29E-06	6.15E-06	6.06E-06	5.98E-06	5.92E-06	5.78E-06	5.72E-06
	11	01.09.17 / 15:30	04.09.17 / 07:00	0.1 M NH_4Cl	1.99E-05	1.98E-05	7.10E-06	6.93E-06	1.78E-05	6.58E-06	6.36E-06	6.29E-06	6.15E-06	6.06E-06	5.98E-06	5.92E-06	1.49E-05	5.72E-06
	12	04.09.17 / 07:00	05.09.17 / 07:00	0.1 M NH_4Cl	1.44E-05	2.40E-05	7.10E-06	6.93E-06	1.78E-05	6.58E-06	6.36E-06	6.29E-06	6.15E-06	6.06E-06	5.98E-06	5.92E-06	1.23E-05	5.72E-06
	13	05.09.17 / 07:00	06.09.17 / 07:00	0.1 M NH_4Cl	1.08E-05	1.83E-05	7.10E-06	6.93E-06	1.44E-05	6.58E-06	6.36E-06	6.29E-06	6.15E-06	6.06E-06	5.98E-06	5.92E-06	1.18E-05	5.72E-06
	14	06.09.17 / 07:00	06.09.17 / 16:00	0.1 M NH_4Cl	3.31E-05	1.74E-05	7.10E-06	6.93E-06	1.32E-05	6.58E-06	6.36E-06	6.29E-06	6.15E-06	6.06E-06	5.98E-06	5.92E-06	1.14E-05	5.72E-06
	15	06.09.17 / 16:00	07.09.17 / 07:30	0.1 M NH_4Cl	1.07E-03	3.07E-03	1.67E-04	5.21E-04	1.02E-04	1.37E-05	6.49E-05	6.80E-06	2.95E-05	6.06E-06	1.06E-05	5.92E-06	1.60E-05	5.72E-06
	16	07.09.17 / 07:30	07.09.17 / 17:00	0.1 M NH_4Cl	1.00E-03	2.85E-03	1.55E-04	4.85E-04	8.45E-05	1.18E-05	5.42E-05	6.29E-06	2.75E-05	6.06E-06	1.04E-05	5.92E-06	1.33E-05	5.72E-06
	17	07.09.17 / 17:00	08.09.17 / 07:30	0.1 M NH_4Cl	1.04E-03	3.00E-03	1.65E-04	5.14E-04	8.78E-05	1.19E-05	5.72E-05	6.80E-06	2.96E-05	6.06E-06	1.08E-05	5.92E-06	1.38E-05	5.72E-06
	18	08.09.17 / 07:30	08.09.17 / 17:00	0.1 M NH_4Cl	1.61E-02	4.64E-02	2.61E-03	7.83E-03	1.03E-03	1.37E-04	5.51E-04	1.05E-04	4.54E-04	6.73E-05	1.64E-04	1.94E-05	1.13E-04	1.53E-05
	19	08.09.17 / 17:00	11.09.17 / 10:00	0.1 M NH_4Cl	2.71E-02	7.85E-02	4.41E-03	1.32E-02	1.84E-03	2.43E-04	9.09E-04	1.75E-04	7.63E-04	1.13E-04	2.74E-04	3.18E-05	1.78E-04	2.54E-05

		Start Collection [date/h]	End Collection [date/h]	Solution	La [mM]	Ce [mM]	Pr [mM]	Nd [mM]	Sm [mM]	Eu [mM]	Gd [mM]	Tb [mM]	Dy [mM]	Ho [mM]	Er [mM]	Tm [mM]	Yb [mM]	Lu [mM]
	20	11.09.17 / 10:00	12.09.17 / 12:00	0.1 M NH_4Cl	2.53E-02	7.35E-02	4.12E-03	1.22E-02	1.63E-03	2.13E-04	8.33E-04	1.59E-04	6.83E-04	1.01E-04	2.48E-04	2.89E-05	1.63E-04	2.31E-05
	21	12.09.17 / 12:00	13.09.17 / 07:10	0.1 M NH_4Cl	2.07E-02	6.00E-02	3.37E-03	1.03E-02	1.28E-03	1.66E-04	6.80E-04	1.28E-04	5.53E-04	8.12E-05	1.99E-04	2.33E-05	1.31E-04	1.82E-05
	22	13.09.17 / 07:10	13.09.17 / 17:10	0.1 M NH_4Cl	1.78E-02	5.21E-02	2.89E-03	8.94E-03	1.09E-03	1.42E-04	5.76E-04	1.09E-04	4.61E-04	6.73E-05	1.65E-04	1.91E-05	1.09E-04	1.53E-05
	23	13.09.17 / 17:10	14.09.17 / 07:10	0.1 M NH_4Cl	1.60E-02	4.71E-02	2.60E-03	7.90E-03	9.64E-04	1.24E-04	5.14E-04	9.63E-05	4.12E-04	6.03E-05	1.49E-04	1.78E-05	1.00E-04	1.37E-05
	24	14.09.17 / 07:10	14.09.17 / 17:10	0.1 M NH_4Cl	1.44E-02	4.21E-02	2.33E-03	7.14E-03	8.65E-04	1.12E-04	4.59E-04	8.56E-05	3.65E-04	5.28E-05	1.32E-04	1.53E-05	8.73E-05	1.22E-05
	25	14.09.17 / 17:10	15.09.17 / 07:10	0.1 M NH_4Cl	1.30E-02	3.78E-02	2.08E-03	6.51E-03	7.71E-04	9.94E-05	4.11E-04	7.61E-05	3.24E-04	4.75E-05	1.18E-04	1.40E-05	7.86E-05	1.09E-05
	26	15.09.17 / 07:10	15.09.17 / 17:10	0.1 M NH_4Cl	1.20E-02	3.57E-02	1.94E-03	5.95E-03	7.12E-04	9.15E-05	3.84E-04	6.92E-05	2.95E-04	4.22E-05	1.06E-04	1.27E-05	7.28E-05	9.54E-06
	27	15.09.17 / 17:10	18.09.17 / 07:10	0.1 M NH_4Cl	1.06E-02	3.14E-02	1.70E-03	5.30E-03	6.32E-04	8.09E-05	3.41E-04	6.14E-05	2.58E-04	3.77E-05	9.33E-05	1.11E-05	6.36E-05	8.46E-06
	28	18.09.17 / 07:10	19.09.17 / 07:10	0.1 M NH_4Cl	9.00E-03	2.66E-02	1.46E-03	4.42E-03	5.27E-04	6.78E-05	2.82E-04	4.98E-05	2.14E-04	3.08E-05	7.71E-05	9.23E-06	5.39E-05	7.32E-06
	29	19.09.17 / 07:10	19.09.17 / 15:10	0.1 M NH_4Cl	8.35E-03	2.46E-02	1.35E-03	4.17E-03	4.94E-04	6.32E-05	2.68E-04	4.70E-05	1.96E-04	2.87E-05	7.05E-05	8.58E-06	5.11E-05	6.63E-06
	30	19.09.17 / 15:10	21.09.17 / 07:10	0.1 M NH_4Cl	7.63E-03	2.26E-02	1.23E-03	3.76E-03	4.56E-04	5.77E-05	2.47E-04	4.33E-05	1.83E-04	2.61E-05	6.52E-05	7.93E-06	4.65E-05	6.23E-06
	31	21.09.17 / 07:10	21.09.17 / 18:10	0.1 M NH_4Cl	7.11E-03	2.10E-02	1.15E-03	3.54E-03	4.28E-04	5.38E-05	2.30E-04	3.93E-05	1.69E-04	2.41E-05	5.98E-05	7.10E-06	4.33E-05	5.72E-06
	32	21.09.17 / 18:10	22.09.17 / 17:10	0.1 M NH_4Cl	6.49E-03	1.93E-02	1.05E-03	3.31E-03	3.90E-04	4.91E-05	2.12E-04	3.57E-05	1.53E-04	2.23E-05	5.55E-05	6.57E-06	4.06E-05	5.72E-06
	33	22.09.17 / 17:10	25.09.17 / 07:10	0.1 M NH_4Cl	7.85E-03	2.35E-02	1.28E-03	3.90E-03	4.68E-04	5.91E-05	2.52E-04	4.35E-05	1.85E-04	2.72E-05	6.70E-05	7.93E-06	4.74E-05	6.17E-06
Column 2	1	23.08.17 / 17:00	24.08.17 / 15:30	DI water	2.15E-05	2.73E-05	7.10E-06	6.93E-06	1.89E-04	7.30E-05	6.36E-06	6.29E-06	6.15E-06	6.06E-06	5.98E-06	5.92E-06	5.78E-06	5.72E-06
	2	24.08.17 / 15:30	25.08.17 / 07:30	DI water	5.04E-05	1.11E-04	7.10E-06	1.88E-05	1.74E-04	6.65E-05	6.36E-06	6.29E-06	6.15E-06	6.06E-06	5.98E-06	5.92E-06	5.78E-06	5.72E-06
	3	25.08.17 / 07:30	25.08.17 / 16:00	DI water	3.64E-05	8.28E-05	7.10E-06	1.34E-05	1.11E-04	4.22E-05	6.36E-06	6.29E-06	6.15E-06	6.06E-06	5.98E-06	5.92E-06	5.78E-06	5.72E-06
	4	25.08.17 / 16:00	28.08.17 / 07:00	DI water	9.43E-06	1.91E-05	7.10E-06	6.93E-06	2.48E-05	9.21E-06	6.36E-06	6.29E-06	6.15E-06	6.06E-06	5.98E-06	5.92E-06	5.78E-06	5.72E-06
	5	28.08.17 / 07:00	28.08.17 / 16:30	DI water	7.20E-06	1.33E-05	7.10E-06	6.93E-06	2.79E-05	1.07E-05	6.36E-06	6.29E-06	6.15E-06	6.06E-06	5.98E-06	5.92E-06	5.78E-06	5.72E-06

	Start Collection [date/h]	End Collection [date/h]	Solution	La [mM]	Ce [mM]	Pr [mM]	Nd [mM]	Sm [mM]	Eu [mM]	Gd [mM]	Tb [mM]	Dy [mM]	Ho [mM]	Er [mM]	Tm [mM]	Yb [mM]	Lu [mM]
6	28.08.17 / 07:00	29.08.17 / 07:00	DI water	1.12E-05	2.31E-05	7.10E-06	6.93E-06	2.27E-05	8.49E-06	6.36E-06	6.29E-06	6.15E-06	6.06E-06	5.98E-06	5.92E-06	5.78E-06	5.72E-06
7	29.08.17 / 07:00	30.08.17 / 07:00	DI water	8.85E-06	1.96E-05	7.10E-06	6.93E-06	1.98E-05	7.17E-06	6.36E-06	6.29E-06	6.15E-06	6.06E-06	5.98E-06	5.92E-06	5.78E-06	5.72E-06
8	30.08.17 / 07:00	31.08.17 / 07:00	DI water	7.20E-06	1.16E-05	7.10E-06	6.93E-06	1.39E-05	6.58E-06	6.36E-06	6.29E-06	6.15E-06	6.06E-06	5.98E-06	5.92E-06	5.78E-06	5.72E-06
9	31.08.17 / 07:00	01.09.17 / 08:00	0.1 M NH_4Cl	7.20E-06	8.85E-06	7.10E-06	6.93E-06	6.65E-06	6.58E-06	6.36E-06	6.29E-06	6.15E-06	6.06E-06	5.98E-06	5.92E-06	5.78E-06	5.72E-06
10	01.09.17 / 08:00	01.09.17 / 15:30	0.1 M NH_4Cl	4.69E-04	1.41E-03	7.74E-05	2.32E-04	3.47E-05	6.58E-06	1.32E-05	6.29E-06	1.14E-05	6.06E-06	5.98E-06	5.92E-06	5.78E-06	5.72E-06
11	01.09.17 / 15:30	04.09.17 / 07:00	0.1 M NH_4Cl	7.20E-06	8.06E-06	7.10E-06	6.93E-06	6.65E-06	6.58E-06	6.36E-06	6.29E-06	6.15E-06	6.06E-06	5.98E-06	5.92E-06	5.78E-06	5.72E-06
12	04.09.17 / 07:00	05.09.17 / 07:00	0.1 M NH_4Cl	3.98E-04	1.22E-03	6.54E-05	1.96E-04	2.94E-05	6.58E-06	6.36E-06	6.29E-06	8.74E-06	6.06E-06	5.98E-06	5.92E-06	5.78E-06	5.72E-06
13	05.09.17 / 07:00	06.09.17 / 07:00	0.1 M NH_4Cl	7.20E-06	7.14E-06	7.10E-06	6.93E-06	6.65E-06	6.58E-06	6.36E-06	6.29E-06	6.15E-06	6.06E-06	5.98E-06	5.92E-06	5.78E-06	5.72E-06
14	06.09.17 / 07:00	06.09.17 / 16:00	0.1 M NH_4Cl	1.63E-03	4.73E-03	2.51E-04	7.63E-04	1.47E-04	3.66E-05	4.72E-05	9.82E-06	4.40E-05	6.49E-06	1.61E-05	5.92E-06	6.01E-06	5.72E-06
15	06.09.17 / 16:00	07.09.17 / 07:30	0.1 M NH_4Cl	3.01E-02	8.85E-02	4.50E-03	1.37E-02	1.94E-03	2.72E-04	1.20E-03	1.80E-04	7.88E-04	1.17E-04	2.83E-04	3.32E-05	1.92E-04	2.63E-05
16	07.09.17 / 07:30	07.09.17 / 17:00	0.1 M NH_4Cl	5.94E-02	1.74E-01	8.94E-03	2.72E-02	3.69E-03	4.50E-04	2.32E-03	3.45E-04	1.50E-03	2.22E-04	5.37E-04	6.27E-05	3.68E-04	5.00E-05
17	07.09.17 / 17:00	08.09.17 / 07:30	0.1 M NH_4Cl	2.91E-02	8.64E-02	4.38E-03	1.34E-02	1.81E-03	2.14E-04	1.08E-03	1.65E-04	7.14E-04	1.05E-04	2.55E-04	2.90E-05	1.64E-04	2.36E-05
18	08.09.17 / 07:30	08.09.17 / 17:00	0.1 M NH_4Cl	5.05E-02	1.50E-01	7.66E-03	2.33E-02	3.07E-03	3.65E-04	1.90E-03	2.79E-04	1.20E-03	1.78E-04	4.27E-04	4.96E-05	2.88E-04	3.97E-05
19	08.09.17 / 17:00	11.09.17 / 10:00	0.1 M NH_4Cl	4.38E-02	1.30E-01	6.66E-03	2.02E-02	2.67E-03	3.14E-04	1.61E-03	2.38E-04	1.01E-03	1.48E-04	3.56E-04	4.19E-05	2.39E-04	3.33E-05
20	11.09.17 / 10:00	12.09.17 / 12:00	0.1 M NH_4Cl	3.05E-02	9.06E-02	4.63E-03	1.40E-02	1.81E-03	2.09E-04	1.06E-03	1.53E-04	6.58E-04	9.58E-05	2.33E-04	2.72E-05	1.53E-04	2.17E-05
21	12.09.17 / 12:00	13.09.17 / 07:10	0.1 M NH_4Cl	2.50E-02	7.42E-02	3.80E-03	1.16E-02	1.48E-03	1.68E-04	8.46E-04	1.23E-04	5.18E-04	7.52E-05	1.85E-04	2.15E-05	1.20E-04	1.73E-05
22	13.09.17 / 07:10	13.09.17 / 17:10	0.1 M NH_4Cl	2.16E-02	6.46E-02	3.30E-03	9.98E-03	1.27E-03	1.45E-04	7.25E-04	1.07E-04	4.42E-04	6.49E-05	1.57E-04	1.78E-05	1.00E-04	1.44E-05
23	13.09.17 / 17:10	14.09.17 / 07:10	0.1 M NH_4Cl	1.78E-02	5.72E-02	2.91E-03	8.87E-03	1.13E-03	1.27E-04	6.22E-04	9.25E-05	3.88E-04	5.60E-05	1.37E-04	1.53E-05	8.55E-05	1.24E-05
24	14.09.17 / 07:10	14.09.17 / 17:10	0.1 M NH_4Cl	1.57E-02	5.11E-02	2.59E-03	7.90E-03	9.98E-04	1.13E-04	5.54E-04	8.12E-05	3.42E-04	4.89E-05	1.22E-04	1.35E-05	7.40E-05	1.11E-05

	Start Collection [date/h]	End Collection [date/h]	Solution	La [mM]	Ce [mM]	Pr [mM]	Nd [mM]	Sm [mM]	Eu [mM]	Gd [mM]	Tb [mM]	Dy [mM]	Ho [mM]	Er [mM]	Tm [mM]	Yb [mM]	Lu [mM]
25	14.09.17 / 17:10	15.09.17 / 07:10	0.1 M NH_4Cl	1.48E-02	4.78E-02	2.43E-03	7.42E-03	9.31E-04	1.05E-04	5.11E-04	7.61E-05	3.13E-04	4.58E-05	1.12E-04	1.24E-05	6.82E-05	1.06E-05
26	15.09.17 / 07:10	15.09.17 / 17:10	0.1 M NH_4Cl	1.28E-02	3.93E-02	2.12E-03	6.48E-03	8.25E-04	9.15E-05	4.32E-04	6.42E-05	2.70E-04	3.93E-05	9.63E-05	1.11E-05	5.77E-05	8.63E-06
27	15.09.17 / 17:10	18.09.17 / 07:10	0.1 M NH_4Cl	1.15E-02	3.54E-02	1.91E-03	5.84E-03	7.38E-04	8.23E-05	3.82E-04	5.82E-05	2.41E-04	3.46E-05	8.67E-05	9.53E-06	5.15E-05	7.77E-06
28	18.09.17 / 07:10	19.09.17 / 07:10	0.1 M NH_4Cl	9.14E-03	2.83E-02	1.53E-03	4.66E-03	5.83E-04	6.46E-05	2.94E-04	4.57E-05	1.85E-04	2.71E-05	6.70E-05	7.10E-06	3.71E-05	6.17E-06
29	19.09.17 / 07:10	19.09.17 / 15:10	0.1 M NH_4Cl	8.06E-03	2.49E-02	1.36E-03	4.13E-03	5.15E-04	5.64E-05	2.50E-04	3.92E-05	1.62E-04	2.32E-05	5.79E-05	6.16E-06	3.10E-05	5.72E-06
30	19.09.17 / 15:10	21.09.17 / 07:10	0.1 M NH_4Cl	7.42E-03	2.30E-02	1.25E-03	3.83E-03	4.72E-04	5.17E-05	2.27E-04	3.60E-05	1.46E-04	2.09E-05	5.33E-05	5.92E-06	2.81E-05	5.72E-06
31	21.09.17 / 07:10	21.09.17 / 18:10	0.1 M NH_4Cl	6.39E-03	1.99E-02	1.09E-03	3.30E-03	4.03E-04	4.48E-05	1.89E-04	3.06E-05	1.24E-04	1.76E-05	4.50E-05	5.92E-06	2.17E-05	5.72E-06
32	21.09.17 / 18:10	22.09.17 / 17:10	0.1 M NH_4Cl	5.53E-03	1.73E-02	9.44E-04	2.90E-03	3.54E-04	3.95E-05	1.58E-04	2.64E-05	1.09E-04	1.56E-05	3.82E-05	5.92E-06	1.77E-05	5.72E-06
33	22.09.17 / 17:10	25.09.17 / 07:10	0.1 M NH_4Cl	4.78E-03	1.51E-02	8.23E-04	2.54E-03	3.08E-04	3.38E-05	1.36E-04	2.29E-05	9.29E-05	1.32E-05	3.29E-05	5.92E-06	1.44E-05	5.72E-06

Continued…

	No.	Start Collection [date/h]	End Collection [date/h]	Solution	Chloride [mM]	Nitrate [mM]	Phosphate [mM]	Sulphate [mM]
	1	23.08.17 / 17:00	24.08.17 / 15:30	DI water	0.76	0.00	0.00	0.00
	2	24.08.17 / 15:30	25.08.17 / 07:30	DI water	1.28	0.00	0.00	0.00
	3	25.08.17 / 07:30	25.08.17 / 16:00	DI water	1.03	0.00	0.00	0.00
	4	25.08.17 / 16:00	28.08.17 / 07:00	DI water	0.50	0.00	0.00	0.00
	5	28.08.17 / 07:00	28.08.17 / 16:30	DI water	0.30	0.00	0.00	0.01
	6	28.08.17 / 07:00	29.08.17 / 07:00	DI water	0.25	0.00	0.00	0.01
	7	29.08.17 / 07:00	30.08.17 / 07:00	DI water	0.21	0.00	0.00	0.01
	8	30.08.17 / 07:00	31.08.17 / 07:00	DI water	0.20	0.00	0.00	0.01
	9	31.08.17 / 07:00	01.09.17 / 08:00	0.1 M NH_4Cl	0.12	0.00	0.00	0.01
	10	01.09.17 / 08:00	01.09.17 / 15:30	0.1 M NH_4Cl	0.15	0.00	0.00	0.01
	11	01.09.17 / 15:30	04.09.17 / 07:00	0.1 M NH_4Cl	0.19	0.00	0.00	0.01
	12	04.09.17 / 07:00	05.09.17 / 07:00	0.1 M NH_4Cl	0.21	0.00	0.00	0.01
	13	05.09.17 / 07:00	06.09.17 / 07:00	0.1 M NH_4Cl	0.19	0.00	0.00	0.01
	14	06.09.17 / 07:00	06.09.17 / 16:00	0.1 M NH_4Cl	0.20	0.00	0.00	0.01
Column 1	15	06.09.17 / 16:00	07.09.17 / 07:30	0.1 M NH_4Cl	27.92	0.00	0.00	0.04
	16	07.09.17 / 07:30	07.09.17 / 17:00	0.1 M NH_4Cl	103.8	0.00	0.00	0.04
	17	07.09.17 / 17:00	08.09.17 / 07:30	0.1 M NH_4Cl	105.5	0.00	0.00	0.04
	18	08.09.17 / 07:30	08.09.17 / 17:00	0.1 M NH_4Cl	97.0	0.08	0.05	0.15
	19	08.09.17 / 17:00	11.09.17 / 10:00	0.1 M NH_4Cl	105.5	0.08	0.05	0.17
	20	11.09.17 / 10:00	12.09.17 / 12:00	0.1 M NH_4Cl	113.7	0.08	0.05	0.16
	21	12.09.17 / 12:00	13.09.17 / 07:10	0.1 M NH_4Cl	113.7	0.08	0.05	0.15
	22	13.09.17 / 07:10	13.09.17 / 17:10	0.1 M NH_4Cl	97.6	0.08	0.05	0.15
	23	13.09.17 / 17:10	14.09.17 / 07:10	0.1 M NH_4Cl	108.88	0.08	0.05	0.15
	24	14.09.17 / 07:10	14.09.17 / 17:10	0.1 M NH_4Cl	113.67	0.08	0.05	0.14
	25	14.09.17 / 17:10	15.09.17 / 07:10	0.1 M NH_4Cl	112.83	0.08	0.05	0.14
	26	15.09.17 / 07:10	15.09.17 / 17:10	0.1 M NH_4Cl	113.67	0.08	0.05	0.13
	27	15.09.17 / 17:10	18.09.17 / 07:10	0.1 M NH_4Cl	115.08	0.08	0.05	0.13
	28	18.09.17 / 07:10	19.09.17 / 07:10	0.1 M NH_4Cl	108.88	0.08	0.05	0.12

	No.	Start Collection [date/h]	End Collection [date/h]	Solution	Chloride [mM]	Nitrate [mM]	Phosphate [mM]	Sulphate [mM]
	29	19.09.17 / 07:10	19.09.17 / 15:10	0.1 M NH_4Cl	119.88	0.08	0.05	0.11
	30	19.09.17 / 15:10	21.09.17 / 07:10	0.1 M NH_4Cl	110.85	0.08	0.05	0.12
	31	21.09.17 / 07:10	21.09.17 / 18:10	0.1 M NH_4Cl	110.29	0.08	0.05	0.12
	32	21.09.17 / 18:10	22.09.17 / 17:10	0.1 M NH_4Cl	111.42	0.08	0.05	0.12
	33	22.09.17 / 17:10	25.09.17 / 07:10	0.1 M NH_4Cl	112.26	0.08	0.05	0.11
	1	23.08.17 / 17:00	24.08.17 / 15:30	DI water	0.76	0.00	0.00	0.00
	2	24.08.17 / 15:30	25.08.17 / 07:30	DI water	1.28	0.00	0.00	0.00
	3	25.08.17 / 07:30	25.08.17 / 16:00	DI water	1.03	0.00	0.00	0.00
	4	25.08.17 / 16:00	28.08.17 / 07:00	DI water	0.50	0.00	0.00	0.00
	5	28.08.17 / 07:00	28.08.17 / 16:30	DI water	0.30	0.00	0.00	0.01
	6	28.08.17 / 07:00	29.08.17 / 07:00	DI water	0.25	0.00	0.00	0.01
	7	29.08.17 / 07:00	30.08.17 / 07:00	DI water	0.21	0.00	0.00	0.01
	8	30.08.17 / 07:00	31.08.17 / 07:00	DI water	0.20	0.00	0.00	0.01
	9	31.08.17 / 07:00	01.09.17 / 08:00	0.1 M NH_4Cl	0.12	0.00	0.00	0.01
	10	01.09.17 / 08:00	01.09.17 / 15:30	0.1 M NH_4Cl	0.15	0.00	0.00	0.01
	11	01.09.17 / 15:30	04.09.17 / 07:00	0.1 M NH_4Cl	0.19	0.00	0.00	0.01
	12	04.09.17 / 07:00	05.09.17 / 07:00	0.1 M NH_4Cl	0.21	0.00	0.00	0.01
Column 2	13	05.09.17 / 07:00	06.09.17 / 07:00	0.1 M NH_4Cl	0.19	0.00	0.00	0.01
	14	06.09.17 / 07:00	06.09.17 / 16:00	0.1 M NH_4Cl	0.20	0.00	0.00	0.01
	15	06.09.17 / 16:00	07.09.17 / 07:30	0.1 M NH_4Cl	27.92	0.00	0.00	0.04
	16	07.09.17 / 07:30	07.09.17 / 17:00	0.1 M NH_4Cl	103.80	0.00	0.00	0.04
	17	07.09.17 / 17:00	08.09.17 / 07:30	0.1 M NH_4Cl	105.49	0.00	0.00	0.04
	18	08.09.17 / 07:30	08.09.17 / 17:00	0.1 M NH_4Cl	97.03	0.08	0.05	0.15
	19	08.09.17 / 17:00	11.09.17 / 10:00	0.1 M NH_4Cl	105.49	0.08	0.05	0.17
	20	11.09.17 / 10:00	12.09.17 / 12:00	0.1 M NH_4Cl	113.67	0.08	0.05	0.16
	21	12.09.17 / 12:00	13.09.17 / 07:10	0.1 M NH_4Cl	113.67	0.08	0.05	0.15
	22	13.09.17 / 07:10	13.09.17 / 17:10	0.1 M NH_4Cl	97.59	0.08	0.05	0.15
	23	13.09.17 / 17:10	14.09.17 / 07:10	0.1 M NH_4Cl	108.88	0.08	0.05	0.15
	24	14.09.17 / 07:10	14.09.17 / 17:10	0.1 M NH_4Cl	113.67	0.08	0.05	0.14

No.	Start Collection [date/h]	End Collection [date/h]	Solution	Chloride [mM]	Nitrate [mM]	Phosphate [mM]	Sulphate [mM]
25	14.09.17 / 17:10	15.09.17 / 07:10	0.1 M NH_4Cl	112.83	0.08	0.05	0.14
26	15.09.17 / 07:10	15.09.17 / 17:10	0.1 M NH_4Cl	113.67	0.08	0.05	0.13
27	15.09.17 / 17:10	18.09.17 / 07:10	0.1 M NH_4Cl	115.08	0.08	0.05	0.13
28	18.09.17 / 07:10	19.09.17 / 07:10	0.1 M NH_4Cl	108.88	0.08	0.05	0.12
29	19.09.17 / 07:10	19.09.17 / 15:10	0.1 M NH_4Cl	119.88	0.08	0.05	0.11
30	19.09.17 / 15:10	21.09.17 / 07:10	0.1 M NH_4Cl	110.85	0.08	0.05	0.12
31	21.09.17 / 07:10	21.09.17 / 18:10	0.1 M NH_4Cl	110.29	0.08	0.05	0.12
32	21.09.17 / 18:10	22.09.17 / 17:10	0.1 M NH_4Cl	111.42	0.08	0.05	0.12
33	22.09.17 / 17:10	25.09.17 / 07:10	0.1 M NH_4Cl	112.26	0.08	0.05	0.11

Table B.3 All element concentrations eluted from the barium chloride and ammonium chloride column experiments (in duplicates).

Appendix C

Model Inputs

C.1 Modelling CEC in PHREEQC

	Exchangeable Species on Clay (initial state at pH 7) [meq/100g]		Equilibrium with 0.5 M $BaCl_2$ Exchangeable Species on Clay [mM]		In Solution [meq/100g]	
without Al	HX	0	Ca	2.84	HX	2.74E-05
	NaX	2.90	Mg	1.33	NaX	0.04
	KX	1.35	Na	2.86	KX	0.07
	CaX_2	2.90	K	1.28	CaX_2	0.06
	MgX_2	1.35	Mn	1.34	MgX_2	0.02
	MnX_2	1.35			MnX_2	0.01
					BaX_2	7.58
with Al	HX	0	Ca	0.965	HX	0.04150
	NaX	0.7	Mg	0.583	NaX	0.01731
	KX	0.3	Na	0.683	KX	0.02690
	CaX_2	1	K	0.273	CaX_2	0.03519
	MgX_2	0.6	Mn	0.298	MgX_2	0.01708
	MnX_2	0.3	Al	7.063	MnX_2	0.00222
	AlX_3	7.1			BaX_2	12.89699
					AlX_3	0.03715

Table C.1 Input and output conditions for PHREEQC modelling of two CEC scenarios: with Al and without Al.

C.2 Modelling Batch Tests in PEST

PEST (Doherty, 1994) was used to determine the optimised exchange constants that describe all REE exchange reactions with kaolinite (in the batch REE dataset). PEST required three input files to run PHREEQC through the command line. These are:

- Command file: supplies PEST with all the template and instruction files, names of model input & output files, the problem size, control variables, initial parameter values, measurement values, weights etc.
- Instruction file: informs PEST where the model output data is and defines the character length.
- Template file: copy of PHREEQC input file except the adjustable parameters are specified.

The input file that PHREEQC required was called the inp.dat. These four input files are shown in tabular form in this section.

PHREEQC Input File	
DATABASE C:\phreeqc\database\w_data.dat	
EXCHANGE_SPECIES	
Yt+3 + 3X- = YtX3	
log_k	2.28974119
La+3 + 3X- = LaX3	
log_k	2.28974119
Ce+3 + 3X- = CeX3	
log_k	2.28974119
Pr+3 + 3X- = PrX3	
log_k	2.28974119
Nd+3 + 3X- = NdX3	
log_k	2.28974119
Gd+3 + 3X- = GdX3	
log_k	2.28974119
Tb+3 + 3X- = TbX3	
log_k	2.28974119
Dy+3 + 3X- = DyX3	
log_k	2.28974119
Ho+3 + 3X- = HoX3	
log_k	2.28974119

PHREEQC Input File

```
Er+3 + 3X- = ErX3
log_k                 2.28974119

Tm+3 + 3X- = TmX3
log_k                 2.28974119

Yb+3 + 3X- = YbX3
log_k                 2.28974119

Lu+3 + 3X- = LuX3
log_k                 2.28974119


SELECTED_OUTPUT 1
   -file               C:\Models\PEST\Fin_Files\SLR1to9_output.dat
   -reset              false
   -simulation         true
   -active             true
   -user_punch         true

USER_PUNCH
   -headings Y La Ce Pr Nd Gd Tb Dy Ho Er Tm Yb Lu
   -start
10 PUNCH TOT("Yt") TOT("La") TOT("Ce") TOT("Pr") TOT("Nd")
TOT("Gd") TOT("Tb") TOT("Dy") TOT("Ho") TOT("Er") TOT("Tm")
TOT("Yb") TOT("Lu")
  -end

PRINT
   -reset              false
   -exchange           true
   -headings           true
   -surface            true
   -totals             true
   -selected_output    true
   -warnings           100

SOLUTION 1
units                 mol/kgw
temp                  25.00
pH                    6.98
pE                    11.18
Cl                    1.00
Ba                    0.50
Ca                    3.9E-04
Mg                    2.1E-04
NaX                   5.4E-04
K                     1.4E-05
Al                    2.8E-03
Mn                    3.5E-06
Zn                    6.0E-04
```

PHREEQC Input File

```
EXCHANGE 1
NaX             5.50E-04
KX              1.50E-05
CaX2            4.00E-04
MgX2            2.10E-04
MnX2            4.00E-06
AlX3            2.83E-03
ZnX2            6.00E-04
YtX3            1.69E-06
LaX3            6.30E-06
CeX3            4.74E-05
PrX3            8.20E-07
NdX3            4.69E-06
SmX3            1.03E-06
EuX3            6.30E-07
GdX3            1.45E-07
TbX3            2.30E-08
DyX3            1.21E-07
HoX3            1.50E-08
ErX3            4.20E-08
TmX3            1.50E-09
YbX3            1.40E-08
LuX3            1.00E-08
   -pitzer_exchange_gammas true
END

USE solution 1

EXCHANGE 2
NaX             5.00E-04
KX              1.00E-05
CaX2            4.00E-04
MgX2            2.45E-04
MnX2            4.00E-06
AlX3            3.23E-03
ZnX2            6.00E-04
YtX3            2.00E-06
LaX3            9.40E-06
CeX3            6.61E-05
PrX3            1.32E-06
NdX3            7.10E-06
SmX3            1.80E-06
EuX3            1.20E-06
GdX3            1.98E-07
TbX3            3.10E-08
DyX3            1.68E-07
HoX3            2.00E-08
ErX3            5.20E-08
TmX3            4.00E-09
YbX3            2.00E-08
LuX3            1.15E-08
   -pitzer_exchange_gammas true
END
```

PHREEQC Input File

```
USE solution 1

EXCHANGE 3
NaX             4.00E-04
KX              9.00E-06
CaX2            4.00E-04
MgX2            3.00E-04
MnX2            5.00E-06
AlX3            3.67E-03
ZnX2            6.00E-04
YtX3            2.50E-06
LaX3            1.25E-05
CeX3            8.85E-05
PrX3            1.80E-06
NdX3            9.40E-06
SmX3            2.40E-06
EuX3            1.70E-06
GdX3            2.97E-07
TbX3            4.20E-08
DyX3            2.11E-07
HoX3            2.60E-08
ErX3            7.00E-08
TmX3            7.00E-09
YbX3            3.40E-08
LuX3            1.30E-08
   -pitzer_exchange_gammas true
END

USE solution 1

EXCHANGE 4
NaX             7.00E-04
KX              2.00E-05
CaX2            6.00E-04
MgX2            4.50E-04
MnX2            1.00E-03
AlX3            4.00E-03
ZnX2            6.00E-04
YtX3            3.30E-06
LaX3            1.70E-05
CeX3            1.31E-04
PrX3            2.30E-06
NdX3            1.35E-05
SmX3            3.20E-06
EuX3            1.90E-06
GdX3            4.81E-07
TbX3            6.20E-08
DyX3            3.09E-07
HoX3            3.90E-08
ErX3            9.80E-08
TmX3            1.05E-08
YbX3            5.50E-08
```

```
LuX3                1.80E-08
   -pitzer_exchange_gammas true
END

USE solution 1

EXCHANGE 5
NaX                 0.0006
KX                  0.000008
CaX2                0.0004
MgX2                0.00045
MnX2                0.0000209
AlX3                0.004
ZnX2                0.0006
YtX3                0.0000034
LaX3                0.0000184
CeX3                0.0001514
PrX3                0.0000026
NdX3                0.0000142
SmX3                0.0000036
EuX3                0.0000026
GdX3                0.000000583
TbX3                0.000000072
DyX3                0.000000377
HoX3                0.000000046
ErX3                0.000000109
TmX3                1.15E-08
YbX3                0.00000008
LuX3                0.000000019
   -pitzer_exchange_gammas true
END

USE solution 1

EXCHANGE 6
NaX                 7.00E-04
KX                  9.00E-06
CaX2                4.00E-04
MgX2                1.00E-05
MnX2                5.00E-06
AlX3                4.00E-03
ZnX2                6.00E-04
YtX3                3.80E-06
LaX3                2.18E-05
CeX3                1.82E-04
PrX3                3.20E-06
NdX3                1.98E-05
SmX3                3.90E-06
EuX3                3.00E-06
GdX3                7.02E-07
TbX3                7.80E-08
DyX3                4.45E-07
HoX3                5.20E-08
```

```
ErX3                1.23E-07
TmX3                1.60E-08
YbX3                1.14E-07
LuX3                2.00E-08
   -pitzer_exchange_gammas true
END

USE solution 1

EXCHANGE 7
NaX                 7.00E-04
KX                  2.00E-05
CaX2                4.00E-04
MgX2                6.00E-04
MnX2                1.50E-05
AlX3                4.33E-03
ZnX2                5.00E-04
YtX3                4.49E-06
LaX3                2.53E-05
CeX3                2.21E-04
PrX3                4.05E-06
NdX3                2.42E-05
SmX3                4.50E-06
EuX3                3.40E-06
GdX3                9.01E-07
TbX3                1.03E-07
DyX3                5.64E-07
HoX3                6.40E-08
ErX3                1.61E-07
TmX3                1.80E-08
YbX3                1.31E-07
LuX3                2.30E-08
   -pitzer_exchange_gammas true
END

USE solution 1

EXCHANGE 8
NaX                 6.00E-04
KX                  2.00E-05
CaX2                4.00E-04
MgX2                7.00E-04
MnX2                8.00E-06
AlX3                5.00E-03
ZnX2                5.00E-04
YtX3                5.30E-06
LaX3                3.02E-05
CeX3                2.64E-04
PrX3                4.80E-06
NdX3                2.83E-05
SmX3                4.90E-06
EuX3                3.70E-06
GdX3                1.10E-06
```

PHREEQC Input File

```
TbX3                1.25E-07
DyX3                6.72E-07
HoX3                8.15E-08
ErX3                1.86E-07
TmX3                2.20E-08
YbX3                1.69E-07
LuX3                2.70E-08
   -pitzer_exchange_gammas true
END

USE solution 1

EXCHANGE 9
NaX                 7.00E-04
KX                  8.00E-05
CaX2                4.00E-04
MgX2                8.50E-04
MnX2                1.40E-05
AlX3                5.67E-03
ZnX2                5.00E-04
YtX3                6.20E-06
LaX3                3.34E-05
CeX3                3.23E-04
PrX3                5.70E-06
NdX3                3.36E-05
SmX3                5.20E-06
EuX3                4.00E-06
GdX3                1.42E-06
TbX3                1.49E-07
DyX3                8.11E-07
HoX3                9.90E-08
ErX3                2.30E-07
TmX3                2.80E-08
YbX3                2.15E-07
LuX3                3.30E-08
   -pitzer_exchange_gammas true
END
```

Continued…

PEST Template File

```
DATABASE C:\phreeqc\database\w_data.dat
EXCHANGE_SPECIES

Yt+3 + 3X- = YtX3
log_k                   #k          #

La+3 + 3X- = LaX3
log_k                   #k          #

Ce+3 + 3X- = CeX3
log_k                   #k          #

Pr+3 + 3X- = PrX3
log_k                   #k          #

Nd+3 + 3X- = NdX3
log_k                   #k          #

Gd+3 + 3X- = GdX3
log_k                   #k          #

Tb+3 + 3X- = TbX3
log_k                   #k          #

Dy+3 + 3X- = DyX3
log_k                   #k          #

Ho+3 + 3X- = HoX3
log_k                   #k          #

Er+3 + 3X- = ErX3
log_k                   #k          #

Tm+3 + 3X- = TmX3
log_k                   #k          #

Yb+3 + 3X- = YbX3
log_k                   #k          #

Lu+3 + 3X- = LuX3
log_k                   #k          #


SELECTED_OUTPUT 1
   -file                 C:\Models\PEST\Fin_Files\SLR1to9_output.dat
   -reset                false
   -simulation           true
   -active               true
   -user_punch           true

USER_PUNCH
   -headings Y La Ce Pr Nd Gd Tb Dy Ho Er Tm Yb Lu
```

PEST Template File

```
   -start
10 PUNCH TOT("Yt") TOT("La") TOT("Ce") TOT("Pr") TOT("Nd")
TOT("Gd") TOT("Tb") TOT("Dy") TOT("Ho") TOT("Er") TOT("Tm")
TOT("Yb") TOT("Lu")
  -end

PRINT
   -reset              false
   -exchange           true
   -headings           true
   -surface            true
   -totals             true
   -selected_output    true
   -warnings           100

SOLUTION 1
units                  mol/kgw
temp                   25.00
pH                     6.98
pE                     11.18
Cl                     1.00
Ba                     0.50
Ca                     3.9E-04
Mg                     2.1E-04
NaX                    5.4E-04
K                      1.4E-05
Al                     2.8E-03
Mn                     3.5E-06
Zn                     6.0E-04

EXCHANGE 1
NaX                    5.50E-04
KX                     1.50E-05
CaX2                   4.00E-04
MgX2                   2.10E-04
MnX2                   4.00E-06
AlX3                   2.83E-03
ZnX2                   6.00E-04
YtX3                   1.69E-06
LaX3                   6.30E-06
CeX3                   4.74E-05
PrX3                   8.20E-07
NdX3                   4.69E-06
SmX3                   1.03E-06
EuX3                   6.30E-07
GdX3                   1.45E-07
TbX3                   2.30E-08
DyX3                   1.21E-07
HoX3                   1.50E-08
ErX3                   4.20E-08
TmX3                   1.50E-09
YbX3                   1.40E-08
LuX3                   1.00E-08
```

```
   -pitzer_exchange_gammas true
END

USE solution 1

EXCHANGE 2
NaX             5.00E-04
KX              1.00E-05
CaX2            4.00E-04
MgX2            2.45E-04
MnX2            4.00E-06
AlX3            3.23E-03
ZnX2            6.00E-04
YtX3            2.00E-06
LaX3            9.40E-06
CeX3            6.61E-05
PrX3            1.32E-06
NdX3            7.10E-06
SmX3            1.80E-06
EuX3            1.20E-06
GdX3            1.98E-07
TbX3            3.10E-08
DyX3            1.68E-07
HoX3            2.00E-08
ErX3            5.20E-08
TmX3            4.00E-09
YbX3            2.00E-08
LuX3            1.15E-08
   -pitzer_exchange_gammas true
END

USE solution 1

EXCHANGE 3
NaX             4.00E-04
KX              9.00E-06
CaX2            4.00E-04
MgX2            3.00E-04
MnX2            5.00E-06
AlX3            3.67E-03
ZnX2            6.00E-04
YtX3            2.50E-06
LaX3            1.25E-05
CeX3            8.85E-05
PrX3            1.80E-06
NdX3            9.40E-06
SmX3            2.40E-06
EuX3            1.70E-06
GdX3            2.97E-07
TbX3            4.20E-08
DyX3            2.11E-07
HoX3            2.60E-08
ErX3            7.00E-08
```

```
TmX3                7.00E-09
YbX3                3.40E-08
LuX3                1.30E-08
   -pitzer_exchange_gammas true
END

USE solution 1

EXCHANGE 4
NaX                 7.00E-04
KX                  2.00E-05
CaX2                6.00E-04
MgX2                4.50E-04
MnX2                1.00E-03
AlX3                4.00E-03
ZnX2                6.00E-04
YtX3                3.30E-06
LaX3                1.70E-05
CeX3                1.31E-04
PrX3                2.30E-06
NdX3                1.35E-05
SmX3                3.20E-06
EuX3                1.90E-06
GdX3                4.81E-07
TbX3                6.20E-08
DyX3                3.09E-07
HoX3                3.90E-08
ErX3                9.80E-08
TmX3                1.05E-08
YbX3                5.50E-08
LuX3                1.80E-08
   -pitzer_exchange_gammas true
END

USE solution 1

EXCHANGE 5
NaX                 0.0006
KX                  0.000008
CaX2                0.0004
MgX2                0.00045
MnX2                0.0000209
AlX3                0.004
ZnX2                0.0006
YtX3                0.0000034
LaX3                0.0000184
CeX3                0.0001514
PrX3                0.0000026
NdX3                0.0000142
SmX3                0.0000036
EuX3                0.0000026
GdX3                0.000000583
TbX3                0.000000072
```

DyX3	0.000000377
HoX3	0.000000046
ErX3	0.000000109
TmX3	1.15E-08
YbX3	0.00000008
LuX3	0.000000019

-pitzer_exchange_gammas true
END

USE solution 1

EXCHANGE 6

NaX	7.00E-04
KX	9.00E-06
CaX2	4.00E-04
MgX2	1.00E-05
MnX2	5.00E-06
AlX3	4.00E-03
ZnX2	6.00E-04
YtX3	3.80E-06
LaX3	2.18E-05
CeX3	1.82E-04
PrX3	3.20E-06
NdX3	1.98E-05
SmX3	3.90E-06
EuX3	3.00E-06
GdX3	7.02E-07
TbX3	7.80E-08
DyX3	4.45E-07
HoX3	5.20E-08
ErX3	1.23E-07
TmX3	1.60E-08
YbX3	1.14E-07
LuX3	2.00E-08

-pitzer_exchange_gammas true
END

USE solution 1

EXCHANGE 7

NaX	7.00E-04
KX	2.00E-05
CaX2	4.00E-04
MgX2	6.00E-04
MnX2	1.50E-05
AlX3	4.33E-03
ZnX2	5.00E-04
YtX3	4.49E-06
LaX3	2.53E-05
CeX3	2.21E-04
PrX3	4.05E-06
NdX3	2.42E-05
SmX3	4.50E-06

PEST Template File

EuX3	3.40E-06
GdX3	9.01E-07
TbX3	1.03E-07
DyX3	5.64E-07
HoX3	6.40E-08
ErX3	1.61E-07
TmX3	1.80E-08
YbX3	1.31E-07
LuX3	2.30E-08

-pitzer_exchange_gammas true
END

USE solution 1

EXCHANGE 8

NaX	6.00E-04
KX	2.00E-05
CaX2	4.00E-04
MgX2	7.00E-04
MnX2	8.00E-06
AlX3	5.00E-03
ZnX2	5.00E-04
YtX3	5.30E-06
LaX3	3.02E-05
CeX3	2.64E-04
PrX3	4.80E-06
NdX3	2.83E-05
SmX3	4.90E-06
EuX3	3.70E-06
GdX3	1.10E-06
TbX3	1.25E-07
DyX3	6.72E-07
HoX3	8.15E-08
ErX3	1.86E-07
TmX3	2.20E-08
YbX3	1.69E-07
LuX3	2.70E-08

-pitzer_exchange_gammas true
END

USE solution 1

EXCHANGE 9

NaX	7.00E-04
KX	8.00E-05
CaX2	4.00E-04
MgX2	8.50E-04
MnX2	1.40E-05
AlX3	5.67E-03
ZnX2	5.00E-04
YtX3	6.20E-06
LaX3	3.34E-05
CeX3	3.23E-04

PEST Template File	
PrX3	5.70E-06
NdX3	3.36E-05
SmX3	5.20E-06
EuX3	4.00E-06
GdX3	1.42E-06
TbX3	1.49E-07
DyX3	8.11E-07
HoX3	9.90E-08
ErX3	2.30E-07
TmX3	2.80E-08
YbX3	2.15E-07
LuX3	3.30E-08
-pitzer_exchange_gammas true	
END	

Continued…

PEST Instruction File

pif @

@Y@ @La@ @Ce@ @Pr@ @Nd@ @Gd@ @Tb@ @Dy@ @Ho@ @Er@ @Tm@ @Yb@ @Lu@

l1 [o1]19:29	[o2]35:45	[o3]51:61	[o4]67:77	[o5]83:93	[o6]99:109	[o7]115:125	[o8]131:141	[o9]147:157	[o10]163:173	[o11]179:189	[o12]195:205	[o13]211:221
l1 [o14]19:29	[o15]35:45	[o16]51:61	[o17]67:77	[o18]83:93	[o19]99:109	[o20]115:125	[o21]131:141	[o22]147:157	[o23]163:173	[o24]179:189	[o25]195:205	[o26]211:221
l1 [o27]19:29	[o28]35:45	[o29]51:61	[o30]67:77	[o31]83:93	[o32]99:109	[o33]115:125	[o34]131:141	[o35]147:157	[o36]163:173	[o37]179:189	[o38]195:205	[o39]211:221
l1 [o40]19:29	[o41]35:45	[o42]51:61	[o43]67:77	[o44]83:93	[o45]99:109	[o46]115:125	[o47]131:141	[o48]147:157	[o49]163:173	[o50]179:189	[o51]195:205	[o52]211:221
l1 [o53]19:29	[o54]35:45	[o55]51:61	[o56]67:77	[o57]83:93	[o58]99:109	[o59]115:125	[o60]131:141	[o61]147:157	[o62]163:173	[o63]179:189	[o64]195:205	[o65]211:221
l1 [o66]19:29	[o67]35:45	[o68]51:61	[o69]67:77	[o70]83:93	[o71]99:109	[o72]115:125	[o73]131:141	[o74]147:157	[o75]163:173	[o76]179:189	[o77]195:205	[o78]211:221
l1 [o79]19:29	[o80]35:45	[o81]51:61	[o82]67:77	[o83]83:93	[o84]99:109	[o85]115:125	[o86]131:141	[o87]147:157	[o88]163:173	[o89]179:189	[o90]195:205	[o91]211:221
l1 [o92]19:29	[o93]35:45	[o94]51:61	[o95]67:77	[o96]83:93	[o97]99:109	[o98]115:125	[o99]131:141	[o100]147:157	[o101]163:173	[o102]179:189	[o103]195:205	[o104]211:221
l1 [o105]19:29	[o106]35:45	[o107]51:61	[o108]67:77	[o109]83:93	[o110]99:109	[o111]115:125	[o112]131:141	[o113]147:157	[o114]163:173	[o115]179:189	[o116]195:205	[o117]211:221
l1 [o118]19:29	[o119]35:45	[o120]51:61	[o121]67:77	[o122]83:93	[o123]99:109	[o124]115:125	[o125]131:141	[o126]147:157	[o127]163:173	[o128]179:189	[o129]195:205	[o130]211:221

Continued…

PEST Control File

```
pcf
* control data
restart  estimation
  1  130  1  0  1
  1  1  single point  1  0  0
  5.0  2.0  0.3  0.03  10
  3.0  3.0  0.001  0
0.1
  30  0.01  3  3  0.01  3
  1  1  1
* parameter groups
k   relative  0.01  0.0  switch  2.0  parabolic
* parameter data
k  none relative  2.300  1.000000E-1   1.000000E+1  k  1.0000   0.0000  1
* observation groups
obsgroup
* observation data
o1                0.00000      1.0  obsgroup
o2                0.00000      1.0  obsgroup
o3                0.00000      1.0  obsgroup
o4                0.00000      1.0  obsgroup
o5                0.00000      1.0  obsgroup
o6                0.00000      1.0  obsgroup
o7                0.00000      1.0  obsgroup
o8                0.00000      1.0  obsgroup
o9                0.00000      1.0  obsgroup
o10               0.00000      1.0  obsgroup
o11               0.00000      1.0  obsgroup
o12               0.00000      1.0  obsgroup
o13               0.00000      1.0  obsgroup
o14               1.400000E-06  1.0  obsgroup
o15               5.100000E-06  1.0  obsgroup
o16               3.960000E-05  1.0  obsgroup
o17               7.000000E-07  1.0  obsgroup
o18               3.900000E-06  1.0  obsgroup
o19               1.120000E-07  1.0  obsgroup
o20               1.800000E-08  1.0  obsgroup
o21               9.700000E-08  1.0  obsgroup
o22               1.200000E-08  1.0  obsgroup
o23               3.100000E-08  1.0  obsgroup
o24               1.000000E-09  1.0  obsgroup
o25               1.100000E-08  1.0  obsgroup
o26               7.500000E-09  1.0  obsgroup
o27               1.600000E-06  1.0  obsgroup
o28               7.100000E-06  1.0  obsgroup
o29               5.240000E-05  1.0  obsgroup
o30               1.000000E-06  1.0  obsgroup
o31               5.400000E-06  1.0  obsgroup
o32               1.590000E-07  1.0  obsgroup
o33               2.400000E-08  1.0  obsgroup
o34               1.290000E-07  1.0  obsgroup
o35               1.500000E-08  1.0  obsgroup
```

o36	4.000000E-08	1.0	obsgroup
o37	3.000000E-09	1.0	obsgroup
o38	1.600000E-08	1.0	obsgroup
o39	8.000000E-09	1.0	obsgroup
o40	1.800000E-06	1.0	obsgroup
o41	9.100000E-06	1.0	obsgroup
o42	6.380000E-05	1.0	obsgroup
o43	1.600000E-06	1.0	obsgroup
o44	6.700000E-06	1.0	obsgroup
o45	2.080000E-07	1.0	obsgroup
o46	2.900000E-08	1.0	obsgroup
o47	1.520000E-07	1.0	obsgroup
o48	1.800000E-08	1.0	obsgroup
o49	5.000000E-08	1.0	obsgroup
o50	5.000000E-09	1.0	obsgroup
o51	2.100000E-08	1.0	obsgroup
o52	9.000000E-09	1.0	obsgroup
o53	2.200000E-06	1.0	obsgroup
o54	1.130000E-05	1.0	obsgroup
o55	8.660000E-05	1.0	obsgroup
o56	1.600000E-06	1.0	obsgroup
o57	9.000000E-06	1.0	obsgroup
o58	3.120000E-07	1.0	obsgroup
o59	4.100000E-08	1.0	obsgroup
o60	2.130000E-07	1.0	obsgroup
o61	2.500000E-08	1.0	obsgroup
o62	6.600000E-08	1.0	obsgroup
o63	7.000000E-09	1.0	obsgroup
o64	3.600000E-08	1.0	obsgroup
o65	1.100000E-08	1.0	obsgroup
o66	2.400000E-06	1.0	obsgroup
o67	1.280000E-05	1.0	obsgroup
o68	1.070000E-04	1.0	obsgroup
o69	1.900000E-06	1.0	obsgroup
o70	1.030000E-05	1.0	obsgroup
o71	4.040000E-07	1.0	obsgroup
o72	4.900000E-08	1.0	obsgroup
o73	2.580000E-07	1.0	obsgroup
o74	3.200000E-08	1.0	obsgroup
o75	7.600000E-08	1.0	obsgroup
o76	8.000000E-09	1.0	obsgroup
o77	5.200000E-08	1.0	obsgroup
o78	1.200000E-08	1.0	obsgroup
o79	2.800000E-06	1.0	obsgroup
o80	1.530000E-05	1.0	obsgroup
o81	1.280000E-04	1.0	obsgroup
o82	2.300000E-06	1.0	obsgroup
o83	1.390000E-05	1.0	obsgroup
o84	5.050000E-07	1.0	obsgroup
o85	5.000000E-08	1.0	obsgroup
o86	3.090000E-07	1.0	obsgroup
o87	3.600000E-08	1.0	obsgroup
o88	8.900000E-08	1.0	obsgroup

PEST Control File			
o89	1.100000E-08	1.0	obsgroup
o90	7.900000E-08	1.0	obsgroup
o91	1.200000E-08	1.0	obsgroup
o92	3.100000E-06	1.0	obsgroup
o93	1.740000E-05	1.0	obsgroup
o94	1.530000E-04	1.0	obsgroup
o95	2.800000E-06	1.0	obsgroup
o96	1.640000E-05	1.0	obsgroup
o97	6.220000E-07	1.0	obsgroup
o98	6.900000E-08	1.0	obsgroup
o99	3.860000E-07	1.0	obsgroup
o100	4.400000E-08	1.0	obsgroup
o101	1.100000E-07	1.0	obsgroup
o102	1.200000E-08	1.0	obsgroup
o103	8.700000E-08	1.0	obsgroup
o104	1.400000E-08	1.0	obsgroup
o105	3.500000E-06	1.0	obsgroup
o106	1.990000E-05	1.0	obsgroup
o107	1.770000E-04	1.0	obsgroup
o108	3.200000E-06	1.0	obsgroup
o109	1.880000E-05	1.0	obsgroup
o110	7.330000E-07	1.0	obsgroup
o111	8.100000E-08	1.0	obsgroup
o112	4.260000E-07	1.0	obsgroup
o113	5.200000E-08	1.0	obsgroup
o114	1.250000E-07	1.0	obsgroup
o115	1.400000E-08	1.0	obsgroup
o116	1.050000E-07	1.0	obsgroup
o117	1.600000E-08	1.0	obsgroup
o118	3.800000E-06	1.0	obsgroup
o119	2.100000E-05	1.0	obsgroup
o120	1.990000E-04	1.0	obsgroup
o121	3.600000E-06	1.0	obsgroup
o122	2.150000E-05	1.0	obsgroup
o123	8.850000E-07	1.0	obsgroup
o124	9.100000E-08	1.0	obsgroup
o125	4.800000E-07	1.0	obsgroup
o126	5.900000E-08	1.0	obsgroup
o127	1.410000E-07	1.0	obsgroup
o128	1.700000E-08	1.0	obsgroup
o129	1.250000E-07	1.0	obsgroup
o130	1.790000E-08	1.0	obsgroup
* model command line			
C:\phreeqc\phreeqc.exe C:\Models\PEST\Fin_Files\in.dat C:\Models\PEST\Fin_Files\in.dat.out C:\phreeqc\database\w_data.dat			
* model input/output			
C:\PEST\temp.tpl C:\Models\PEST\Fin_Files\in.dat			
C:\PEST\inst.ins C:\Models\PEST\Fin_Files\SLR1to9_output.dat			

Table C.2 Pest input files to model the REE batch dataset.

C.3 Modelling Soil Column Experiments in TRN

The TRN input files for simulation of the barium chloride columns are shown in this section. Six input files were required to model the barium chloride columns. These are:

- trn.ini ⇒ defines the global parameters
- box.dat ⇒ defines cell data
- qIn.dat ⇒ defines inflow solutions
- element.dat ⇒ defines chemical elements
- exch.ini ⇒ defines ion exchange species
- phase.ini ⇒ defines equilibrium phases

Two input solutions were required (created in PHREEQC) to run TRN. These are:

- 005_bacl.sol ⇒ file name of aqueous inflow solution
- CEC.sol ⇒ file name for initial mobile water

trn.ini			**Description**
BOXN	10		total number of cells
DELT	1.57	// h	time step
T_END	400 // h	// h	simulation time
AREA	0.001256	// m^2	cross section of column
DISP	1		0-without dispersion, 1-with dispersion
REAC	0		0-without kinetics, 1-with kinetics
PHAS	1		0-without mineral equilibrium, 1 with mineral equilibrium
EXCH_TYP	3	// 1-resin, 2-soil, 3-resin-cation	
EXCH_POR	2	// 0-mobile, 1-stagnant, 2-both	
DBL_POR	1		0-single porosity, 1-dual porosity
MIX_VOL	0 0.00785	// in m3	volume of upstream mix cell
DILU	0 0 0	// on/off diluT 1st_dilu_box	
RESIN_FLOW	0 494 3	// on/off nR_steps NR_cells mix_cells	
MIX_SOL	Pink2_eqREE_conc.sol		initial water in upstream mix (file name)
RESIN_SOL	Pink2_eqREE_conc.sol		
EXCH_DAVIES	1	// activity correction for IX	
ICHM	1		0-without PHREEQC, 1-with PHREEQC
KCHM	1		increment factor for PHREEQC calculations
KOUT	1		increment factor for output in cM_*.txt and cP_*txt
KOUX	1		increment factor for output in profile directories
KOUB	0		
UNSATU	0		
ANALY	0		
ELEM_DO	0	// external Dissolved Oxygen Do	
CTOT	150 0 0	// meq/L plus assym_factor	total ion exchange capacity
CHRG	pH		parameter for chage balance adjustment for t>0

trn.ini			Description
CHRG_IN	pH		parameter for chage balance adjustment for t=0
UNIT	2	// -2 mg/L , +2 mmol/L	
DISP_PHRE	1		
PRN_MASS_UNIT	3		units of mass balance elements
PRN_MASS_EBOX	3	// number of boxes	number of cells in mass balance output
PRN_MASS_FULL	0	// 1 = output per disp-step	type of mass output (0-standard, 1-for each dispersion step)
PRN_END_CELLS	0	// solu-output of all cells	
PRN_BOX_DAT_REVERSE	0	// print box.dat in reverse order	
SI_ONLY_PORE	0	// makeshift for column tests	
PHAS_TO_PORE	0		
FILL_AND_WAIT	0 0	// fill, timesteps after fill	
IX_NO_EQUILIBRATE	1	// no IX equilibrium at t=0	
ELMB_NB	8		number of elements for mass balance
ELMB_01	La		name of first mass balance element
ELMB_02	Ce		name of second mass balance element
ELMB_03	Nd		name of third mass balance element
ELMB_04	Dy		name of fourth mass balance element
ELMB_05	Cl		name of fifth mass balance element
ELMB_06	Ba		name of sixth mass balance element
ELMB_07	Al		name of seventh mass balance element
ELMB_08	Na		name of last mass balance element
REDX_PAIR	0	// redox Fe(2)/Fe(3)	
PHRE_SHOW	0	// -1 no output	time step for PHREEQC-input check
FOUR_DIAG	1		
PE_FIX	0 0	// for pore water	1-without pe changes during reactions
PE_MIN	0 0	// pe_Min = par - pH	parameter to fix minimum pe value
PE_MAX	0 0	// pe_Max = par	parameter to fix maximum pe value
TIME_DIGITS	6		

box.dat			Description
box	1		number of first cell in the section
name	A		name of the section
dx	0.015	// m	cell length
eps	0.1	// m^3/m^3	porosity for mobile phase
epsP	0.5	// m^3/m^3	porosity for stagnant phase
diffu	0	// m^2/s	effective diffusion coefficient
disp	0.001	// m	longitudinal dispersivity
alpha	0.055	// 1/h	exchange rate between between mobile and stagnant water
cell	CEC.sol		file name for initial mobile water

CEC.sol	
SOLUTION 1	
units	mol/kgw
temp	2.50E+01
pH	6.00E+00
pE	4.00E+00
Ca	3.40E-05
Mg	9.00E-06
Na	6.50E-05
K	8.80E-05
S(6)	3.00E-06

CEC.sol	
Cl	7.40E-05
Fe	1.79E-07
Al	5.00E-06
Mn	2.17E-07
N(5)	1.00E-06
P	1.00E-06
Ni	1.70E-07
Zn	2.60E-06
Cu	1.57E-07
Yt	1.12E-08
La	1.02E-08
Ce	2.55E-05
Pr	7.10E-09
Nd	6.93E-09
Sm	8.29E-09
Eu	6.86E-09
Gd	2.22E-08
Tb	6.29E-09
Dy	6.15E-09
Ho	6.06E-09
Er	5.98E-09
Tm	5.92E-09
Yb	5.78E-09
Lu	5.72E-09

EXCHANGE 1	
QH	0.00E+00
QNa	4.74E-04
QK	7.98E-05
QNH4	0.00E+00
Q2Ca	1.58E-04
Q2Ba	0.00E+00
Q2Mg	1.03E-04
Q2Mn	1.40E-06
Q2Fe	0.00E+00
Q3Fe	0.00E+00
Q3Al	7.61E-04
Q3Yt	4.31E-07
Q3La	1.83E-06
Q3Ce	1.04E-05
Q3Pr	1.88E-07
Q3Nd	1.10E-06
Q3Sm	9.36E-06
Q3Eu	3.82E-06
Q3Gd	1.70E-08
Q3Tb	5.00E-09
Q3Dy	2.60E-08
Q3Ho	3.00E-09
Q3Er	8.00E-09
Q3Tm	2.00E-09
Q3Yb	2.00E-09
Q3Lu	2.00E-09

CEC.sol
END

qIn.dat			Description
box	FIRST		name of first cell
Typ	0	\\ should not be changed	
t0	0	\\ h	start of time period
q0	1	\\ should not be changed	inflow scaling at t0
t1	100000		end of time period
q1	1	\\ should not be changed	inflow scaling at t1
nmCX	005_bacl.sol		file name for aqueous inflow solution

005_bacl.sol	
SOLUTION 1	
units	mol/kgw
temp	2.50E+01
pH	6.97E+00
pE	1.06E+01
Cl	1.00E-01
Ba	5.00E-02
O(0)	2.42E-16
END	

phas.ini	
Gypsum	0
Calcite	0
Dolomite	0
Fe(OH)3(a)	0
Al(OH)3(a)	1
Gibbsite	1
Brucite	0
Kaolinite	1
Siderite	0
Silicagel	0
Coffinite	0
Schwertmann_KT(e)	0
Schwertmann_Yu(e)	0
Schwertmann_Bh(e)	0
Schoepite	0
Rutherfordine	0
Uraninite(c)	0
UO2(a)	0
Becquerelite(e)	0
Soddyite(e)	0

Continued…

element.ini	
BDAT	DATA_BASE\w_data.dat
Ca	1 0 0 0
Mg	1 0 0 0
Na	1 0 0 0
K	1 0 0 0
S(6)	1 0 0 0
C(4)	0 0 0 0
Cl	1 0 0 0
Fe(2)	1 0 0 0
Fe(3)	0 0 0 0
Fe	1 0 0 0
Al	1 0 0 0
Mn	1 0 0 0
Ba	1 0 0 0
U	0 0 0 0
U(4)	0 0 0 0
U(6)	0 0 0 0
F	0 0 0 0
C(-4)	0 0 0 0
S(-2)	0 0 0 0
O(0)	1 0 0 0
Sc	1 0 0 0
Yt	1 0 0 0
P	0 0 0 0
Si	1 0 0 0
Cd	0 0 0 0
Mo	0 0 0 0
Zr	0 0 0 0
La	1 0 0 0
Ce	1 0 0 0
Pr	1 0 0 0
Nd	1 0 0 0
Sm	1 0 0 0
Eu	1 0 0 0
Gd	1 0 0 0
Tb	1 0 0 0
Dy	1 0 0 0
Ho	1 0 0 0
Er	1 0 0 0
Tm	1 0 0 0
Yb	1 0 0 0
Lu	1 0 0 0
Y	1 0 0 0

Table C.3 Input files for TRN calculations..

C.4 Modelling Water Flow in HYDRUS 1-D

HYDRUS 1-D	Input
Main Processes	
Water Flow	□
Solute Transport	
Heat Transport	
Root Water Uptake	
CO2 Transport	
Geometry Information	
Length Units	m
Number of Soil Materials	5
Number of Layers for Mass Balances	5
Decline from Vertical Axes	1
Depth of the Soil Profile	6
Time Information	
Time Units	Days
Initial Time	0
Final Time	400
Initial Time Step	0.001
Minimum Time Step	1.00E-05
Maximum Time Step	10
Print Information	
T-level Information	□
Every n time steps	1
Print at Regular Time Interval	
Screen Output	□
Print Fluxes (instead of Temp) for Observation Nodes	□
Hit Enter at End?	□
Number of Print Times	10
Iteration Criteria	
Maximum Number of Iterations	10
Water Content Tolerance	0.001
Pressure Head Tolerance [m]	0.01
Lower Optimal Iteration Range	3
Upper Optimal Iteration Range	7
Lower Time Step Multiplication Factor	1.3
Upper Time Step Multiplication Factor	0.7
Lower Limit of the Tension Interval [m]	1.00E-08
Upper Limit of the Tension Interval [m]	100
Soil Hydraulic Model	
van Genuchten-Mualem	□
Modified van Genuchten	
Brooks-Corey	
Kosugi (log-normal)	
Dual-porosity (Durner, dual van Genuchten - Mualem)	
Dual-porosity (mobile-immobile, water c. mass transfer)	
Dual-porosity (mobile-immobile, head mass transfer)	

Dual-permeabilty (Gerke and van Genuchten, 1993)	
Look-up Tables	
No Hysteresis	□
Hysteresis in retention curve	
Hysteresis in retention curve and conductivity	
Hysteresis in retention curve (no pumping, Bob Lenhard)	
Water Flow Parameters	see Table 6.1
Water Flow Boundary Conditions	
Upper Boundary Condition	
Constant Pressure Head	□
Constant Flux	
Atmospheric BC with Surface Layer	
Atmospheric BC with Surface Run Off	
Variable Pressure Head	
Variable Pressure Head/Flux	
Lower Boundary Condition	
Constant Pressure Head	
Constant Flux	
Variable Pressure Head	
Variable Flux	
Free Drainage	□
Deep Drainage	
Seepage Face	
Horizontal Drains	
Initial Condition	
In Pressure Heads	□
In Water Contents	

Table C.4 HYDRUS 1-D inputs to simulate water flow through a 6 m laterite.